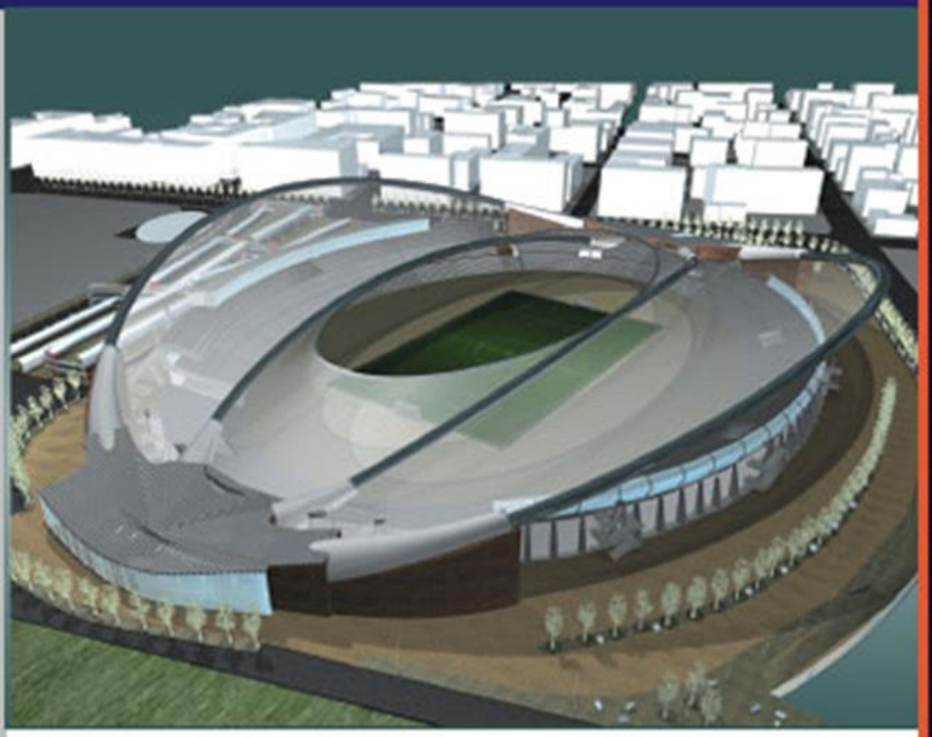

Performance of Wind Exposed Structures

Results of the PERBACCO project

Edited by
Gianni Bartoli
Francesco Ricciardelli
Anna Saetta
Vincenzo Sepe

Firenze University Press

Performance of Wind Exposed Structures
Results of the PERBACCO project

Edited by
Gianni Bartoli
Francesco Ricciardelli
Anna Saetta
Vincenzo Sepe

Firenze University Press

Monografie
Scienze Tecnologiche
15

MONOGRAFIE
SCIENZE TECNOLOGICHE

1. Barbara Mazza, *Le Corbusier e la fotografia. La vérité blanche*, 2002

2. *Information technology ed automazione del progetto*, a cura di Carlo Biagini, 2002

3. Leonardo Casini, Enrico Marone, Silvio Menghini, *La riforma della P.A.C. e la filiera olivicolo-olearia italiana*, 2003

4. Leonardo Casini, Enrico Marone, Silvio Menghini, *OCM seminativi: tendenze evolutive e assetto territoriale*, 2003

5. *E4 Thematic Network: Enchanging Engeneering Education in Europe*, a cura di Claudio Borri, Francesco Maffioli, 2003

6. Paolo Ventura, *Città e stazione ferroviaria.* Seconda edizione rivista, 2004

7. *Ecological design for an effective urban regeneration*, edited by Dimitra Babalis, 2004

8. *Winderful: Wind and Infrastructures : dominatine eolian risk for utilities and lifelines*, edited by Gianni Bartoli, Francesco Ricciardelli, Vincenzo Sepe, 2004

9. Giovanni Allegretti, *Porto Alegre: una biografia territoriale*, 2005

10. Antonino Pellicanò, *Da Galileo Galilei a Cosimo Noferi: verso una Nuova Scienza.* La Travagliata Architettura *un inedito trattato galileiano nella Firenze del 1650*, 2005

11. Giuliano Maggiora, *Sulla retorica dell'architettura*, con contributi di Maria Cristina Chiusa, Rosalba Feltro Grassi, 2005

12. Roberta Gentile, Stefano Mancuso, Silvia Martelli, Simona Rizzitelli, *Il giardino di Villa Corsini a Mezzomonte. Descrizione dello stato di fatto e proposta di restauro conservativo*, 2006

13. Marco Frati, *"De bonis lapidibus conciis": la costruzione di Firenze ai tempi di Arnolfo di Cambio. Strumenti, tecniche e maestranze nei cantieri fra XIII e XIV secolo*, 2006

14. Jan C. J. Bart, *Polymer Additive Analytics. Industrial Practice and Case Studies*, 2006

Performance of Wind Exposed Structures:
Results of the PERBACCO project

Edited by

Gianni Bartoli, Francesco Ricciardelli, Anna Saetta, Vincenzo Sepe

Firenze University Press
2006

Performance of Wind Exposed Structures : results of the PERBACCO project / Edited by Gianni Bartoli, Francesco Ricciardelli, Anna Saetta, Vincenzo Sepe. – Firenze : Firenze university press, 2006.
(Monografie. Scienze Tecnologiche, 15)
http://digital.casalini.it/8884534534
Stampa a richiesta disponibile su http://epress.unifi.it

ISBN 10: 88-8453-453-4 (online)
ISBN 13: 978-88-8453-453-8 (online)
ISBN 10: 88-8453-454-2 (print)
ISBN 13: 978-88-8453-454-5 (print)

624.175 (ed. 20)
Building Aerodynamics – Wind effects – Structural Dynamics

PERBACCO is the title of a Research Project in Wind Engineering co-financed by the Italian Ministry for Education, University and Research (MIUR), carried out by eight Italian Universities for two years (Nov. 2003- Nov. 2005).
This book reports the main results obtained in the project, that was a further attempt to integrate different disciplines aiming at an overall optimization of the performance of a wide range of wind exposed structures and infrastructures.

Project Co-ordinating Institution:

Centro di Ricerca Interuniversitario di
Aerodinamica delle Costruzioni ed Ingegneria del Vento

Università di Firenze, Università di Roma "La Sapienza", Università di Perugia,
Università di Trieste, Università IUAV di Venezia, Università di Chieti-Pescara

Cover photo and image:
the roof of the "Adriatico" Soccer Stadium, Pescara (Italy), and the model tested in the CRIACIV wind tunnel for an undergraduate degree Thesis (2005); by courtesy of Sara Giangreco and Fabio Rizzo *(no reproduction can be made without the written permission of the authors)*

© 2006 Firenze University Press

Università degli Studi di Firenze
Firenze University Press
Borgo Albizi, 28 - 50122 Firenze, Italy
http://epress.unifi.it/

Printed in Italy

INDEX

FOREWORD

Within the PRIN (Progetti di Ricerca di Interesse Nazionale) cofinanced by the MIUR (the Italian "Ministero dell'Istruzione, dell'Università e della Ricerca"), a number of University Departments, which are active in the field of Building Aerodynamics and Wind Engineering promoted in 2003 the launch of a wide research project called on PERBACCO (a free Italian acronym standing for Life-cycle Performance, Innovation and Design Criteria for Structures and Infrastructures Facing AEolian and Other Natural Hazards), aimed at integrating different disciplines to obtain an overall optimization of the performance of a wide range of wind exposed structures and infrastructures. 9 Research Units from 8 different Universities have joined the project, which had its official start in November 2003.

This volume, which is going to be presented at the IN-VENTO-06, the 9th (Italian) National Conference of Wind Engineering, hosted by the University "G. D'Annunzio" of Chieti-Pescara, June 2006, is the main tool for the presentation and dissemination of the scientific outcomes: the present book aims at giving a complete perspective of the topics dealt with by the research units on the different aspects of the performance based design of wind exposed structures.

Out of the many open issues still under discussion, the PERBACCO project has focused on 9 Themes which are deemed to be crucial in view of specific needs. These broad scientific and engineering themes have been considered within the 9 research teams, any of them dealing with one or more of the themes, in a truly intense cooperation network.

More than 50 researchers from the 8 participating Universities in the project have been involved in one or more of the scheduled activities: some 65 papers published on international or national journals or on conference or seminar proceedings, 6 plenary meetings, many cross visits of young researchers carried out for scientific exchanges and/or experimental works. These are some of the figures of the work carried out during the 24 months of contract of the PERBACCO project, which has been concluded in November 2005.

ACKNOWLEDGMENTS

The Editorial Board of this volume wishes to gratefully acknowledge the Scientific Coordinator of the project (Prof. C. Borri) and all involved actors during the entire project life. The precious advices of Dr. C. Bullo and all the staff of Firenze University Press, publisher of the volume, during the overall editing of the manuscripts is also gratefully acknowledged.

A final acknowledgement is also due to the financial contribution of the MIUR.

Firenze, May 23rd, 2006

Gianni Bartoli, Francesco Ricciardelli, Anna Saetta, Vincenzo Sepe

1 Introduction

Claudio Borri
University of Florence

1.1 OBJECTIVES

The project "LIFE-CYCLE PERFORMANCE, INNOVATION AND DESIGN CRITERIA FOR STRUCTURES AND INFRASTRUCTURES FACING EOLIAN AND OTHER NATURAL HAZARDS" (2003-05, in the following referred to as **PERBACCO**, according the semi-acronym that the participants unanimously accepted), within the Research Projects of National Interest (PRIN) of MIUR, has been launched and carried out as a natural follow-up of two previous projects in the same line, namely: "WIND AND INFRASTRUCTURES: DOMINATING EOLIAN RISK FOR UTILITIES AND LIFELINES" (WINDERFUL, 2001-03) and "ANALYSIS, CONTROL AND MITIGATION OF AEOLIAN RISK ON CONSTRUCTIONS AND URBAN ENVIRONMENT" (ACME CUE, 1999-01). These two "predecessors" were run almost by the same research teams as in PERBACCO and giving rise of many questions in terms of risk and performances of major structural systems facing the storm hazard.

It is important to underline, that the research group has reached, in recent years, a very high degree of synergy and cooperation, mainly due to the common large scale research facility given by the large Wind Engineering laboratory of CRIACIV, situated in Prato (nearby Florence) and managed by six Italian Universities (CRIACIV is the Italian acronym for "Interuniversity Research Centre for Building Aerodynamics and Wind Engineering"). About 35 researchers are working together from different places on common projects, including the series of PRINs (all financed in the last 15 years), with the main aim of promoting wind engineering and eolian risk in the country and internationally (important international/European cooperation have also been developed in the last years).

The present volume, which resumes the main outcome of the project, has a double aim: the first is to make the achievements more visible and sustainable for a wider scientific community & audience; the second arises from the more extensive version of the results which have been much deeply evaluated during the time elapsed after the project conclusion (about 4 months). Usually the closure of such a wide bi-annual project requires many efforts (inclusive the administration ones) and the scientific results are normally suffering a reduced space (also due to the web procedures tool available: the MIUR/Cineca web-site).

As an introduction, the present Chapter is far from pretending to exhaust the wide range of activity carried out: in the following 8 Chapters, the contributions of all research Units will be developed and widely presented, under the coordination of a Chapter responsible.

The main objective of the project was to introduce, in the current practice of building construction, the idea of the minimization of the ratio between costs and benefits, rather than the simple minimization of costs, for the entire cycle of life of structures and infrastructures.

This goal is achieved by means of the following intermediate strategic actions:

A) To furnish a unique method to evaluate the concept of "expected performance" and of "risk due to wind and other natural hazards", involving building and infrastructural works, for their full cycle of life, which would be acceptable for all the people involved in the building process, from the owners until the customers;

B) To develop models and tools to the dynamic/evolutionary monitoring of the performances of structures under wind action, integrated in an especially built procedure;

C) To pick up, to record, to refine, to spread and to promote the specific knowledge as it could be received and adopted by the building industry.

A further transversal work is intended to be done, looking for a stricter integration of the national research project with the European one, in the circle of 6 PQ of RST, area 3.3 (New production processes and devices).

The actual project, in fact, is a component of a bigger and all-embracing European project (PERBRISK, proposed and coordinated by CERTH from Thessalonica, GR), in which each of the workgroups (under the guide of the same Institution coordinating the present proposal), is involved specifically in the analysis of the influence of naturals hazards on the performance indicators of some classes of structures, for their entire cycle of life.

The contribution of this Research Program of National Interest (Italian) to the requirements of the European Project Work Package 5a is focused on the following points:

- Innovation of processes and methods;
- Integration of design and demolition/removal phases in the life cycle of the structure;
- Developing/Promotion of new materials and/or innovative procedures to reduce vulnerability;
- Updating of building methods/processes;
- Probabilistic approach to the performance evaluation methodology (expected performances);
- Reduction of construction costs and/or reduction of the ratio costs/benefits;
- Increase of sustainability in the building process and in the quality of living;
- Increase of transport safety.

Even if, formally, it is not possible to joint Research Units out of the University, (Companies, Research Corporations, Insurances, Consulting Companies, Professional Institutions), this project works for positioning itself in the innovative way of strong interaction with building industry and other research institutions (out of the Academy). In cooperation with some of them, several points have been have been identified and analyzed as CASE STUDIES. In particular, with reference to such case studies, the analysis of performance indexes for the full cycle of life (including design and demolition/removal phases), considered crucial for the final objectives, was considered.

Main topics, corresponding, roughly speaking, to the operative research units, are identified as follows: definition of the risk to natural hazards and to the "expected performance" during the full cycle of life; tools and experimental techniques for wind tunnel, cable systems (power lines), bridges and large infrastructures like "life-lines"; towers, pylons and line-like structures; control and damping of vibrations, building and industrial implants, (as, for example, offshore structures and cooling towers); light-weight roofs, mixed deformable structures; telecommunication systems (spars, guyed mast); comfort in urban sites.

The performances for the full cycle of life, the innovation and the updating of design criteria could be referred to a certain number of "key parameters", which would be considered, in each case, amongst safety, resistance, ductility, lightness, durability, sustainability, innovation (of materials and structures), possibility of removal, renewability, quality of life.

In order to define such "key parameters", the Project has taken charge of the following tasks:

- Analysis of extreme events or events which are strongly penalizing the performance of the systems;
- Definition of analysis processes and achievement of the performances;
- Analysis of the key performance factors, by means of the evaluation of the "key indicators";
- Develop of prediction models for the performances;
- Application of the models to the case studies for the determination of the "expected performance"
- Analysis of costs and benefits, each of them corresponding either to a single part or to a full work phase within each Operative Unit, with the goal, in any case, to analyze the already recalled case studies.

1.2 OUTCOMES

In closing this research, the coordinator wishes to emphasize that once again the group of research units have worked with much synergy, passion and competence. The research units have put human resources and own equipments in order to fulfil the proposed aims. As already mentioned before, the wind engineering laboratory of CRIACIV in Prato has been again the binding element from the experimental point of view (an aspect of absolute importance in research activities such as this one). An example of that is the support to the experimental activity of the Units of Perugia (on cable systems), of Chieti-Pescara (on multi-box bridge decks), of Reggio Calabria and Trieste (on vortex-shedding from cylindrical bodies).

In the detail, the activities carried out may be summarised out of the 9 research Units as in the following.

1.2.1 Research Unit of Rome “La Sapienza”

Although the Performance-Based Design (PBD) has developed above all in the field of seismic engineering, it can be extended also to other fields of engineering, among which wind engineering. The research Unit of Roma “La Sapienza” has developed a first attempt to such extension, a particular category of structures has been considered for sake of simplicity, i.e. high buildings.

Suitable target performances has been identified and categorized in two groups:

- Low performance levels:
  1. The probability to exceed the limit state of structural collapse of the building is less than PF1 for a given value of the average return period
  2. The probability to exceed a given level of damage of the facade of the building is less than PF2 for a given value of the average return period
- High performance levels:
  1. The probability that the occupants of the last level of the building feel seek due to the wind induced oscillations is less than PF3 for a given value of the average return period
  2. The probability that discomfort conditions for the pedestrians take place in the surrounding zone of the building, due to wind flow around the building itself, is less than PF4 for a given value of the average return period

According to the selected performance objectives, it is possible to define suitable damage measures (DM) and suitable parameters of structural response (EDP). The damage measure may be based on the evaluation of the repairs required to restore the undamaged state and represented through the fragility curves. It remains opened the problem to develop fragility curves to wind for specific classes of buildings. In this research several methodologies have been proposed.

1.2.2 Research Unit of Florence at CRIACIV

The research Unit of Florence (at CRIACIV, i.e. the coordinating Unit) has investigated the risk connected to aeroelastic instability of structures, with regard to the evaluation of the vulnerability in serviceability condition and to the collapse limit state. In particular, experimental campaigns and numerical studies have been carried out on the phenomena of the vortex-synchronization and flutter.

A) Analysis of the vibration level induced by vortex-shedding. The aeroelastic model of a chimney has been studied experimentally varying the intensity of turbulence of the incoming flow and the mechanical characteristics of the physical model. The results led to the definition of numerical models for the evaluation of the response in synchronization regime and for the fatigue risk assessment. The model has been tested on 27 real chimneys, using the actual distribution of probability of the wind in the location of the chimneys under investigation.

B) Aeroelastic analysis of bridge decks. The research unit has proposed a probabilistic approach to flutter allowing of the definition of the critical wind velocity in a statistical way. Moreover, the possibility of simplifying the approach to the problem has been considered, by reducing the number of the aeroelastic derivatives of interest. This method may be very useful during the preliminary design phase of a bridge. The model has been validated thanks to several data in the literature and also performing experimental tests on a bridge-deck model with trapezoidal cross-section with lateral cantilevers. Moreover, the possibility of using the indicial functions to evaluate the bridge performances has been considered. This part of the research also included the simulation of structural nonlinearities and the evaluation of the effectiveness of different structural schemes. Finally, the research unit has studied the behaviour of a real footbridge in Ruffolo (Siena) under wind excitation.

1.2.3 Research Unit of Chieti/Pescara

Aeolian risk in bridges was the mainly focused and investigated by the Unit at Univ. of Chieti “G. D’Annunzio”, Pescara campus). During the first year, an experimental campaign to measure real wind has been carried out. The objective was to obtain information on the actual characteristic of the turbulence in urban and extra-urban areas. Large area has been put under investigation, considering distances up to several hundred meters. This way, it has been tried to fill a gap in the scientific literature, and the measures may be useful for bridges of different length. As far as the recurrent eolian actions, the research included structural monitoring. In particular, techniques and algorithms for the structural identification has been developed, based on ambient vibration (wind, traffic), without the need of measuring them directly (unknown input).

During the second year of research the aerodynamic and aeroelastic behaviour of multi-box bridge decks has been investigated, from the whole-structure performance point of view. In particular, it has been lead a parametric study on the aeroelastic response of multi-box deck bridges varying the distance between the boxes. The experience acquired by the local coordinator of the unit during the studies for the design of Messina Strait Crossing has been useful in this part of the project. Those studies aimed to the best performances in that specific situation (3300 m main span and the exceptional deck width of 60 m with 10 lanes, two maintenance lanes and two rail tracks). In that situation it was immediately clear that the standard suspension scheme did not require fur-

ther modification (with the shape of the main cable produced by their self-weight and by the weight of the deck transmitted by the hangers). Therefore, the study of the aerodynamics (although complex) was sufficient to guarantee optimal performances in terms of aeroelastic stability and of vortex-induced vibrations. To date, it is necessary to extend the study for the Messina Bridge to different span lengths and different suspension schemes.

The research aimed to investigate the relationship between the required performances of such a bridge in terms of suspension system, traffic volume and span length. The research theme is the opportunity of accept bridge decks with lower aerodynamic characteristics in the cases in which these might be less expensive (as it happens in case of shorter spans). Different structural solutions (such as crossed hangers) may be used to the purpose of obtaining greater torsional stiffness, in such a way as to achieve the same acceptable performances in terms of aeroelastic stability ("flutter"), vortex shedding, etc.

In this project theoretical and numerical analyses and wind tunnel experimental tests has been carried out. Even if one gives only a comparative value to the results obtained so far, they already appear as very encouraging. It is highlighted in fact the possibility of building decks for very long span bridges which are stable even considering a separation between the boxes of the deck which is much smaller of the one that has been considered so far. This reduction of the deck width would result in a remarkable reduction of the building costs.

1.2.4 Research Unit of Perugia

Dynamic behaviour of cables under wind action may be origin of several discomfort, fatigue and other sources of risk; the Unit at Univ. of Perugia has focused its attention on it. This has been done through experimental tests in the wind tunnel (in cooperation with the research Unit at CRIACIV). A specific model has been built and tested under laminar and turbulent flow. At the same time, a numerical model has been developed and the numerical and experimental results have been compared. The numerical model may be used to perform the stochastic characterization of the response by varying the geometrical and mechanical parameters of the cable and of the wind turbulence. A specific experimental campaign for the evaluation of wind action (drag, lift, and moment) on real-scale part of structural system for mobile phone communication has been also carried out, varying the configuration of antennas and parabolic dishes as well as wind direction and velocity. Moreover, in order to improve the performances of such systems, a new typology of cable-stayed antenna has been developed. This is characterized by a specific lattice connection between the body and the stays, which has a positive effect on the moments on the body and increases the elastic stability threshold.

Methods for the estimation of the expected maxima of wind action (applied to low buildings) have been analyzed, together with a mixed model for the correct modelling of pressure field. Finally, a multi-objective optimization procedure has been developed for the dynamic of the considered structural typologies.

Following goals have been fulfilled:

- identification of the parameters required for the description of the structural behaviour of telecommunication towers (considering the single structural elements and the overall system);
- characterization of the force acting on these structures through wind tunnel experimental tests;
- estimation of the maxima starting from finite length time histories;
- identification of the parameters for the evaluation of the expected performances and of the serviceability;
- criteria of optimization of structural systems with following increase of the ratio benefits/costs.

1.2.5 Research Unit of Venice

The research Unit at Univ. IUAV in Venice has developed its work according to the phases summarized in the following.

1. and 2.: analysis of events that penalizes the performance of the structure and definition of the processes of analysis and of performance determination. Load models have been developed through the combination of wind tunnel experimental tests and numerical simulations. Moreover, structural models for the study of the overall mechanical response and for the determination of the expected performance, accounting for the fluid-structure interaction (according to the structural typology: rigid or aeroelastic structures) have been also developed. Simplified analyses based on the proper orthogonal decomposition (POD) of signals have been validated, leading to the synthesis of possible application in the field of structural design;
3.: analysis of performance factors through the calculation of the 'key-indicators'. As far as the light roofs, a synthesis of performance factors have been sketched up through the identification of 'key-indicators', their quantification and the creation of relevance tables between the value of the indicator and the performance level;
4.: development of performance prediction models. The design methodology developed for the large roofs considers the realization of a system 'open' to retrofit solution in case the monitoring of the structures would highlight the necessity of that. This has been applied to the new Braga Stadium;
5.: development and promotion of new materials and of devices for vulnerability reduction: cables equipped with viscous damping systems in their final part near the connections with the deck have been studied. The results show that these systems are more efficient than those with localized damping in the mitigation of vibrations for the modes higher than those for which the system has been optimized;
6.: application to study cases for the evaluation of the expected performance. The above exposed techniques have found an interesting application again in the Braga Stadium (Portugal), which has been analyzed both with simplified analysis tools and with numerical models coupling fluid and structures and including geometrical nonlinearities. These simulations have highlighted that the development of specific numerical models allows a better characterization of the structural response of complex systems like the case studied.

1.2.6 Research Unit of Trieste

According to the initial plan, investigations on risk due to vortex shedding of chimneys and slender structures was carried out by the research Unit at Univ. Trieste, which has reported of following main outcomes:

a) Experimental campaign of aeroelastic model in the wind tunnel.
b) Further development of the experimental campaign on aeroelastic model in the wind tunnel of the CRIACIV, in cooperation with the Firenze-CRIACIV research unit.
c) Real-scale experimental campaign. An experimental campaign has been carried out on the chimney of the new incinerator in Trieste. Displacement and acceleration time-histories at the chimney top have been measured through satellite positioning techniques, together with the wind direction and velocity.
d) Numerical and analytical modelling of the load due to vortex shedding. Simplified laws have been found in lock-in regime, relating the amplitude of the oscillations to the magnitude of the load, its frequency and phase with respect to the oscillation of the structure.
e) In a first phase an iterative analytical procedure has been developed. In a second phase, a numerical model has been derived, based on the same simplified empirical laws.

f) The analyses on the behaviour of suspension bridges in serviceability condition have been further developed in cooperation with the research unit of Chieti-Pescara, with particular regard to vortex induced vibrations.

1.2.7 Research Unit of Reggio Calabria

The problem of comfort analysis under wind action in urban environment has been faced through the analysis of results available in the literature and through experimental tests. The research Unit at Univ. Mediterranea of Reggio Calabria, in particular, analysed the literature reports on experimental and numerical results of the characteristics of the eolian circulation at low heights in the urban environment. These studies were aimed to define the way how polluting substances are diffusing within cities and urban areas. Although the results are very limited in number, they provide useful qualitative and quantitative information on the parameters of the eolian circulation in street canyons. Consequently, the available data have been integrated with those obtained from experimental tests in CRIACIV boundary layer wind tunnel, where the components of wind velocity have been measured on a model of urban area with simple regular geometry. The measurements led to the definition of average velocity profiles, of turbulence indexes and turbulence scales, of Reynolds stresses, of probability density functions and spectra of turbulent components, and of the peak factors. The set of results available has been used for the definition of criteria for the estimate of the characteristics of eolian flow in urban environment.

A second research topic was dealt with by the same Unit, which concerns with the discomfort induced by structural vibrations. Here the literature information has been analyzed, developed and organized. As regard to the particular case of vibrations in pedestrian bridges, an experimental program on pedestrians crossing very flexible footbridges has been started. The first results are already available and have been used to define design criteria for flexible structures.

1.2.8 Research Unit of Naples “Federico II”

The research activities of the Unit at Univ. of Naples "Federico II" have concerned with mainly two topics: the definition of life-long design strategies of control devices (A) and the development of micro-macro behaviour models of the devices (B).

With regard to the topic A, the response to eolian a seismic actions of footbridges and buildings, where passive and semi-active control systems have been installed, has been studied. The results obtained demonstrate that the usage of such devices not only avoid the structural collapse under exceptional events in an economically convenient way, but also completely avoid structural damage with great benefits in terms of the overall durability of the building. The activities consisted in the development and optimization of dynamic control systems included the definition of suitable design methodologies for footbridges and buildings. Studies have been carried out also on the applicability of passive isolation systems and devices for the reduction of the vibrations induced by trains. For the latter aspect, simplified analytical models have also been developed.

As for the topic B, phenomenological models of the control devices have been developed. The validity of such models has been demonstrated in the prediction of the dynamic response of different structures under several vibration inputs. In particular semi-active devices based on magneto-reologic fluid have been considered. For these devices, detailed experimental tests have been performed, aiming to the evaluation of the delays induced by the control electronics and by the mechanic response.

A further result that may be considered a product of the research due to the synergic work of the research units of the PERBACCO project (CRIACIV and Napoli units above all) has been the presentation of a proposal of European project by the CRIACIV, answering to the "Collective Re-

search" notification of the VI Program (published in December 2004) and called MOISER (Market Oriented Innovative SEismic Rehabilitation).

1.2.9 Research Unit of Florence

The research activity at Univ. of Florence, Dept. of Civil Engineering (Firenze-DIC) has almost entirely followed what has been originally planned, i.e. 1. “Global wind actions on structures”, 2. “Local actions on building claddings and surfaces” and 3. “Assessment of eolian vulnerability and risk”

Within topic 1. and 2., Modelling and simulation of non-Gaussian pressure field on the surface of largely extended structures (like an isolated cooling tower) has been performed through a transfer function applied to a Gaussian field for which expressions of the mean and spectral structure have been given. Reconstruction of non-Gaussian pressure field have been measured on wind tunnel models. Some new large roofs of sport plants/arenas have been analyzed in close cooperation with the Unit at CRIACIV, namely: the Olympic soccer stadium in Pyraeus, the new roof of Delle Alpi stadium in Turin, and the new roof of the small Manfredonia stadium.

The research Unit has developed a numerical procedure for the reconstruction, through radial basis neural networks, of non-Gaussian pressure fields based on wind tunnel measures. Simulation of non-Gaussian pressure time-histories through non-linear auto-regressive models has been carried out, developing a non-linear auto-regressive model based on radial basis neural networks. The generation of a scalar progress has been implemented.

As for topic 3., the possibility of reducing the computational cost for the non-linear analysis of the behaviour of cracked reinforced concrete or masonry structures through principal coordinate decomposition of the motion has been studied. Reliable results have been obtained on cooling towers but the methodology does not apply in a satisfactory way to different structures (such as masonry chimneys).

1.3 SOME PRELIMANARY CONCLUSIONS

The previous (allow me to use the expression “impressive”) overview, shows very clearly the outstanding vitality of the research group and its capability to work with a very high synergy effect. Although this might be a natural, long lasting phenomenon due to the many previous projects that the group has performed in previous years, the research outcomes may be considered unique in the entire national scientific scenery.

For sure, the group working in PERBACCO has represented the most accredited and entitled research pole in Wind Engineering in Italy, for a long period, thanks to a successful and efficient cooperation strategy which has become, nowadays, well consolidated.

The Author of this Introductory Chapter, being at the same time the national Scientific the Coordinator of the project, gives the chance to acknowledge sincerely everybody’s contribution to the project in the past 2 years. It would be too long here to mention and thank all the participants (Ph.D students, technicians and administrative staff, research engineers and associates, Professors) who have contributed actively, at different levels.

Only a great “Thank you!” I cannot omit here and this goes to the four Editors of this volume, Prof. Gianni Bartoli (Florence), Prof. Francesco Ricciardelli (Reggio Calabria), Prof. Anna Saetta (Venice) and Prof. Vincenzo Sepe (Chieti/Pescara), and to Dr. Chiara Bullo, of Firenze University Press, for their heavy work and supportive commitment.

1.4 RESEARCH UNITS

Unit #1 **Dipartimento di Ingegneria Strutturale e Geotecnica** – Università degli Studi di Roma "La Sapienza"		
Research Theme:	**General approach to risk evaluation for combined natural hazards and to design criteria aimed at optimal lifelong performances**	
Coordinator:	Giuliano AUGUSTI	Full Professor
Components:	Carlo PAULOTTO	PhD
	Paolo Maria MARIANO	PhD

Unit #2 **CRIACIV** (Centro di Ricerca Interuniversitario di Aerodinamica delle Costruzioni ed Ingegneria del Vento) – Università degli Studi di Firenze		
Research Theme:	**Risk levels definition and performance analysis**	
Coordinator:	Claudio BORRI	Full Professor
Components:	Gianni BARTOLI	Associate Professor
	Serena CARTEI	Secretary
	Carlotta COSTA	PhD student
	Claudio MANNINI	PhD student
	Stefano PASTÒ	PhD student
	Lorenzo PROCINO	Technician

Unit #3 **PRICOS** (Dipartimento di Progettazione Riabilitazione e Controllo delle Strutture Architettoniche) – Università degli Studi "G. D'Annunzio" di Chieti-Pescara		
Research Theme:	**Performance, service conditions and durability of bridges, life-lines and other large infrastructures subject to wind and to other natural loads**	
Coordinator:	Piero D'ASDIA	Full Professor
Components:	Cristina BRUSAPORCI	PhD
	Pasqualino CARUSI	PhD
	Mariella DIAFERIO	Assistant Professor
	Sofia FEBO	PhD student
	Massimiliano ORONZO	Technician
	Marcello PETRANGELI	Consulting Engineer
	Marco PETRANGELI	Associate Professor
	Vincenzo SEPE	Associate Professor
	Massimo TARQUINI GUETTI	Consulting Engineer
	Alberto VISKOVIC	Assistant Professor

Unit #4		
Dipartimento di Ingegneria Civile ed Ambientale – Università degli Studi di Perugia		
Research Theme:	**Expected performance and new design criteria for structural systems used to support communication devices affected by wind loads**	
Coordinator:	Vittorio GUSELLA	Full Professor
Components:	Marco BRECCOLOTTI	PhD student
	Federico CLUNI	PhD student
	Massimilano GIOFFRÈ	Assistant Professor
	Ilaria VENANZI	PhD student

Unit #5		
Dipartimento di Costruzione dell'Architettura – Università IUAV di Venezia		
Research Theme:	**Performance analysis and design criteria for flexible structures under eolian and other natural actions: lightweight roof and suspension systems**	
Coordinator:	Massimo MAJOWIECKI	Associate Professor
Components:	Nicola COSENTINO	PhD
	Massimiliano LAZZARI	PhD
	Emilio MEROI	Associate Professor
	Anna SAETTA	Associate Professor

Unit #6		
Dipartimento di Ingegneria Civile – Università degli Studi di Trieste		
Research Theme:	**Theoretical and experimental studies supporting design of slender structures under wind loads. Design criteria for towers, chimneys and masts**	
Coordinator:	Salvatore NOÈ	Associate Professor
Components:	Claudio AMADIO	Associate Professor
	Luca CARACOGLIA	Consulting Engineer
	Isaia CLEMENTE	PhD
	Boris SOSIC	Technician
	Tatiana SLUGA	PhD
	Gian Andrea RASSATI	Consulting Engineer
	Franco TREVISAN	Technician

Unit #7		
Dipartimento di Meccanica e Materiali – Università degli Studi "Mediterranea" di Reggio Calabria		
Research Theme:	**Wind and vibration induced discomfort on humans and human activities**	
Coordinator:	Francesco RICCIARDELLI	Associate Professor
Components:	Enrico T. DE GRENET	PhD student
	David A. PIZZIMENTI	PhD student
	Santo POLIMENO	Consulting Engineer
	Raffaele PUCINOTTI	Assistant Professor
	Alfonso SANTOSUOSSO	Associate Professor (Univ. of Napoli)

Unit #8		
DAPS (Dipartimento di Analisi e Progettazione Strutturale) – Università degli Studi "Federico II" di Napoli		
Research Theme:	**Innovative devices for life-long vulnerability reduction and performance improvement in constructions**	
Coordinator:	Giorgio SERINO	Full Professor
Components:	Maria Gabriella CASTELLANO	Consulting Engineer
	Paolo CLEMENTE	Consulting Engineer
	Mauro FONTANA	Consulting Engineer
	Mariela LUEGE	Consulting Engineer
	Antonio OCCHIUZZI	Associate Professor
	Concetta ONORII	PhD student
	Antonio ORLANDO	Consulting Engineer
	Emanuele RENZI	Consulting Engineer
	Maria Cristina SPIZZUOCO	PhD
	Simone ZANNELLI	Consulting Engineer

Unit #9		
DIC (Dipartimento di Ingegneria Civile) – Università degli Studi di Firenze		
Research Theme:	**Design criteria for buildings and industrial plants against wind loads and other natural hazards**	
Coordinator:	Paolo SPINELLI	Full Professor
Components:	Alberto ANTONELLI	PhD
	Michele BETTI	PhD
	Paolo BIAGINI	PhD student
	Luca FACCHINI	Associate Professor
	Maurizio ORLANDO	Associate Professor
	Enrico SIBILIO	PhD student

2 First steps towards Performance-Based Wind Engineering[1]

Giuliano Augusti *and* ***Marcello Ciampoli***
Università di Roma "La Sapienza"

2.1 INTRODUCTION

In the last few decades an intense research effort has been devoted to the risks on constructions and infrastructures deriving from natural and man-made hazards with regard to both the design of new artefacts and the restoration and recovery of existing ones, and the consequent problems of design under uncertainties. Several significant hazards should be considered: wind storms, snowfalls, rainfalls, floods, landslides, earthquakes and – recently – terrorist attacks. The lower intensities of these events may be of frequent occurrence and, whilst not causing structural damage, result nevertheless in a degradation of the life-time performance.

Recently, attention has been paid to reconsidering this knowledge in the framework of Performance-Based Design (PBD). Rather than being an alternative to prescription-base codes, PBD is in reality an approach that does not exclude prescriptions, but is aimed directly at the achievement of well specified performance objectives and/or their optimization. (It can be noted that until very recently the code provisions adopted to achieve performance objectives have largely been developed on an empirical basis.)

PBD has been developed mainly in the USA with reference to seismic risk and design [a]: in the "PERBACCO" project an attempt to extend it to Wind Engineering has been made, as described in this Chapter.

For the sake of simplicity, this initial attempt is limited to a particular class of buildings, namely tall buildings and is based on the PEER equation [a], [b]:

$$p(\mathrm{DV}) = \iiint p(\mathrm{DV} \mid \mathrm{DM}) \cdot \left| dp(\mathrm{DM} \mid \mathrm{EDP}) \right| \cdot \left| dp(\mathrm{EDP} \mid \mathrm{IM}) \right| \cdot dp(\mathrm{IM}) \tag{2.1}$$

where:

[1] This Chapter is based on the paper by Carlo Paulotto, M.Ciampoli and G.Augusti: *Some proposals for a first step towards a Performance Based Wind Engineering* presented at the IFED - International Forum in Engineering Decision Making; First Forum, Stoos (CH), December 2004.

- IM (Intensity Measure) denotes a measure of the magnitude of the action;
- EDP (Engineering Demand Parameter) denotes a parameter which is able to describe the structural response;
- DM denotes a damage measure;
- DV denotes a decision variable, i.e. a parameter that governs the design decision;
- p(…) = [1 − P(…)] denotes a probability of exceedance, where in turn P is the cumulative distribution function of (…);
- p(… | …) denotes a conditional probability of exceedance.

In order to apply PBD, the first step to be undertaken is the definition of the performances.
A possible choice is the following:

- Low performance levels (related to structural safety)

1. With reference to the considered building, the probability of failure for the collapse limit state is lower than a P_{F1} value, in a fixed time period.
2. With reference to the envelope of the considered building, the probability of failure for the damage limit state is lower than a P_{F2} value, in a fixed time period.

- High performance levels (related to serviceability or comfort)

1. With reference to the considered building, the probability of failure for the serviceability limit state is lower than a P_{F3} value, in a fixed time period.
2. With the reference to the area around the considered building, the probability of failure for the pedestrian comfort limit state is lower than a P_{F4} value, in a fixed time period.

On the basis of the definition of the performances, appropriate Damage Measures (DMs) and Engineering Demand Parameters (EDPs) should be chosen.

In this first attempt to extend the PBD to Wind Engineering, attention has been focused on the terms of Eq. (1) related to the vulnerability analysis (i.e. dp(DM | EDP) and dp(EDP | IM)). Structural vulnerability are usually expressed by means of fragility curves, that correlate directly DM and IM. Even if the fragility curves formulated in this way are not consistent with the formulation of PBD as defined by Eq. (1), they can be applied if it is assumed that DM coincides with EDP.

In the following Sections, some considerations are developed about low and high performance levels. Concerning high performance levels, a method is proposed in order to develop fragility curves considering the wind-induced oscillations of tall buildings.

2.2 FRAGILITY CURVES

The term “fragility” means the probability of attaining a specific damage state, conditioned on the value of the demand. There are two types of fragility curves: system fragility and component fragility curves. System fragility curves refer to the damage of the entire structure, while component fragility curves are related to a specific component of the structure. The fragility of the entire structure can be obtained by assembling the component fragilities according to some functional logic. Fragility functions can be developed using different methods, that is, heuristic, empirical, analytical or a combination of them.

In the field of Wind Engineering, if D_i and ν denote respectively a generic damage state and the wind speed, fragility curves can be derived by evaluating the function $p(D_i | \nu)$, that represents the probability that the structure will experience a damage state not smaller than D_i when the wind

velocity is ν.

2.2.1 Fragility curves for low performance levels

In case of permanent damage (i.e. low performance levels), DM is generally defined for a generic damaged object on the basis of the repairs that it needs to be restored to the undamaged state, that is in term of repair/replacement costs. In this way, only losses stemmed from property damage are taken into account, overlooking direct and indirect business interruption losses, which pertain to decreases in production, sales or profits. It should be stressed that business interruption losses can dramatically exceed property damage, as reported in [c] for floods and earthquakes.

According to this definition for DM, some sort of "vulnerability curves" (e.g., plots of mean values of losses as a function of the action intensity) can be elaborated on the basis of data collected by the assurance and reassurance companies. This operation is not easy to perform because these data are not always available and directly usable: in fact they are available only for those regions where the penetration of assurance is very strong, and they are often given in an aggregate form (e.g. losses are referred to different types of buildings). Then, before constructing this vulnerability curve for a specific class of building it is often necessary to disaggregate the losses as suggested in [d] (see Fig.2.1).

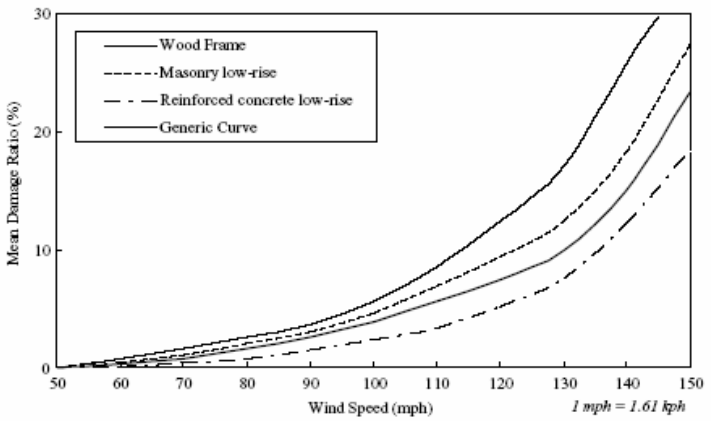

Figure 2.1 Hurricane vulnerability curves for commercial building classes in Puerto Rico [d].
The Mean Damage Ratio at wind speed ν is defined as:

$$\sum_i^n L_i \Big/ \sum_i^n V_i$$

where L_i is the cost to repair the damage, or the loss, to building location i, V_i is the total value of buildings at that location and n is the total number of locations experiencing wind speed ν (ν is 3-s peak gust at 10 m height). The Generic Curve refers to Puerto Rico commercial portfolio.

It has to be noted that the evaluation of losses based on such vulnerability curves is not consistent with decision making: in fact financial appraisal would be mixed up with cost benefit analysis. Furthermore vulnerability curves like those reported in Fig. 2.1 are not suitable for the implementation of PBD according to Eq. (2.1). For each value of the wind speed they give only the mean value of damage; they do not furnish the probability that a specific damage state will occur. Then these vulnerability curves have to be transformed into fragility curves.

Moreover, these fragility curves have to be given not in the usual form losses vs. wind speed

(e.g. DM vs. IM) but as DM vs. EDP. Now a question arises concerning what EDP should be used. On the basis of the results obtained in the field of Performance Based Earthquake Engineering, the displacement of the top of the building should be used for low performance levels: however, in the framework of Wind Engineering, peak pressure value on the building envelope could be better correlated with damage than the displacement of the top of the building.

2.2.2 Fragility curves for high performance levels

High performance levels are closely related to the notion of comfort, that is to human behaviour. First of all it is necessary to define the terms "unacceptable discomfort". As reported in [e], the notion of unacceptable discomfort may be defined in the following way. In any given design situation various degrees of wind-induced discomfort may be expected to occur with certain frequencies that depend upon the degrees of discomfort, the features of the design and the wind climate at the location in question. The discomfort is unacceptable if any of these frequencies is judged to be too high. Statements specifying maximum acceptable mean frequencies of occurrence for various degree of discomfort are known as "discomfort criteria".

Discomfort problems due to wind and concerning tall buildings are generally related to building oscillations and high wind speed at pedestrian level. Fragility curves for discomfort problems can not be evaluated on the basis of the repair/replacement costs. In fact in this case losses do not emanate from property damage. Instead of economic stock measures , flow measures have to be used in order to take into account this type of losses. [f].

According to the flow measures, the value of an asset is defined as the discounted flow of net future returns from its operation. For ordinary property damage, the stock and flow measures represent the same thing and including both in losses estimation would involve double counting. But, for example, if a machine with a useful life of several years is considered to be out of service for few weeks, repair cost and the value of lost production are not likely to be equal. The lost production represents the flow measure of losses.

2.2.2.1 Discomfort problems in tall buildings due to wind induced oscillations

Studies of human response to wind-induced vibrations are based on: i) experimental tests conducted by the aerospace industry; ii) observations about the behaviour of persons placed in motion simulators; observations about the behaviour of the occupants of tall buildings during storms.

In the first case the results relative to frequencies lower than 1 Hz, that are typical for oscillations of tall steel buildings, are extrapolated from the results relative to the frequency range 1 Hz – 35 Hz (proper for the aerospace industry scopes).

In the second case the human behaviour is tested for periodic motions with different frequencies. It was found that the perception thresholds decrease as the frequencies increase. For example, as reported in [g] and [h] and quoted in [e], average perception thresholds were found to vary from about 6 milli-g for frequencies of 0.1Hz to about 3 milli-g for frequencies of 0.25 Hz. The subjects were annoyed while working at their desks if the acceleration exceeds 12 milli-g. The motions were described as extremely annoying or intolerable beyond accelerations of the order of 50 milli-g to 60 milli-g. Since the motion of the structure is a narrowband random excitation inducing bi-axial and torsional response, the use of uni-axial sinusoidal motion is questionable (across-wind response, being vortex-shedding driven, is to some extent similar to the sinusoidal waveform; otherwise the along-wind motion is more random in nature as a result of buffeting). In addition, the absence of visual and audio cues in the test environment neglect critical stimuli.

In the third case the human behaviour is related with the rms value of the top floor

accelerations during the storm. In a study conducted on two tall buildings and presented in [i] and [j] (quoted in [e]), it was found that about 35% and 45% of the persons on the higher floor experienced motion sickness symptoms during the storm respectively for a value of 2 milli-g and 5 milli-g of the rms value of the accelerations of the top floor. Comfort criteria based on rms accelerations, as opposed to peak acceleration, offer a more accurate means of combining response in different directions based on their respective correlations [k]. In the peak acceleration criterion, the first peaks, in each direction, are determined and subsequently combined by an empirical combination rule; however, since different response component may have a different probability structure, requiring different peak factors, care must be exercised.

In a very interesting work, Burton et al. [l] examined the biodynamic human body vibration response occurring during low-frequency (from 0.15 Hz to 1.00 Hz) constant amplitude acceleration. A frequency dependence of this biodynamic response was found, revealing an increasingly magnified acceleration of the head as the acceleration increased. Through the knowledge that the vestibular system is the primary indicator of motion perception, the frequency dependence of the head acceleration can be directly translated into a frequency dependence of motion perception. It can be concluded that with decreasing frequency of oscillation there is an increase in perception threshold, and vice versa. Therefore the assessment of occupant comfort criteria should include frequency dependency of motion.

Further investigations have revealed that the jerkiness of the structural response may primarily be responsible for perception of motion. Quite simply, while humans are capable of adjusting to accelerations, any change in the acceleration will require additional adjustments for equilibrium. As a result, basing perception criteria on a measure of jerk, or the rate of change of acceleration, may better capture the stimulus defining perception thresholds under random motion.

On the basis of these and other studies a series of comfort criteria were proposed. North American practice, for example, uses 10-15 milli-g peak horizontal acceleration at top floor for residential buildings and 20-25 milli-g for office buildings, based upon a 10 year return period; on the contrary the International Standards Organization (ISO) suggests a curve in terms of rms value of the acceleration on the top floor that should not be exceeded more than once in five years on average [m]. According with the last criterion, for example, a rms value of the acceleration equal to 5 milli-g is acceptable for a building with a first period equal to 5 s. This implies that this acceleration will be perceived, but if it only occur once every five years, the functioning and commercial viability of the building will not be adversely affected.

In the Authors opinion should be more rational, especially in the case of office buildings, to agree on a specific discomfort related fragility curve with the occupants and/or owners of a tall building. In this case only one damage state exists: some occupants of the top floors have to leave their workplace or are not able to work because of the building oscillations. Business interruption losses stem from this behaviour.

It can be reasonably assumed that people are not able to work at their desks if the peak acceleration of the building top floor exceeds a value in the range 4-10 milli-g. Taking into account that this value depends on the oscillation frequency in the way that if the frequency decreases the critical peak acceleration increases, a simple triangular probability density function (pdf) can be adopted to represent this phenomenon (see Fig.2.3). The position of the maximum of the pdf depends on the period of the structure and it can be immediately determined. In fact the bounds of the peak acceleration interval 4-10 milli-g can be reasonably related respectively to the frequency 1 Hz and 0.1 Hz, and a linear relation can be assumed between peak acceleration and frequency in logarithmic coordinates. A fragility curve can be obtained from the correspondent cdf (see Fig. 2.3). It is worth noting that this fragility curve is given as DM vs. EDP and then is

suitable for the implementation of PBD according to Eq. (2.1).

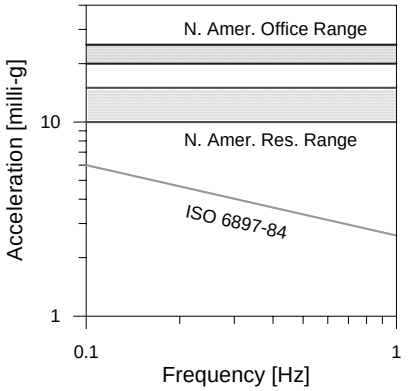

Figure 2.2 Some examples of perception criteria: range of 10 years peak acceleration values at the top floor relative to the North American practice respectively for office building (blue) and residential building (red); 5 years rms values of acceleration suggested by ISO 6897-84 [m]. Note that the last criterion takes into account the oscillation frequency.

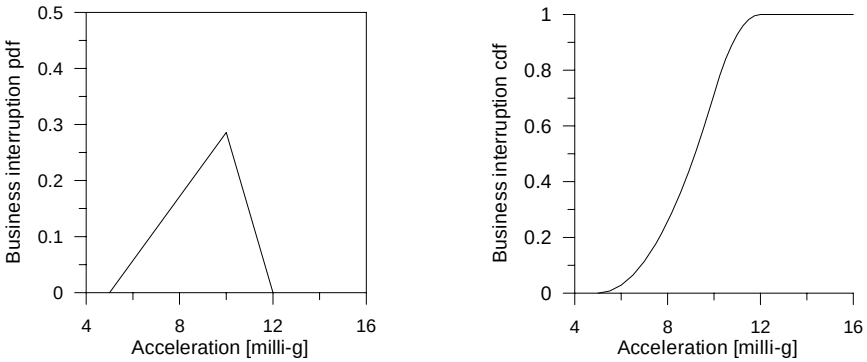

Figure 2.3 A triangular pdf can be adopted to represent the probability of occurrence of business interruption as a function of the peak acceleration of the top floor of a tall building. A fragility curve can be directly derived from the correspondent cdf.

2.3 CONCLUSIONS

In this paper a first attempt to extend PBD to Wind Engineering is presented. First of all, with reference to tall buildings, low and high performance levels are defined. Then the paper focuses on the aspects of PBD related to vulnerability analysis. Concerning the low performance levels, the features of the building vulnerability curves, that were found in the Wind Engineering devoted literature and that are not consistent with the PBD philosophy, are pointed out: i) these curves are not probabilistic; ii) they are generally given as losses vs wind speed (e.g. DM vs. IM) instead of DM vs. EDP; iii) they are not consistent with decision making. Concerning high performance levels a method is presented to obtain fragility curves related to business interruption losses due to wind induced oscillations.

2.4 BASIC REFERENCES

[a] Giovenale P. 2002. *Valutazione del rischio sismico di strutture: caratterizzazione dell'azione e tecniche di analisi*. PhD Thesis, Department of Structural and Geotechnical Engineer, University of Rome "La Sapienza".

[b] Moehle J., Deierlen G.G. 2004. A framework methodology for Performance-Based Earthquake Engineering. *Proc. of International Workshop on Performance-Based Design*, June 28 – July 2 , Bled, Slovenia.

[c] Tierney K. 1997. Impacts of recent disasters on business: the 1993 Midwest floods and 1994 Northridge earthquakes. In *Economic consequences of earthquakes: preparing for the unexpected*, B. Jones (Ed.), MCEER, Buffalo, NY.

[d] Khanduri A.C., Morrow G.C. 2003. Vulnerability of buildings to windstorms and insurance loss estimation. *Journal of Wind Engineering and Industrial Aerodynamics*, Vol. 91, pp. 455-467.

[e] Simiu E., Scanlan R.H. 1996. *Wind effects on structures*. John Wiley & Sons, New York.

[f] Rose A., Lim D. 2002. Business interruption losses from natural hazards: conceptual and methodological issues in the case of the Northridge earthquake. *Enviromental Hazards*, Vol. 4, pp. 1-14.

[g] Yamada M., Goto T. 1975. *Criteria for motions in tall buildings*. College of Engineering, Hosei University, Koganei, Tokyo, Japan.

[h] Goto T. 1981. Human perception and tolerance of motion. *Monograph of Council on Tall Buildings and Urban Habitat*, Vol. PC, 817-859.

[i] Hansen R.J., Reed J.W., Vanmarcke E.H. 1973. Human response to wind-induced motion. *J. Struct. Div.*, ASCE, 98, No. ST7, pp. 1589-1605.

[j] Reed J.W. 1971. *Wind-induced motion and human discomfort in tall buildings*. Research Report No. R71-42, Department of Civil Engineering, MIT, Cambridge, Mass.

[k] Kareem A. 1992. Serviceability issues and motion control of tall buildings. *Proceedings of Structures Congress*, San Antonio.

[l] Burton M., Denoon R.O., Roberts R.D., Kwok K.C.S., Hitchcock P.A. 2003. A Motion Simulator to Investigate Effects of Wind-Induced Building Motion. *Proceedings of the 11th International Conference of Wind Engineering*, Lubbock, Texas.

[m] ISO 1984. *Guidelines for the evaluation of response of occupants of fixed structures, especially buildings and off-shore structures to low-frequency horizontal motion (0.063 to 1 Hz)*. ISO6897-1984(E), International Organization for Standardization, Geneva.

2.5 LIST OF PUBLICATIONS

[1] Paulotto C., Ciampoli M., Augusti G. 2004. Some proposals for a first step towards a Performance Based Wind Engineering. *IFED-International Forum in Engineering Decision Making; First Forum*, Stoos, December 2004; www.ifed.ethz.ch.

3 Bridges

Vincenzo Sepe
University "G. D'Annunzio" of Chieti-Pescara

3.1 INTRODUCTION

Researchers of the "Perbacco" project have been dealing with the structural behaviour of bridges subject to wind loads for several years. The past research, funded by the Italian Ministry for University and Research and by the European Commission, has dealt both with long span and with pedestrian bridges, and has included theoretical, numerical and experimental analyses; the main results are reported in [l], for this and for other subject studied by the national research group coordinated by the CRIACIV Unit.

During this two-years research project, the attention has mainly been devoted, as concerns bridges, to long span bridges and to techniques to evaluate their behaviour from a numerical and experimental point of view. The following sections of this chapter summarise the main results, details being reported in the quoted published papers.

3.2 DEVELOPMENTS IN THE MODELISATION OF FLUID-STRUCTURES INTERACTIONS FOR LONG SPAN BRIDGES : INDICIAL FUNCTIONS FOR SELF-EXCITED AND BUFFETING FORCES

Among the topics faced during the research program of the CRIACIV Unit, load models in time-domain for the aeroelastic analysis of bridges have been analyzed.

In particular, the indicial approach for self-excited forces has been discussed, that is an alternative in the pure time-domain to the aeroelastic derivatives [b]. The history of motion is expressed as a series of infinitesimal step-wise increments; indicial functions describe the non-stationary evolution in time of loads due to translational velocities and rotation. In particular, $\Phi_{Rr}(t-\tau)$ is the normalized load component $R = F_x, F_z, M_y$ at time t due to a unit velocity (or rotation) $r = \dot{x}, \dot{z}, \alpha_y$ that occurred at time τ. The wind loads are then given by the convolution integrals of the indicial functions with the motion history:

$$
\begin{aligned}
F_x^{ai} &= q_0 B \int_{-\infty}^{t} \left[k_{F_x\dot{x}} \Phi_{F_x\dot{x}}(t-\tau) \frac{\ddot{x}(\tau)}{U} + k_{F_x\dot{z}} \Phi_{F_x\dot{z}}(t-\tau) \frac{\ddot{z}(\tau)}{U} + k_{F_x\alpha} \Phi_{F_x\alpha}(t-\tau) \dot{\alpha}(\tau) \right] d\tau \\
F_z^{ai} &= q_0 B \left[k_{Z\dot{x}} \int_{-\infty}^{t} \Phi_{Z\dot{x}}(t-\tau) \frac{\ddot{x}(\tau)}{U} d\tau + k_{Z\dot{z}} \int_{-\infty}^{t} \Phi_{Z\dot{z}}(t-\tau) \frac{\ddot{z}(\tau)}{U} d\tau + k_{Z\alpha} \int_{-\infty}^{t} \Phi_{Z\alpha}(t-\tau) \dot{\alpha}(\tau) d\tau \right] \\
M_y^{ai} &= q_0 B^2 \left[k_{M\dot{x}} \int_{-\infty}^{t} \Phi_{M\dot{x}}(t-\tau) \frac{\ddot{x}(\tau)}{U} d\tau + k_{M\dot{z}} \int_{-\infty}^{t} \Phi_{M\dot{z}}(t-\tau) \frac{\ddot{z}(\tau)}{U} d\tau + k_{M\alpha} \int_{-\infty}^{t} \Phi_{M\alpha}(t-\tau) \dot{\alpha}(\tau) d\tau \right]
\end{aligned}
\tag{3.1}
$$

where k_{Rr} are constant coefficients depending on the aerodynamic coefficients and their derivatives.

Experimental procedures to identify indicial functions have been achieved only recently [k] and are not yet so well established as those to obtain aeroelastic derivatives. Alternatively, it is possible to provide a parametric analytical expression of indicial functions through exponential filters [f]:

$$
\Phi_{Rr}(s) = 1 - \sum_{h=1}^{N_{Rr}} a_h^{Rr} e^{-b_h^{Rr} s} \tag{3.2}
$$

where $s = 2Ut/B$ is a non-dimensional time, a_h^{Rr} and b_h^{Rr} are non-dimensional coefficients and N_{Rr} is the number of terms chosen to express the indicial function.

Introducing harmonic motions in the expression of self-excited forces through aeroelastic derivatives and indicial functions, it is possible to express both models in the frequency domain. If exponential filters in Eq. (3.2) are substituted in Eq. (3.1), the convolution integrals can be solved analytically. Thus, the two load models can be compared, and a relationship between indicial function coefficients and aeroelastic derivatives can be obtained. Subsequently, indicial functions coefficients can be identified by means of a non-linear least-square optimization procedure on aeroelastic derivatives (that are measured at discrete values of reduced frequency). Details on the identification procedure are given in [m].

During this research project, sets of indicial coefficients have been obtained for streamlined and bluff sections; rectangular sections have been especially addressed, allowing a parametric discussion for several dimensional ratios. The feasibility of the selected approach has been demonstrated, at least in the case of cross-sectional analyses, by the identification of critical flutter condition, pre-critical and post-critical behavior. Comparisons amongst wind tunnel tests, numerical and analytical procedures have been carried out; as an example of the analyses performed, a comparison between numerical and experimental results obtained in the CRIACIV boundary layer wind tunnel are shown (in Figure 3.1).

No direct comparison, involving time-domain simulations of cross-sectional response and experimental tests, was found in literature, neither analyses on the effect of different group of coefficients on the dynamic behavior of the section. During the research project, however, it has been shown that, in the case of streamlined section, aeroelastic behavior can be represented with sufficiently good approximation with only one exponential group, while more ’bluff’ geometries require an augmented number of states [2]. In the ’bluff’ case, in fact, a limited number of indicial coefficients does not represent in an adequate manner the unsteady contribution of self-excited forces. With an adequate number of coefficients, however, coupled and torsional flutter conditions are well captured by the adopted load model.

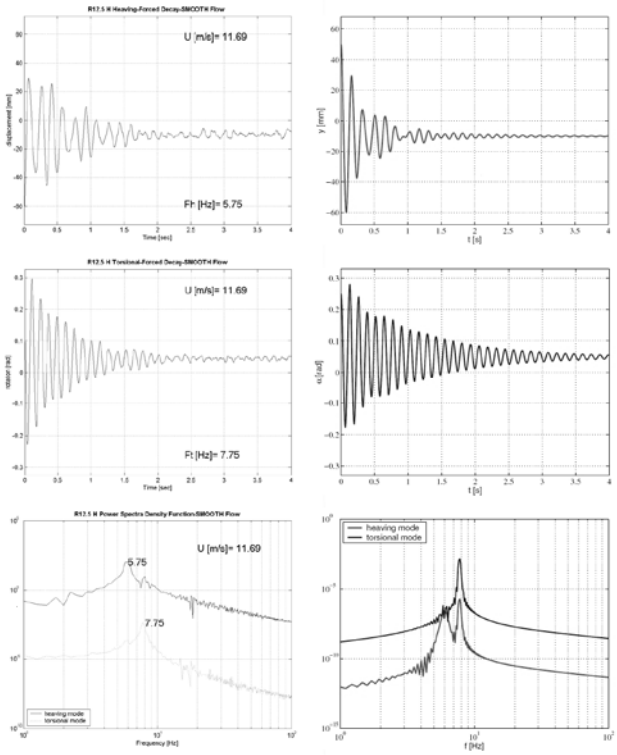

Figure 3.1 Experimental test (left) vs. numerical simulation (right) - U = 11.69 m/s

The possibility of utilizing an indicial approach for modeling buffeting forces has also been investigated. In fact, buffeting forces on bridge decks are commonly modeled by Sears' function [12]. However, it is known that Sears' function is reliable only for very streamlined bridge deck sections and that a complete load model for wind action should require a suitable formulation of buffeting forces in time domain. Analytical and experimental studies (e.g. [i][j]) suggest a way to treat the problem of admittance functions for bridges; functions based on experimental data like flutter derivatives [2] can be used in the definition of buffeting loads, and they are preferable to the common employed Sears' function. Following this suggestion, a complete time-domain model for cross-sections including vertical turbulence has been arranged [13]. Equal indicial functions are applied for definition of self-excited and buffeting loads. Corresponding aerodynamic admittance functions have been numerically evaluated and compared with experimental and analytical results.

Rectangular sections have been taken into account, their characteristic dimensions being the width *B* and the thickness *D*. Results for lift and moment admittance functions are shown in Figure 3.2. It results that admittance functions obtained from indicial functions well approximate the experimentally obtained admittance functions. In particular, the estimate of admittance functions having the structure of Sears-like functions can be compared with experimental results provided by [d] (Figure 3.3); qualitative agreement is observed for sections with different dimensional ratios. By this approach, the possibility of the use of parameters typical of self-excited forces to model turbulent action with an acceptable error is proved and a complete model of wind loads by means of indicial functions can be presented.

In this model, the point of view remains strictly two-dimensional and drag forces and longitudinal turbulence components are neglected; however, any span-wise coherence effect can be accounted for.

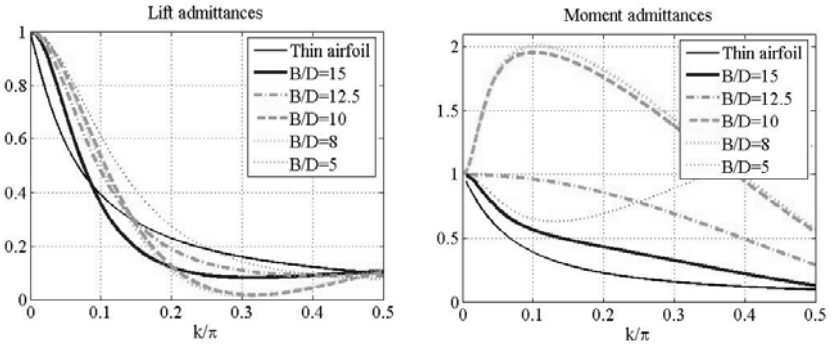

Figure 3.2 Lift and moment admittance functions for rectangular sections

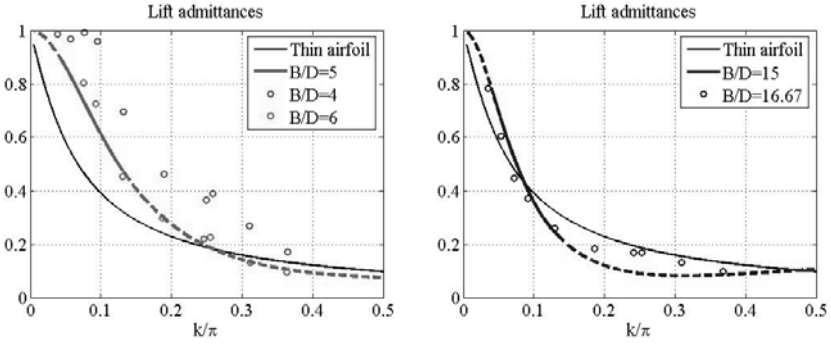

Figure 3.3 Comparison of lift admittance function calculated by means of indicial functions for a rectangular section with B/D= 5 and B/D=15 with Sears' function and experimental results [d]

Although some attempts have been made to directly measure indicial functions in experimental tests [k], and Computational Fluid Dynamics seems to offer a promising tool [p], the most feasible procedure consists to date in choosing a parametric analytical expression of indicial functions and in identifying the parameters from quantities measured in the wind tunnel. Exponential filters [f] are considered. Several nonlinear optimization algorithms have been studied and a reliable procedure based on a combination of bounded trust-region algorithm and Gauss-Newton algorithm has been developed for the identification of indicial function coefficients [d]. An example of identification for lift derivatives is reported in Figure 3.4.

The effects of experimental data scattering on the definition of critical flutter conditions have also been investigated. In particular, classical flutter analysis is compared with the relatively young indicial function approach. As the identification of indicial functions play a crucial role in the numerical simulations, the performance of automatically identified functions have been tested via a Monte-Carlo procedure [5]. Three main results are obtained:

1) The critical wind speed and the critical frequency based on the non-scattered data almost coincide with the mean values of the distribution obtained.

2) The variances obtained with indicial functions are much lower than those obtained through aeroelastic derivatives. The indicial functions, in fact, take into account all the reduced frequencies and, therefore, some scattering can be compensated.
3) The distribution of critical condition obtained through indicial functions are narrow-banded, in spite of the broad boundaries of the indicial functions that produced them.

At least for the considered streamlined section and with respect of the critical condition, a great reliability of the indicial function model is therefore proved.

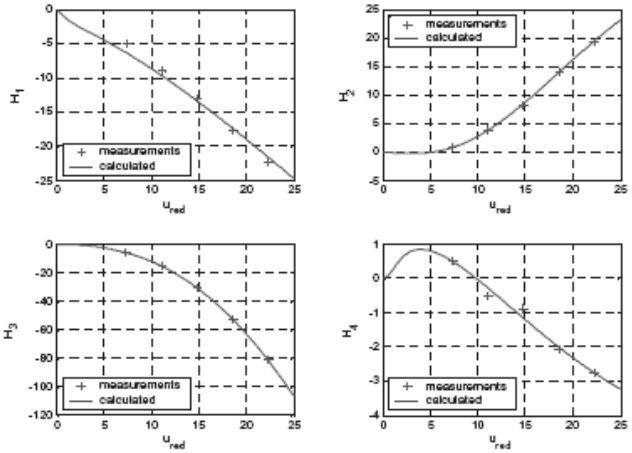

Figure 3.4 Identification of lift indicial function from aeroelastic derivatives for a rectangular cross-section with with/high ratio B/D=5.

3.3 FINITE ELEMENTS ANALYSIS FOR THE RESPONSE AND THE OPTIMISATION OF LARGE SPAN BRIDGES WITH RESPECT TO THE AEROELASTIC INSTABILITY

3.3.1 Numerical models

Numerical simulations have also been performed in the CRIACIV Unit to study several aspects related to suspension bridge performances. Several different structural models have been used, from very simple ones to verify theoretical considerations to full bridge finite element models. An ad hoc finite element program for the analysis of bridges under wind action has been developed [1]. This includes a pre-processor for the parametric generation of the bridge FE model, a multi-correlated wind velocity field generator based on auto-regressive filters, an FE solver for non-linear dynamic problems, several analysis types specific for bridge aerodynamic and aeroelasticity in time- and frequency-domain, the implementation of steady and unsteady history dependent load models, and a post-processor.

Full 3D models have been used in [7] with two different goals:

(i) evaluate the influence of the mean static deformed configuration on the stability threshold;
(ii) evaluate the effects of load nonlinearities on structural response.

For these purposes, the quasi-steady load model has been employed, as aerodynamic data dependent on the angle of attack are easily available whereas aeroelastic derivatives are seldom measured with dependence on the angle of attack.

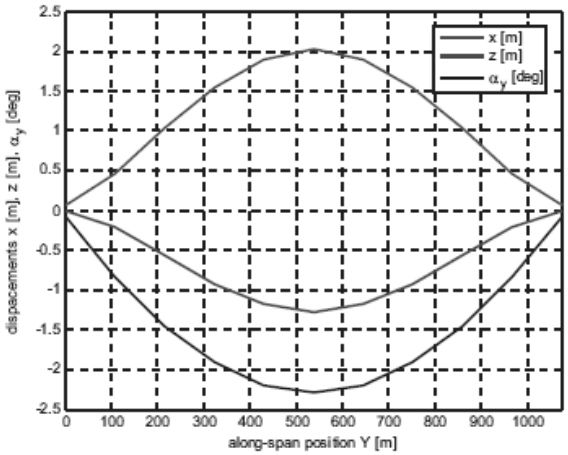

Figure 3.5 Static displacements at critical wind velocity of a sample bridge**.**

As regard to the first investigated topic, a specific numerical procedure for aerodynamic stability evaluation has been developed. The results shows that the mean deformations (Figure 3.5) induces changes in the mean angle of attack and in the structural modes, which in turn result in different mean wind velocities. In a sample bridge, neglecting the mean deformations results in a critical wind velocity of 26.4m/s, whereas if the deformations are taken into account both for the structural modes and for the aerodynamics the critical wind velocity for flutter stability is of 22.8m/s. That means that the calculation neglecting the deformations might induce errors not on the safety side. On the other hand, the critical mode shape (Figure 3.6) is only slightly influenced by the change of configuration (at least in the considered examples).

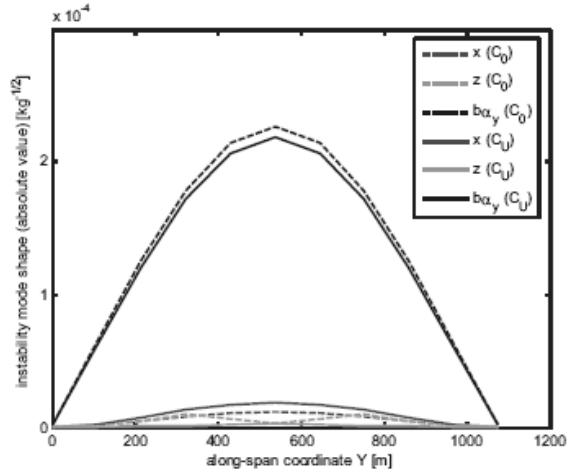

Figure 3.6 Instability mode shape (absolute value) evaluated with the aerodynamic and modes in reference configuration (dashed lines) and in the mean configuration evaluated through static analysis (full lines).

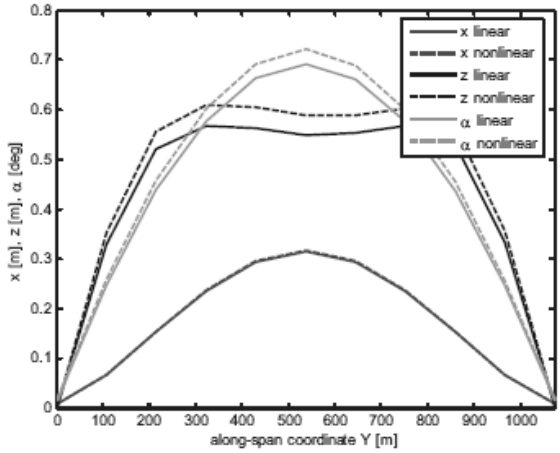

Figure 3.7 RMS of sample bridge response to turbulent wind: linearized (full lines) vs nonlinear (dashed lines) quasi-steady models.

As regard to the second investigated topic, it turned out that nonlinearities may result in larger buffeting response as visualized in Figure 3.7.

A non-linear simplified (2-cross-section) model of suspension bridge has also been consider (Figure 3.8). It allows to investigate the secondary instability modes as described in [1] and to take into account the effects of structural nonlinearities and of along-span wind correlation in buffeting simulations (including unsteady self-excited forces).

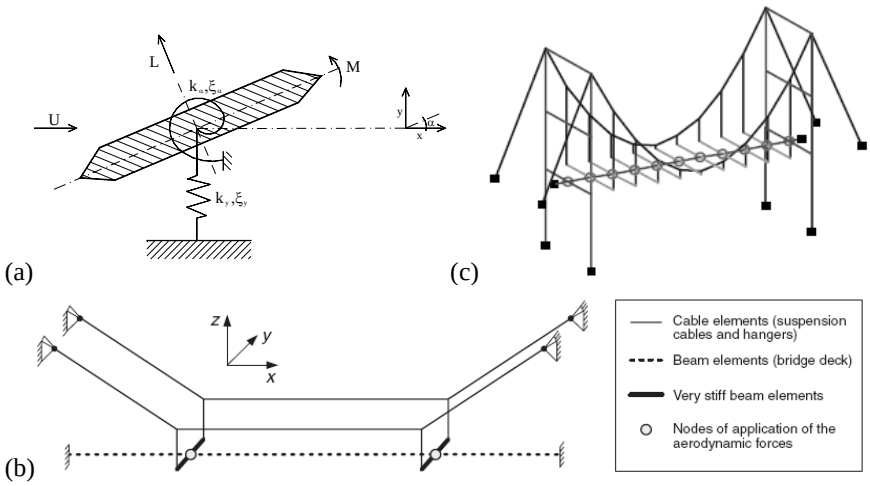

Figure 3.8 (a): cross-sectional model with 2DoFs; (b): simplified model with two cross-section; (c): 3D full bridge model.

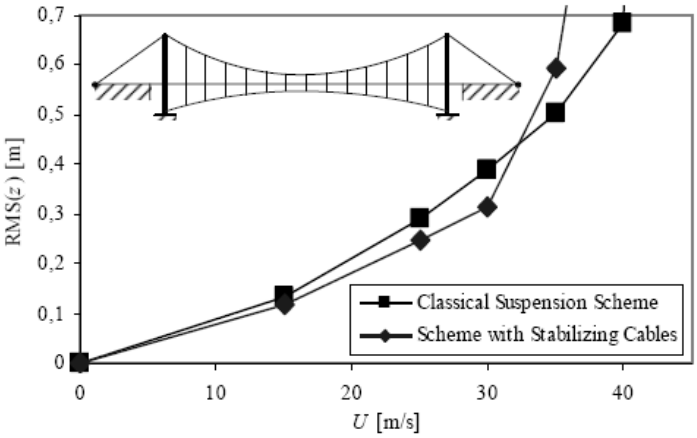

Figure 3.9 Vertical response at mid-span of a sample suspension bridge under buffeting excitation (including unsteady self-excited forces): evaluation of the effects of secondary cables with opposed curvature.

Some first evaluation of aeolian risk mitigation strategies have also been proposed in [6] where the effect of secondary cables with opposed curvature has been evaluated (Figure 3.9). A comparison of the behaviour against the wind action of two structural schemes is presented. A 'classical' suspension scheme and two 'Musmeci'-type solutions are accounted for, with stabilizing cables of different materials. Computer simulation techniques are used to generate wind forces on the bridge, including both buffeting and self-excited forces. Attention is focused on dynamic analyses, to evidence advantages and disadvantages of both schemes. In particular, it is shown that the 'Musmeci' solutions present advantages in terms of serviceability conditions, under the action of turbulent flow. A strong dependence of critical flutter velocity on additional cable and deck mass and stiffness is, on the other hand, observed. Different combinations of geometries, mass and pre-stress can give rise to a wide scenario in terms of critical flutter velocity, being very important the modal shapes and frequency obtained. The double-curvature solution appears to be very interesting and further analyses are in progress. In particular, a even better efficiency is expected for non-planar cable systems.

3.3.2 Aeroelastic analysis in time domain

The study of dynamic response of bridges to wind action can be described in the time or frequency domain. The contribution of the IUAV Unit of Venice [3][4][10][11] has dealt with two basic formulations for time domain analysis: a "*quasi-steady"* formulation (*QS*) and a formulation derived from the "*extension of aeroelastic derivatives to the time domain*" (*DA*). Writing the aeroelastic force equations with the two different approaches involves different simplification hypotheses:

- the "*quasi-steady"* formulation can include non-linearity of wind angle of incidence (actual wind angle of incidence on bridge deck) and geometrical non-linearity of the entire structure alike neglecting system frequency dependence;
- the formulation based on the "*extension of aeroelastic derivatives to the time domain*" considers aeroelastic force frequency dependence but the final equation comes from superimposition of linear impulse function.

Both formulae have been applied for studying "*stress ribbon*" pedestrian bridge [4][8][10], like the Sacramento footbridge designed by Jiri Strasky & Co. (Figure 3.10), which can be considered aerodynamically similar to a thin airfoil immersed in a fluid. In this hypothesis the aeroelastic derivatives are shown in Figure 3.11.

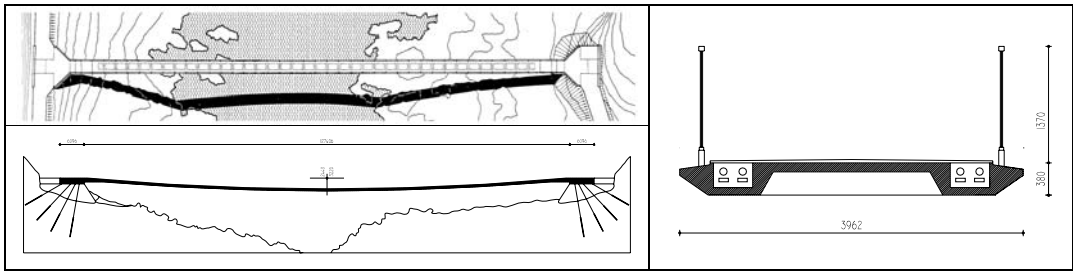

Figure 3.10 "Stress ribbon" pedestrian bridge over the Sacramento river: plan (a) and longitudinal section (b) and cross section

In particular for both the formulations, QS and DA, two different analyses have been carried out: the frequency analysis and a direct time integration analysis.

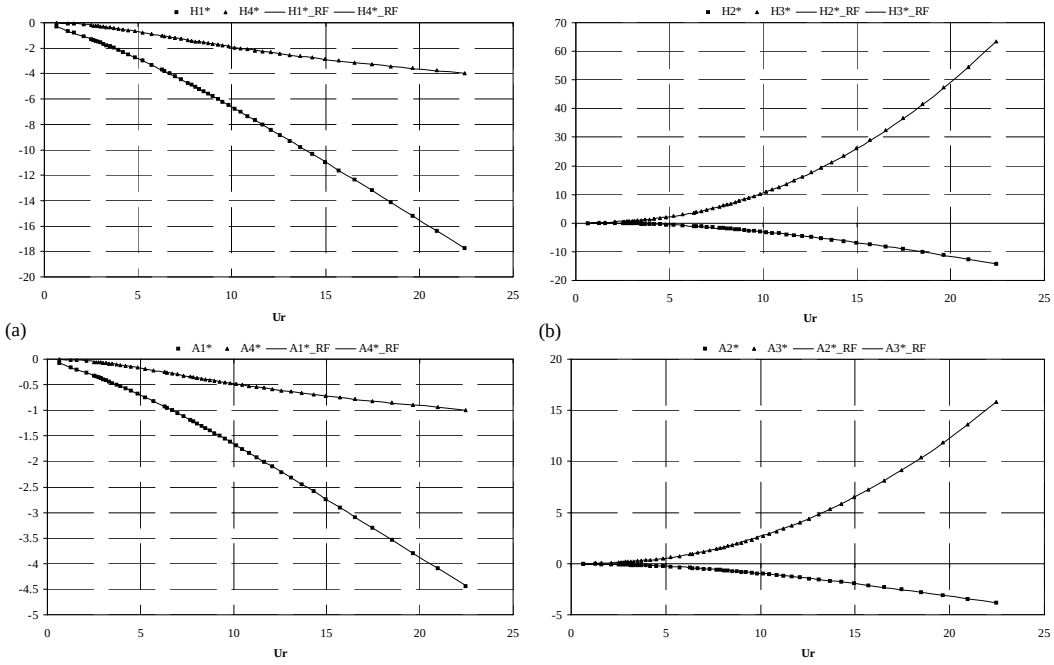

Figure 3.11 Flutter derivatives ($H_1^*, H_4^*, A_1^*, A_4^*$ (a) and $H_2^*, H_3^*, A_2^*, A_3^*$ (b)) and rational function approximation ($H_{1\_RF}^*, H_{4\_RF}^*, A_{1\_RF}^*, A_{4\_RF}^*$ (a) and $H_{2\_RF}^*, H_{3\_RF}^*, A_{2\_RF}^*, A_{3\_RF}^*$) for the thin airfoil.

Quasi Steady Formulation (*QS*)

As described in more detail in the quoted papers, taking the reference axis to be that identified by wind-structure relative velocity U_r, (Figure 3.12a) the equations for forces for parallel or orthogonal wind (Lift, Drag e Moment) can be written:

$$F_L = \frac{1}{2}\rho U_r^2 B C_L(\alpha_e)\ ;\ F_D = \frac{1}{2}\rho U_r^2 B C_D(\alpha_e)\ ;\ M = \frac{1}{2}\rho U_r^2 B^2 C_M(\alpha_e) \tag{3.3}$$

where ρ is the air density, B the deck width, C_L, C_D and C_M are the aerodynamic coefficients for lift (L), drag (D) and torsion (M), function of actual angle of incidence α_e, and U_r is the relative velocity

Figure 3.12b shows the flexural and torsional frequencies changes of the system as a function of the incident wind speed: if the wind velocity increases the torsional frequency decreases until it coincides with flexural frequency. The frequency change is a consequence of aeroelastic forces definition: no contribution is introduced directly into the flexural component, whose frequency thus does not change. The diagram of Figure 3.12b indicates that for the example under consideration the critical flutter velocity is about 82 m/s (intersection point of the two curves), for which the two movements are perfectly coupled and the system can lead to structural aeroelastic instability: the torsional frequency of the system is equal to the flexural frequency ($n_{F,1}$ = 0.346 Hz and $\omega_{F,1}$ = 2.17 rad/sec).

Time domain studies confirm the results obtained from frequency analysis, as specified at the diagram of Figure 3.13a, since aeroelastic analysis corresponds to the study of system free motion. The structural system is still damping at an incident velocity of 81 m/s (as shown in Figure 3.12b, while at the flutter velocity of 82 m/s there is a continuous increasing of displacement and rotation with equal frequency but out of phase, as shown in the displacement-rotation diagram of Figure 13b and in the time series shown in Figure 3.13a.

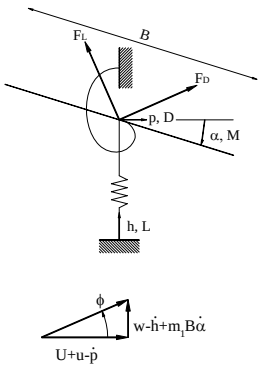

(a)

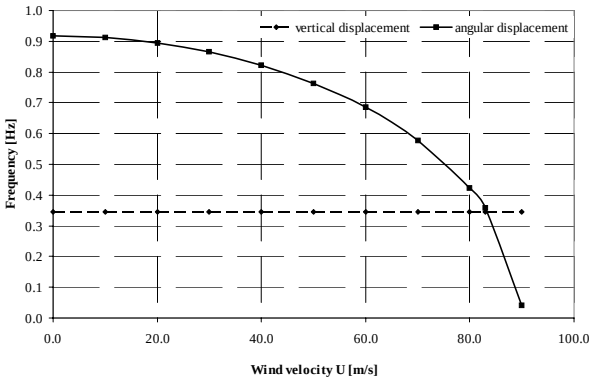

(b)

Figure 3.12 (a) two degrees of freedom model for quasi steady formulation and (b) frequency variation of the vertical and torsional displacement as a function of the reduced velocity - (QS formulation)

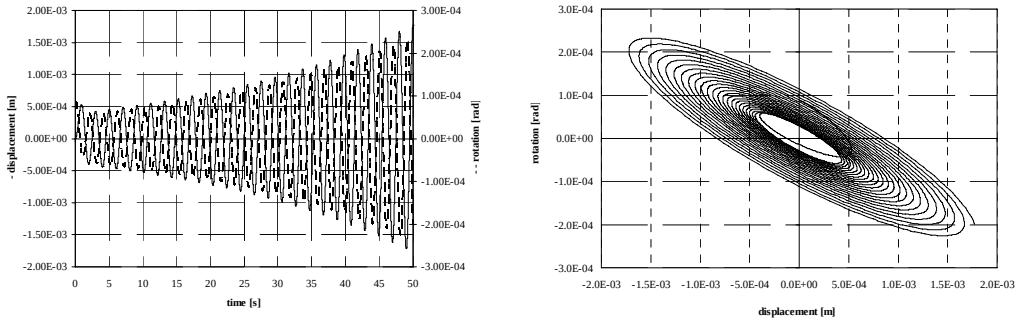

Figure 3.13 Structural response (a) time history of the vertical and torsional displacement and (b) diagram vertical – torsional displacement with wind velocity U = 82 m/s - (QS formulation)

Development of aeroelastic derivatives in the time domain (*DA* formulation)

Closed expression of aerodynamic coefficients for current bridge with "*bluff*" sections cannot be assessed starting from the theory of fluids and resort must be made to wind tunnel testing. Connection between forces, displacement and velocity terms is carried out by aeroelastic derivatives $H_i^*(K)$, $A_i^*(K)$ i=1,4 measured in a wind tunnel. According to the Scanlan theory [e], for harmonic frequency ω movement the forces can be described with the following equations:

$$L_{se}(t)=\frac{1}{2}\rho U^2 B\left(KH_1^*\frac{\dot{h}}{U}+KH_2^*\frac{B\dot{\alpha}}{U}+K^2H_3^*\alpha+K^2H_4^*\frac{h}{B}\right);\ M_{se}(t)=\frac{1}{2}\rho U^2 B^2\left(KA_1^*\frac{\dot{h}}{U}+KA_2^*\frac{B\dot{\alpha}}{U}+K^2A_3^*\alpha+K^2A_4^*\frac{h}{B}\right) \tag{3.4}$$

The *DA* formulation based on the "*extension of aeroelastic derivatives to the time domain*" considers aeroelastic force frequency dependence but the final equation comes from superimposition of linear impulse function.

Eq. (3.4) represent self-excited forces, that are expressed into the mixed frequency-time domain in terms of aeroelastic derivatives. Starting from the hypothesis that self-excited forces derives from superposed linear mechanisms, it can be used a model describing aeroelastic forces in terms of integral convolution between structural movement and impulsive forces (indicial functions, cf. Sec.3.2.1), e.g. [h]:

$$L_{se}(t)=\frac{1}{2}\rho U^2\int_{-\infty}^{t}\left(I_{L_{seh}}(t-\tau)h(\tau)+I_{L_{sep}}(t-\tau)p(\tau)+I_{L_{sea}}(t-\tau)\alpha(\tau)\right)d\tau \tag{3.5}$$

As described in [3][8][10][11], the development of the anti-transformed for return to the time domain requires using a continuous function of equation (3.5) and not discrete values, as obtained for instance in the wind tunnel. As a consequence, the commonest approximation form normally used in aerodynamics is "*approximation by rational functions*", e.g. [a][c]:

$$\overline{I}^*_{L_{seh}}(i\omega)=a_0+a_1\left(\frac{i\omega B}{U}\right)+a_2\left(\frac{i\omega B}{U}\right)^2+\sum_{g=3}^{m+2}\left(\frac{a_g 4\pi^2}{d_l^2U_r^2+4\pi^2}+i\frac{a_g 2\pi d_l U_r}{d_l^2U_r^2+4\pi^2}\right) \tag{3.6}$$

$$K^2H_4^*=a_0-\frac{4\pi^2}{U_r^2}a_2+\sum_{l=3}^{m+2}a_l\frac{4\pi^2}{d_l^2U_r^2+4\pi^2}\qquad K^2H_1^*=a_1\frac{2\pi}{U_r}+\sum_{l=3}^{m+2}a_l\frac{2\pi d_l U_r}{d_l^2U_r^2+4\pi^2} \tag{3.7}$$

Coefficients a_0, a_1, a_2, a_g, g=3,m+2 can be assessed with linear or non-linear approximation to minimum square method by using values obtained from aeroelastic derivatives wind tunnel testing. Return to the time domain is now possible with anti-transformation:

$$L_{seh}(t)=\frac{\rho U^2}{2}a_0 h(t)+a_1\frac{B}{U}\dot{h}(t)+a_2\left(\frac{B}{U}\right)^2\ddot{h}(t)+\sum_{g=3}^{m+2}\int_{-\infty}^{t}a_g e^{\left(-\frac{d_g U}{B}(t-\tau)\right)}\dot{h}(\tau)d\tau \qquad K^2H_i^*=a_1\frac{2\pi}{U_r}+\sum_{i=3}^{m+2}a_1\frac{2\pi d_i U_r}{d_i^2U_r^2+4\pi^2} \tag{3.8}$$

The last term of the Eq. 3.8 (i.e. the memory term) represents memory of the phenomenon and its assessment at instant t depends on the entire time history of $\dot{h}(\tau)$ (non-stationary status of the force).

Torsional and flexural frequency variations between the two force models (*QS* and *DA*) are comparable and correspond to substantially constant flexural frequency and to marked torsional frequency reduction. It is worth noting that this trend relates to the specific structure of the footbridge, but could change significantly in other studies. While *QS* formulation does not affect flexural rigidity, *DA* formulation includes this change, though it results negligible in some cases.

The results obtained by extending aeroelastic derivatives to the time domain in terms of flutter velocity are also in good agreement with the close formulation for flutter problem described, for example, in [11]. Further details can be found in [3][8][10].

3.3.3 Design alternatives and optimisation of long span bridges

In [9] the first results obtained by the research Unit of Chieti-Pescara have been presented of a research on very long span bridges, characterised by innovative decks with respect to truss decks or single-box decks so far built: in particular, the so-called multi-box steel decks, consisting of longitudinal boxes and transversal beams, the latter suspended through hangers to the main cables, and longitudinal space between boxes filled with grids that can also be used as safety lanes.

As far as the writer know, the only multi-box bridge that has really been designed in detail is the Bridge on the Messina Strait; the design of 1992 consists of three longitudinal boxes (two for motorway lanes and one for railway lane) and grids used for safety and service lanes.

The aerodynamic design of the deck played a crucial role [g], and the design was optimised for the 3300 meters span and for a deck about 60 meters large.

According to new design request, however, it has deemed interesting to compare the 1992 design with other alternatives, defined for a smaller number of lanes and therefore for narrower decks. In this case, it seems sensible to accept also some worse aerodynamic performance of the deck, provided that appropriate structural solutions (e.g. crossed hangers, “mono-dual cables”, stabilising cables, etc.) guarantee the respect of all ultimate and serviceability limit states, if this can turn in a significant reduction of the overall costs.

The research so far developed, whose results are reported in detail in [9], assumes different alternatives with respect to the 1992 deck, varying the distance between the longitudinal boxes; as a consequence of smaller deck loads and therefore of a lighter deck, the transversal beams and the main cables become lighter, and this allow a significant reduction in the cost of the bridge, as summarised in Table 1, where the weight reduction is evident.

All the analyses are based on the aerodynamic characterisation of such decks performed in the CRIACIV wind tunnel in Prato. Figure 3.14 shows the cross section of the 1992 deck of the Messina bridge, while Figure 3.15 shows the scheme for four different decks obtained by varying the space between longitudinal boxes.

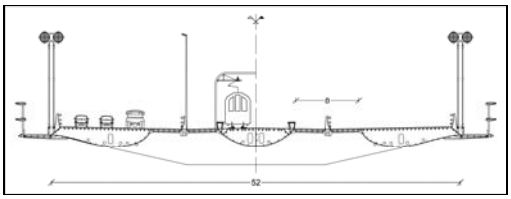

Figure 3.14 1992 design of the Messina Bridge deck

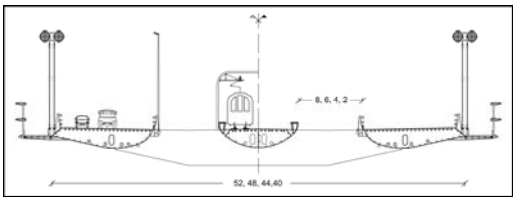

Figure 3.15 Modified decks

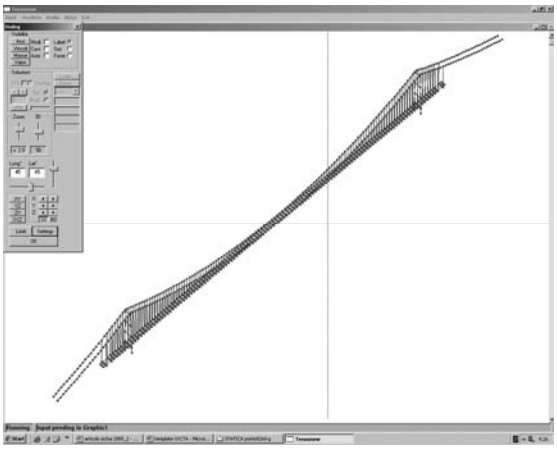

Figure 3.16 3D FEM model – software TENSO 8 (D'Asdia et al.)

The FEM code used for the numerical analyses is TENSO 8 (Figure 3.16), an *ad hoc* software for static and dynamic step by step analysis of nonlinear structures, implemented and continuously improved by the research group.

Weight	Messina '92	52 m	48 m	44 m	40 m
Deck [t/m]	18.8	15.6	14.8	14.3	14.1
Main cables [t/m]	29.9	24.7	23.8	23.2	23.1
Tower [t/m]	58.3	49.5	48.0	46.9	46.5
Steel weight reduction, %	--	17%	20%	22%	23%

Table 3.1 Weight of the steel structure

An analysis has also been performed on the aeroelastic stability of the 1992 design and of the modified bridges, using the aerodynamic characterisation obtained through tests in the CRIACIV wind tunnel. Details can be found in Chapter 8.

3.4 BASIC REFERENCE

[a] Fung Y. C. 1955. *An Introduction to the Theory of Aeroelasticity*, John Wiley & Sons, New York.

[b] Scanlan R. H., Béliveau J.-G. et al. 1974. Indicial aerodynamics functions for bridge decks. *Journal of Engineering Mechanics* **100**: 657-672.

[c] Roger K.L. 1977. Airplane math modeling methods for active control design: structural aspects of active control. *AGARD-CP- 8, Advisory Group for Aerospace Research and Development*, Neuilly-sur-Seine, France.

[d] Jancauskas E. D., Melbourne W. H. 1986. The aerodynamic admittance of two-dimensional rectangular section cylinders in smooth flow. *Journal of Wind Engineering and Industrial Aerodynamics* **23**: 395-408.

[e] Simiu E., Scanlan R. 1996. *Wind effects on Structures*. John Wiley & Sons, New York

[f] Höffer R. 1997. *Stationäre und instationäre Modelle zur Zeitbereichssimulation von Windkräften an linienförmigen Bauwerken*. Dept. Civil Eng. Bochum, TU-Bochum. Ph.D.

[g] D'Asdia P., Sepe V. 1998. Aeroelastic instability of long-span suspended bridges: a multi-mode approach. *Journal of Wind Engineering and Industrial Aerodynamics*, **1998** (74-76): 849-857.

[h] Ding Q., Lee P.K.K. 2000. Computer simulation of buffeting actions of suspension bridges under turbulent wind. *Journal of Computer and Structures*, **76**: 787-797.

[i] Scanlan R. H. 2001. Reexamination of sectional aerodynamic force functions for bridges. *Journal of Wind Engineering and Industrial Aerodynamics*, **89** (14-15): 1257-1266.

[j] Hatanaka A., Tanaka H. 2002. New estimation method of aerodynamic admittance function. *Journal of Wind Engineering and Industrial Aerodynamics*, **90**: 2073–2086.

[k] Caracoglia L., Jones N. P. 2003. A methodology for the experimental extraction of indicial functions for streamlined and bluff deck sections. *Journal of Wind Engineering and Industrial Aerodynamics*, **91**: 609-636.

[l] Bartoli G., Ricciardelli F., Sepe V. (edited by) 2004. *WINDERFUL – Wind and INfrastructures: Dominating Eolian Risk for Utilities and Lifelines*, ISBN 88-8453-137-3, Firenze University Press.

[m] Borri C., Salvatori L., Zahlten W. 2005. On the Identification of Indicial Functions from measured Aeroelastic Derivatives. *6th European Conference on Structural Dynamics EURODYN'05*, Paris, France, 4-7 September 2005.

3.5 LIST OF PUBLICATIONS

[1] Salvatori L., Spinelli P. 2004. Influence of structural non-linearities on the response of suspended bridges under wind excitation: numerical simulations on simplified structures. *8° convegno nazionale di ingegneria del vento, IN-VENTO-2004*, Reggio Calabria, 21-23 giugno 2004

[2] Zahlten W., Salvatori L. et al. 2004. On the identification of indicial functions from measured aeroelastic derivatives. *8° convegno nazionale di ingegneria del vento, IN-VENTO-2004*, Reggio Calabria, 21-23 giugno 2004

[3] Lazzari M., Saetta A., Vitaliani R., 2004. Aeroelastic forces and dynamic response of long-span bridges. *Int. Journal for Numerical Methods in Engineering*, **60**: 1011-1048.

[4] Lazzari M., Saetta A., Vitaliani R. 2004. Analisi aeroelastica di ponti nel tempo: i ponti a nastro teso, *8° convegno nazionale di ingegneria del vento, IN-VENTO-2004*, Reggio Calabria, 21-23 giugno 2004

[5] Borri C., Salvatori, L. et al. 2005. On the identification of indicial functions from measured aeroelastic derivatives. *6th European Conference on Structural Dynamics EURODYN'05*, Paris, France, 4-7 September 2005.

[6] Costa C., Salvatori L., et al. 2005. Re-thinking the classical scheme of very long suspension bridges under wind loading. *6th European Conference on Structural Dynamics EURODYN'05*, Paris, France, 4-7 September 2005.

[7] Salvatori, L., Spinelli P. 2005. Three-dimensional simulations of suspension bridges under wind load: influence of mean steady configuration and effects of load nonlinearities. *EACWE-4*, Prague.

[8] Gasparini A., Lazzari M., Vitaliani R., Saetta A. 2005. Large span footbridge performance: strengthening and retrofitting solutions, *CONMAT'05 3rd International Conference on Construction Materials: Performance, innovations and structural implications*, Vancouver, Canada, August 22-24, 2005

[9] D'Asdia P., Sepe V., Bartoli G., Febo S. 2005. Multi-box steel decks and suspension system for very long span bridges. *XX Conference C.T.A. "Advances in steel constructions"*, 26-28 September 2005, Ischia, Italy. (pp. 269-276).

[10] Lazzari M., Vitaliani R., Saetta A. 2005. Aeroelastic analysis in time domain: the stress-ribbon bridge, *6th European Conference on Structural Dynamics EURODYN'05*, Paris, France, 4-7 September 2005

[11] Lazzari M, 2005. Time domain modeling of aeroelastic bridge decks: a comparative study and an application. *Int. Journal for Numerical Methods in Engineering*. **62**(8): 1064-1104.

[12] Costa C. 2006. Aerodynamic admittance functions and buffeting forces for bridges via indicial functions. *J. Fluids Struct*. in print.

[13] Costa C., Borri C. 2006. Application of indicial functions in bridge deck aeroelasticity. *Journal of Wind Engineering and Industrial Aerodynamics*, accepted for publication.

WITH CONTRIBUTION FROM:

Gianni Bartoli, University of Florence
Carlotta Costa, University of Florence
Piero D'Asdia, University "G. D'Annunzio" of Chieti-Pescara
Sofia Febo, University "G. D'Annunzio" of Chieti-Pescara
Massimiliano Lazzari, University of Padova
Anna Saetta, University IUAV of Venezia
Luca Salvatori, University of Florence

4 Large span roofs

Massimo Majowiecki
University IUAV of Venezia

4.1 INTRODUCTION

Within the framework of wind engineering problems, it is widely established that to obtain realistic results from model tests, it is necessary to accurately model both the object being studied and the characteristics of the wind affecting it.

In particular every complete modelling of suspension systems as well as lightweight roof systems involves an accurate fluid/structure analysis. Both the modelling of wind flows over the structure and the mechanical model of the structure itself, within the framework of geometrically non linear field, must be introduced, by considering aeroelastic interaction. The pressure field, by considering the effect of vortex shedding, as well as the pressure coefficients have to be evaluated.

The drastic reduction in the ratio of permanent weight to variable load makes lightweight structures particularly sensitive to the effects of wind and snow. The dynamic nature of wind action can cause oscillations and deformations of such amplitude that they jeopardisethe function of the roof and, in the worst cases, its structural stability. On the other hand, the static effect of snow represents an extremely heavy load for this type of structure, even reaching as high as 70-80% of the total load. Melchers demonstrated that one of the primary causes of collapse (corresponding to approximately 45% of the cases analyzed) lies in an erroneous evaluation of the loading conditions and of the structural response. With improvements in the methods for in-depth analysis in the design of lightweight wide-span roofing, theoretical studies can and must be used in combination with experimental tests performed in wind tunnels and in situ. From the observation of structures that have completely or partially collapsed:

- due to snow, e.g. the Hartford Coliseum (1978), the Pontiac Stadium (1982), the Milan Sports Hall (1985) and the Montreal Olympic Stadium (1992);
- due to wind, e.g. the Montreal Olympic Stadium (1988);
- due to the effects of water, e.g. the Minnesota Metrodome (1983) inflatable roof

information has been collected and design specifications have been obtained for the verification of such structures in ultimate limit and serviceability states.

For flexible structures, and particularly for lightweight roofs, the wind action represents one of the main natural hazards. In this chapter, the past experiences in the wind tunnel investigation, the

numerical simulation of pressure fields (including simplified techniques, such as the POD) and the generation of multivariate wind speed fields, will be specified for the flexible roofs, towards their practical use in structural design. The possibility of using follower forces (important task in modelling wind action) has been tested and implemented in a structural analysis software.

Since the wind action is one of the main problem in designing and analysing large span roofs, the attention has been particularly focused on the wind-structure interaction and on the dynamic behaviour of flexible structures. Hence, the next two paragraphs show some useful simplified tools and some advanced numerical techniques, respectively, for the analysis of dynamic response of flexible structures and, in particular, large span roofs; the next two paragraphs show the role of experimental investigation in the design stage, from the preliminary wind tunnel tests to the full scale validation of the structure.

4.2 USE OF SIMPLIFIED TOOLS IN ANALYSING WIND EFFECTS ON LARGE SPAN ROOFS

Due to the geometric complexity, the flexibility which induce large displacement and the small inherent damping, several aspects have to be taken into account during the design stage of a suspended large span roof. The analysis of wind induced vibration requires, for instance, the evaluation of the pressure coefficients, the structural response analysis, the investigation of possible aeroelastic effects, etc, up to the design of additional energy dissipative system to reduce the vibrations themselves, if necessary. A particularly interesting application of recent techniques to study the cited problems has been made for the new Stadium built in Braga (Portugal) for the Euro 2004 Games. The main objective of this paragraph is to study the structural response and its mitigation whit relatively simple analysis tools which allow to control the numerical results without using heavy analysis software and without loosing in precision. The appropriate use of orthogonal decomposition techniques is very helpful at this scope. Another goal is to review the design process from a unitary point of view. In fact, in the Authors experience, the different problems are usually studied by different specialists and the interference between the various aspects is often lost.

The wind induced response analysis is firstly reported. Then, the main results of an aeroelastic experimental study are given. A sensibility analysis will show some important aspects to take into account in evaluating the structural reliability. Finally, since the wind induced vibrations were found to be quite large, the preliminary design of an additional damping system is shown. Fig. 4.1 shows a general view of the Stadium and a scheme of the roof indicating the references used below.

4.2.1 Wind Induced Response Analysis

Wind pressures are derived from a wind tunnel study, on a rigid scaled model, carried out by the RWDI. Since the pressure time histories were simultaneously measured at different points, within the upper and the lower sides of the roof panels, the instantaneous pressure fields were available.

The orthogonal decomposition techniques have been adopted to simplify the pressure representation, and to reduce the computational effort. Following the simplified procedure suggested by Vickery [a], the structural response to wind actions has been determined by separately evaluating (1) the mean response, (2) the quasi-steady response and (3) the resonant response. The first term simply takes into account the mean pressure distributions. The second one is obtained by performing a classical covariance proper orthogonal decomposition (POD). The third one takes into account the dynamic amplification of a suitable number of structural vibration modes, each one of them being excited by the unsteady wind pressures.

The static responses and the modal parameters used in the above cited calculations have been evaluated by mean of a finite element model of the structure, implemented on the FE software STRAND. Cable and shell and beam finite elements have been used to model the suspension cables, the roof panels and the connectors respectively. Linear analyses have been performed, the geometric stiffness matrix corresponding to the equilibrium configuration under gravity loads.

Wind Tunnel Data

Wind tunnel results were provided in terms of pressure coefficient time history series. Pressures on the concrete roof panels were simultaneously measured at 200 points, distributed on both the upper and the lower surfaces. Details on pressure taps distribution were reported by RWDI [b]. Time series were provided for 36 wind directions, 10° spaced. The pressure coefficients were referenced to the mean dynamic pressure measured at a height equivalent to 600m (full scale) during the wind tunnel tests. The Cp data were listed as individual Cp's (i.e., they provided the top and underside pressures separately). Approximately 12250 points of Cp data were provided for each pressure tap location.

Acquisitions were made at 512 samples per second for 24 seconds (corresponding to approximately 1 hour at full scale). The wind tunnel test speed at height equivalent to 600 m full scale was approximately 14.6 m/sec. Following the appropriate data scaling, from the model to the prototype scale (length scale L_s = 400, velocity scale V_s = 3.2, time scale T_s = 125), the measured pressures have been transformed in nodal (referred to the FEM model) values by mean of cubic spline interpolation.

General statistic features of pressure fields

In order to obtain the distribution of differential pressures main statistics, the unsteady pressure fields have been interpolated (cubic spline) and combined (upward and downward faces) for each record time instant. Differential pressure mean values, standard deviations, minima and maxima were evaluated for different incident wind directions. Mean values are used to evaluate the generic mean response (load, deflection, etc.) of the structure to wind actions. Standard deviations and extreme values are representative of local fluctuations and are used for local design evaluations. Fig. 4.2 reports the pressure coefficient mean values and standard deviations for a wind incidence of 270° from true north (the worst wind loading condition).

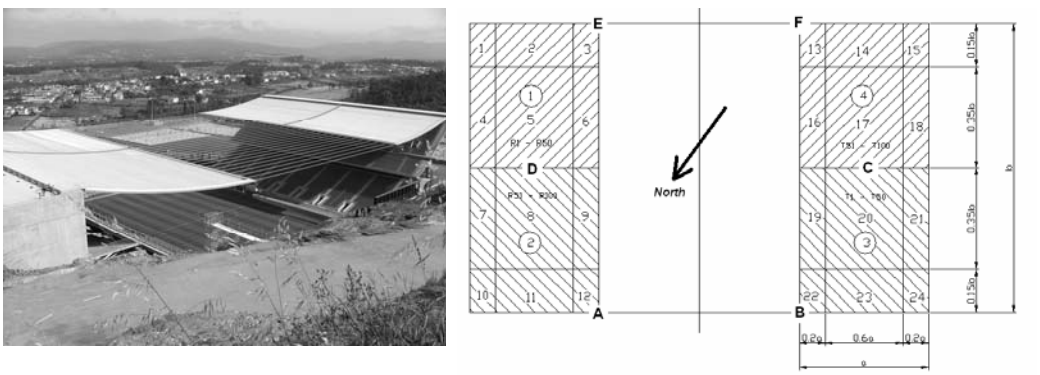

Figure 4.1 View of the Stadium from the south (a) and scheme of the roof (b).

Classical covariance Proper Orthogonal Decomposition - POD

An unsteady multivariate pressure field can be usefully simplified by projecting (Proper Orthogonal Decomposition - POD) it on the space generated by the eigenvectors of the covariance matrix of the original field. Two main advantages can be achieved by this technique. Firstly, the new fields (pressure modes) are mutually uncorrelated, giving rise to advantages which will be explained in the next section. Secondly, the energy content of the complete multivariate field is usually well represented by few components in the transformed space, allowing the representation of the effective pressure field by mean of few pressure modes. A possible third advantage, which is still debated by the scientific community, consists in the physical correlation between pressure modes and aerodynamic phenomena (such as incident wind turbulence, vortex shedding, etc.). As a matter of fact, since the covariance is fully representative of the correlation only for Gaussian random processes, the pressure modes are mutually uncorrelated only for Gaussian multivariate pressure fields. It means that the POD method can usefully applied for global actions (were the non-Gaussianity becomes negligible) but not for the evaluation local loads.

Analytically, let $\boldsymbol{p}(t)=\{p1(t) \ldots pm(t)\}^T$ be a Gaussian stationary nil mean m-variate random process. Let $\mathbf{C}_p$ be the covariance (for $\tau = 0$) matrix of $\boldsymbol{p}(t)$. This matrix is symmetric and positive definite, thus it admits the modal decomposition:

$$\mathbf{C}_p = \sum_{k=1}^{m} \phi_k \phi_k^T \lambda_k \tag{4.1}$$

where λ_k and ϕ_k are k^{th} eigenvalue and eigenvector of $\mathbf{C}_p$. The eigenvalues are real and positive; the eigenvectors follow the orthogonality properties:

$$\phi_i \phi_j^T = \delta_{ij}; \qquad \phi_i^T \mathbf{C}_p \phi_j = \delta_{ij} \lambda_j \ ; \qquad (\text{i, j =1, …m}) \tag{4.2}$$

where δ is the Kroneker's delta. By virtue of Eq. (4.2a), the eigenvectors of $\mathbf{C}_p$ constitute a base in the class of vectors with dimension m. The covariance transformation law is defined by:

$$\mathbf{p}(t) = \sum_{k=1}^{m} \phi_k x_k(t) \tag{4.3}$$

where $\boldsymbol{x}(t)=\{x_1(t) \ldots x_m(t)\}^T$ is the m-variate random process, image of $\boldsymbol{p}(t)$ in the transformed

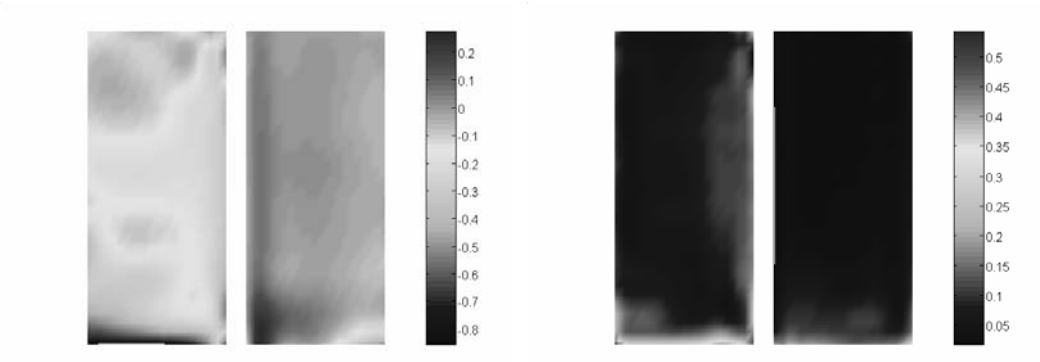

Figure 4.2 Pressure coefficient mean values (a) and standard deviations (b) for wind incidence 270° from true north.

space. Furthermore, the Eq. (4.2b) shows that the covariance matrix $\mathbf{C}_x$ of $\boldsymbol{x}(t)$ is diagonal and its terms are the eigenvalues of $\mathbf{C}_p$. It means that, in the transformed space, $\boldsymbol{x}(t)$ is a vector of m uncorrelated (for $\tau = 0$) processes. By sorting the eigenvalues in decreasing order, Eqs. (4.1) and (4.2) may be cut off after a term of order s, suitably less than m.

Fig. 4.3 shows the eigenvectors ϕ_k and the eigenvalues λ_k (which represents the variance of the image field $x_k(t)$) for the firsts two pressure modes, for a wind incidence of 270° from north. Since the eigenvectors are steady quantities, the POD has been directly carried out on the measured pressure coefficients; then, the cubic spline interpolation has been applied to each eigenvector to obtain the nodal differential (upward and downward faces) values.

Quasi-steady effects

By virtue of Eq. (4.3) and after a cut off after a term of order s, the generic response $R(t)$ of a linear system to the load $\boldsymbol{p}(t)$ can be expressed as:

$$R(t) = \sum_{k=1}^{s} x_k(t) \cdot R_k \tag{4.4}$$

where R_k is the generic response (load, deflection, etc.) due to the static distribution ϕ_k. Thanks to the uncorrelation between $x_i(t)$ and $x_j(t)$ if $i \neq j$, the variance of the generic response, if resonant effects are neglected, is given by:

$$\sigma_{R,qs}^2 = \sum_{k=1}^{s} \sigma_{x_k}^2 R_k^2 \tag{4.5}$$

Finally, the quasi-steady peak (minimum and maximum) response can be obtained as:

$$R_{qs} = \overline{R} \pm g_{qs}\sigma_{R,qs}; \qquad \sigma_{R,qs} = \sqrt{\sigma_{R,qs}^2} \tag{4.6}$$

g_{qs} being the quasi-steady gust factor. For the case study of Braga Stadium, 38 pressure modes have been considered. The gust factor g_{qs} has been assumed to be 3.6 for each pressure mode. In Tab. 4.1, the mean, quasi-steady and resonant effects (see below) are compared, for the 270° from north wind direction, in terms vertical displacements (positive upward) of 6 significant roof points (as indicated in Fig. 4.1b).

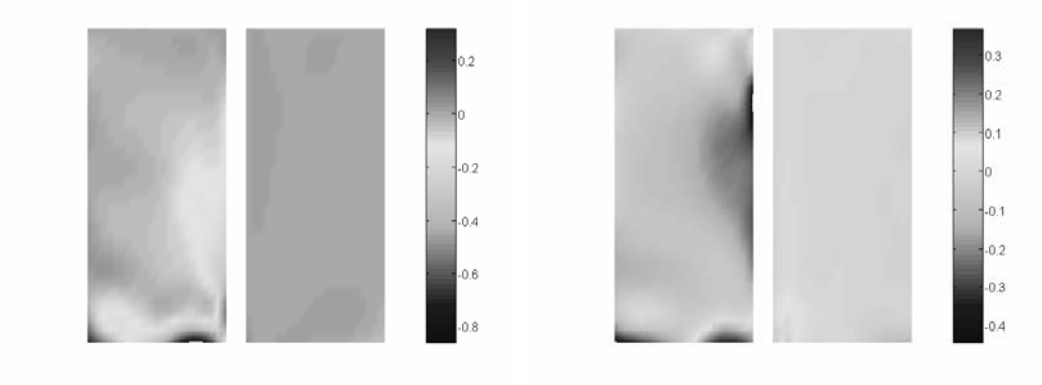

Figure 4.3 Cp modes (POD), wind 270° from true north: (a) Mode 1, $\sigma^2 = 0.1449$; (b) Mode 2 - $\sigma^2 = 0.0748$.

Resonant effects

The resonant effects can be evaluated by using the relationship:

$$R_{qs+res} = \overline{R} \pm \sqrt{g_{qs}^2 \sigma_{R,qs}^2 + g_{res}^2 \sigma_{R,res}^2} \; ; \qquad g_{res}^2 \sigma_{R,res}^2 = \sum_{h=1}^{n} g_h^2 \sigma_{R_h}^2 \tag{4.7}$$

In Eq. (4.7b), n is the number of structural vibration modes which are considered to be sensitive to resonant effects; g_h is the h^{th} modal gust factor

$$g_h = \sqrt{2\ln(f_h T)} + \frac{0.577}{\sqrt{2\ln(f_h T)}}, \tag{4.8}$$

f_h being the natural frequency of the h^{th} mode and T the sample length (typically one hour); σ^2_{Rh} the variance of response R associated to the mode h. The latter can be computed from modal analysis. Let $\psi_h(x,y)$ be the h^{th} mode shape, R_h the response corresponding to this deflection; $m(x,y)$ the mass per unit area; ξ_h the h^{th} modal damping. The h^{th} modal mass and load are:

$$M_h = \int_A m(x,y) \cdot \psi_h^2(x,y) \cdot dA \; ; \qquad Q_h(t) = \int_A p(x,y,t) \cdot \psi_h(x,y) \cdot dA \tag{4.9}$$

Finally:

$$\sigma_{R_h}^2 = R_h^2 \frac{\pi}{4 \cdot \xi_h} \frac{f_h \cdot S_{Q_h}(f_h)}{(2 \cdot \pi \cdot f_h)^4 M_h^2}, \tag{4.10}$$

$S_{Qh}(f)$ being the modal force spectrum. For the case study of Braga Stadium, 10 structural vibration modes have been considered. The damping ratio $\xi_h = 0.01$ has been assumed for all modes. The already cited Tab. 4.1 shows the strong influence of resonant effects in determining the global structural response.

Comments

The experimental data show the pressure coefficients to be significantly lower – both in mean values and standard deviation – than those reported by standards (EC1) for similar geometry. Large values are essentially confined to the roof borders, corresponding to local vortex shedding. Hence, vortex induced pressures seem to not affect the global roof dynamics even if they can induce significant local stresses on the roof panels.

The POD has been used to simply evaluate the quasi-steady effects. The derived responses result lower than those derived by the standard (EC1) approach. Hence, the spatial uncorrelation effects should be greater than those approximately taken into account by the EC1 simplified procedures.

Node	$\overline{R}$	$g_{qs}^2 \sigma_{R,qs}^2$	$\overline{R} \pm \sqrt{g_{qs}^2 \sigma_{R,qs}^2}$	$g_{res}^2 \sigma_{R,res}^2$	$\overline{R} \pm \sqrt{g_{qs}^2 \sigma_{R,qs}^2 + g_{res}^2 \sigma_{R,res}^2}$
A	0,1550	0,0250	0,3131	0,3027	0,7275
B	-0,0837	0,0115	-0,1910	0,3076	-0,6486
C	-0,0441	0,0014	-0,0812	0,0433	-0,2555
D	0,0930	0,0052	0,1652	0,0419	0,3101
E	0,0621	0,0092	0,1582	0,2040	0,5238
F	-0,0198	0,0016	-0,0599	0,2018	-0,4709

Table 4.1 Comparison of mean, quasi-steady and resonant contributions: vertical displacement, wind 270° from north.

Very important resonant effects have been found. They are dominant in determining the peak responses for most of the wind directions. These effects are strictly related to the damping ratio which has been assumed to be 1% for all considered vibration modes: the monitoring system which has just been arranged on the real structure, seems to show values of ξ even smaller.

4.2.2 The Aeroelastic Study

The tests, carried out at the Politecnico di Milano [d], were performed on a 1:70 aeroelastic model of the Braga stadium in both laminar flow (without surrounding topography, to check the presence of possible forms of aeroelastic instabilities) and turbulent flow (with surrounding topography, in order to establish the response of the roof structure to the action of turbulent wind). Roof acceleration, displacement, strain and related mean drag forces were measured at different significant points. The following results were pointed out (see also Diana et al., 2003):

- The aeroelastic stability has been proved, up to 7 m/s, corresponding to 58m/s at full scale;
- The response to turbulent wind, with the effect of surrounding topography, showed, at the nominal design speed with 20% turbulence, amplitude levels that, at full scale, are of the order of 40÷50 cm, with acceleration due to the first modes that reach peaks up to 1.5÷2 m/s^2 and RMS values of 0.46 m/s^2 A peak value of 2 m/s^2 means that the overload due to dynamic motion is 20% of the dead load.
- The amplitudes of vibration generally found at the maximum speed are to be considered not acceptable, since there are uncertainties on the effective value of the turbulence on site and of the damping of the structure, which can cause a significant variation from the values found on the model. Therefore, in order to decrease such levels, and control their variation due to the parameters uncertainties (real damping and turbulence level), damping devices can be installed on the structure.
- In order to simulate their effect, proper dampers have been designed and implemented on the model, in order to increase the structural damping up to a maximum value of 7-8%. This allow to decrease the vibrations at 50% of the original global levels of vibration while the amplitude of the torsional frequency is reduced by a factor three, so showing the effectiveness of such devices. In the full scale, the required damping of each of the four dampers is in the range 100-l50 kNs/m, i.e. as an ordinary ant-yaw dampers of train.

4.2.3 A Sensibility Analysis

This section presents a reliability analysis of the roof of the Stadium of Braga under random wind loads without consideration of the dynamic amplification due to the structural response. The extensive explanation of the problem can be found in Bertero et al. [e]. The following results are obtained: a) the sensibility of the failure probability of the roof to the spatial random distribution of wind loads, b) the wind direction that drive the structure to fail with most probability (considering all wind direction with a uniform distribution), c) the points of the roof that will fail with most probability, and d) the spatial distribution of wind loads that drive the structure to fail with most probability. Wind pressures are derived from the RWDI wind tunnel study. The roof was divided in 24 sectors where the wind pressure was measured and averaged at any time t. Therefore, the wind loads on the roof are represented as randomly distributed pressures $\mathbf{X}$ in n (=24) sectors with mean values $\boldsymbol{\mu}$ and covariance matrix $\boldsymbol{C}$. In the analysis of the roof, the bending moments at m (=130) points will be considered.

A probabilistic model of the roof to random wind loads is analyzed classifying the data in deterministic and probabilistic as follows. Deterministic data are: n = Number of roof sectors = 24; m = Number of points on the plate to evaluate the reliability = 130; k = Number of the load case considered acting simultaneously with the wind load = 1 = dead loads; $\mathbf{M_{Gx}}$, $\mathbf{M_{Gy}}$, $\mathbf{M_{Gxy}}$ =

Bending and torsional moment vectors for load case k (rows = 130); $\mathbf{A_x}$, $\mathbf{A_y}$, $\mathbf{A_{xy}}$ = Matrix formed by the bending-torsional moments originated at each point of the plate by an unitary pressure in each sector (rows = 130, columns = 24); $\mathbf{M_{Upx}}$, $\mathbf{M_{Upy}}$, $\mathbf{M_{Unx}}$, $\mathbf{M_{Unx}}$ = Ultimate resistance positive-negative bending moments for each plate point (rows = 130).

For each wind direction the following probabilistic description was considered for the randomly distributed pressures $\boldsymbol{X}$ in the n sectors: $\boldsymbol{\mu}$ = Vector of mean values of $\boldsymbol{X}$; $\boldsymbol{C}$ = Covariance Matrix of the randomly distributed pressures $\boldsymbol{X}$; $\boldsymbol{f_X(X)}$ = Probability density function of the random variables**.** Correlated normal distribution with parameters $\boldsymbol{\mu}$ and $\boldsymbol{C}$.

Sets of correlated normal variables $\boldsymbol{X}$ can be simulated from sets of uncorrelated standard normal distribution variables $\boldsymbol{Z}$ by using the Cholesky decomposition of the correlation matrix $\boldsymbol{C}$:

$$\mathbf{X} = \mathbf{L} \cdot \mathbf{Z} + \boldsymbol{\mu}_X \,, \qquad \mathbf{C} = \mathbf{L} \cdot \mathbf{L}^T \,, \tag{4.11}$$

L being an inner triangular matrix obtained by the Cholesky decomposition of **C** and **Z** is a vector of uncorrelated standard normal distributed variables. Lets assume that a wind pressure ΔX_j is simulated for each zone or the roof j. For each point of the slab, i, the bending and torsional moments, M_x, M_y and M_{xy} can be computed as follow:

$$M_{h,i} = M_{Gh,i} + \sum_{j=1}^{n} A_{h,ij} \cdot \Delta X_j \,, \qquad h = x,\ y,\ xy. \tag{4.12}$$

Considering the bending moments in each direction, the failure functions at each point of the plate ($1 \le r \le 130$), $G_r(\mathbf{X})$, are the following hyperplanes:

$$M_{Uph} - \left(M_{Gh,i} + \sum_{j=1}^{n} A_{h,ij} \cdot \Delta X_j \right) < 0 \ , \text{ and } \quad M_{Unh} - Abs\left(M_{Gh,i} + \sum_{j=1}^{n} A_{h,ij} \cdot \Delta X_j \right) < 0 \tag{4.13}$$

where $G_r \le 0$ is failure and M_{Uxy} is computed from the Johanssen Theory as the smallest of $(M_{Upx}+M_{Upy})/2$ and $(M_{Unx}+M_{Uny})/2$. The failure condition is obtained when failure is reached at any point of the plate, i.e., the structural failure can be defined as $(G_1 \le 0) \cup (G_2 \le 0) \cup \ldots \cup (G_{130} \le 0)$. The failure probability is given by the probability that an outcome of the random variables $\boldsymbol{X}$ belongs to the failure domain, $\boldsymbol{D_f}$, defined by equations above. This probability is expressed by the following integral:

$$\int_{D_f} f_X(X) \cdot d(X) \tag{4.14}$$

The Orientated Simulation Method [f] was used to evaluate the probability of the Eq. (4.14). In order to identify the most dangerous wind direction, the minimum reliability index β for each direction was calculated. Fig. 4.4b summarizes the obtained index β for each direction. Therefore 300° is the wind direction that drives the structure to fail with most probability. Fig. 4.4a shows the distribution of β values along the slab. The zone with smallest values of β is related to the zone with maximum bending moment for the gravity load on the border where the wind load attack the roof.

Note that this method provides the worst spatial wind load distribution associated to the wind variability and the weakness of the roof. Therefore, at this purpose, this reliability-based method can be better than the POD, since in the POD method the obtained distribution depend only on the wind load variability itself. It was found that the spatial distribution of wind loads that drive the

structure to fail with most probability is considerably different to that assumed in codes for design. However, the values are acceptable for static wind analysis.

4.2.4 Preliminary Design Of An Additional Damping System

The analysis of wind effects showed that the wind induced vibrations can reach very high amplitudes. Vibration amplitudes are very sensitive to the inherent structural damping ratio (approximately inversely proportional to $\sqrt{\xi}$). In those analysis a damping ratio of 1% was assumed for each natural vibration mode, but strong uncertainties characterize this value. Whenever the actual inherent damping will be lower than 1%, the wind induced vibrations could reach even larger amplitudes than the estimated ones. Hence, it seems important to monitor the actual structural damping. If it results insufficient to adequately contain the vibration amplitudes, it will be necessary to add a damping system which guaranties an acceptable level of wind induced oscillations. In the following, the main properties of such a damping system have been preliminary evaluated.

The presence of a stiff beam at the inner borders of the roof (from points B to F and A to E in Fig. 4.1b) induces the firsts natural modes, which are the most excited by the wind turbulence, to have the largest amplitudes at the ends of the beams themselves. Thus, the beam ends (points A, B, E and F) are among the most quoted to locate external dampers. These are also among the few locations compatible with the architectural requirements.

Hence, the analyzed damping system consists of four linear viscous dampers located at the inner vertices of the roof, C being the damping coefficients of dampers installed at points A, B, E and F. As a matter of fact, the dampers will be located at the ground level and connected to the roof by mean of tensile strands. Thus, a mass or a spring will be necessary to avoid compression in the cables. Nevertheless, in the present preliminary analysis the only presence of a simple linear viscous damper has been considered, without taking into account the added mass or stiffness, the mean value of the cable tensile force, etc.

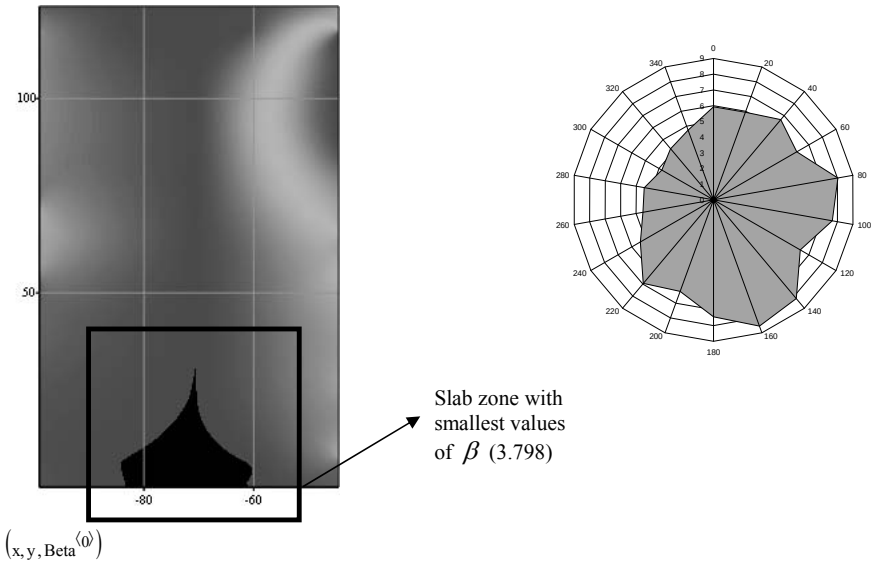

Figure 4.4 Mapping of the β values for wind direction of 300° and minimun β value for different wind directions.

A deeper stage of the design should evaluate the specific problems as, for instance, the opportunity to realize a friction damping system rather than a viscous one, the devices to avoid the cable slackening, the support induced cable excitation, etc.

Estimation of the added damping ratio through complex eigenvalue analysis

A preliminary estimation of the damping system efficiency has been carried out by mean of the eigenvalue analysis of the non-classical damped system. The eigenproblem is formulated by considering the firsts 10 modes of the undamped structure and the 4 added linear viscous dampers. The firsts 4 complex modes have been analyzed (the higher ones requiring a more refined model). Fig. 4.5a shows the damping ratio associated to such modes, for different damping values. Additional damping ratio of 4% and more and a significant reduction of the oscillation amplitudes on the firsts non-classical modes can be achieved by using viscous dampers with a damping coefficient C=15000 kg_f s/m. Fig. 4.5b shows the real part of the 1st complex eigenvector.

In order to validate the analysis of the damping ratio, the time history analysis of free vibration induced by different impulses has been numerically carried out (modal superposition of the firsts 21 undamped modes). The modal identification has been made by the POD of the time series and the subsequent evaluation of the logarithmic decrement. The analyzed conditions substantially confirm the above evaluated damping ratio.

Effects of the damping system on the wind induced vibrations

In order to evaluate the realistic behavior of the damping system and the maximum force produced by the dampers, different time history analysis of the structure subjected to the pressure fields measured in the wind tunnel have been carried out. Tab. 4.2 shows a comparison of the structural responses (in terms of vertical displacements at the most significant points) in absence and with external dampers; the wind pressures were derived from RWDI wind tunnel tests, with the wind blowing from 270° to the true north. The velocity amplitude at the damper locations are also reported.

A significant reduction of the oscillation amplitudes (see standard deviations) can be obtained by using viscous dampers with a damping coefficient C=15000 kgf s/m. The subsequent damping force will reach an amplitude (derived from the value of $V_{max,damp}$ reported in Tab. 4.2) of about 6 tons, as order of magnitude.

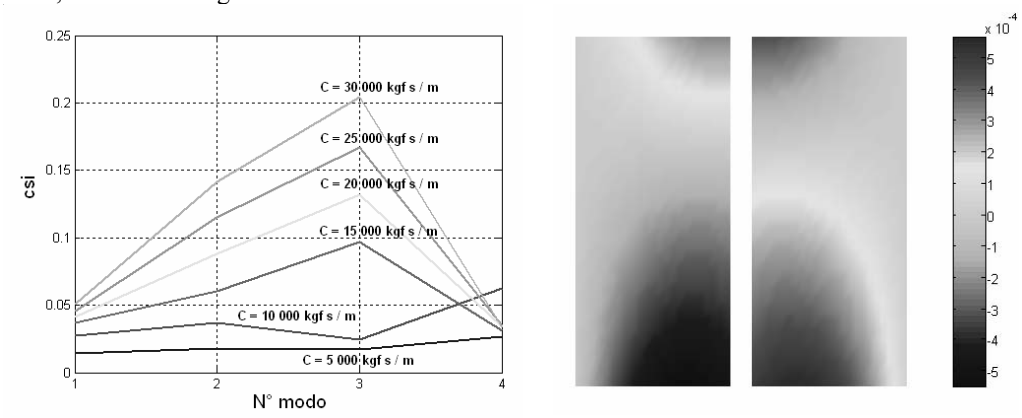

Figure 4.5 Damping ratio of complex modes and real part of the 1st complex eigenvector - f_1=0,28 Hz - ξ_1=3,7%.

	ξ_i=1% - C=0 kg_f s/m				ξ_i=1% - C=15000 kg_f s/m				
	min [cm]	*max* [cm]	μ [cm]	σ [cm]	*min* [cm]	*max* [cm]	μ [cm]	σ [cm]	$V_{max,damp}$ [m/s]
A	-34	+32	+2	10,6	-11	+14	+2	3,8	≈0,27
B	-46	+39	-6	11,1	-24	+10	-6	4,9	≈0,37
E	-35	+48	+8	16,4	-13	+31	+8	6,0	≈0,41
F	-60	+26	-15	16,2	-38	+3	-15	6,8	≈0,34

Table 4.2 Comparison of the structural responses (vertical displacements) in absence and with external dampers.

4.3 NUMERICAL ANALYSES OF LARGE ROOFS

4.3.1 Montreal Olimpic Stadium (Canada)

The roof over the baseball stadium in Montreal is a lightweight structure of the cable-stayed system type, with a membrane having a double curvature that covers an ellipse-shaped opening 200 m long and 140 m wide (Fig. 4.6). The shape of the membrane, which forms a globally hyperbolic curvature, was obtained by means of a uniform elliptic prestressing, adopting as the geometric boundary conditions an anchorage at 17 points around the perimeter and a suspension from 26 internal points.

Such a structure has been subject of a failure occurred in presence of a wind of low intensity (approximately 19 m/s) coming to bear at an angle corresponding to approximately 60° between the direction of the wind and the main axis of the roof (Fig. 4.7a). Moreover, the structure was characterized prior to collapse by an antimetric dynamic movement with respect to its lesser dimension inducing an oscillation with an amplitude of around 5 meters.

Starting from data on the geometry, materials, and design details, in the following we present some results carried out from a non linear static as well as dynamic analyses based on a new numerical model of the structure (Fig. 4.7b). The principal results of such analyses are extensively presented in publications [3] to [6].

The finite element model of the structure (Fig. 4.7b) uses two types of element: four-node membrane elements and two-node cable elements. The characteristics of each of the finite elements implemented in the Loki code are described e.g. in [g], [2]. Conservative surface loads have been adopted for the simulation of loads due to snow, while the simulation used non-conservative "follower" loads for a realistic description of wind action.

Membrane
"Panama" fabric of Kevlar 49 aramidic fibers, 16420 den;
coated with PVC type "B 1086";
self weight 29 N/m²;
modulus of elasticity is E = 16MN/m,
strength, 620-640 kN/m in the direction of the warp and 580 kN/m in the direction of the weave

Cables: galvanized harmonic steel strands with an open or closed Z-shaped cross-section:
minimum ultimate strength 1600 N/mm²,
the equivalent modulus of elasticity E = 160000 N/mm²

Figure 4.6 External view of the Montreal stadium roof and principal characteristics of materials

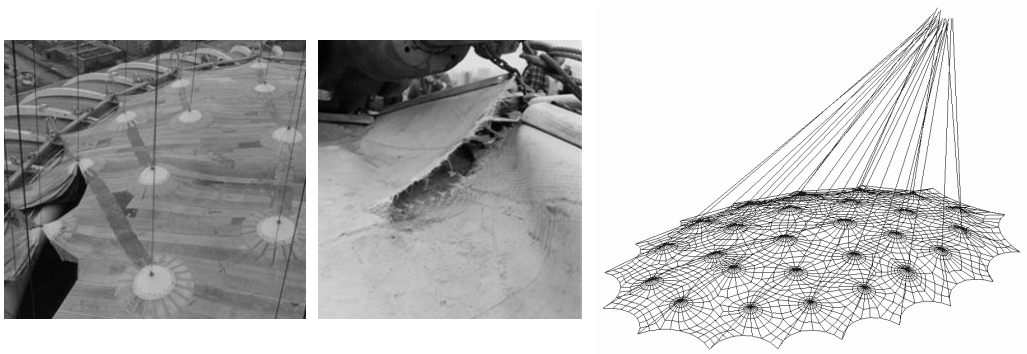

Figure 4.7 Membrane failures between the suspension cones and numerical model of the roof

Fig. 4.8 shows some results of the non linear static analysis in term of displacements and stresses of membrane elements as load increases (the diagrams refer to a central zone of the roof), both due to snow and wind loading. It is evidenced the high non linear behaviour of the structure: in particular, there is clearly a drastic reduction in the 2nd principal stress in the membrane and a stiffening effect deriving from the increment in the displacements. Similarly Fig. 4.9 shows the displacements and stresses to load ratio diagrams for cable elements obtained by the non linear snow and wind static analysis. The large displacements behaviour is evidenced by the non-linear displacement-load ratio that can be observed in all three displacement components.

Some further considerations can be carried out by the results of the static analyses (widely described, e.g. in [3] and [6]): the structure demonstrates a marked difference in the behaviour between the front (the southern side) and the back (northern side), that is a markedly unsymmetrical response. In particular under snow loading this effect can be observed mainly for displacements and for some stress concentration near the suspension cones (i.e. the weakest part of the membrane). Moreover under wind load, the stress in the principal suspension cables diminishes sensibly and such a loss of tension on the suspension cables releases the membrane from the intermediate supports and the roof, as mentioned earlier, acquires a pressostatic behaviour. Concerning non linear dynamic analysis, due to the flexibilty of the Montreal Olympic Stadium roof, fluid acts on the directly exposed outer surface of roof as well as on its internal surface depending on the internal volume changes. Therefore the dynamic analysis takes into account such an effect, by introducing some simplifications:

- structural deformation has no effect on the fluid motion field;
- wind speed is simulated with a classical Gaussian distribution and speed is transformed into pressure with a quasi-static formula;
- the constrained fluid volume effect modified by structural movements is introduced with a simplified model for which: structural model speed are small when compared to fluid pressure wave propagation rate; and structural periods are high compared with time required for overcoming internal pressure propagation-induced transition.

Based on these hypotheses, internal pressure can be considered as distributed quasi-homogeneously and structural dynamics can be described in a simplified form.

The final fluid-structure effect in the foregoing hypotheses is thus given by the algebraic sum of external and internal pressures, both of follower type, due to the structural motion.

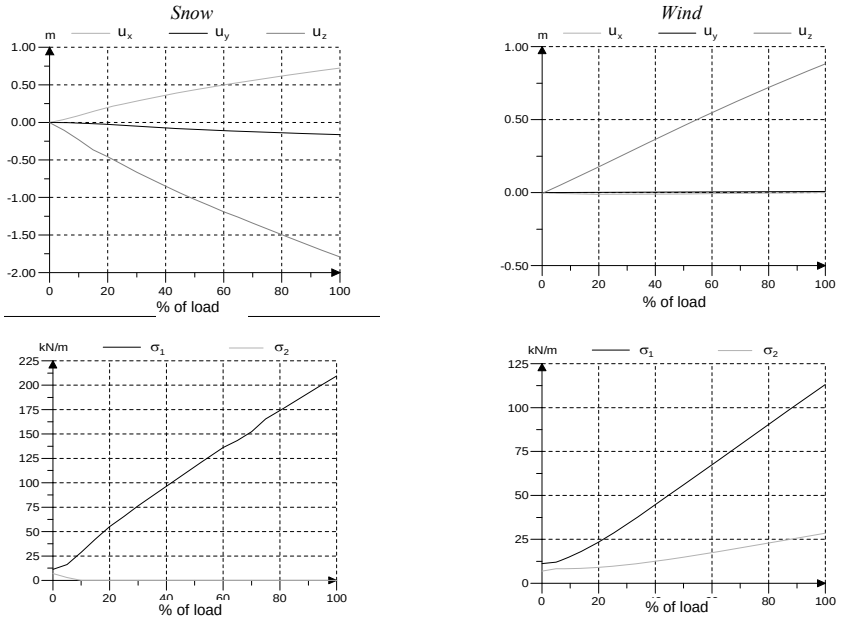

Figure 4.8 Typical snow and wind response – membrane displacements and stresses

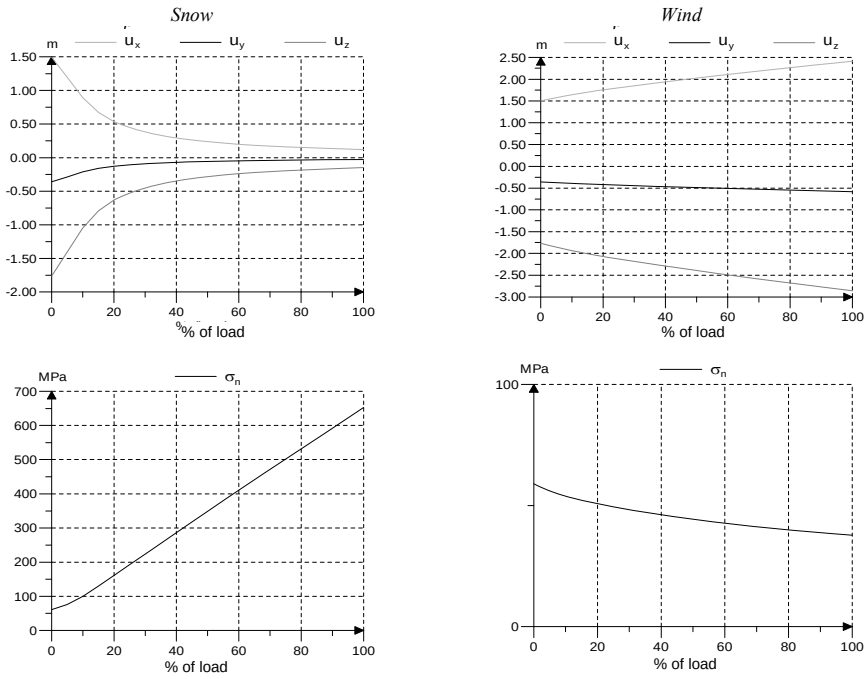

Figure 4.9 Typical snow and wind response –suspension cable displacement and stress.

These hypotheses thus enable concentrating on the overall macroscopic variables of fluid volume and average internal pressure tied to the environmental conditions, i.e. temperature. Such variables are connected by a non-linear law implemented and solved in the time domain by the LOKI calculation code, according to the scheme depicted in Fig. 4.10.

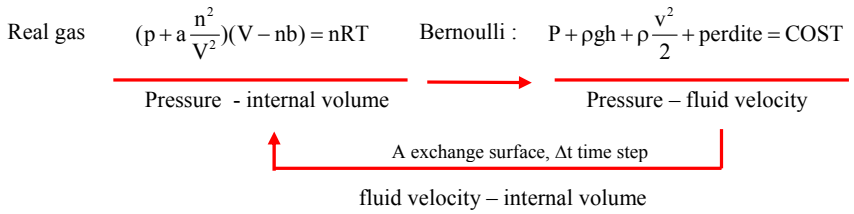

Figure 4.10 Interaction simply model between structures model – internal volume.

The wind load field is obtained by the simulation of the wind velocity and pressure coefficients measured by wind tunnel tests: the speed field was simulated at a 60° angle of incidence between average wind direction and main structure axis, this being the wind angle that had led to the membrane roof failure.

Dynamic analyses on the structure were performed with three different boundary conditions and the wind applied was the same for all the following analyses:

- analysis I: exchange surface ∞, no fluid structure interaction effect;
- analysis II: 100 m^2 exchange surface, permeable structure;
- analysis III: 50 m^2 exchange surface, permeable structure.

Fig. 4.11 shows the results for the first two analyses in terms of internal volume – exchange volume. In the case of no fluid structure interaction effect (Fig. 4.11a) it is worth noting that no aerodynamic resonance appears, so no risk factors are added and the displacements and stresses remain limited. The other analysis (Fig. 4.11b) indicate the onset of aerodynamic resonance (that increases as external exchange surface decreases), that is to say as the structure becomes more stiff and dissipates less energy due to decreased fluid volume pushed out or re-called by internal volume.

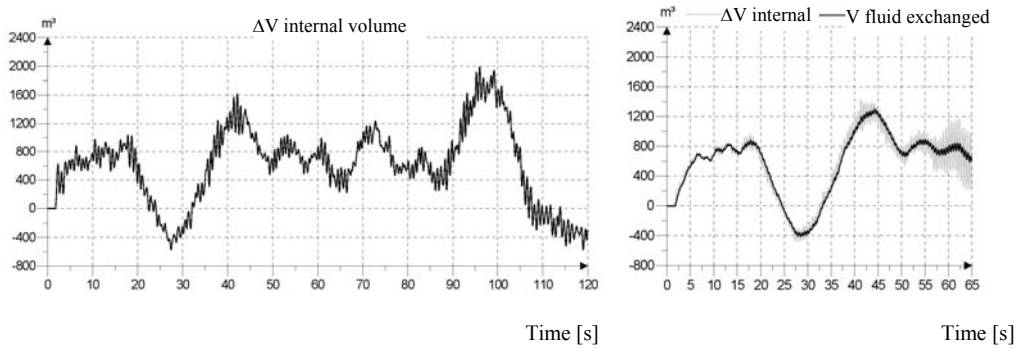

Figure 4.11 Global parameters: internal volume – exchange volume (a) ∞ m^2, (b) 100 m^2.

4.3.2 Braga Stadium (Portugal)

The large roof of the new football stadium built in Braga (Portugal) for the European Championship 2004, is schematically shown in Figure 4.12. On two sides the stadium is closed by stands parallel to the long side of the football field; one of the short sides is closed by the hill while the other one is open to the valley. The structure is sustained by parallel large diameter cables positioned at regular distance. The cables are fixed to the lateral concrete stands, which provide a rigid restraint. As a consequence to the particular geometry, the roof behaves as two flexible stripes, with a low flexural stiffness which is concentrated on the two sides. From an aerodynamic point of view it corresponds to two stripes (i.e. Stress-Ribbon structures) immersed in a fluid.

The characteristics of the structure, its innovative structural shape, the low flexural stiffness and its intrinsic tendency to an aeroelastic behaviour leads immediately to the need of analysing its response to the wind action by means of coupled fluid-structure numerical analyses.

The aerodynamic analysis is based on the wind test carried out at the Canadian wind tunnel RWDI (Rowan Williams Davies & Irwin Inc.) on a rigid model, Fig. 4.13a. In particular, the pressure histories have been scaled to transform the values obtained for the rigid model to the real scale. Then the resulting time histories have been applied to the numerical model, which take into account the non linear geometry behaviour as well as the dependence of the forces on the structural displacement. Moreover the results of the analyses have been be compared with those obtained from the three wind tunnel tests carried out respectively by: RWDI on a rigid model (Fig. 4.13a), DMI on aeroelastic small model and Politecnico of Milano - Italy on aeroelastic large model (Fig. 4.13b).

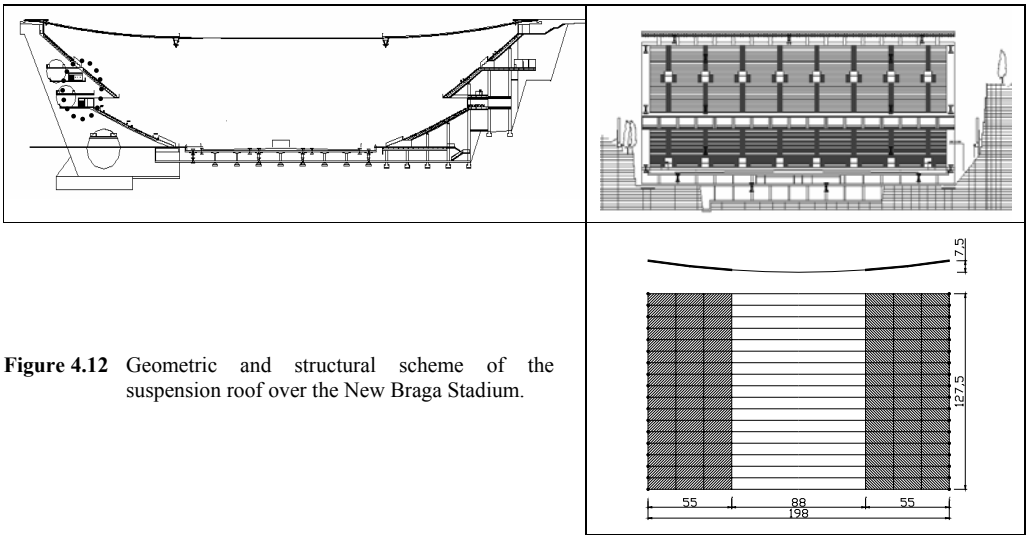

Figure 4.12 Geometric and structural scheme of the suspension roof over the New Braga Stadium.

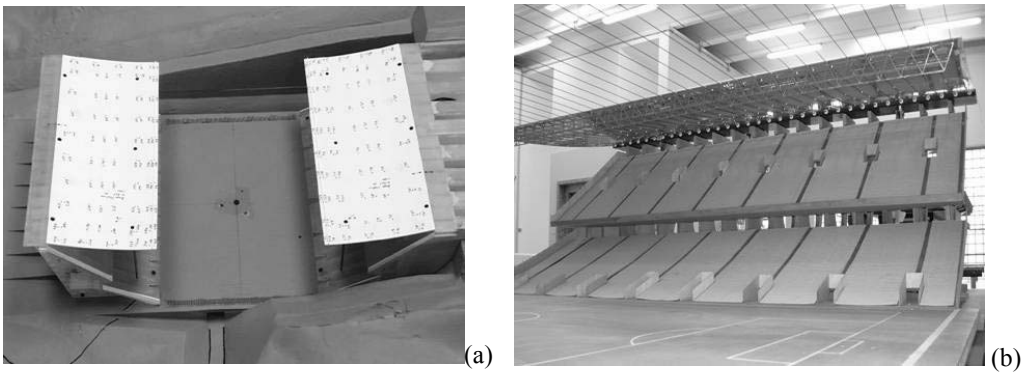

(a) (b)

Figure 4.13 Models used for the wind tunnel tests: rigid model (a), aeroelastic model (b)

Two different configuration of the structure, regarding wind action, have been considered: the first assumes the hypothesis of "open structure" between the superior and the inferior tiers, according to the design imposition; the second one assumes the closure condition, since this is the solution actually realized. The differences between the two hypotheses are due a significant modification of the fluid flux, affecting the dynamic behaviour of the whole structure. In fact even a limited variation of the opening produces a consistent modification of the wind flux as well as of the pressure field, which acts on the roof structure.

Fig. 4.14 and 4.15 show the pressure and the displacement diagrams obtained from the numerical analyses compared with the data obtained by the wind tunnel test on the rigid model. Both the hypothesis of open and close structure are taken into account.

Due to the dynamic behaviour of the roof structure, both the pressures and the incoming wind flux suffer some significant modifications, so producing self-oscillations of the structure. Such synchronization appears with both the considered models. However in the hypothesis of close structure we can observe a more regular response, in term of structural motion, while for an open structure an anticipated synchronization starting can be recognized.

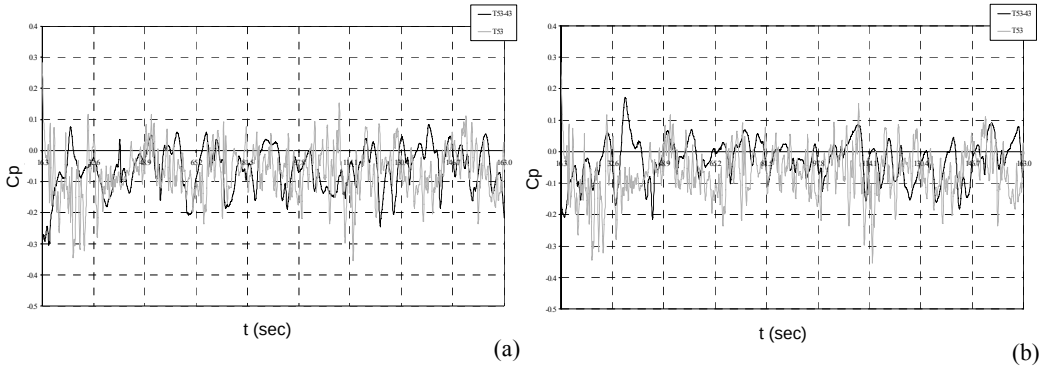

(a) (b)

Figure 4.14 Pressure coefficients vs time (black line numerical – grey line wind tunnel): open structure (a) close structure (b)

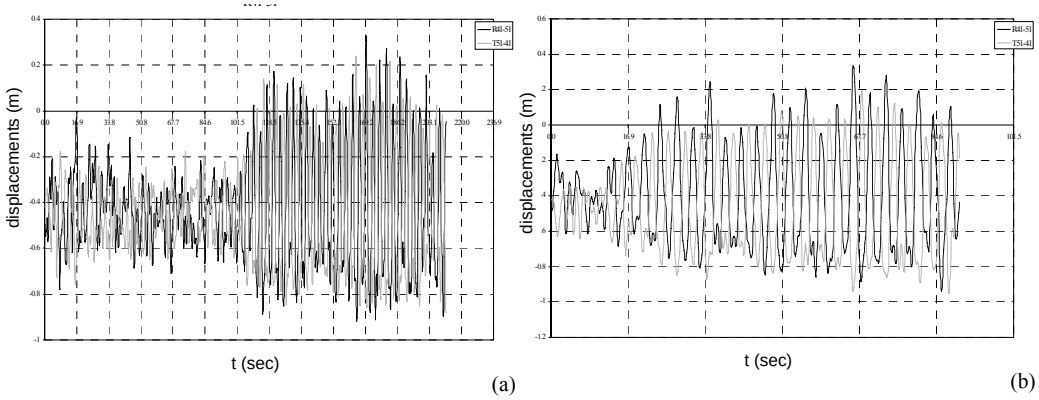

Figure 4.15 Displacements vs time (black line left part – grey line right part): open structure (a) close structure (b)

For such a structure the actual behaviour is strongly dependent on the wind interaction phenomenon and on the dimensions of the real openings. In particular the latter aspect represents an important issue in the dynamic analysis of such a roof structure: in fact as a consequence of a small variation in the geometry data, a significant variation in the dynamic response of the whole structure may follow. This is a typical case of great uncertainty in the phase of design and validation of the theoretical as well as numerical analyses that should be carried out for such roof typologies.

4.4 WIND TUNNEL TESTING

A wide experimental campaign has been carried out during the research program at the CRIACIV Boundary Layer Wind Tunnel (BLWT). In the following, the main experiences on large span roofs are resumed.

4.4.1 "Karaiskaki" stadium in Piraeus

The first case is relative to a rigid model of the new Olympic Stadium in Piraeus. The roof, almost horizontal, covers all the stands of the stadium by means of 14 cantilevered lattice structures spanning about 33 meters. 20 incoming wind directions have been analyzed and for each the mean values, the standard deviation and the maxima and minima of the pressure coefficients have been evaluated. Finally the recorded data have been used for performing the numerical simulations in time domain, whose objective is the definition of the design loads for the steel structures. The BLWT model has been realized (Fig. 4.16) in scale 1:250. The roof of the model has been equipped with 252 pressure taps: 126 located on the upper surface and 126 to the soffit in order to evaluate the net pressure coefficient.

The recorded data refer to the net pressures (difference between the pressure on the upper surface and the soffit), measured at the 126 couples of taps. The time histories of the net pressures have been divided by the dynamic pressure at the mean height of the roof (103 mm in model scale, around 25 m in real scale) in order to obtain the pressure coefficients. A wind profile typical of the sea has been reproduced whose parameters, in real scale, have been chosen from literature data and experimental tests: profile exponent $\alpha = 0.15 \div 0.18$, roughness length $z_0 = 50 \div 150$ mm, integral scale length $L_U = 50 \div 100$ m.

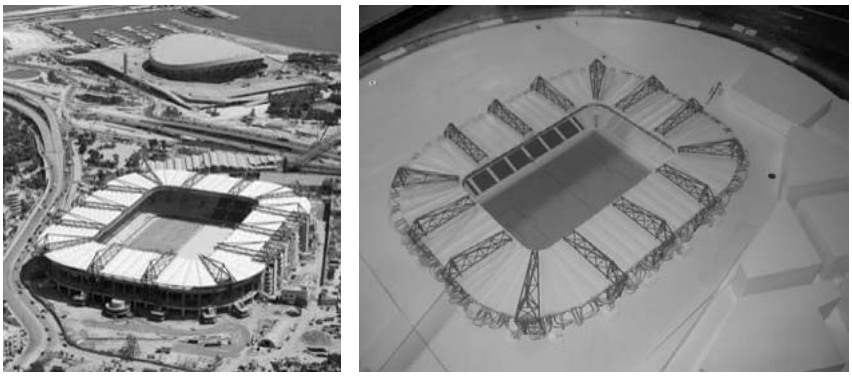

Figure 4.16 View of the building site of the stadium (left); boundary layer wind tunnel model (right).

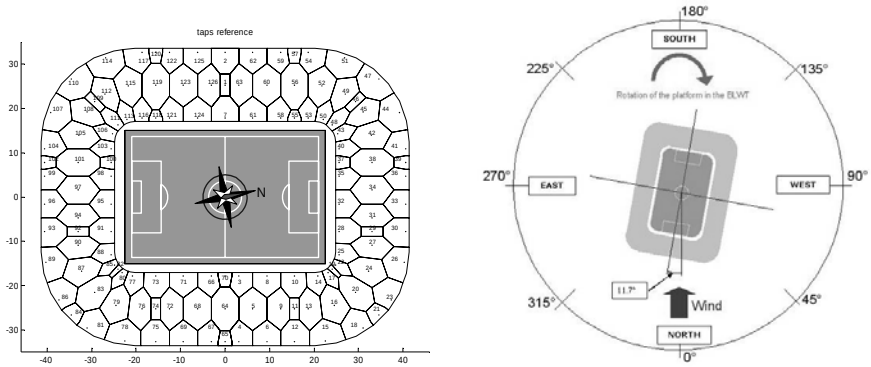

Figure 4.17 Position of the pressure taps (each point corresponds to a couple of pressure taps at the outer and inner surface of the roof) and reference system for the incoming wind direction.

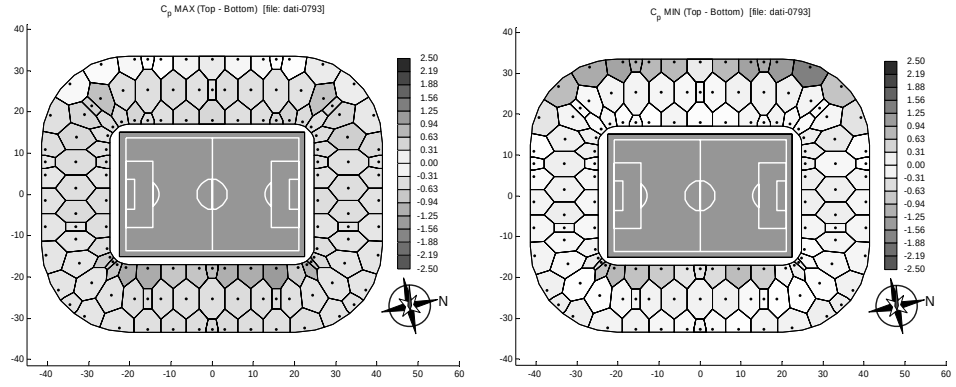

Figure 4.18 Design maxima (left) e minima (right) for the net pressure coefficient (incoming wind direction: 79.3°).

For each incoming wind direction 30s long time histories have been recorded, with a sampling frequency of 250 Hz.

The extremes of each time history has been modelled using the Gumbel method by means of the BLUE correction (Best Linear Unbiased Estimators) [i], the values of the parameters characterizing the extreme values distribution of each pressure coefficient have been obtained. The design value, maximum or minimum, has been finally assumed as the value that, in the extreme values distribution, has a 22% probability to be overcome, according to the indications provided by Cook and Mayne [n], and according to the procedure that has also been used in the draft of the Eurocode 1.

Results of the wind tunnel tests have been used for performing a series of FEM numerical analysis in time domain of the whole structure. The numerical model in real scale, made by 3779 mono-dimensional elements, has been created using the FEM code SAP 2000 [l].

For the numerical analysis the pressure time histories relative to eight of the 20 incoming wind directions have been taken into account. Furthermore, as the coordinates of the pressure taps didn't coincide with the FE model nodes, a special algorithm for the wind load simulation (described in the following) has been adopted.

Using the similitude laws, the sampling frequency of 250 Hz in the wind tunnel corresponds to a frequency of 1.93 Hz in real scale, that is 30 seconds of recording in BLWT correspond to a storm of 64 minutes in real scale sampled with a time step of 0.516 (=1/1.93) seconds.

Since the first eigenfrequencies of the structure are a few less than 1 Hz (T 1 s), it results that the sampling rate is not sufficiently small to dynamically excite the structure, therefore the analysis performed directly considering the time histories recorded in wind tunnel will assume the form of a quasi-static analysis, leading to neglect the resonant response.

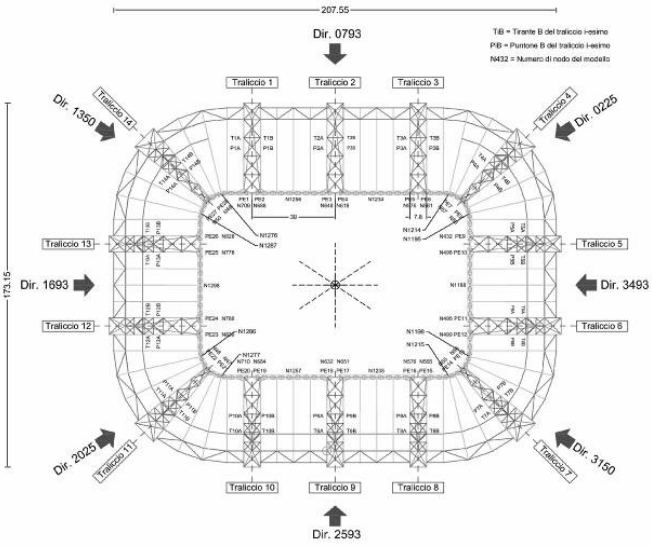

Figure 4.19 Analysed incoming wind directions.

To obviate to such drawback it has been decided to analyse the signal acquired in wind tunnel in order to obtain a new signal sampled at a higher frequency which is able to excite the higher frequencies of the structure.

In such sense a special algorithm, developed to the Department of Civil Engineering of Florence, has been adopted. Once defined the position of the pressure taps and the correspondent acquired signals, the procedure allows the simulation of time histories in points of the domain different from those correspondents to the pressure taps.

The software is based on a RBF based artificial neural network which acts on the pressure field, variable in space and time and considered orthogonal to the reference surface. One of the main assumptions made in the case of the Piraeus stadium was that the acquired signal was Gaussian. Naturally many cases exist in which the Gaussianity hypothesis is more or less correct; nevertheless, in the examined case, the analysis of the statistical properties of the single signals has allowed to ascertain that such assumption was indeed permissible.

The procedure is based on the construction of the power spectral density function (PSDF) of the single signals and on the corresponding cross PSDF, that provide information on the time-space correlation between the acquired signals.

Finally, the actual pressure field, in correspondence of the pressure taps, is approximated by a series expansion and, if required, extended to additional point on the reference surface.

In the case of the Piraeus stadium 128 time histories of pressure coefficient have been simulated and finally transformed into the corresponding nodal forces, to be applied on the numerical model, through the respective influence areas.

The frequency of the simulated signal has been increased up to 50 Hz ($\Delta t = 0{,}02$ s), allowing to consider the contribution of the first 15 modal shapes of the roofing structure.

Once completed the time domain analysis, the analysis of the extreme values for the structural response has been conducted, especially considering the members forces in the main structural elements of the roofing structure, such as struts and ties of the cantilevered structures. For this task, in the time history of the members forces the initial transitory has been cut out and the resulting signal has been divided in 10 temporal windows, each one characterized by 1050 samples. For every window the maximum (or minimum) value has been determined, as shown in the Fig. 4.20a.

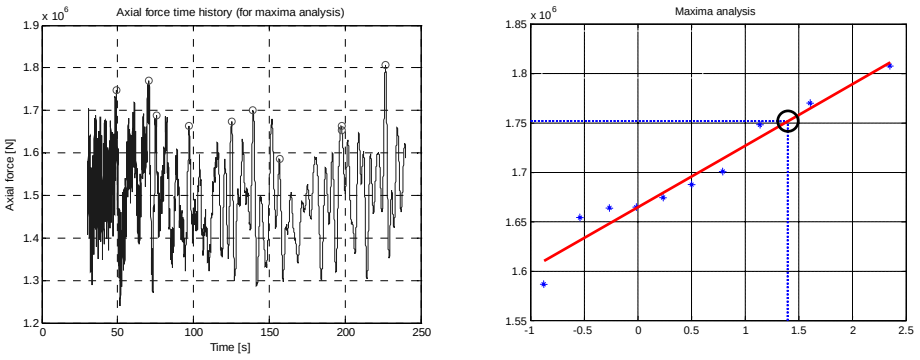

Figure 4.20 Maxima for the axial force TH in the main struts of the cantilevered structure and linear regression for the estimation of the design value for the member axial force.

The maxima have been ordered and placed in a Gumbel diagram and finally, through a linear regression, the design value of the generic member force has been determined as the value that present a 22% of overcoming probability (Fig. 4.20b).

4.4.2 "Delle Alpi" stadium in Turin

The second case is relative to a rigid model of the new roofing structure of the "Delle Alpi" stadium in Turin. The new roofing structure should be inserted under the existing one, moving the inner perimeter toward the centre of the stadium for about 22 meters (Fig. 4.21). The wind tunnel model (in scale 1:250) also includes the adjacent buildings within a distance of 250 m from the centre of the stadium. The roof in the BLWT model has been equipped with 256 pressure taps (128 couples), 126 for the inner and outer surface plus two pressure taps for the reference pressures. In this way it has been possible to measure the net pressure on the roof surface.

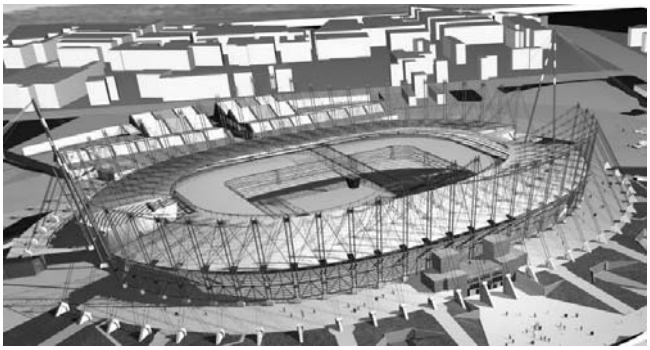

Figure 4.21 Rendering of the architectural model of the new Delle Alpi stadium in Turin.

The tests have been performed for 16 incidence wind directions (from 0° to 360° increasing of 22.5°) and for two different configurations (with or without the "old" roofing structure). The 0° direction coincides with the geographical North and is rotated counterclockwise of 18° with respect to the longitudinal axis of the stadium (Fig. 4.23). For each wind direction and configuration of the model two sessions of measurements have been performed: the first one to acquire the 64 couples of pressure taps along the four sides of the stadium and the second to acquire the remainder 64 couples set in correspondence of the corner. A third set of measurements has been carried out by instrumenting 64 couples of pressure taps spread on the whole surface in order to rebuild the correlation structure of the pressure field.

For the evaluation of the maximum and minimum design values of the pressure coefficients, a Gumbel analysis has been carried out, dividing the time histories into several time windows, each one correspondent to about 10 minutes in real scale. For each wind direction the following parameters have been evaluated: mean value and standard deviation of the aerodynamic coefficients c_p, maximum and minimum values of the c_p. Finally, a comfort analysis has been performed by the individualization of the wind motion fields in the areas between the roof structure and the stands.

The distribution of the pressure coefficients on the new roof for the configuration in which it is also present the old one clearly underlines the shielding effect of this last towards the new structure. The Fig. 4.24 shows the distribution of the maxima and minima for the net pressure

coefficients, assuming an incoming wind direction coincident with the longitudinal axis of the stadium.

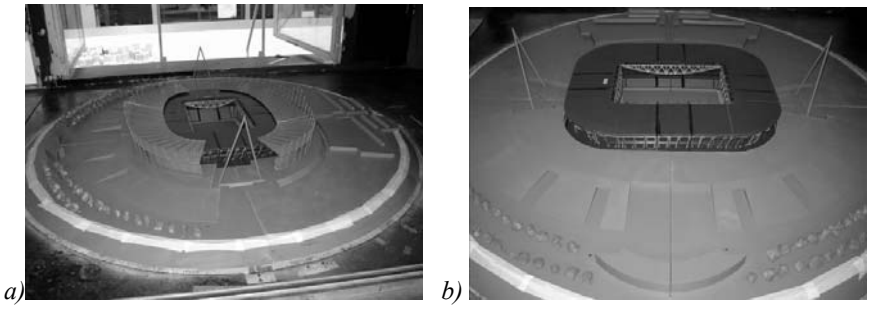

Figure 4.22 View of the wind tunnel model with (a) e without (b) the old roofing structure.

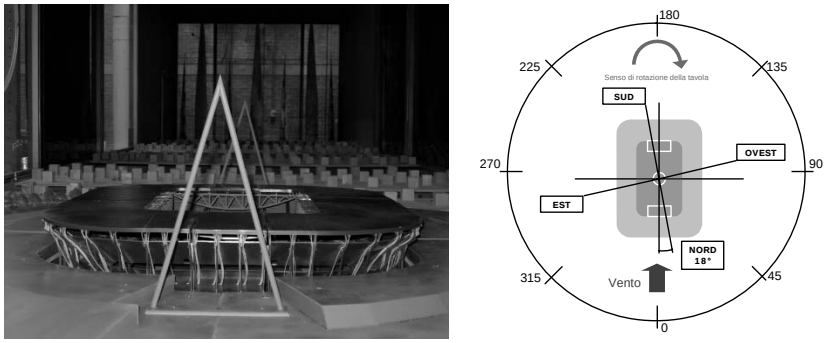

Figure 4.23 View of the wind tunnel model without the old roofing structure and reference system: teflon tubes are visible near the stadium stands.

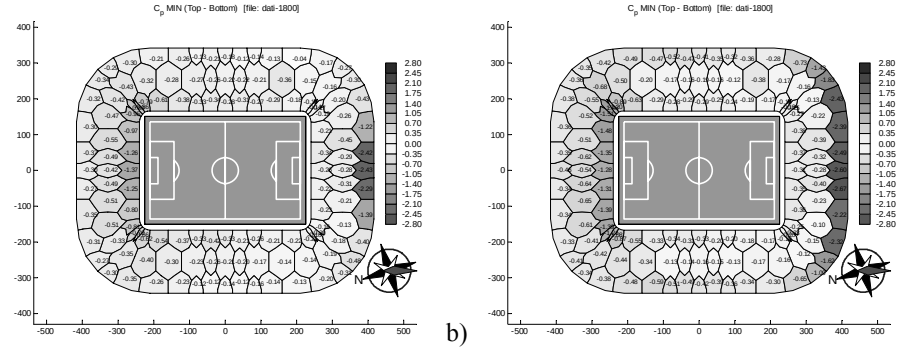

Figure 4.24 Net pressure coefficient minima distribution for the two configurations analysed: a) with the old roofing structure and b) without the old roofing structure.

The study of the comfort for the spectators due to the wind action in a specified area provides a description of the physiological and psychological effects that the people can experience in a particular windy situation. The principal factors that concur to the definition of the comfort are: the conditions of local air flows motion, the characteristics of the wind motion field under undisturbed conditions and in presence of urban elements in the analysis site, the intensity of turbulence, that influences in a very complex way the motion field in urban environment.

It is possible to obtain a classification of the pedestrian comfort based on some criteria that analyze different disturbing factors. One of the possible classifications are that reported in [o], that divides the uneasiness in the following four points: mechanical effects due to the wind, "cold wind" (effect of cooling caused by the wind in combination with low temperatures), thermal effects present in environments where the temperatures considerably differ from the bodily temperature, psychological effects. The criterions for the evaluation of the zones subjected to discomfort for the spectators (or of the pedestrians) evolved very much in the last years. They introduced an increasing number of variables capable to quantify in more and more exact way the phenomenon. Although these criteria face the problem from different points of view they all fix one or more thresholds of speed of the wind in order to identify the various condition of comfort. Therefore a description based on the uneasiness for the people, assumed an incident wind direction, will be assigned to each of these conditions.

The scales of human discomfort in comparison to the wind speed are assumed as base for the definition of the criteria for the classification of the comfort of a site. Therefore some dimensionless isovelocity maps of have been created with respect to the V_{ref} and, once the incoming wind intensity has been chosen, the zones of greater uneasiness can be defined.

The model used for the pressure evaluation has properly been modified to allow the study of the motion field on a vertical plane, placed in the transversal direction of the stadium, through the PIV technique(Particle Image Velocimetry). The characterization of the incident flow on a body through the PIV technique consists in the individualization of the instantaneous motion field of the fluid in a given configuration.

Tests have been carried out for the Delle Alpi stadium for the two configurations: "with" and "without" the old roofing structure and for only one incoming wind direction, parallel to the minor axis of the stadium and hence perpendicular to the grand stands.

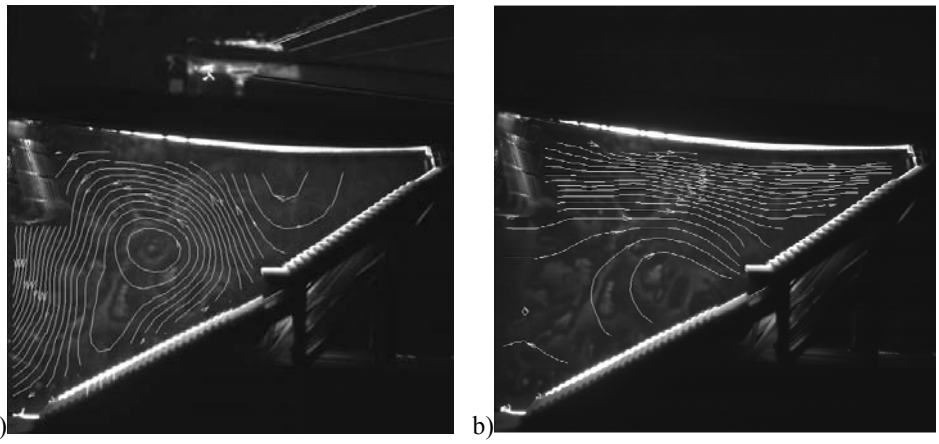

Figure 4.25 Instantaneous vector fields for the two configurations: a) without the old roof, b) with the old roof.

The used system allows acquisitions for a maximum frequency of 15 vector fields per second. The images have been processed with the cross-correlation function and vectors validation by means of moving average.

In the Fig. 4.25, the vector maps for the motion fields measured in the wind tunnel are shown. These maps provide the numerical values to be multiplied for the reference/design wind velocity (V_{ref}), fixed depending on the required performance standards; in this way the resultant map of the actual wind velocity can be obtained.

Results show a noticeable variation of the net pressure coefficients on the new roofing structure depending on the preservation of the old roofing. In the first case the existing stands and roof provide a shielding action on the new roofing structure. The instant vector fields of the flow velocity show a greater flow regularity and better conditions of air circulation in the configuration without old roof.

4.5 FULL SCALE DYNAMIC CHARACTERIZATION

Since the wind induced response is sensitive to the modal shapes, frequencies and, especially, damping, the knowledge of the actual dynamic properties becomes essential to confirm the design assumptions, based on theoretical calculations and wind tunnel tests, or to introduce mitigation devices. In order assess the dynamic behavior of the New Braga Stadium large span suspension roof, the dynamic characterization of the real structure has been per-formed. Two test types were carried out: classical sudden load release, used to identify the frequencies of the first vibration modes, and harmonic excitation, at different structure points, with subsequent measurement of the free vibration decay. The testing program on the complete roof structure is part of a design and verification strategy, according to the Eurocode - Basis of Structural Design - that gives general indications about the Design Assisted by Testing; in the specific case, the full scale testing has been performed to reduce the uncertainties on the dynamic damping parameters and to check the vibration mode shapes and frequencies, as indicated in the Annex D of the cited Eurocode.

The experimental evaluation of the modal damping ratio values - which are difficult to be foreseen in absence of very similar structures - allows to increase the reliability of the theoretically calculated response to dynamic loads and, in particular to the wind action. In addition, the measured natural modal shapes and frequencies allow to validate and to calibrate the numerical models which have been arranged during the design stage, for their use during the monitoring and the maintenance phases. This is an essential step in the evaluation of the structural subsequent performances.

The high flexibility and the large roof mass, consisting of two huge concrete slabs supported by suspension cables 202 m free span, result in low frequency values for the first vibration modes. Hence, the structure testing, under harmonic excitation, required the setup of a special excitation system, capable to induce appreciable oscillations of the structure in the range 0,2 - 1,0 Hz.

The tests have been performed in May (Test Series 1) and July 2004 (Test Series 2). They substantially consisted in measuring the dynamic response of the structure to impulsive and to harmonic loads. The response was measured in terms of acceleration in some significant points of the structure itself. The recorded accelerations were analyzed to recognize the excited modal shapes and to determine the corresponding modal damping ratios. The experimentally recognized modal shapes are compared to the numerical model derived ones. The ascertained values of the damping ratios - whose magnitude was variable, depending also on the stiffness type of the excited mode - have been used to confirm or to review the response predictions derived from numerical analyses and wind tunnel tests.

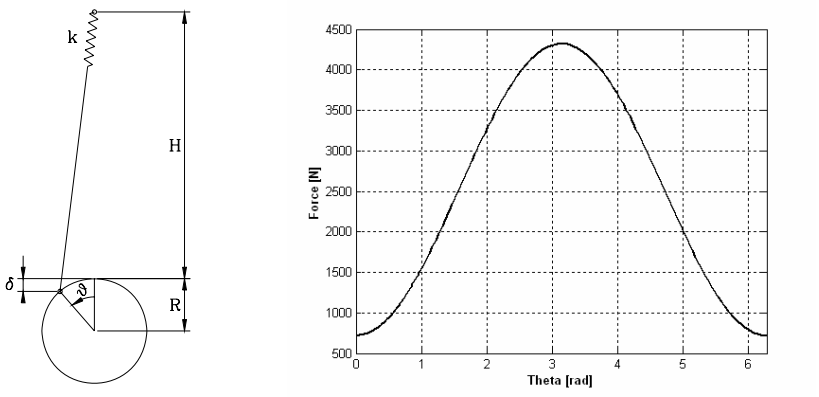

Figure 4.26 Scheme of the harmonic exciting system (left); spring force vs engine angular position (right).

4.5.1 Experimental Setup

Two different exciting systems were used. During the Test Series 1, the structure was excited by impulsive loads, by releasing an approximately 5 tons mass, preliminary suspended to the roof edge steel girder by mean of a cable.

Within the Test Series 2, the structure was excited by periodic, approximately harmonic loads, at different frequencies. The forces were provided by a cable, linked to the edge steel girder by mean of a pre-tensioned spring, sinusoidally moved at the other end. Since the spring was sufficiently flexible, the roof movement was negligible in comparison to the cable one; hence, the force was nearly sinusoidal, as shown in Fig. 4.26. The cable movement was provided by an electric engine, through an eccentric link (Fig. 4.27).

The actual induced force was measured by mean of a force transducer located between the roof girder and the spring. The force transducer output was sampled and recorded at 10 Hz.

In order to excite the first significant vibration modes, both the impulsive and the harmonic loads were applied in two different significant points of the structure: an inner roof corner and a roof border steel girder mid span. The exciting positions are schematically shown in Fig. 4.28, where they are named as EXC A and EXC B respectively.

Figure 4.27 View of the electric engine with the eccentric link (left) and of the girder linked spring (right).

In order to measure the structural dynamic response under the applied dynamic loads and the free vibrations decay after the loading excitation stop, 6 accelerometers were placed on the roof slab. The sensor positions and their order number (ACC 1 to ACC 6) are schematically shown in Fig. 4.28.

The accelerometers are part of the structural monitoring system which is installed in the stadium. They are Tri-axial Force Balance Accelerometer type, consisting in a mass-spring resonator with optical mass pickoff sensing, working within a frequency range of 0 to 60 Hz.

The vertical acceleration component only has been taken into account, in the calculations for the present work. In fact, it is sufficient to describe the behavior of the more flexible vibration modes, which are substantially the wind excited ones, the vertical component being prevailing for these modes. The accelerations at the 6 sensors were simultaneously acquired and recorded during the tests at 250 Hz frequency sampling.

4.5.2 Testing Program

During the Test Series 1 the structure was excited by impulsive loads, by releasing an approximately 5 tons mass preliminary suspended to the roof. The main purpose of these tests was to identify the main natural frequencies of the structure.

This first analysis allowed to simplify the successive harmonic excitation, which could be focused around the recognized natural frequencies. On the other hand, the impulsive force had to be - for safety reasons - relatively small (if compared to the involved inertial forces). Hence, the relative structural response was not sufficiently wide and clear to be used for the modal shapes and damping identification.

Once the main natural frequencies of the roof were identified by mean of the Test Series 1, the harmonic excitations were focused around those frequencies. The purpose of this second test series (namely the Test Series 2) was to significantly excite the main natural vibration modes, by mean of resonant harmonic forces.

For this purpose, different excitation frequencies were tried, close to the preliminary identified ones, until the best fitting of the resonant frequency was reached for each mode. Fig. 4.29 shows a summary of the main forcing and response parameters involved in this test series. The plot of the A/F values is shown to point out the resonant conditions; Freq is the forcing frequency (Hz); the ratio A/F is representative of the dynamic magnification due to the resonant effects, being A the roof acceleration half-amplitude (g) in correspondence of the exciting system, at the frequency Freq and F the force half-amplitude (kN) at the same frequency (after a frequency filtering which isolates the only components around Freq).

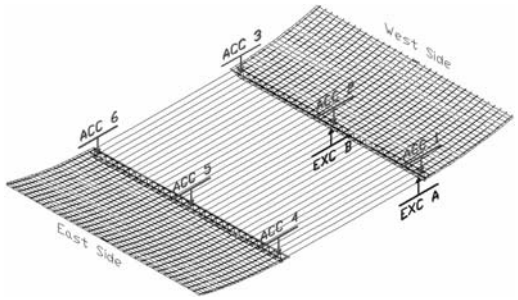

Figure 4.28 Accelerometers and exciting system position.

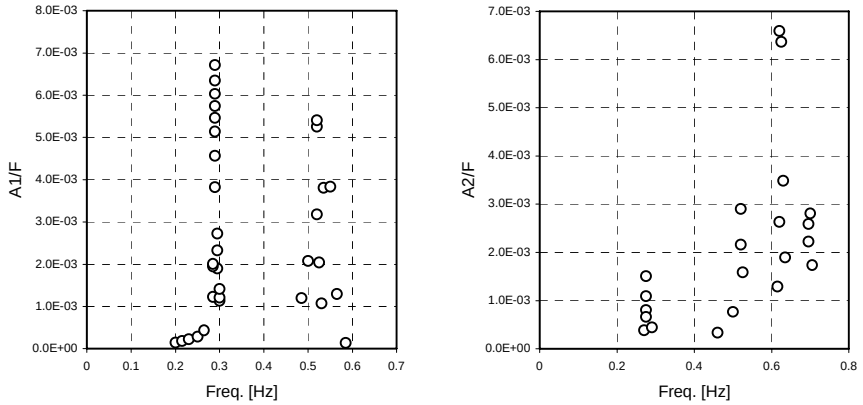

Figure 4.29 Dynamic response ratio A/F vs excitation frequency: force in EXC A (left) and EXC B (right).

4.5.3 The dynamic characterization

The free vibration decay time series, recorded after the resonant harmonic excitation stop, are among the most appropriate data to evaluate the natural modal shapes and the corresponding modal damping. For this purpose, the measured acceleration fields have been numerically treated. Firstly, a frequency filtering has been performed to isolate the frequency range involved by the given vibration mode. Then, the obtained signals have been projected on the covariance matrix eigenvector generated space (the POD - Proper Orthogonal Decomposition - has been performed).

This procedure points out the dominant modal shape, within the considered frequency range, and the corresponding time history. This latter, whenever it includes free vibration intervals, allows to evaluate the logarithmic decrement and, thus, to determine the modal damping ratio. In addition, if the free vibration time history is sufficiently long to follow the motion from large to small amplitudes, the logarithmic decrement can be evaluated within different intervals and the damping ratio can be separately obtained for different vibration amplitudes.

In Fig. 4.30 the results of the above described analysis is shown for one of the performed tests. The following information are reported: a 3D view of the identified modal shape (in terms of its values in the 6 monitored points ACC 1 to ACC 6); the modal acceleration time history within the free vibration interval and the relative PSDF - with an indication of the natural frequency - including an outline of the logarithmic decrement curve for intermediate vibration amplitudes and the numerical values of the modal damping ratios; the theoretical corresponding mode (from the same FEM model as the one used to evaluate the wind induced response) with the corresponding theoretical natural frequency.

Different main modes have been experimentally identified. Due to the limited number of excitation positions, other modes have not been excited during the test campaign. In addition, some of the theoretical modal frequencies are very close each to one other: they are substantially dual modes and the excited one depends on and is very sensitive to the excitation position. On the other hand, the identified modes are sufficient to characterize the dynamic behavior of the structure in terms of modal damping ratio and modal shapes and frequencies to be compared to the theoretical ones.

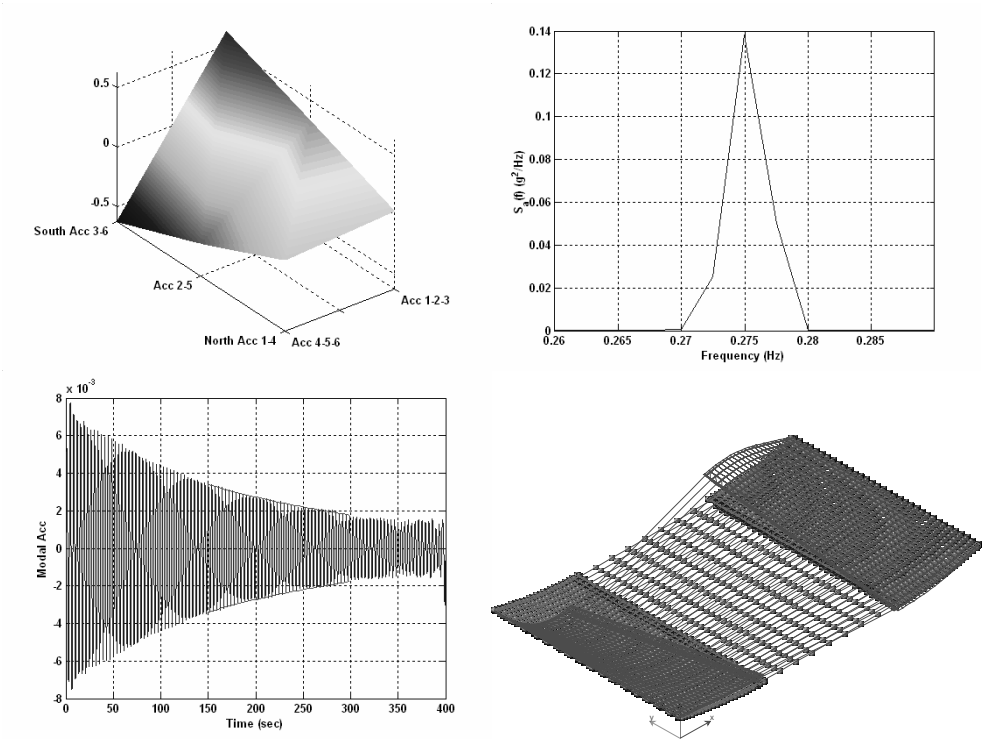

Figure 4.30 First mode dynamic properties. Test n. EXCB06; experimental frequency f_{exp} = 0,275 Hz; experimental damping ratios: $\xi_{large\ amplitudes}$ = 3,0‰ - $\xi_{mean\ amplitudes}$ = 2,5‰ - $\xi_{small\ amplitudes}$ = 2,3‰; FEM theoretical frequency f_{theor} = 0,274 Hz.

The comparison between the theoretical and the experimentally recognized mode shapes and frequencies, pointed out that the anti-symmetric modes (with reference to a cable plane section) are very accurately represented by the FEM model, while the symmetric ones are lightly stiffer than the theoretical predicted ones and the respective frequencies are slightly higher.

It seems important to observe that the symmetric modes heavily involve the cables elongation, the stiffness of the substructure and the geometric stiffness, while the anti-symmetric ones are substantially determined by the geometric stiffness matrix only.

Regarding the determined modal damping ratios, it can be observed that, as it can be expected, for large oscillation amplitudes the damping values are higher than for small amplitudes. The largest excited amplitudes give rise to damping ratios of 3‰, as order of magnitude, for approximately all the excited modes.

The modes which involve the bending deformation of the steel border girder partially collaborating with the concrete slab, are characterized by slightly higher values of the damping ratio. These modes are quite stiff and, hence, they are not particularly significant in determining the wind induced response.

4.6 BASIC REFERENCE

[a] Vickery, B.J. 1993, *Wind loads on the Olympic Stadium: Orthogonal Decomposition and Dynamic (Resonant) Effects.* Report BLWT-SS28A-1993.

[b] RWDI 2001. *Wind tunnel study of roof wind pressures, Braga Stadium*. Report 01-327, October 2001.

[c] Ove Arup 2001. *Wind climate analysis report, Braga Stadium*. Report 66161, September 2001.

[d] Diana G., Bocciolone M., Collina A., Tosi A., Rocchi D. 2003. *Wind tunnel investigation on Braga Stadium*. Final Report, February 2003.

[e] Bertero R.D., Carnicer R., Puppo A.H. 2003. Sensibility wind analysis of the roof structural system - Stadium of Braga – Portugal. Final Report, September 2003.

[f] Puppo A.H., Bertero R.D. 1992. Evaluation of Probabilities using Orientated Simulation. *Journal of Structural Engineering, ASCE*, **118** (6).

[g] Lazzari M., Saetta A., Vitaliani R. 2001. Non-linear dynamic analysis of cable-suspended structures subjected to wind actions. *Journal of Computers and Structures*, **79** (9): 953-969.

[h] Augusti G., Spinelli P., Borri C., Bartoli G., Giachi M., Giordano S. 1995. The C.R.I.A.C.I.V. Atmospheric Boundary Layer Wind Tunnel. In *Wind Engineering : retrospect and prospect*, IAWE, International Association for Wind Engineering, Vol. 5, Wiley Eastern Limited, New Delhi.

[i] Box G.E.P., Jenkins G. N., Reinsel G.C. 1994. *Time series analysis for casting and control*. 3rd Edition, Prentice Hall.

[j] Cook N.J., Mayne J.R. 1980. A refined working approach to the assessment of wind loads for equivalent static design. *J. Wind Engrg. & Ind. Aerodyn*, **6**: 125-137.

[k] Galsworthy J., Vickery B.J., Mikitiuk M., Kong L., Surry D. 2002. *The Athens Olympic stadium roof and velodrome roof Athens, Greece*. AG Davenport BLWT Lab., SS50-2002

[l] Wilson E.L., Habibullah A. 2004. *SAP2000. Structural Analysis Program*. Computers and Structures, Inc. 1995 University Ave. Berkeley, California.

[m] Borri C., Bartoli G., Orlando M., Procino L., Spinelli P. 2004. *Nuova Struttura di Copertura dello Stadio delle Alpi a Torino - Prove in galleria del vento per la determinazione di pressioni sulla copertura e del comfort in tribuna*. Rapporto finale della Convenzione di Ricerca tra CRIACIV e JUVENTUS F.C. Spa"

[n] Hunt J.C.R., Poulton E.C., Mumford J.C. 1976. The effects of wind on people: new criteria based on wind tunnel experiments. *Building Environ.*, **11**.

[o] Koss H., Blackmore P., Kuismanen K. 2002. *Wind comfort criteria in different countries and physiological psychological aspects*. COST Action C14.

[p] Isymov N., Davenport A.G. 1974. A Probabilistic Approach to the Prediction of Snow Loads, *Canadian Journal of Civil Engineering.*

[q] Murakami S., Uehara K., Deguchi K. 1980. Wind Effects on Pedestrians: New Criteria Based on Outdoor Observation of Over (2000) Persons. In: *Cermak (ed.) Proceedings of the 5th International Conference on Wind Engineering*, Fort Collins, Colorado.

[r] Penwarden A.D., Wise A.F.E. 1975. *Wind environment around buildings*. Building Research Establishment Report, HMSO

[s] Vickery B.J., Apperley L. W. 1973. *On the Prediction and Evaluation of the Ground Wind Environment*. The University of Sydney, Department of Civil Engineering Research Report R227, Sydney

4.7 LIST OF PUBLICATIONS

[1] Cosentino N., Majowiecki M. 2004. Analysis and mitigation of the wind induced response of large span suspended roofs: the case of the new Braga Stadium. *Atti dell'8° Convegno Nazionale di Ingegneria del Vento - IN-VENTO-2004*, Reggio Calabria, Giugno 2004.

[2] Lazzari M, Vitaliani RV, Majowiecki M, Saetta A. 2003. Dynamic behavior of a tensegrity system subjected to follower wind loading. *Computer & Structures*, **81** (22-23): 2199-2217.

[3] Lazzari M, Vitaliani RV, Majowiecki M, Saetta A. 2002. F.E. Analysis of Montreal Stadium Roof Under Variable Loading Conditions. *IABSE Symposium*, Melbourne, Australia, September 11-13, 2002.

[4] Lazzari M., Majowiecki M., Saetta A., Vitaliani R. 2002. Comportamento non lineare per geometria dello Stadio Olimpico di Montreal. *7° Conv. Naz. di Ingegneria del Vento, ANIV IN-VENTO-2002,* Milano - September, 19-22 2002.

[5] Lazzari M., Majowiecki M., Saetta A., Vitaliani R. 2006. Il Comportamento Strutturale della Copertura dello Stadio Olimpico di Montreal. *CRASC'06 - Crolli e Affidabilita' delle Strutture Civili, Università degli Studi di Messina*, Messina, 20-22 Aprile 2006.

[6] Lazzari M, Vitaliani RV, Majowiecki M, Saetta A. 2006. F.E. Analysis of Montreal Stadium Roof under Variable Loading Conditions, *submitted to Int. Journal.*

[7] Marini, M., Cosentino, N., Majowiecki, M. 2005. Dynamic characterization of the New Braga Stadium large span suspension roof. *International Conference on Experimental Vibration Analysis for Civil Engineering Structures, EVACES*, Bordeaux, France, October 2005

[8] N. Cosentino, M. Majowiecki, C. Utili 2005. Optimal Damping Systems for Flexible Footbridges. *Proc. of Footbridge 2005 - 2nd International Conference*, Venice December 2005

WITH CONTRIBUTION FROM:

Gianni Bartoli, University of Florence
Paolo Biagini, University of Florence
Claudio Borri, University of Florence
Nicola Cosentino, Structural Engineer - Bologna
Luca Facchini, University of Florence
Massimiliano Lazzari, University of Padova
Maurizio Orlando, University of Florence
Anna Saetta, University IUAV of Venezia

5 Masts and cables

Salvatore Noè
University of Trieste

5.1 INTRODUCTION

Vertical or sub-vertical slender and highly flexible structures like masts and cables are often subjected to non-linear wind loading that sometimes overlaps non-linear structural behaviour.

In the frame of the research project, both experimental and theoretical studies have been dedicated to these phenomena.

The characteristics of the wind load on cables have been experimentally investigated by means of wind tunnel tests and numerically simulated, in the aim of collecting data useful to define the spectral properties necessary to perform fatigue analyses.

The vortex shedding induced load in lock-in conditions or close to it have been modelled both analytically and a numerically. The numerical model has been implemented in a general purpose f.e. code for the non-linear dynamic analysis under wind loads.

5.2 FATIGUE SAFETY OF CABLES UNDER WIND ACTION

Cables are used as structural elements in many applications of civil engineering, such as suspended bridges and stayed musts. When engineers are involved in the design, maintenance and retrofitting of suspended bridge, they must account for random actions, such as vehicular load and wind action, which may induce stress variations in the primary cables and eventually lead to component fatigue. Concerning in particular with the dynamic behaviour of cable under wind action, it is important to understand and evaluate the stochastic characteristics of the response. This may be achieved estimating the statistical quantities mean, coefficient of variation, skewness and kurtosis: these estimates provide information on the distribution of the response. In fact, to perform an accurate fatigue safety analysis, it is necessary to highlight the deviation, or not, from normal distribution due to the nature of wind load and to the non-linearity of the dynamic behaviour of the cable.

5.2.1 The wind tunnel tests

The wind tunnel experimental tests were carried out at the boundary-layer wind tunnel of CRIACIV (Centro di Ricerca Interuniversitario di Aerodinamica delle Costruzioni e Ingegneria del Vento) in Prato (Italy). The experimental model of the cable was build using 48 cylinders, each one with a diameter of 40 mm and a length of 40 mm, connected by a 0.7 mm-diameter strand made of steel [1]. The cable was placed at middle height in the test section, with a sag to span ratio of 1/10, which is typical of cables used in suspension bridges. The horizontal component of cable tension, H, assumed in this case the value of 22 N. The Irvine number, λ^2, which account for both geometric and elastic effect, assume a value greater than 256 π^2.

The cable was supported at its ends by means of two identical devices capable of measuring both the axial load and the overall drag force acting on the cable by means of two load cell at both ends of the cable. Due to the design of the supports, the friction and torsion in the cable, which may corrupt the measure of the axial load, and the overall friction of the slide were the cells were mounted on, which may corrupt the measure of the drag force, were proved to be negligible. The cells could measure forces up to ÷ 120 N.

The displacement components of the middle point of the cable were measured by means of a laser system. The vertical and longitudinal component of the velocity at the midspan of the cable and the along wind velocity at the distance of 400 mm along the span were measured by means of two hot-wire anemometers. Moreover, two pitot tubes were used to estimate the mean value of the wind speed near the roof of the tunnel and at the cable level.

The tests were performed both in laminar and in turbulent flow. In laminar test, the mean wind speed varied in the range U = 10 ÷ 30 m/s, where U is the mean wind speed at the cable level. The measured intensity of turbulence was less than 1 percent (see Fig. 5.1a). The turbulent flow was obtained by means of a grid placed 4.00 m upstream of the model. The mean wind speed varied in the range U = 10 ÷ 20 m/s. The intensity of turbulence measured was about 14 percent in the along-wind direction and about 11 percent in the across-wind direction (see Fig. 1.1a). The integral scale of turbulence was found by fitting the normalized spectrum of logged data to Von Karman one (Fig. 1.1b), obtaining a value for L_u of 0.18 m [2].

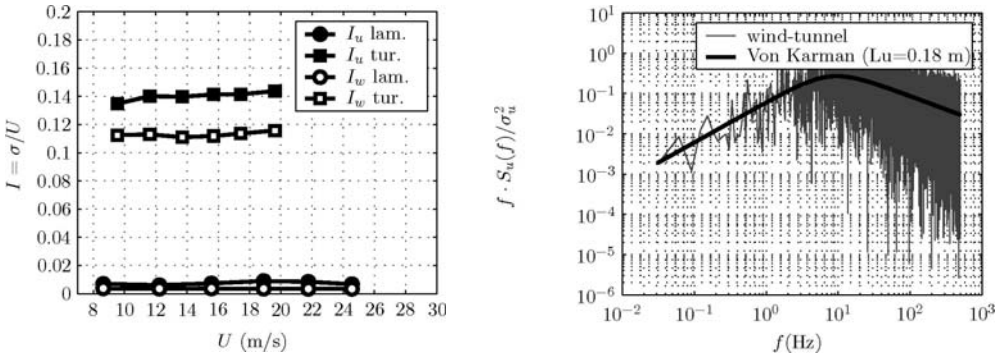

Figure 5.1 (a) Intensity of turbulence vs. wind mean speed, measured in the tunnel without the cable; (b) Spectral Density of turbulent flow.

5.2.2 Data analysis

As previously stated, the tests were performed in laminar and in turbulent flow condition. Two set of data were logged for each condition: in one set of measures the arm supporting the pitot and the hot-wire anemometers was at a distance of 0.30 m from the cable (in its initial position), in the other set it was 1.10 m distant. The logged data were:

- the axial load at the supports,
- the reaction at the supports in the along-wind direction,
- wind mean values measured by the pitot,
- wind instantaneous speed measured by the hot-wire anemometers.

Furthermore, in a different set of measurements in laminar flow, the displacement of the middle point of the cable, both along-wind and across wind, were measured by means of the laser system.

The first analysis was performed in order to assess the effect of the presence of the cable on turbulent flow. In Fig. 1.2 are reported the measured value of the intensity of turbulence at increasing wind mean speed U for the four test configuration (d is the distance between the cable and the anemometers). (In the following figures, 'test 1' are tests in laminar flow with d = 1.10 m, 'test 2' are tests in laminar flow with d = 0.30 m, 'test 3' are tests in turbulent flow with d = 1.10 m and 'test 4' are tests in turbulent flow with d = 0.30 m).

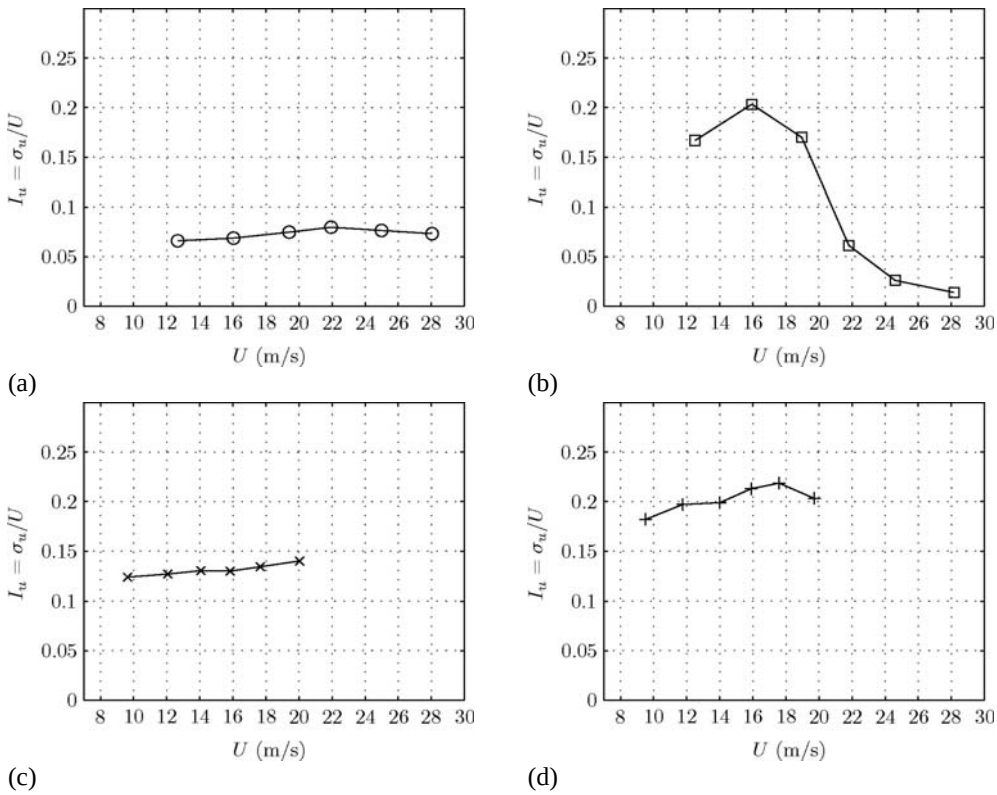

Figure 5.2 Intensity of turbulence for increasing wind speed in test 1 (a), test 2 (b), test 3 (c) and test 4 (d).

As it can be seen, when the anemometers were placed 1.10 m behind the cable the intensity of turbulence was almost constant at increasing wind speed: in turbulent flow it assumed the value measured when the cable was not present, while in laminar flow the value was about 5% greater than the one found without the cable: the difference to be ascribed to the turbulence generated by the cable. In the tests with the anemometers placed 0.30 m behind the cable, the intensity of turbulence increased its value at lowest wind speeds while at greatest wind speeds, since the cable arose above the level of the anemometers, it tended to the value obtained without the cable.

The data logged by the load cells were elaborated [3] to obtain the mean values of the increment of axial force and of the overall drag force for increasing wind speed in dimensionless units as follows:

$$K_T = \frac{1}{2}\frac{\Delta T_{sx} + \Delta T_{dx}}{T_0}$$

$$C_D = 2\frac{F_{D,sx} + F_{D,dx}}{\rho \cdot B \cdot L' \cdot U^2}$$

$$Re = \frac{U \cdot B}{\nu}$$

where ΔT_{sx}, ΔT_{dx}, $F_{D,sx}$ and $F_{D,dx}$ are the values of the increment of axial load, ΔT, from the value corresponding to the cable in its initial, without wind flow, position (T_0 = 23.5 N) and of the along-wind reaction F_D, measured at both ends of the cable; B is the diameter of wood cylinders, ν is the kinematic viscosity of air, ρ is density of air and is L' the horizontal projection of the length of the cable in its initial position; Re is Reynolds' number. The obtained values for K_T and C_D are reported in Fig. 5.3.

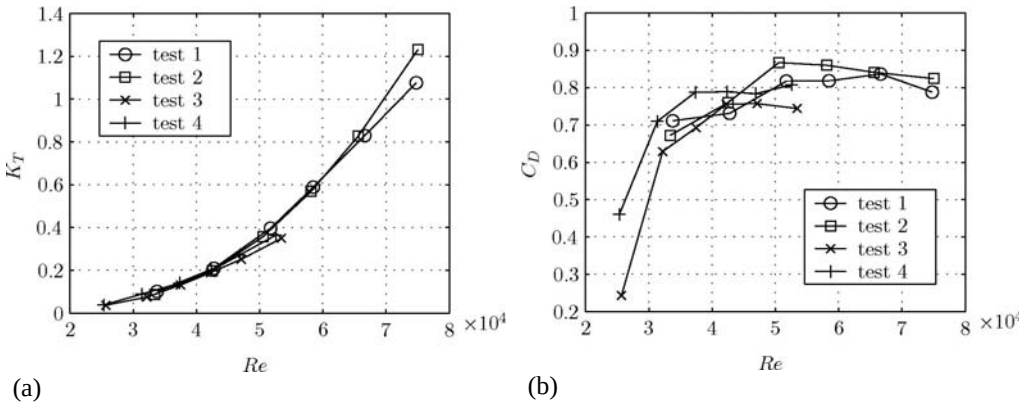

Figure 5.3 Diagram of the increment of axial load (a) and of the overall drag force (b), in dimensionless units, versus the Reynolds' number.

The data shown in Fig. 5.3b suggest that, in present case, the transition region, maybe because of the surface roughness of the cable model and to the flow turbulence [a], occur at Reynolds numbers smaller than those available in literature. It should be noted that the data shown in Fig. 5.3b can be assumed as an estimation of the drag coefficient of a cable supported at its ends. Moreover, the present case was very complicated since being three-dimensional (i.e. not a single section of the cable), the model changed its position with regard to the flow when subjected to

increasing wind speed and the porosity of the experimental model, due to the interspace of 8 mm between wood cylinders, may also affect the evolution of the drag force with increasing wind speed. Besides, these data can hardly be compared to available ones since similar tests are not present in the literature the authors are acquainted with.

The logged data were successively elaborated to obtain the Spectral Density Function. In Fig. 5.4 are reported the spectra obtained for the axial load cells and the overall drag force cells, both in laminar and in turbulent flow, for a wind mean speed of about 16 m/s. The figure shows several peaks which are in agreement with the frequencies of the natural modes of the cable that can be found by analytical analysis, as in [b]; The first three analytical frequencies for each kind of motion of the cable are reported in Tab. 5.1.

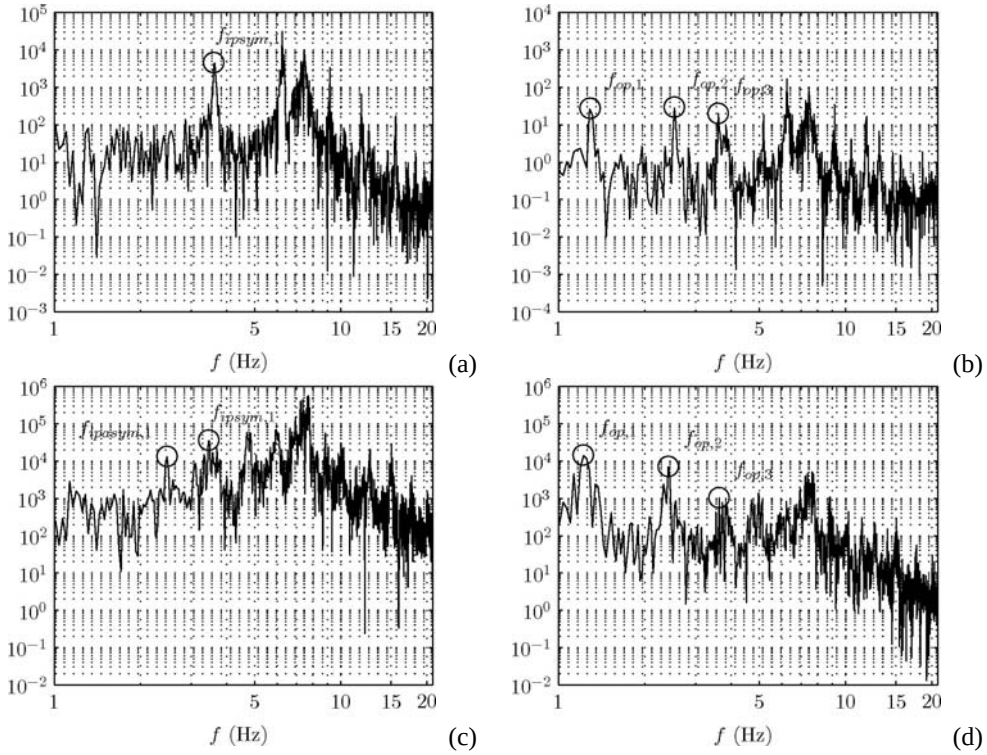

Figure 5.4 Density Spectra with a mean wind speed U about 16 m/s: (a) Laminar flow, axial load cell; (b) Laminar flow, drag force cell; (c) Turbulent flow, axial load cell; (d) Turbulent flow, drag force cell.

In Fig. 5.4 peaks with the identification of corresponding frequency were highlighted. In particular, it can be observed from Fig. 5.4a and Fig. 5.4c the peaks corresponding to out-of-plane modes: this seems obvious for test in turbulent flow, but it was also found in laminar flow due to the small natural turbulence of wind tunnel, even in smooth conditions, and to the wake efforts on the cable.

Motion	f_1 (Hz)	f_2 (Hz)	f_3 (Hz)
Out of plane	1.22	2.43	3.65
In plane, antisymmetric	2.43	4.86	7.30
In plane, symmetric	3.48	5.97	8.45

Table 5.1 First three natural frequencies for cable motion

Eventually, The data logged from the cells measuring the axial load and the along-wind reaction were elaborated to check their stochastic characteristics (in terms of standard deviation, skewness and kurtosis). The results were reported in Fig. 5.5.

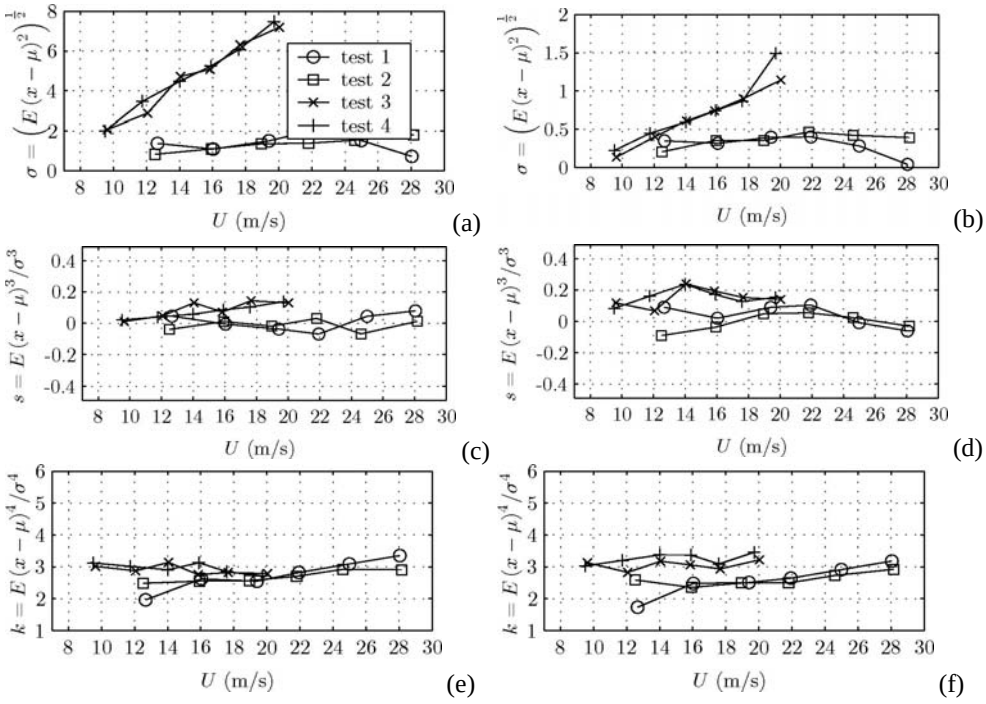

Figure 5.5 Standard deviation (a), skewness (c) and kurtosis (e) of axial load cells and standard deviation (b), skewness (d) and kurtosis (f) of drag load cells.

From the figures, it can be observed that the standard deviation σ in turbulent flow assumed bigger values that in laminar flow. Moreover, it tended to increase with increasing wind speed. Differences can be found analyzing the skewness: actually, even if the value remained quite close to 0, which corresponds to a symmetric distribution, in laminar flow it was almost constant, while in turbulent flow it showed a slight increasing trend. Finally, analyzing the kurtosis, it can be observed that, while in turbulent flow the values were about 3 in the whole range of wind speed, in laminar flow, at low speed, the distribution was less outlier-prone than the normal one. Nevertheless, from the elaborated data of performed test, it can be observed that in turbulent flow the values do not differ significantly from those corresponding to a Gaussian distribution ($s = 0$ and $k = 3$). These results are of significant interest in the evaluation of fatigue life of cables,

where a complete statistical characterization of the forces induced by wind turbulence is necessary.

5.2.3 Numerical modeling of the cable

The cable was modeled numerically assuming a geometrical non-linear behaviour. To solve the problem, the Finite Element Method was used adopting a 3-D two joints truss. The elastic and geometric stiffness matrices were determined assuming large displacements, large rotations and small deformations [c] simplifying in this way the model. The problem was solved by means of a modified Newton-Raphson algorithm; the analysis in time domain was carried out by means of H.H.T. (Hilbert-Hughes-Taylor) method, which is a generalization of Newmark method [4, 5].

The cable used in experimental tests was modeled assuming for the axial stiffness, the mass density, the overall length and the initial sag the values of the experimental model.

To check the behavior of the numerical model of the cable, a first comparison was performed using the data obtained from the experimental tests. At first, the comparison was performed by means of a quasi-static analysis, adopting the drag coefficient estimated above. In Fig. 5.6 the increment of axial force and the along-wind midspan displacement are reported for experimental tests and numerical analysis, and a good agreement can be observed.

Then, to analyze the dynamical behaviour of the cable a simulation of wind field acting on the cable was performed, through a simplified approach which considered the wind loads to be independent stochastic processes [6]. The simulation of wind time histories was performed by means of superposition of sinusoidal waves as in [d]. The results obtained in terms of the coefficient of variation, skewness and kurtosis of the axial load in the cable are reported in Fig. 5.7.

A good agreement between the numerical and experimental results can be noticed in terms of the statistical moments: in particular, the numerical results seems to confirm that the response of the cable used in the present work is almost Gaussian, with a skewness of about 0 and a kurtosis of 3. Nevertheless, skewness shows a slight increasing tendency at increasing wind speeds

Further experimental and numerical test are planned to check the influence of different flow characteristics and sag-to-span ratio on the stochastic characteristics of the response: a first step is shown in [7].

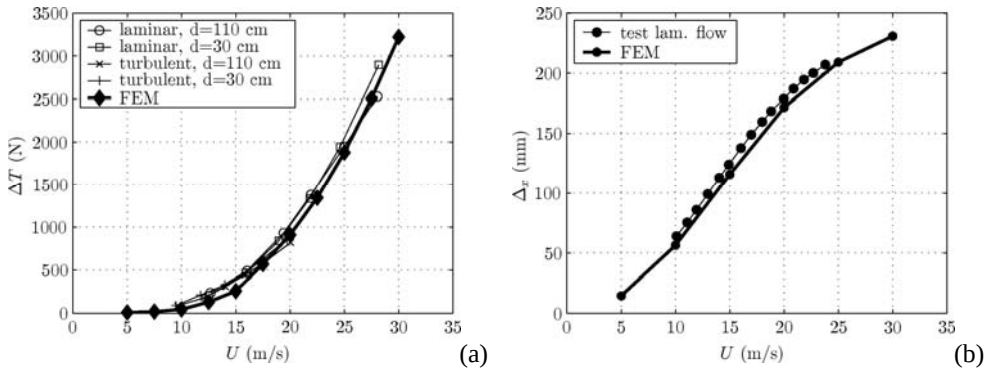

Figure 5.6 Comparison of increments of axial load (a) and along-wind displacement (b).

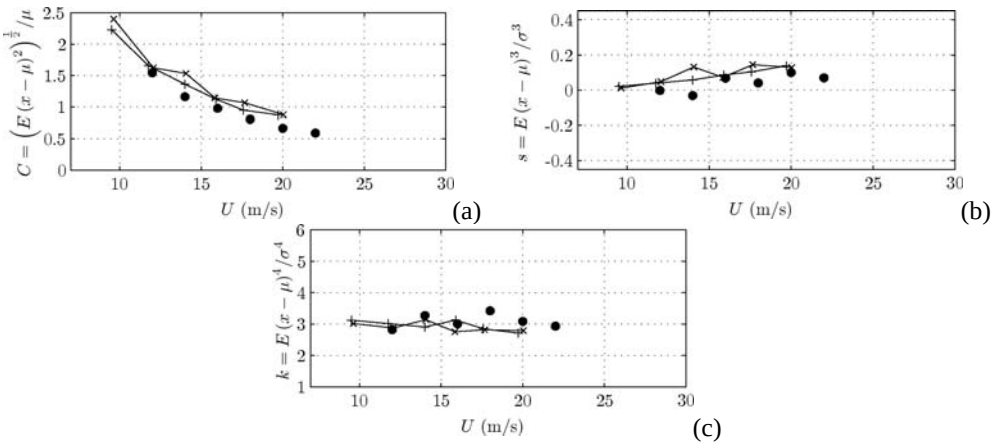

Figure 5.7 **C**omparison between numerical and experimental results in turbulent flow: (a) coefficient of variation, (b) skewness, (c) kurtosis

5.3 VORTEX SHEDDING INDUCED LOAD

An analytical model and a numerical model of the interaction between the action due to vortex shedding in lock-in condition and the response of the structure subjected to this loading situation have been developed.

5.3.1 Analytical model

The analytical model is based on empirical relations between the oscillation amplitude with a) the lock-in range amplitude; c) the lift coefficient value and c) the phase between the motion and the load.

The model estimates the value of the oscillation amplitude of an elastically suspended and mechanically dumped cylinder under vortex shedding load in stationary conditions as a function of the wind speed

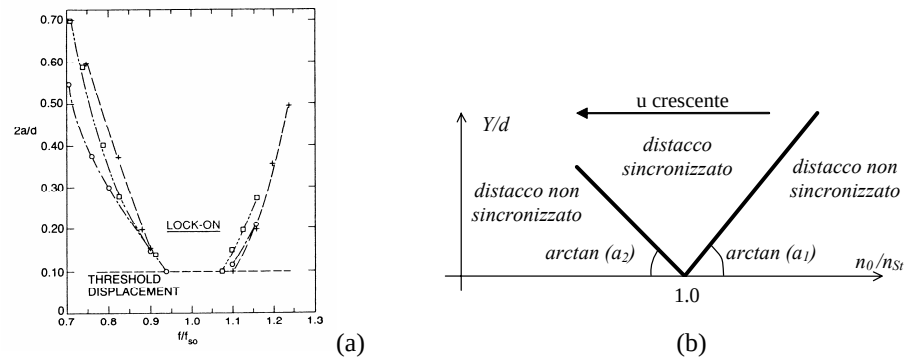

Figure 5.8 Experimental [e] (a) and simplified relationship between oscillation amplitude and lock-in range amplitude

The simplified relationships adopted in the model are compared with the original experimental ones in Figures 5.8, 5.9 and 5.10.

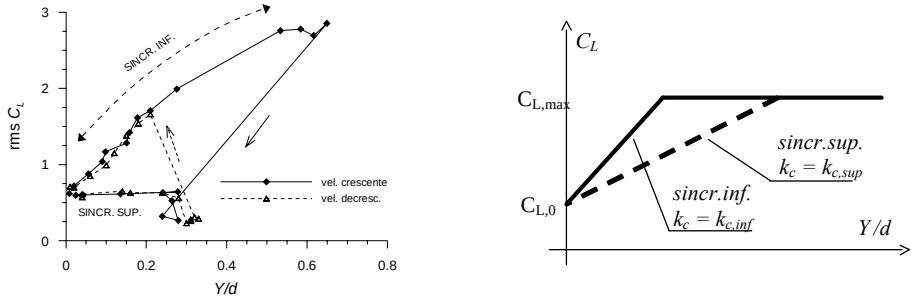

(a) (b)

Figure 5.9 Experimental [f] (a) and simplified relationship between oscillation amplitude and the lift coefficient

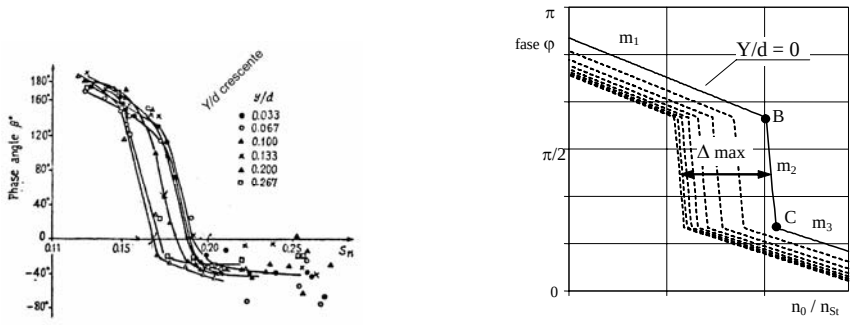

(a) (b)

Figure 5.10 Experimental [h] *($\beta = \varphi$; $S_M = St\ n_c/n_S$; y=Y)* (a) and simplified relationship between oscillation amplitude and the lift coefficient

The equivalent analytical expressions are:

Lock-in range vs. oscillation amplitude:

$$if\ \ Y/D \geq a_{i=1,2}\left(n_0/n_{St} - 1\right)\ \ then \quad n_{she} = n_c \cong n_0 \qquad (lock\text{-}in)$$

$$se\ \ Y/D < a_{i=1,2}\left(n_0/n_{St} - 1\right)\ then \quad n_{she} = n_{St}$$

Lift coefficient vs. oscillation amplitude and force-motion phase

$$C_L\left(Y/D, \varphi\right) = C_{L,0}\left[1 + k_c\left(\varphi\right)\frac{Y}{D}\right]\ ;\ \ C_L \leq C_{L,\max}$$

Phase shift vs. oscillation amplitude (Figure 5.10 (b))

$$\Delta\left(Y/d\right) = \Delta_{\max}\left(1 - e^{-k_\varphi Y/d}\right)$$

The evaluation of the oscillation amplitude Y corresponding to the wind speed $\bar{u}$ is made by means of an iterative process which is schematically described in Figure 5.11.

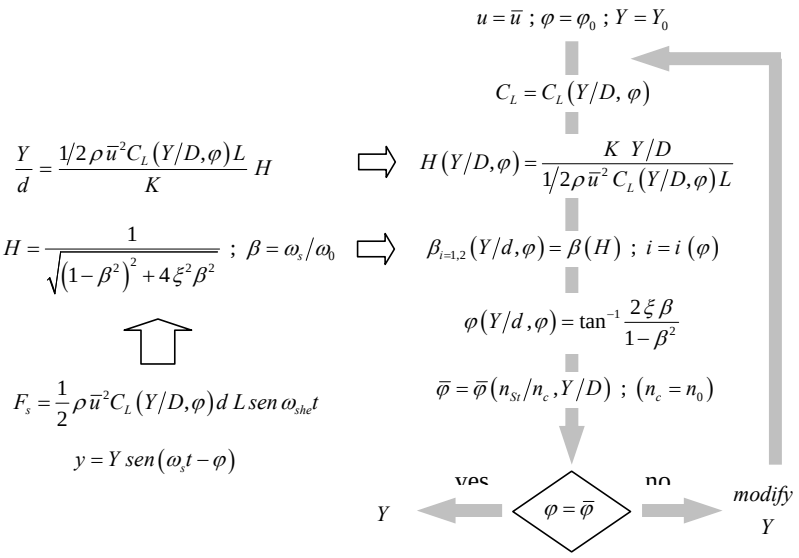

Figure 5.11 Iterative procedure for the evaluation of the oscillation amplitude in the analytical model

Theoretical previsions obtained from the analytical model match fairly with experimental observations. An example is shown in Figure 5.12

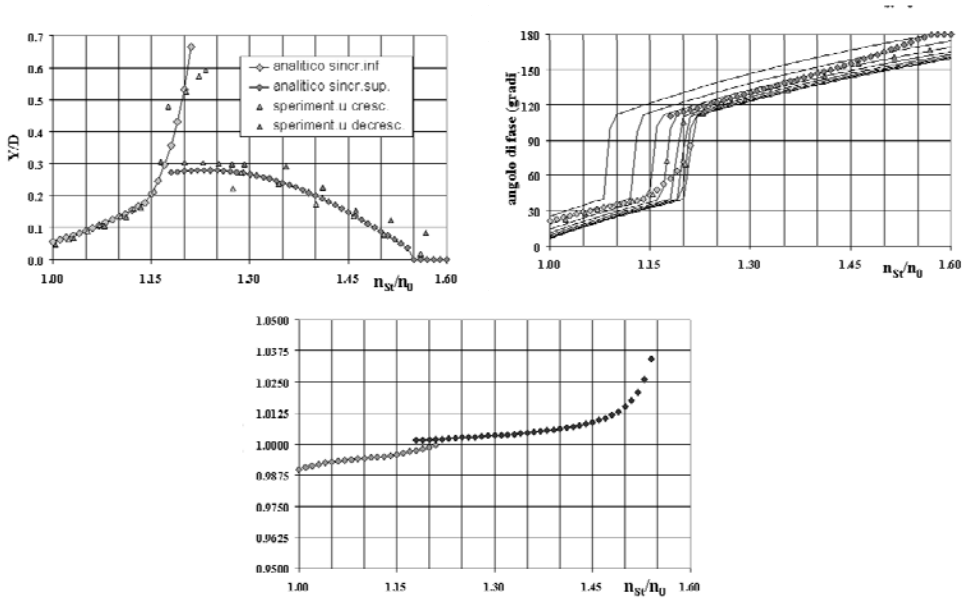

Figure 5.12 Tests DS4S e DS4D [f]: Comparison between experimental results and analytical simulation [8]

5.3.2 Numerical model

The analytical model can only estimate the maximum response amplitude of the oscillating system in stationary conditions. In order to simulate the response under a general wind speed history, a numerical model has been derived from the analytical one. The numerical model has been implemented in a general purpose f.e. code used for aeroelastic analyses of bridges, chimneys and cables. The model has been tested with reference to the usual wind tunnel experimental condition of a cylinder elastically suspended and mechanically dumped. The response to different wind speed histories have been obtained in the time domain by means of the β-Newmark method.

The basic principles remains the same of the analytical approach. In particular the numerical model adopts the same simplified relationship between oscillation amplitude, lift coefficient and load – motion phase described in Figures 5.9 and 5.10.

The load frequency at time t $n_{she}(t)$ is evaluated as $n_{she} = \beta(\varphi) n_o$, determining the value of $\varphi(Y/d)$ with the iterative process of Figure 5.13.

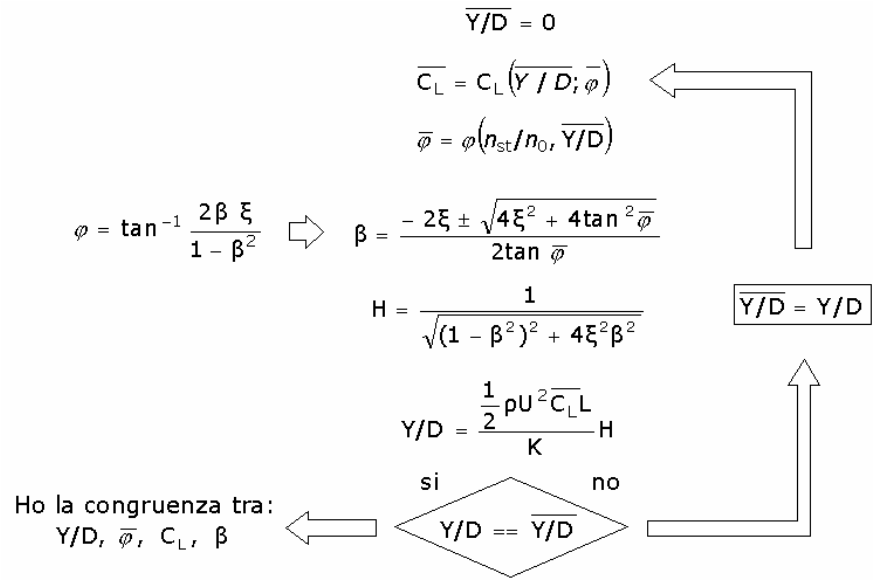

Figure 5.13 Iterative procedure for the evaluation of the load-motion phase and lift coefficient in the numerical model [9]

The same iterative process gives at the same time the value of the lift coefficient C_L

Differently from the case of the analytical model the amplitude of the lock-in range is not pre-determined as a function of the amplitude of the motion. The load frequency $n_{she}(t)$ is put identical to the Strouhal frequency $n_{St}(t)$ if the calculated force –motion phase is equal to 0 or 2π.

The numerical model is able to reproduce the hysteretic behaviour typical of the lock-in. The differences between the cases of increasing or decreasing wind speed is shown in Figures 5.14 and 5.15.

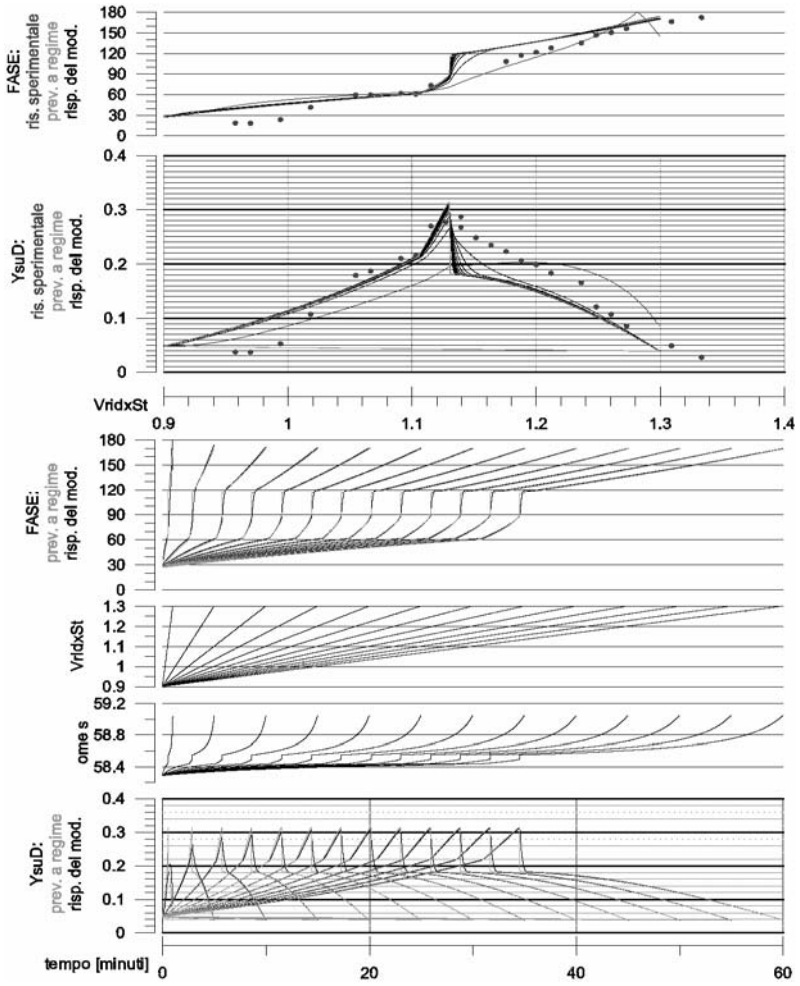

Figure 5.14 Numerical simulation in comparison with the experimental results (Feng 1968 ξ=0.181% [g])

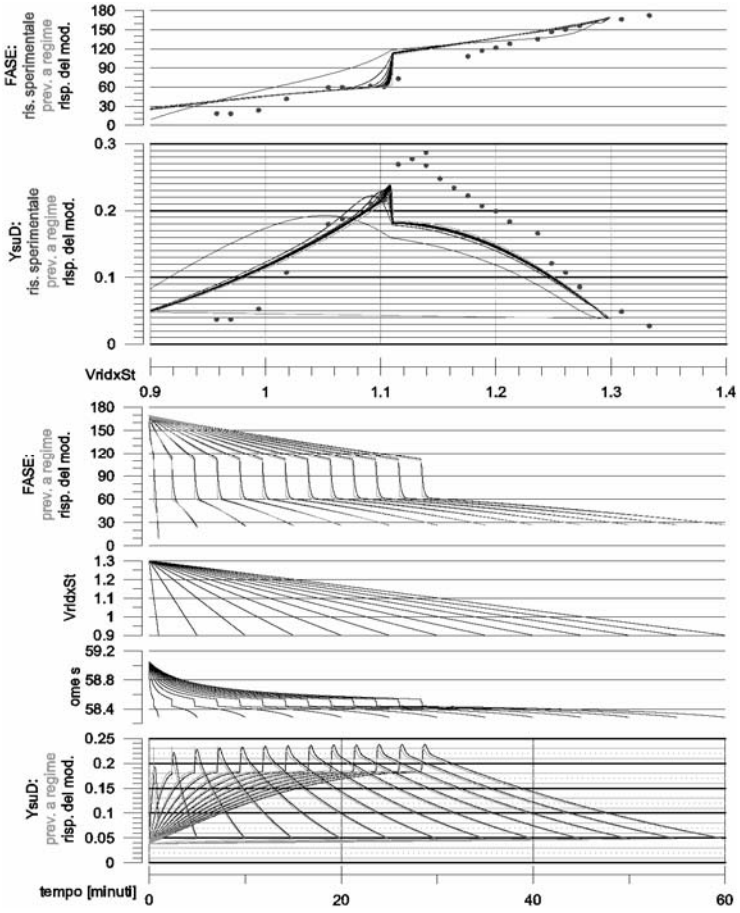

Figure 5.15 Numerical simulation in comparison with the experimental results (Feng 1968 ξ=0.181% [g])

5.4 BASIC REFERENCE

[a] ESDU 1980: *Data Item 80025, Mean forces, Pressures and Flow Field Velocities for Circular Cylinderical Structures: Single Cylinder with Two-dimensional Flow*. ESDU International Inc., London

[b] Irvine M. 1981. *Cable Structures*. Dover Pubblica-tions Inc., New York

[c] Bathe K.-J.1982. Finite element procedures in engineering analysis. Prentice-Hall Inc., New Jersey

[d] Shinozuka, M., Jan., C.-M. 1972. Digital simulation of random processes and its applications. *Journal of Sound and vibration* **25**(1), 111-128

[e] Koopmann G.H. 1967. The vortex wakes of vibrating cylinders at low Reynolds numbers. Journal of Fluid Mechanics, 28, p. 501.

[f] Fathi S. 2001.Vibrazioni strutturali across-wind per distacco di vortici. Tesi di dottorato, Università degli Studi "G. d'Annunzio" di Chieti-Pescara, 2001

[g] Feng C.C. 1968. The measurement of vortex induced effects in flow past stationary and oscillating circular and D-section cylinders. Master Dissertation, University of British Columbia (USA).

[h] Yano T., Takahara S. 1971. Study on unsteady aerodynamic forces on an oscillating cylinder. 3th International Conference on Wind Effects on Building and Structures, Tokio, p. 737

5.11 LIST OF PUBLICATIONS

[1] Bartoli G., Cluni F., Gusella V., Procino L. 2004. Dinamica del cavo sotto l'azione del vento: analisi sperimentale in galleria del vento. *Proc. 8° Conv. Nazionale Ingegneria del Vento (IN-VENTO-2004), Reggio Calabria, Italy*

[2] Bartoli G., Cluni F., Gusella V. 2004. Wind Tunnel Scale Model Testing of Suspended Cables, *Proc. 5th Inter. Coll. .Bluff Body Aerodyn. App. - BBAA V, Ottawa, Canada*

[3] Bartoli G., Cluni F., Gusella V., Procino L. 2006. Dynamics of cable under wind action: wind tunnel experimental analysis". *Journal of Wind Engineering and Industrial Aerodynamics*, **94**, 259-273

[4] Cluni F., Gusella V. 2004. Random vibrations of cables under wind loading: experimental tests and numerical comparison. *Proc. 3rd Int. Conf. on Adv. Struct. Eng. .Mech. (ASEM'04), Seul, Korea*

[5] Cluni F., Gusella V. 2004. Analisi numerica delle vibrazioni del cavo sotto vento e confronto sperimentale. *Proc. 2° workshop "Problemi di vibrazioni nelle strutture civili e nelle costruzioni meccaniche", Perugia, Italy*

[6] Cluni F., Gusella V. 2005. Fatigue safety of cables under wind loading. *Proc. Safety Reliab. Eng. Syst. Struct. (ICOSSAR 2005), Rome, Italy*

[7] Cluni F. 2005. Comportamento dinamico dei cavi sotto l'azione del vento: modelli numerici e prove sperimentali. *Proc. 17° Congr. Mecc. Teor. Appl. (AIMETA'05), Firenze, Italy*

[8] Noè S., Fathi S., D'Asdia P. 2004. Modello analitico per la stima della ampiezza di oscillazione per distacco di vortici. *Proc. 8° Conv. Nazionale Ingegneria del Vento (IN-VENTO-2004), Reggio Calabria, Italy*

[9] Noè S, Chessa P. 2006. Modello numerico del carico da distacco di vortici. *Proc. 9° Conv. Nazionale Ingegneria del Vento (IN-VENTO-2006), Pescara, Italy*

WITH CONTRIBUTION FROM:

Gianni Bartoli, University of Florence
Federico Cluni, University of Perugia
Vittorio Gusella, University of Perugia
Lorenzo Procino, University of Florence

6 Pedestrian wind comfort

Francesco Ricciardelli
University of Reggio Calabria

6.1 INTRODUCTION

Besides safety assessments, the issue of the serviceability of wind exposed structures is relevant. The discomfort associated with wind induced vibrations is in many cases the most stringent condition to be considered in the design stage of a large variety of wind exposed structures. In addition to that there is the direct effect of wind on humans which, even though not associated with any structural behaviour, has to taken into account in urban planning and building architecture. These two causes of discomfort and their effects have been summarised in figure 6.1, in which wind is seen as the main cause of discomfort, and the structure as a filter of the wind input to the human perception. Disregarding the indirect effects of wind, that is those deriving from structural vibration which have been deeply investigated in the past (e.g. Griffin 1990), in this chapter some issues concerning the direct action of wind on humans in the urban environment will be dealt with. In particular the two topics of the human perception and of the wind characteristics will be considered, to be seen as a resistance and an action, respectively, if the language of structural design is adopted.

6.2 PEDESTRIAN WIND COMFORT

Wind can be a direct cause of discomfort for humans, when particular orographic conditions or building arrangements give rise to a high windiness at the street level. Street channelling flows, diverting effects caused by tall buildings, particular geometric arrangements of buildings and other constructions can all be caused of particular local flow conditions, to be considered in the planning of new developments or in the design of new buildings.

A fully consistent approach to the problem would require two sets of data, which in most cases are available only with a certain degree of approximation. On the one hand, the human perception of windiness, which is strongly related to factors such ad psychology and physiology, and the human reaction (to be measured through capability of individuals of persisting in their activities in a windy environment), not easily described in a mathematical way. On the other hand, statistics are required of the wind speed at the locations of interest, which require knowledge of the local wind climate and of the characteristics of the flow at particular locations in the lower Urban

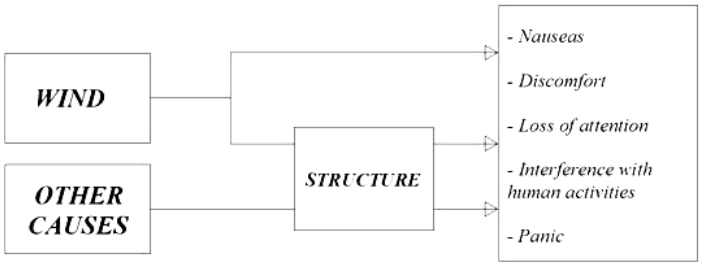

Figure 6.1 Direct and indirect wind-induced discomfort

Boundary Layer. Based on the difficulty of achieving a consistent description of the availability (i.e. of the maximum windiness acceptable) and of the demand (i.e. of the windiness of the site), usually rather simple models are used, in which the human perception is related to only one parameter of the wind velocity, and the windiness is characterised by the statistics of the same parameter.

The results of the assessments provide a measure of the quality of the open spaces, therefore of their commercial value. In addition, very high winds and in particular highly gusty winds at the street level can also become dangerous for pedestrian, in which case the issue of safety of pedestrian has also to be considered , together with that of comfort.

6.3 WIND PERCEPTION AND EFFECTS ON HUMANS

Perception of the wind discomfort cannot be described through an objective numerical parameter, as perception itself is subjective. Therefore the evaluation of the pedestrian wind comfort is usually carried out through the analysis of the outcome of interviews carried out on populations of pedestrians. An example of the results obtained using such approach is shown in figure 6.2, taken from Sasaki et al. (2000). The figure confirms the belief that the sensibility to the pure wind velocity is moderate and, therefore, for a consistent evaluation of the wind comfort a number of parameters have to be taken into account. These parameters are of a physical nature (e.g. humidity, temperature, exposure to solar radiation etc.) and of a physiological and psychological nature (e.g. type of activity, exposure time, expectations, etc.), with the two families of parameters contributing by the same amount to the final perception. Based on this observation a complex “perception” index would be required to appropriately define the effects of the climate on the human activities. Such an approach has been used in the past to evaluate indoor comfort, but to the best of the present knowledge it has not yet been applied to engineering evaluations of outdoor comfort. While a numerical description can be given for physical parameters, the difficulty in accounting for physiological and psychological parameters is in that only a qualitative description of their effects is available. The interaction among non-physical parameters is schematised in figure 6.3.

What is, instead, usually done is define threshold values of the wind velocity (either mean or peak value), which allow a certain activity to be carried out with prescribed levels of comfort, and this can be done either in a deterministic or in probabilistic form. In other words, for a range of possible activities the maximum values of the wind velocity are given, allowing that particular activity to be carried out, e.g., with ease, with some difficulties or with major difficulties. A second approach is that which is based on one single reference wind velocity, for which it is given

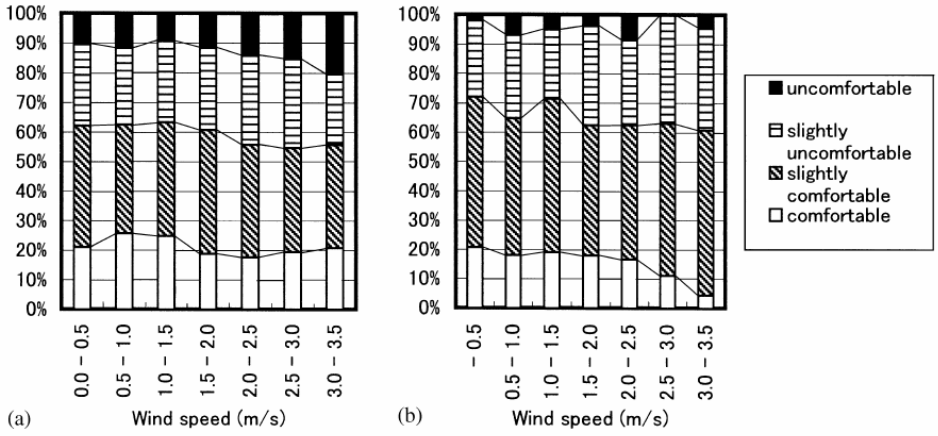

Figure 6.2 Variation of the wind comfort after Sasaki et al. (2000)

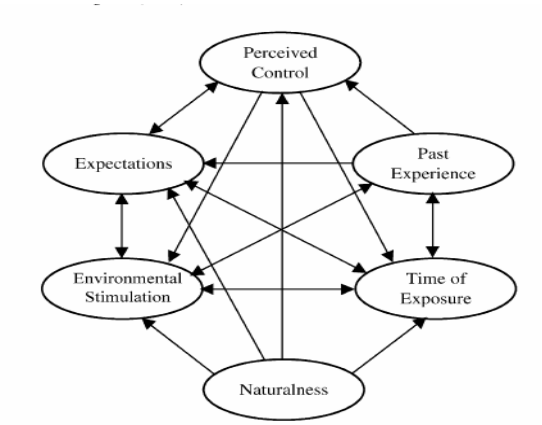

Figure 6.3 Interaction of physiological and psychological parameters (after *Nikolopoulou & Steemers., 2003*)

the probability that each activity is carried out at given level of comfort. A detailed list of threshold valued of the wind velocity can be found in Bottema (2000).

The criteria in use in worldwide Institutions have been summarised by Delpech et al. (2005). The criterion in use in France at CSTB refers to a gust speed evaluated adding to the mean wind velocity evaluated over a period of 15 minutes one standard deviation of the turbulent fluctuations. The probability distribution of such gust speed is evaluated based on the available data, and compared to the threshold value of 3.6 m/s. The maximum acceptable probability of exceedance of the threshold is then given, depending on the activity. In particular, for a steady position the gust velocity must exceed the value of 3.6 m/s with a frequency lower than 0.05, for a

Activity	Area	Wind comfort level		
		Acceptable	Unpleasant	Very unpleasant
Quick walk	Pavements, paths	0.43	0.50	0.53
Slow walk	Parks, working areas	0.23	0.34	0.53
Standing/sitting Short time	Malls, promenades	0.06	0.15	0.53
Standing/sitting Long time	Street restaurants and theatres	0.001	0.03	0.53

Table 6.1 Maximum probability of exceedance of the 5 m/s threshold mean wind velocity

Activity	Wind comfort level	
	Acceptable	Unacceptable
Quick walk	8.25 m/s with P<0.02	10.95 m/s with P<0.02
Slow walk	5.6 m/s with P<0.06	8.25 m/s with P<0.04
Standing	3.35 m/s with P<0.06	5.6 m/s with P<0.06
Sitting	3.35 m/s with P<0.04	5.6 m/s with P<0.01

Table 6.2 Maximum probability of exceedance of the threshold wind velocities

regular walking it must exceed the threshold with a frequency lower than 0.10, and for a brisk walking the maximum frequency of exceedance is 0.20.

The criterion used at DNW following the Dutch code NEN 8100 is based on the statistics of the mean velocity. Five different classes of comfort are defined, and the class of a given site depends on the probability of exceedance of the threshold value of 5 m/s by the mean wind velocity. In particular for class A, B, C and D this probability has to be lower than 0.025, 0.05, 0.10, 0.20. Locations not classified in any of the above classes are considered of class E.

The mean wind velocity is considered also in Canada at Concordia University, averaged over a period of one hour, and the reference threshold is 4 m/s in winter and 6 m/s in the summer, which somehow implicitly accounts for factors other than the simple wind speed, such as temperature, humidity and pedestrian expectations. The threshold values must not be exceeded for more that 0.10 of the time in parks and sitting areas, for more that 0.15 of the time in main streets and areas of dense circulation of pedestrians, and for more than 0.25 of the time in secondary streets and areas of fast walking.

A more detailed criterion is that used in Denmark at DMI, based again on the statistics of the mean wind speed, to be compared with the threshold value of 5 m/s. In table 6.1 the levels of performance are given for four different activities, each associated with possible locations.

Finally, the criterion used in the United Kingdom at BRE refers to threshold values of the mean wind velocity corresponding to the Beaufort wind velocity scale. In table 6.2 the wind velocities and the maximum probabilities of exceedance are given for four different activities.

6.4 CHARACTERISATION OF WIND ACTION

The statistics of the mean or peak wind velocity used in the criteria mentioned in the previous section are the result of the combination of the wind climate with the characteristics of the air circulation in the lower Urban Boundary Layer. What is usually done is relate the statistics of either the mean or the gust wind velocity at locations at the pedestrian level to those of the mean wind velocity at a reference height.

The probability that the mean wind speed at reference height exceeds a given threshold is usually described through a Weibull distribution, whose parameters are calibrated based on a meteorological study, consistently with what commonly done in other fields of Wind Engineering. The characteristics of the wind flow in the urban environment are known to be quite different from those of a Turbulent Boundary Layer naturally developed over a homogeneous rough surface (Ricciardelli & Polimeno, 2006). The boundary layer over a city centre is made of an External Layer, in which the characteristics of the flow are not influenced by the change in roughness occurring in the city, and an Urban Boundary Layer, in which the characteristics of the flow are associated with the large scale, inhomogeneous roughness which characterises the city centre, and in which the hypotheses of the Monin-Obukhov Similarity theory are not met. The lower portion of the Urban Boundary Layer is termed Internal Layer or Surface Layer, which extends up to an elevation of approximately 10% the total depth of the boundary layer. In the Surface Layer the flow is strongly affected by the local geometry, i.e. the one-point characteristics of the flow can be quite different from their spatially averaged values. The Surface Layer can be further separated into an Inertial Sublayer and a Roughness Sublayer, with the separation ranging between an elevation of twice to five times the average height of the buildings (the lower bound being the most common value in the literature). This is also the elevation where the Reynolds stresses take their maximum values. The characteristics of the flow in the Roughness Sublayer is strongly dependent on the building arrangement, and relevant parameters are the uniformity of the building height and the building aspect ratio, i.e. the ratio of the average building height to the average street width, H/W.

Based on these observations it is clear that a consistent description of the characteristics of the flow at the pedestrian level can be achieved only through a direct measurement in the wind tunnel, which confirm that the characteristics of the wind fluctuations are quite different from those found in the upper Boundary Layer. To show this, in figure 6.4 the Probability Density Functions of the longitudinal turbulent fluctuations are shown, in a rectangular street arrangement, at an elevation of about 3 m, in a transversal and longitudinal street canyon, respectively. From the plots it can be seen that while in the case of a longitudinal canyon the Probability Density Function of the velocity fluctuations can be reasonably and with acceptable accuracy assumed of a Gaussian shape, in the transversal canyon the Probability Density Function is strongly skewed to the left. That non-Gaussianity of the Probability Density Function of the turbulent fluctuations was reported by Yim el al. (2000) who suggested that Gram-Charlier distribution be used instead.

The non-Gaussianity of the probability distribution of the wind velocity fluctuations is reflected in the values of the gust factor. In figure 6.5 the profiles of the gust factors are shown, as measured in the wind tunnel, for two locations in a transversal and in a longitudinal street canyon, as evaluated on a averaging time of 3600 sec. At both locations the gust factors in the Canopy Layer are larger than the value of 3.5, appropriate for a Gaussian white noise and commonly adopted in the evaluation of wind loads. Especially in the transversal canyon, the gust factor can reach values as high as 6.5, and takes a value of 5.9 at the pedestrian level. Above the canopies, however, the values of the peak factor tend to be again in the range of 3 to 4. In the figure the

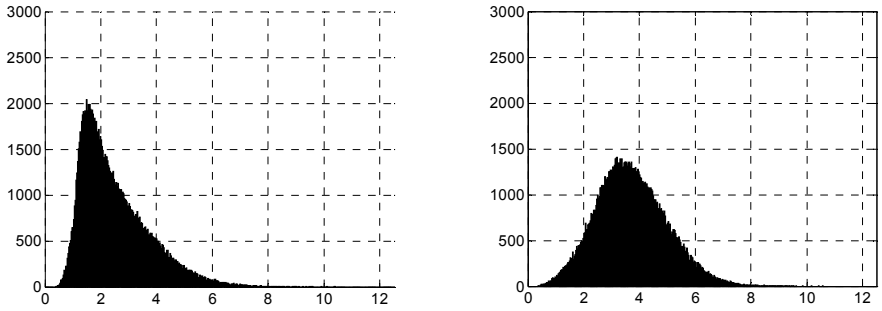

(*a*) (*b*)

Figure 6.4 Probability distribution of the wind velocity fluctuations in a transversal (*a*) and longitudinal (*b*) street canyon

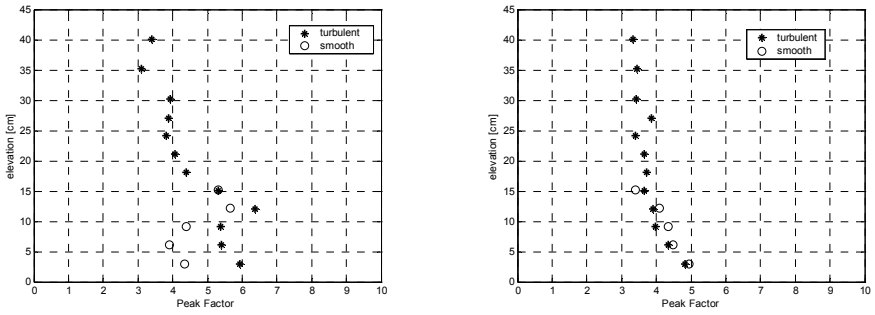

(*a*) (*b*)

Figure 6.5 Gust factor the wind velocity in a transversal (*a*) and longitudinal (*b*) street canyon

peak factors measured in the case of an oncoming smooth flow are also shown, as measured in the Canopy Layer. In the longitudinal canyon these are rather similar to the values measured for a turbulent oncoming flow, but in the transversal canyon the values measured for the two flow condition are different, with lower values measured in smooth flow. This confirms that two qualitatively different types of flow exist, one taking place in longitudinal canyons, where a channelling effect exists making the characteristics of the flow in the canyon similar to those taking place above the canopies, and one taking place in the transversal canyons whose characteristics are very little related to those of the oncoming flow, but rather related to the local geometry of the constructions.

To better justify this statement, in figure 6.6 the spectra of the longitudinal turbulence are shown. In figure 6.6a and 6.69b the spectra at a location in the transversal canyon are plotted, at elevations z/H=0.2, z/H=0.6 and z/H=1, H being the building height, in smooth and turbulent flow, respectively. It can be seen that for each elevation the spectra in smooth and turbulent flow are almost the same. In figure 6.6c and 6.6d the spectra at a location in the longitudinal canyon are shown, for the same values of z/H, again for the smooth and turbulent flow conditions. In this case the spectra are rather different for the two flow regimes, with those of the turbulent flow regime being centred at much lower frequencies than those of the smooth flow regime.

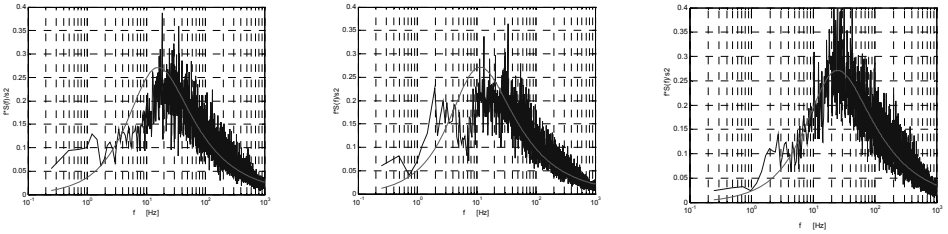

(*a*) – transversal canyon - smooth

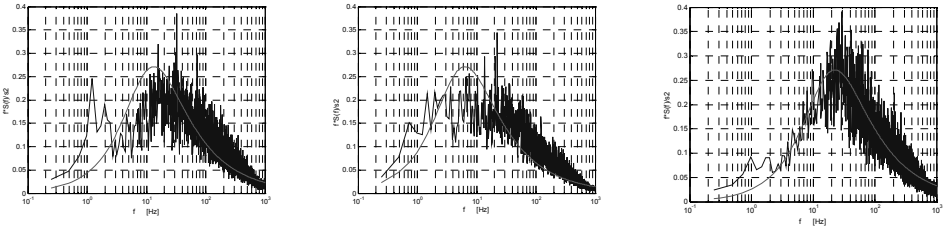

(*b*) – transversal canyon - turbulent

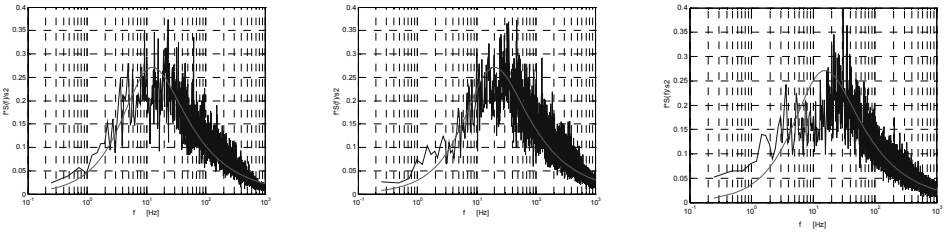

(*c*) – longitudinal canyon - smooth

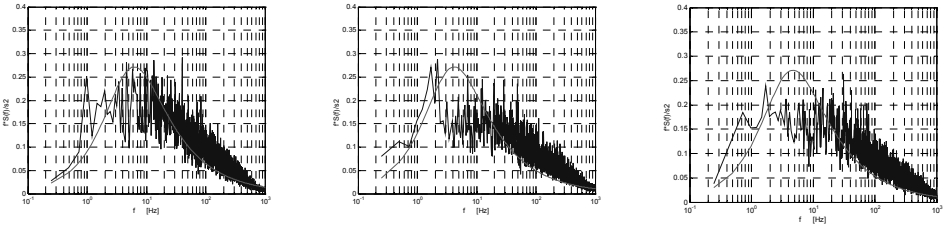

(*d*) – longitudinal canyon - turbulent

Figure 6.6 Spectra of the wind velocity fluctuations in a transversal and longitudinal street canyon, for a smooth and turbulent oncoming flow

6.5 SIMPLIFIED COMFORT ASSESSMENT

The criteria of section 1.3 are now applied to the flow measurements carried out in the wind tunnel on a regular orthogonal street arrangement. This allows comparing the results obtained

through the application of the different criteria, and gives a tool for the preliminary assessment of the comfort in a regular street arrangement, associated with given wind climate.

It is assumed that the distribution of the reference mean wind velocities is given through a Weibull distribution, that is the probability that the reference mean wind velocity U_{10} is larger than a prescribed value u is:

$$P_{U_{10}}(u) = \exp\left[-\left(\frac{u}{c}\right)^k\right] \tag{6.1}$$

If the ratio R between the mean velocity at a prescribed point at the pedestrian level $\overline{u}_p$, and the reference wind velocity U_{10} is known from wind tunnel measurements, and if it is assumed that aerodynamics is linear, then the probability distribution of eq. (6.1) can be applied also to the pedestrian mean velocity, that is:

$$P_{\overline{u}_p}(u) = \exp\left[-\left(\frac{u}{R \cdot c}\right)^k\right] \tag{6.2}$$

Eq. (6.2) can be directly used for the criteria based on the mean wind velocity to relate the two parameters c and k of the Weibull distribution, i.e. to evaluate the maximum value of the c parameter that fulfils the criterion requirement for a specified value of the k parameter. That is:

$$c \le \frac{\overline{u}}{R}\left[-\ln\left(-\overline{P}\right)\right]^{-1/k} \tag{6.3}$$

in which $\overline{u}$ is the mean wind velocity threshold and $\overline{P}$ is the maximum probability of exceedance of $\overline{u}$, both associated with the particular comfort criterion applied.

A similar approach can be used for the criteria based on the gust velocity, in which case eq. (6.2) becomes:

$$P_{\hat{u}_p}(u) = \exp\left[-\left(\frac{u - g\sigma}{R \cdot c}\right)^k\right] \tag{6.4}$$

in which σ is the RMS of the turbulent fluctuations and g a prescribed gust factor. In this case eq. (6.3) becomes:

$$c \le \frac{\overline{u} - \sigma}{R}\left[-\ln\left(-\overline{P}\right)\right]^{-1/k} \tag{6.5}$$

Eqs. (6.3) and (6.5) have been applied to the results of wind tunnel flow measurements on an orthogonal street arrangement presented in Ricciardelli & Polimeno 2006. Two locations have been considered, in a transversal and in a longitudinal street canyon, respectively. The quantities of interest are given in table 6.3.

In figures 6.7 through 6.11 the results of the calculations are shown. Figure 6.7 presents the results from the application of the criterion in use at DNW, and figure 6.8 those of the criterion in use at Concordia University, both based on the mean wind velocity. Comparison of the two sets of results shows that comfort level of DNW roughly correspond to acceptable comfort levels for a wintertime assessment after the Concordia criterion. In particular, comfort level D of the DNW criterion roughly corresponds to an acceptable level of comfort for secondary streets following the Concordia criterion. Comfort level C of the DNW criterion corresponds to an acceptable level of

	U_{10} [m/s]	$\overline{u}$ [m/s]	□ [m/s]	R
Transversal	6.7	2.5	1.2	0.37
Longitudinal		3.6	1.3	0.54

Table 6.3 Flow parameters measured in the wind tunnel

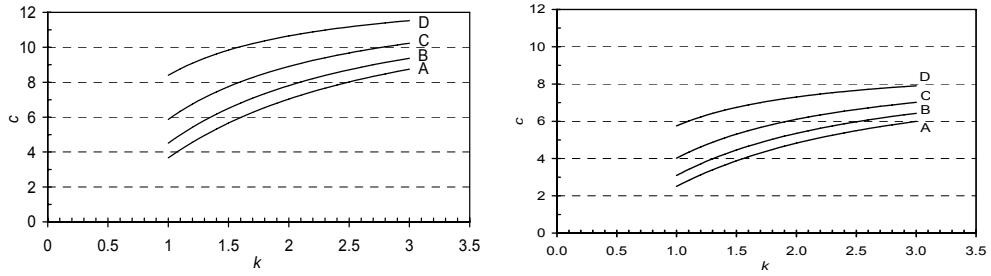

Figure 6.7 Results for the DNW criterion applied to the transversal (a) and longitudinal (b) canyon flow

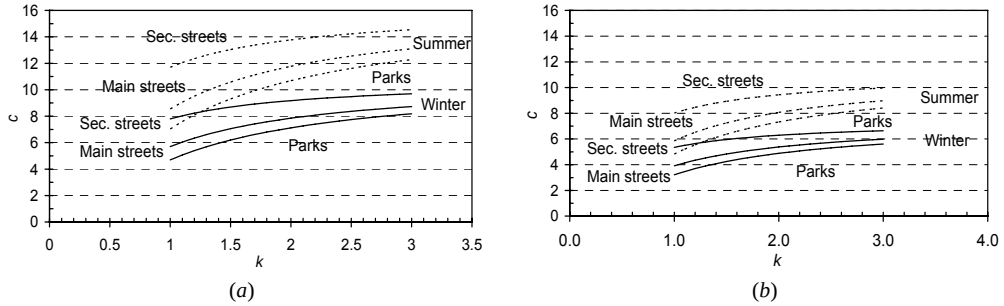

Figure 6.8 Results for the Concordia criterion applied to the transversal (a) and longitudinal (b) canyon flow

comfort for main streets following the Concordia criterion. Finally comfort level B and A are comparable to an acceptable level of comfort for parks when the Concordia criterion is applied.

In figure 6.9 the results of the application of the DMI criterion are shown. Comparison of these with those of the DNW criterion shows that comfort level D of the DNW criterion roughly corresponds to an acceptable level of comfort for a slow walk following the DMI criterion. Comfort level C of the DNW criterion corresponds to an acceptable level of comfort for a short time standing of the DMI criterion. Finally comfort level B and A are comparable to an acceptable level of comfort for a long time standing when the DMI criterion is applied.

In figure 6.10 the results deriving from the application of the BRE criterion are shown. Comparison of the curves obtained with those associated with the same activities and obtained through the application of the DMI criterion indicate that the two approaches bring quite different results.

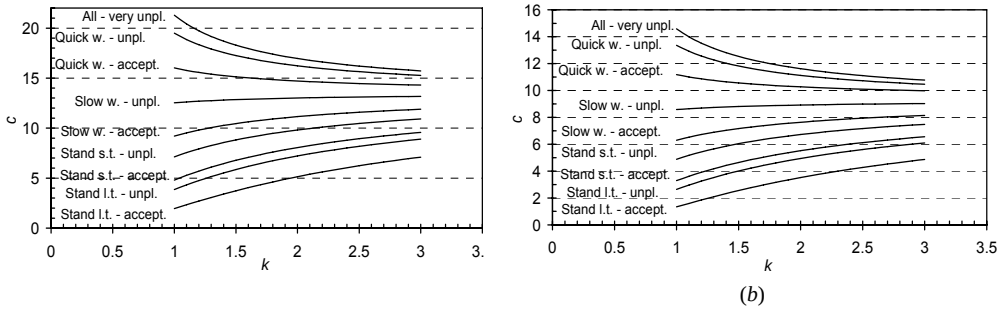

Figure 6.9 Results for the DMI criterion applied to the transversal (a) and longitudinal (b) canyon flow

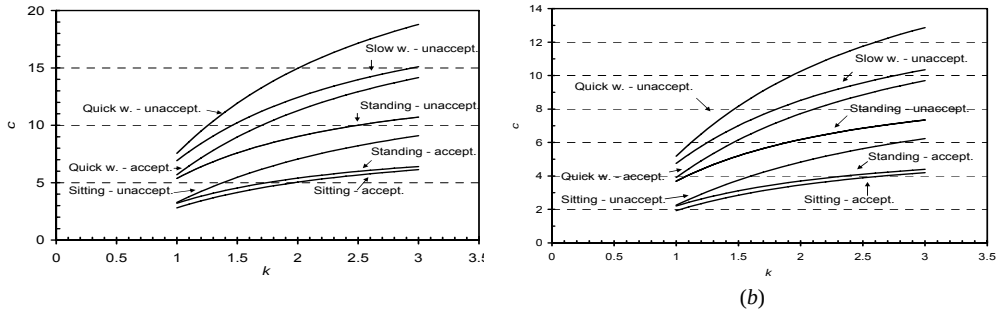

Figure 6.10 Results for the BRE criterion applied to the transversal (a) and longitudinal (b) canyon flow

Finally, in figure 6.11 the results obtained through the application of the CSTB criterion, which are based on a conventional peak velocity. Also in case comparison with the curves obtained from the application of the criteria in use at other Institutions shows a quite evident disagreement.

To summarise the results obtained, the particular case of k=2 is considered, that is the case in which a Raleigh distribution is used to describe the probability of exceedance of the mean wind velocity. In table 6.4 the values of the c constant are reported, as evaluated through the different criteria.

6.6 BASIC REFERENCE

[a] Griffin M.J. 1990. *Handbook of human vibration*. Elsevier Academic Press

[b] Sasaki R., Yamada M., Uematsu Y., Saeki H. 2000. Comfort environment assessment based on bodily sensation in open air: relationship between comfort sensation and meteorological factors. *J. Wind Eng. Ind. Aero*., 87, 93-110

[c] Bottema M. 2000. A method for optimization of wind discomfort criteria. *Building and Environment*, 35, 1-18

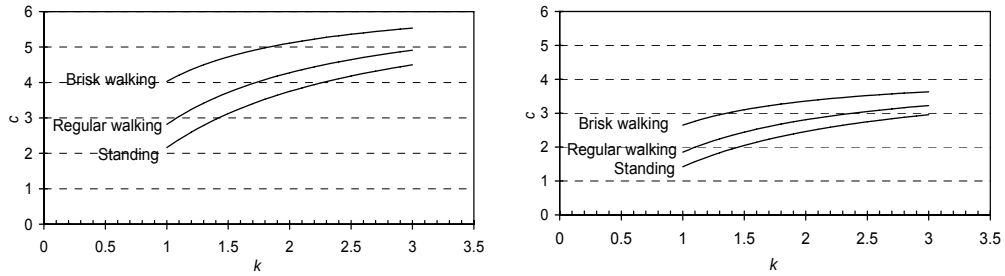

Figure 6.11 Results for the CSTB criterion applied to the transversal (a) and longitudinal (b) canyon flow

[d] Delpech P., Baker C.J., Blackmore P.A., Koss H., Sanz-Andres A., Stathopoulos T., Willemsen E. 2005. Pedestrian wind comfort assessment: a comparative study. *EACWE4, Fourth Euro. Afr. Conf. Wind Eng.*, Prague

[e] Yim Z.J., Chou C.R., Huang W.P. 2000. A study on distributions of the measured fluctuating wind velocity components. *Atmospheric Environ.*, 34, 1583-1590

6.7 LIST OF PUBLICATIONS

[1] Ricciardelli F., Polimeno S. 2004. Some experimental results concerning the characteristics of the wind flow in the canopy layer. *Urban Wind Engineering & Building Aerodynamics*, COST Action C14, Rhode-Saint-Genese

[2] Bartoli G, Ricciardelli F, Sepe V. 2004. Italian contribution to research in the field of Urban Wind Engineering and Building Aerodynamics: the WINDERFUL Project. *Urban Wind Engineering & Building Aerodynamics*, COST Action C14, Rhode-Saint-Genese

[3] Ricciardelli F., Polimeno S. 2004. Analisi delle caratteristiche dei campi di vento a bassa quota in ambiente urbano. *IN-VENTO 2004*, 8° Convegno Italiano di Ingegneria del Vento, Reggio Calabria

[4] Ricciardelli F., Polimeno S. 2006. Characteristics of the wind flow in the lower Urban Boundary Layer. *J. Wind Eng. Ind. Aero.*, to appear

WITH CONTRIBUTIONS FROM:

Carmela Lombardo, University of Reggio Calabria
Santo Polimeno, University of Reggio Calabria
Lorenzo Procino, CRIACIV

Activity	Institution	comments	*c* - transversal	*c* - longitudinal
Standing	DMI	Short time - acceptable	8.06	5.52
		Short time - unpleasant	9.81	6.72
		Long time - acceptable	5.14	3.52
		Long time - unpleasant	7.22	4.94
	BRE	Acceptable	5.40	3.70
		Unacceptable	9.02	6.18
	CSTB		3.75	2.46
Standing or sitting	Concordia	Winter	7.12	4.88
		Summer	10.69	7.32
Sitting	BRE	Acceptable	5.05	3.46
		Unacceptable	7.05	4.83
Slow walking	CSTB		4.27	2.81
	DMI	Acceptable	11.15	7.64
		Unpleasant	13.01	8.91
	BRE	Acceptable	9.02	6.18
		Unacceptable	12.43	8.52
Walking	Concordia	Main streets - winter	7.85	5.38
		Main streets - summer	11.77	8.07
		Main streets - winter	9.18	6.29
		Main streets - summer	13.77	9.43
Fast walking	CSTB		5.11	3.36
	DMI	Acceptable	14.71	10.27
		Unpleasant	16.23	11.12
	BRE	Acceptable	11.27	7.72
		Unacceptable	14.96	10.25
General	DNW	A	7.04	4.82
		B	7.81	5.35
		C	8.91	6.10
		D	10.65	7.30

Table 6.4 Comparison of the c parameter for the Raleigh distribution

7 On site experimental tests

Massimiliano Gioffrè
University of Perugia

7.1 INTRODUCTION

Experimental tests are the base of any scientific discipline since they can provide information to validate hypothesis on the observed phenomena. In particular, for engineering structures the results of experimental tests are fundamental for the accurate identification and modeling of complex structural systems and/or load and load-structure interactions.

When dealing with wind engineering problems the need of experimental information becomes even more crucial and this explain the great effort of the worldwide scientific community toward the development of experimental methods using both wind tunnel and on site tests. Although very important, the results obtained from wind tunnel tests have to be carefully interpreted given the well known scale problems that make the reproduction of the actual phenomena very difficult.

For this reason a part of the PERBACCO research project has been also devoted to on site full-scale experimental investigations, beside wind tunnel tests, to better understand two complex problems such as the identification of a special class of cable stayed masts used to support communication devices for mobile phone networks and the effects of the vortex-shedding load, with particular reference to the lock-in conditions, on the response of a cylindrical concrete chimney.

7.2 A REMOVABLE GUYED MAST FOR COMMUNICATION DEVICES

The main components of the mobile phone networks are the base stations. These are systems used to link mobile phones to the rest of mobile and fixed phone network and are mainly composed by the supporting structure, the communication devices (antennas and/or dishes), and the shelter used to place the equipment for controlling and running the transmission apparatus. The need to accommodate for the required volume of users at any given area in the different times of the year brings to base stations that have to be easily removable ("raw land site").

Several non trivial problems arise when designing, constructing and maintaining the supporting structure of such a site, which is usually a cable stayed mast. Among them, the estimation of the appropriate wind loads is quite difficult given the complex flow-structure interactions. The effectiveness of the stays is reduced because of their large angle with the

Figure 7.1 View of the cable stayed mast with the truss systems and the two pipe rods.

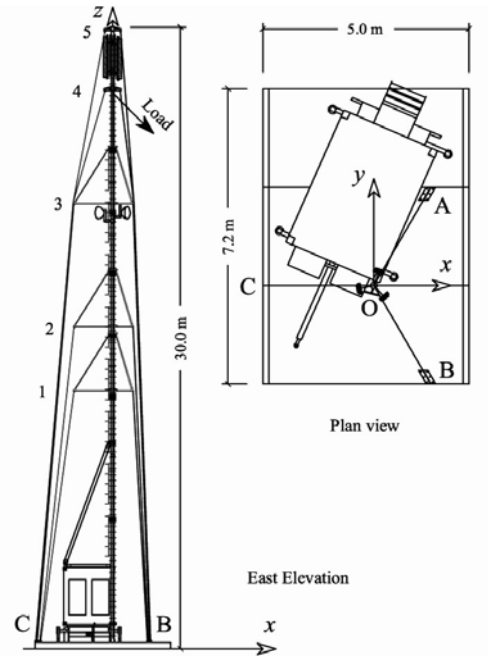

Figure 7.2 Elevation and plan view of the base station with the five orders of stays (1-5) and their plan positions (A-C).

ground, in order to limit the base dimensions of the mobile base station, and because of the cable slacking. The inherent slenderness of the structural system makes it prone to stability issues. The low-stiffness foundations, made of an assembly of steel beams and concrete slabs simply placed on the ground to obtain fast and removable installations, can easily increase the overall displacements. The soil-foundation-structure interactions are different from a site to another and they have to be accurately modeled to obtain reliable response evaluations. Deeper insights on these topics can be found in [a,b,c] where the results of wind tunnel tests to estimate the drag and lift coefficients on full-scale structural portions that support communication devices are reported.

The structural system studied in this research project by the Perugia Research Unit is a special class of cable-stayed mast where the connections between the cables and the post are made of a truss system (Fig. 7.1). This solution was introduced by Elettromontaggi s.r.l., Massa Martana, Perugia, Italy, on the classic cable stayed mast reported in [c] to improve its dynamic behavior and to overcome serious problems in terms of structural stability. The stays of the previous structural system were in fact at a very large angle with the ground giving very low lateral stiffness since they were directly connected to the mast.

The adopted truss system resembles what is used in the sailing boat masts where the stays are almost vertical but their performance in terms of lateral stiffness is improved connecting the stays to the crosstrees. Furthermore, the peak bending moments are reduced and the distribution of the internal forces along the mast height is more uniform then in the cable-stayed mast without the truss system.

Both these structures are quite sensitive to the assembling stage that makes the structural layout seldom predictable. It follows that the structural behavior is influenced by several

uncertain parameters that directly affect the response. The accurate modeling of the complex structural systems under investigation can be obtained with the information given by suitable on site experimental tests. Part of the research project was therefore focused on a set of experimental tests using load cells and strain gauges to record the static and dynamic response at several locations on the actual structure equipped with the truss system.

7.2.1 The supporting structure

The investigated structure is a cable stayed mast where the stays are connected to the post by a truss system. The prototype used in the tests is very similar to the structure described in [c] where more detailed information can be found.

The four main elements of the base station are the post, the stays with the truss systems, the foundation slab, and the shelter (Fig. 7.2).

The post is composed by five steel pipe elements of 6 m length connected by bolted flanges. All the elements but the higher have diameter 168.3 mm and thickness 12.5 mm. The last six meters are made of a steel pipe with smaller diameter and thickness of 139.7 mm and 10.0 mm, respectively. The mast supports the safety ladder, the cable racks, the connections to fix the stays, and the truss systems.

The stays have diameter of 10 mm and their directions form 120° angles in the plan view (A, B, and C in Fig. 7.2}). Two orders of three stays are directly connected to the post (heights 30 m and 27 m), while other three orders (heights 21 m, 15 m, and 12 m) are connected to the two-elements truss system with rectangular steel tube section (dimensions 60 mm x 40 mm, thickness 3 mm). One of the elements is horizontal and carries mainly compression force, while the other is diagonal and principally bears tensile force. All the cables are connected to the foundation slab by a tightening system used to provide a pre-tension of about 10KN in the installation stage.

The foundation slab is made of three precast elements, mixing steel beams and reinforced concrete, with plan dimension of 7.2 m x 5.0 m and thickness of 30 cm. The elements are connected by bolted flanges to give appropriate base stiffness. The supporting structure is designed to sustain up to six prismatic antennas (1.3 m or 2.0 m height) and up to four dishes with 60 cm diameter.

The prismatic shelter has aluminium supporting structure mounted on wheels to be easily moved. During the installation stage the wheels are unloaded using four extensible stabilizers and the mast is directly connected to the shelter with hinges at heights 0.93 m and 3.76 m. Furthermore, two pipe steel rods (thickness 10 mm) connect the upper part of the shelter frame to the post increasing its lateral stiffness.

7.2.2 Experimental setup

The main interest in planning the experimental setup was to have a sort of permanent full-scale laboratory that could be used several times preserving accuracy and effectiveness of the measurements.

The internal forces at some significant sections of the structural system are indirectly measured using pairs of strain gauges (120 Ohm electric resistance with temperature compensation) glued on the steel surface. In particular, two sections of the truss system connecting the stay of the third order, position C, are equipped with four strain gauges on the tube lateral surfaces near the connection with the post. Figure 7.3 shows one of the two strain gauges on the diagonal element at height of about 24 m.

Figure 7.3 Strain gauge on the diagonal element of the truss system protected from the environmental conditions..

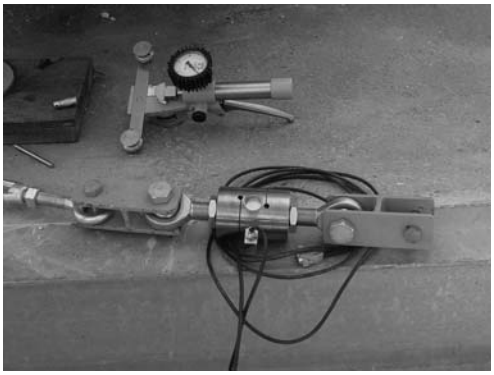

Figure 7.4 Load cell ready to be mounted in the stay and tensiometer for the manual measurements.

The coupled strain gauge is on the opposite lateral face at the same height, while the other two sensors are on the horizontal element at height of about 21 m. The instruments are protected against aggressive environmental conditions using special plastic covered by a silver foil to obtain a robust installation that can effectively perform during the load tests carried out at different times of the year. The picture in this figure also shows the bolted flange connection between the two higher pipe elements of the post and the hinged link of the diagonal member to the mast.

Four more sections on the post at heights of 21 m, 18 m, 12 m, and 9 m, are provided with pairs of strain gauges to measure the deformation in the OA plane (8 strain gauges) and OC plane (8 strain gauges). In order to obtain adequate durability of the sensors, special care was adopted in the installation procedures (e.g. preparing the steel surfaces, gluing and protecting the strain gauges, connecting the transmission cables) even if the access and working conditions were very difficult.

The axial load in the third order stays is measured by three load cells placed near the connections to the foundation slab (positions A, B, and C). A load cell is also used to measure the static load applied during one of the tests. Each cell has capacity of 75 KN and accuracy 2 mV/V. Figure 7.4 shows one of the load cells with the connecting system and the tensiometer used during the static load test to measure the axial load in the un-monitored stays.

The signals of the strain gauges and the load cells are converted by two synchronized Spider-8 acquisition systems each with 8 ADC digitizers, which use the 4.8 kHz carrying frequency technique and are connected to a personal computer by a serial interface RS-232.

The wiring system is optimized to reduce the signal loss minimizing the cable length using the cable rack that is completely available since no communication devices, such as antennas and/or dishes, are installed during the experimental tests. For the same reason the acquisition system and the personal computer are placed inside the shelter, which gives the possibility to execute the test with every kind of environmental conditions.

The mast displacements during the static load test are surveyed by a topographic station and a system of 20 reflecting targets and two optical prisms.

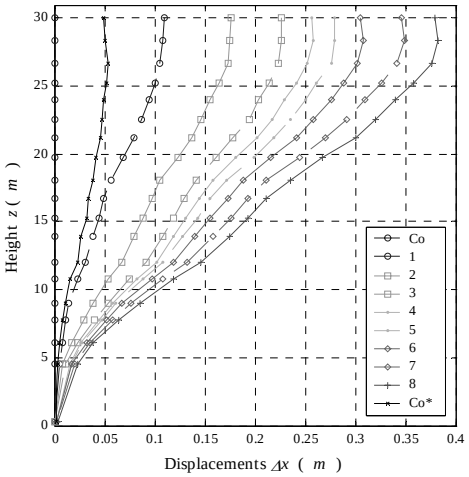

Figure 7.5 Relative displacements of the mast.

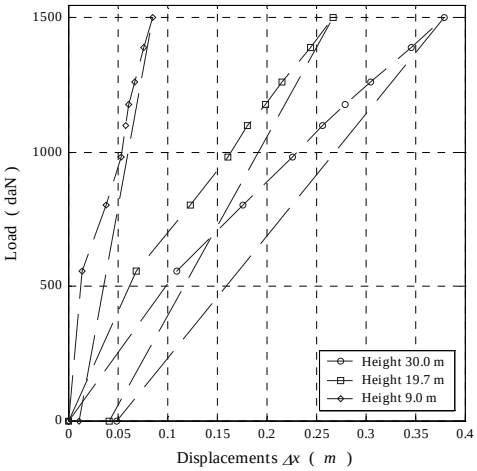

Figure 7.6 Relative displacements of the mast at three heights.

7.2.3 Experimental tests

Several experimental tests were performed on the prototype structure under investigation. In the following, the main results obtained during a static load test, a free vibration test, and a dynamic test recording the wind induced structural response will be reported.

The four load cells were calibrated with the unloaded configuration so that the absolute measure of the axial load was obtained. The strain gauges were calibrated with reference to the initial layout Co where all the stays are preloaded with approximately the same axial force of about 800 daN and the mast was placed in vertical position by sight inspection, like it is usually done in the actual installations.

During the static test the structure was point loaded by a winch that pulled a steel cable connected to the structure at the height of 27 m in the OC plane (i.e. plane x-z in Figure 7.2) and forming an angle of about 45° with the ground. The acquisition system continuously logged (sampling frequency 1 Hz) the strain time histories in the truss system (4 sensors) and the post (8 sensors in the OC plane), together with the axial load time series in the third order stays and in the load cable. The load was given with 8 incremental steps at the end of which the mast displacements were surveyed from the initial layout Co to the final unloaded structure Co*.

As a first tentative test, the free vibrations were obtained shaking one of the stays of the structure and recording simultaneously the structural response in the four strain gauges on the third order truss system, the eight strain gauges on the mast in the OA plane, and the three load in cells in the third order stays with a sampling frequency of 100 Hz. The structural response to wind load is also logged with sampling frequency of 200 Hz.

7.2.4 Experimental results

Figure 7.5 shows the mast displacements in *x* direction at each of the load steps relative to the initial configuration Co. The mast deformation reflects the effect of the stays with the truss system that induce curvature changes and a more uniform distribution of the bending moment diagram if

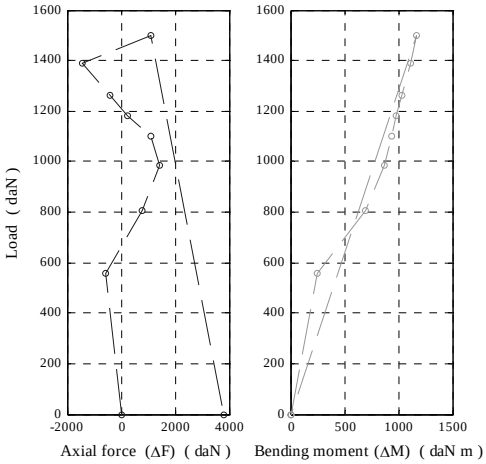

Figure 7.7 Internal forces increments at height 12 m.

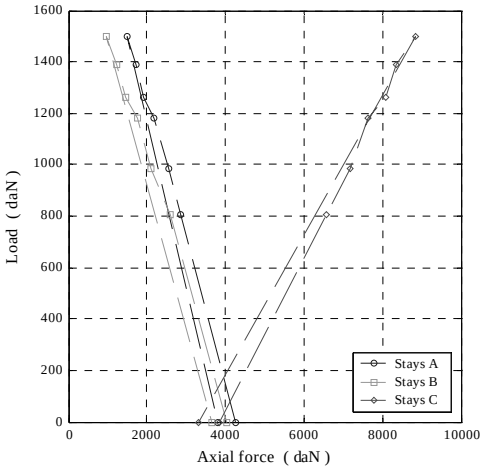

Figure 7.8 Total axial force in the stays at each position.

compared with the structural model in [c]. This feature improves the structural behavior especially with regard to instability phenomena.

The relative displacements measured with the reflecting targets at heights 30 m, 20 m, and 9 m are plotted as a function of the applied load in Figure 7.6. It can be noted a linear piece-wise behavior alternating softening and hardening zones. This demonstrates the complexity of such a structural system where the bolted connections and the different order of stays play an unpredictable role.

The complex behavior is also highlighted by the internal forces diagrams in the truss system, in the mast, and in the stays. As an example the axial force and the bending moment in the mast at height 12 m are plotted vs. the applied load in Figure 7.7. These diagrams report the internal forces increments from the initial condition Co because they were calculated from the strain gauges that were set to zero in this state (i.e. it was not possible to have the axial force and bending moment corresponding to load zero).

Figure 7.8 reports the sum of the axial forces in the stays at each position (A, B, and C) as a function of the applied load. The sum is performed over the data measured both with the load cells and the tensiometer. The total axial force in the stays in position A and B decreases but do not reaches zero values. Only the first order stay in position B loses all the pre-load when the applied load is about 1390 daN.

The first attempt in order to identify the main dynamic parameters of the complex system under investigation was performed shaking the third order stay at position B and recording the free vibrations time histories. Figure 7.9 shows the three axial load time series in the third order stays and the corresponding normalized spectral density from which it is possible to estimate some of the natural frequencies quite clearly.

Figure 7.10 reports the bending stress and the axial stress time series in the horizontal element (strut) of the third order stay's truss system. These recordings are at the same time of those reported in Figure 7.9 and the spectral densities obtained by the strain gauges series confirm the natural frequencies obtained by the load cells series.

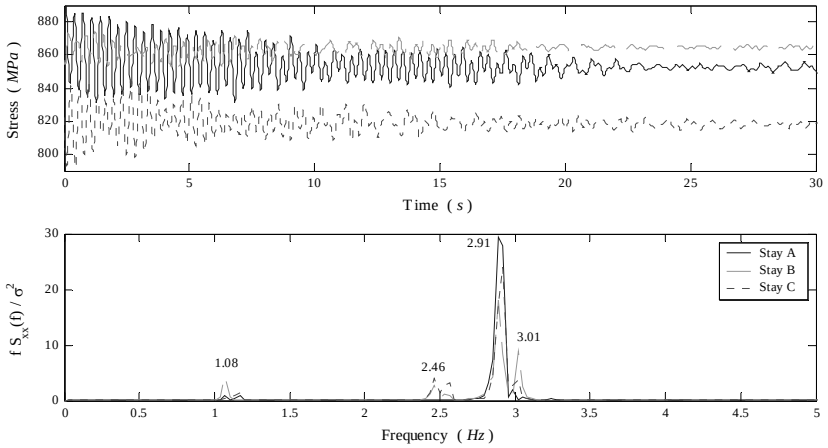

Figure 7.9 Axial force time series for the third order stays (above) and corresponding normalized spectral densities (below).

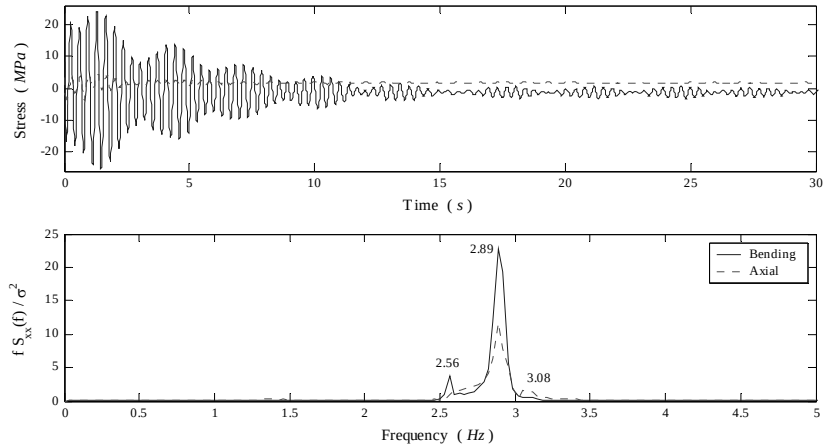

Figure 7.10 Relative stress time histories in the truss system (above) and corresponding normalized spectra (below).

The analysis of the free vibrations recorded by all the sensors indicates clear peaks at the following frequencies: 1.08, 1.17, 2.45, 2.56, 2.9, 3,0, and 6,04 Hz.

Some of the signals can also be used to obtain raw estimates of the damping ratio interpolating the decreasing amplitude with the classic exponential decay function. In particular the damping ratio associated to the frequency 1.1 Hz is about 4.5% and the one corresponding to 2.56 Hz is found in the range between 7.5 and 8.3%.

During this research it was also possible to record the wind induced vibration using all the aforementioned sensors. As already noted no communication devices, such as antennas and/or dishes, were installed so that the wind load acting on the structure was lower then the one in the actual layouts. Nevertheless the effect of the stays, the truss systems, the cable rack, the safety ladder, the cables for the monitoring system is reflected in the mast response time series. Figure 7.11 reports the bending moment stress oscillations induced by the wind load at height 12 m on

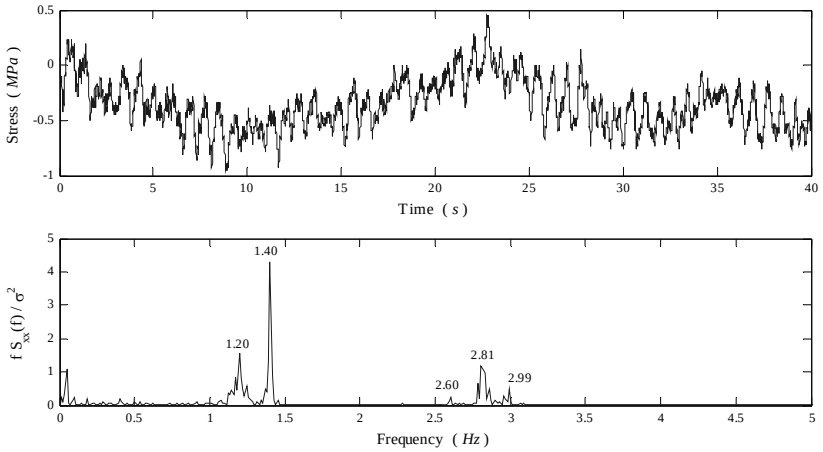

Figure 7.11 Wind induced vibrations in the mast (above) and corresponding normalized spectra (below).

the mast. The peaks in the spectral density are slightly different from those found in the free vibration test indicating response sensitivity to uncertain parameters such as the cable tension and the assembly layout. The described differences in the spectra peaks might be caused by the fact that the wind load test was performed some months later than the free vibration test and slackening was found in some of the stays.

A preliminary numerical model was also developed. Figure 7.12 shows the first three modes of vibration to which correspond the frequency of 1.36, 1.65, and 2.45 Hz respectively. It looks like the torsional mode (third mode), mainly involving the truss system and the stays, perfectly matches the experimental findings. On the other hand, the first two modes indicate that the numerical model is stiffer than the actual structure and has to be better calibrated (e.g. refining the constraint modeling).

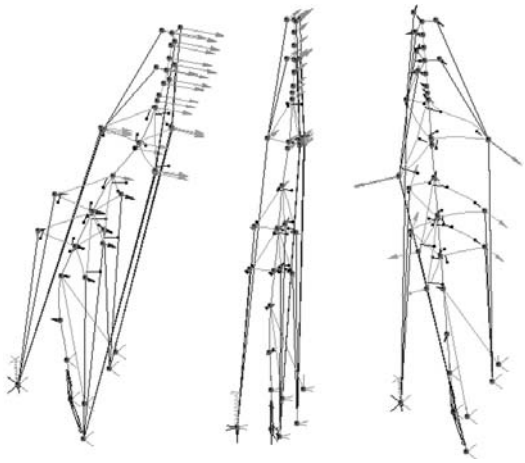

Figure 7.12 First three modes of vibration from the numerical model.

The results obtained from this experimental investigation confirmed the complexity of the studied structural system and were used to estimate the natural frequencies and the associated damping ratios. These results represent a starting point for the structural identification that could be improved using more accurate methods.

7.3 THE TRIESTE CYLINDRICAL CONCRETE CHIMNEY

The Trieste Research Unit contributed to the PERBACCO project continuing the experimental work on the concrete chimney of the new municipal waste disposal incinerator in Trieste [d]. The cylindrical stack has height of 100.0 m and diameter of 6.3 m. Time series of the structural dynamic response to wind loads have been recorded together with the wind velocity using a biaxial accelerometer, an anemometer, a wind-vane, and a GPS antenna.

7.4 BASIC REFERENCE

[a] Gioffrè M., Gusella V., Materazzi A. L., 2002. Problemi di progettazione di antenne per telefonia mobile, *Proc. 7th Italian Conference on Wind Engineering* (IN-VENTO-2002). Milano, Italy

[b] Gioffrè M., Gusella V., Materazzi A. L., Venanzi I., 2003. Optimal design of raw land sites for mobile phone networks. *Proc. 11th Int. Conf. Wind Eng, Lubbock (11ICWE)*, Texas, USA

[c] Gioffrè M., Gusella V., Materazzi A. L., Venanzi I., 2004. Removable guyed mast for mobile phone networks: wind load modelling and structural response. *Journal of Wind Engineering & Industrial Aerodynamics*, 92(6), 463-475

[d] D'Asdia P., Noè S., 1998. Vortex induced vibration of reinforced concrete chimneys: in situ experimental and numerical previsions. *Journal of Wind Engineering & Industrial Aerodynamics*, 74-76, 765-776

7.5 LIST OF PUBLICATIONS

[1] Gioffrè M., Gusella V., Materazzi A.L., Venanzi I., Morbidoni S., Frontoni A. 2004. Modelli e verifiche sperimentali per l'ottimizzazione di strutture rimovibili per reti di telefonia mobile, *Atti dell'8° Convegno Nazionale di Ingegneria del Vento, IN-VENTO-2004*, Reggio Calabria, 21-23 Giugno 2004, pp. 349-356.

[2] Gioffrè M., Gusella V., Morbidoni S. 2005. Identification of a special class of removable guyed mast. *Proceedings, Sixth European Conference on Structural Dynamics (EURODYN 2005)*, Paris, France, September 4-7, 2005, vol.3, pp. 2237-2242.

WITH CONTRIBUTION FROM:

Vittorio Gusella, Università degli Studi di Perugia
Annibale Luigi Materazzi, Università degli Studi di Perugia
Salvatore Noè, Università degli Studi di Trieste
Ilaria Venanzi, Università degli Studi di Perugia

8 Wind tunnel tests

Gianni Bartoli
University of Florence

8.1 INTRODUCTION

One of the main topics in which a correct assessment of a Performance-Based design procedure has to be defined, is certainly related to bridge aerodynamics. As a matter of fact, such structures are so sensitive to wind actions from so many points of view that a correct definition of the requested performances is certainly necessary. Among others, the following aspects require a deeper analysis and a correct definition of the safety level essential for the structure:

- from a serviceability point of view, the first required performance is the control of vibrations due to buffeting forces (that is the amplification of the structural response due to the dynamic characteristics excited by wind turbulence): large oscillation could mainly cause discomfort to the bridge's users but, in some cases, could produce interruptions in the use of the bridge (i.e. when a train transit has to be considered);
- considering a limit state design, the correct definition of the performance with respect to the possible collapse of the bridge (i.e. due to dynamic instability like the one due to flutter instability) should be considered, by correctly analyzing the distribution of probability of the wind speed which could cause the structural collapse.

In the following, the results of some wind tunnel tests performed at the CRIACIV-DIC boundary layer wind tunnel will be illustrated. In detail, three experiences will be reported:

- the first section reports some results obtained by a study on the span-wise correlation of aerodynamic forces on a rectangular cylinder for different vibration regimes (vortex shedding, buffeting and flutter);
- in the second part, some details will be given about the analyses performed on a trapezoidal single-box girder with lateral cantilevers; this typology is very common for medium-span cable-stayed and suspension bridges, so that an extensive experimental and numerical campaign has been performed in the framework of the PERBACCO project;
- in the last section, a sensitivity analysis of a multi-box girder (similar to the one proposed in the design for Messina Strait Bridge) will be described, being this solution an innovative one for very long-span bridges.

8.2 SPAN-WISE CORRELATION OF AERODYNAMIC FORCES ON A RECTANGULAR CYLINDER

The span-wise correlation of aerodynamic forces and pressure fluctuations on vibrating cylinders, bridge decks, and other elongated structures has been studied long since. In particular, it is well known that to an increase in the oscillation amplitude an increase in the correlation is associated ([a], [b]). Reference [c] reports an investigation on the influence of turbulence on the correlation of torque on a rectangular prism with an aspect ratio of 6.7:1, driven into vertical and torsional motion at different reduced wind speeds. Other recently carried out studies aimed at characterising the aerodynamic forces and pressure fluctuations acting on a bridge box deck section for the three different vibration regimes of forced motion, torsional lock-in and torsional flutter have been reported in [d]; it was observed that the characteristics of the aerodynamic forces and pressure distributions are strongly dependent on the vibration regime. Moreover, POD application revealed that the aerodynamic forces are the sum of components due to different excitation mechanisms, coexisting at each vibration regime [e].

In the experimental campaign which is presented here, some additional analyses on the influence of the oscillation amplitude on the span-wise correlation of aerodynamic forces and pressure fluctuations on a rectangular prism have been performed. Wind tunnel tests were carried out on a rectangular prism (BxD=30x6 cm): the 232 cm long model (made of carbon fibre composite to minimise the weight, Fig. 8.1) was placed in the test section, with the suspension system placed outside the tunnel. Springs with different stiffness were used to obtain target oscillation frequencies, and the ratio between the torsional and vertical natural frequencies was varied in the range of 1 to 2 changing the eccentricity of the attachment points. Two conditions were tested of smooth flow and turbulent flow, with an intensity of turbulence of 0.17 and an integral scale of 0.21 m; in the following, only the smooth flow condition is discussed. Dynamic tests were performed for following frequency ratios: setup #1: f_h=4.5, f_α=10.1 (f_α/f_h=2.24), setup #2: f_h=7.3, f_α=16.1 (f_α/f_h=2.21), setup #3: f_h=7.3, f_α=10.7 (f_α/f_h=1.47), setup #4, f_h=f_α=10.8 (f_α/f_h=1.0). Damping coefficients in the range from 0.1% to 0.2% were measured, depending on the DoF and on the setup.

The model was instrumented with 210 pressure taps arranged in seven arrays of 30 (ten on the upper and lower sides, five on the windward and leeward sides). The arrays were located at the following distance from midspan: array #1: -80 cm; array #2: -40 cm; array #3: -20 cm; array #4: midspan; array #5: +10 cm, array #6: +30 cm; array #7: +80 cm. This allowed evaluating the span-wise correlation for 13 values of the separation δ from a minimum of 10 cm (δ/D=1.7) to a maximum of 160 cm (δ/D=27). In addition to the pressure measurements, in the dynamic tests three laser displacement transducers were used to measure the dynamic response, while in the static tests six load cells were used to measure the overall forces. The static tests were carried out for 12 angles of attack and at U=16 m/s, reading from arrays #1, #3, #4 and #7. The pressures were sampled for 30 sec at 250 Hz. In the dynamic tests measurements were taken from arrays #3, #4, #5 and #7, for 210 sec at 250Hz. In the following, results obtained on setup #1 and #4 are discussed, corresponding to a SDoF and to a coupled 2-DoF behavior, respectively. In Fig. 8.2 the STD of the vertical and torsional amplitudes of oscillation, and in Fig. 8.3 the excitation frequency are plotted as a function of the wind speed.

In setup #1, for wind speeds of 1.4 and 2.4 m/s a vertical vortex shedding lock-in is observed (f_s=4.5 Hz). For U=3.3 m/s the shedding frequency locks to the torsional natural frequency (10.0 Hz). At higher wind speeds, up to 11.7 m/s the shedding frequency follows the Strouhal law with St=0.128, and the model goes into a forced motion in both DOFs. Starting at 12.3 m/s the model goes into torsional flutter, with an excitation frequency of 9.8 Hz, close to the torsional frequency in still air.

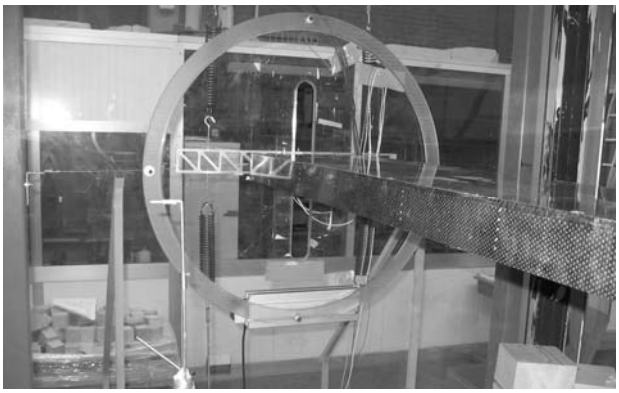

Figure 8.1 Rectangular section: wind tunnel model with pressure taps

In setup #4, for wind speeds in the range of 2.59 to 3.50 m/s a torsional vortex shedding lock-in takes place at 10.8 Hz. For wind speeds of 3.51 to 3.90 m/s the frequency of excitation changes to 8.0 Hz and the response switches to the vertical DoF, also at 8.0 Hz, 26% lower than the natural frequency. From 3.90 to 12.0 m/s the shedding frequency follows the Strouhal law, and the model goes into a forced motion in both DoFs. At 12.0 m/s torsional flutter starts, with an excitation frequency of 10.7 Hz, coincident with the natural frequency.

8.2.1 Correlation coefficents

Four wind speeds have been selected for discussion of setup #1, corresponding to different vibration regimes: U=3.3 m/s for lock-in, U=10.0 m/s for forced motion, U= 12.1 m/s for flutter with a STD of the torsional rotation similar to that measured at lock-in (0.070 rad vs. 0.066 rad), U= 15.3 m/s for fully developed flutter. Following the same criterion, five wind speeds will be discussed for setup #4: U=3.2 m/s for torsional lock-in, U=3.7 m/s for vertical lock-in, U=10.0 m/s for forced motion, U=12.7 m/s for torsional flutter with STD rotation (0.074 rad) equal to that at lock-in (0.073 rad), U=15.6 m/s for fully developed flutter. In addition, results of the static tests will be shown for reference.

For the above wind speeds the correlation coefficients of torque, lift and drag, together with those of the stagnation and base pressures were evaluated as:

$$R_{C_i}(\delta/D) = \mathrm{cov}\left[C_i(\delta/D)\right] \big/ \mathrm{var}\left[C_i\right] \tag{8.1}$$

in which C_i= C_M, C_L, C_D, C_{ps}, C_{pb}.

The following exponential low was used to describe the correlation coefficient function:

$$R_{C_i}(\delta/D) = \exp\left[-c \cdot \left(\delta/D - k\right)\right] + d \tag{8.2}$$

in which c is the exponential decay coefficient, d is an horizontal asymptote and k is a constant required to meet the condition $R_{Ci}(0)$=1, given as:

$$k = 1/c \cdot \ln\left(1 - d\right) \tag{8.3}$$

In the literature a simple exponential function is usually taken for the correlation coefficient, as it is assumed that correlation vanishes as separation increases. The need of introducing a non-zero asymptote stems from the observation that for some vibration regimes, even at large separations (δ/D>15) the correlation coefficients take a finite value. This is explained as the result of the exis-

tence of a fully correlated portion of the aerodynamic forces and pressures, associated with an aeroelastic behavior. These forces are functions of the section displacement and velocity (for a rigid model are the same for all sections) and therefore are fully correlated. The remaining portion of the aerodynamic forces and pressures are due to oncoming and signature turbulence, to flow separation and reattachment, and to vortex shedding, and loose coherence as separation increases.

In Tab. 8.1 and 8.2 the values of c and d coefficients of forces and pressures are shown, for setup #1 and #4. In Fig. 8.4 the correlation coefficients are shown, and interpolated using Eq. (8.2).

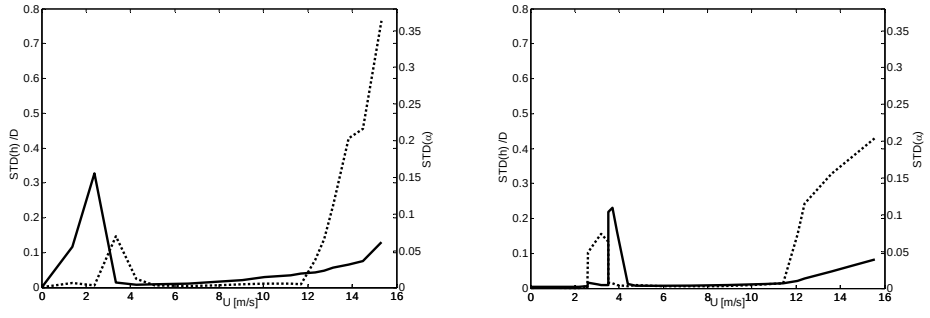

Figure 8.2 STD of the vibration amplitudes for setup #1 and #4 (solid line: vertical displacement; dotted line: angle of torsion)

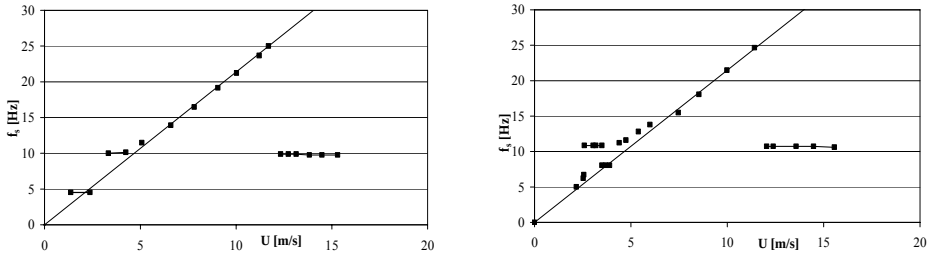

Figure 8.3 Excitation frequency as a function of the wind speed for setup #1 and #4

8.2.2 Discussion of the experimental results

For the static case, consistently with the assumption that only self-excited forces and pressures are fully correlated, the d coefficient is expected to be zero. This was found but for the stagnation pressure, for which the value d=0.06 was calculated. To satisfy the physical model adopted, such value was forced to zero in the evaluation of the exponential decay coefficient. In the static case the decay of correlation is slower for lift than for torque and drag, the latter being the result of a rapid decay of correlation of stagnation (c=0.952) and base (c=0.526) pressures.

Being infinite the correlation length of the self-excited forces and pressures, the correlation length of the non-correlated components are evaluated as:

$$L_i/D = \int_0^\infty \exp\left[-c\delta/D\right] d\left(\delta/D\right) = 1/c \tag{8.4}$$

In Tab. 8.3 the correlation length of the aerodynamic forces and pressures are shown.

For the forced motion regime (U=10.0 m/s) the d parameter is either zero or takes, in the case of the base pressure in setup #4, a quite low value, consistently with the low amplitude response. Only the stagnation pressure has finite values of the d coefficient, of 0.17 and 0.19 for setup #1 and #4, respectively. The correlation decay is slower than measured in the static case, even though the amplitudes of oscillation are very small in both DoFs. As for the static case lift is the most correlated component, but for the forced motion regime the correlation length is twice that (L_{CL}=7.3D and L_{CL}=8.6D for setups #1 e #4, respectively). A similar result is find for torque (L_{CM}=3.2D and L_{CM}=4.1D) and for drag (L_{CD}=3.3D and L_{CD}=4.5D). In addition, it can be observed that in the forced motion regime for setup #1 the correlation lengths are smaller than for setup #4.

	response		Asymptotic value (d)					Decay coefficient (c)				
	$\widetilde{h}$	$\widetilde{\alpha}$	M	L	D	S	B	M	L	D	S	B
static	-	-	0.00	0.00	0.00	0.00	0.00	0.462	0.234	0.512	0.952	0.526
U=3.3 m/s	0.014	0.070	0.54	0.14	0.10	0.14	0.11	0.648	5.000	1.78	5.000	2.260
U=10.0 m/s	0.029	0.005	0.00	0.00	0.00	0.17	0.04	0.308	0.137	0.306	0.868	0.347
U=12.7 m/s	0.049	0.066	0.39	0.22	0.00	0.12	0.05	0.289	0.088	0.219	0.389	0.235
U=15.3 m/s	0.130	0.363	0.89	0.78	0.35	0.43	0.10	0.186	0.027	0.120	1.136	0.080

Table 8.1 Dynamic response and correlation parameters for setup #1

	response		Asymptotic value (d)					Decay coefficient (c)				
	$\widetilde{h}$	$\widetilde{\alpha}$	M	L	D	S	B	M	L	D	S	B
static	-	-	0.00	0.00	0.00	0.00	0.00	0.462	0.234	0.512	0.952	0.526
U=3.2 m/s	0.010	0.074	0.24	0.50	0.15	0.15	0.17	0.507	0.457	0.484	2.150	0.783
U=3.7 m/s	1.384	0.007	0.76	0.48	0.00	0.23	0.04	0.535	0.236	0.088	1.773	0.135
U=10.0 m/s	0.011	0.004	0.00	0.00	0.00	0.19	0.00	0.241	0.116	0.224	0.929	0.222
U=12.1 m/s	0.022	0.073	0.35	0.00	0.02	0.15	0.03	0.245	0.075	0.183	0.362	0.183
U=15.6 m/s	0.083	0.200	0.77	0.68	0.31	0.16	0.13	0.329	0.041	0.145	0.219	0.106

Table 8.2 Dynamic response and correlation parameters for setup #4

Setup #1						**Setup #4**					
	M	L	D	S	B		M	L	D	S	B
static	2.2	4.3	2.0	1.1	1.9	static	2.2	4.3	2.0	1.1	1.9
U=3.2 m/s	1.5	0.20	0.56	0.20	0.44	U=3.2 m/s	2.0	2.2	2.1	0.46	1.3
U=10.0 m/s	3.2	7.3	3.3	1.2	2.9	U=3.7 m/s	1.9	4.2	11.4	7.4	0.56
U=12.7 m/s	3.5	11.4	4.6	2.6	4.3	U=10.0 m/s	4.1	8.6	4.5	1.1	4.5
U=15.3 m/s	5.4	37.0	8.3	0.88	12.5	U=12.1 m/s	4.1	13.3	5.5	5.5	2.8
						U=15.6 m/s	3.0	24.4	6.9	9.4	4.6

Table 8.3 Correlation length for setup #1 and #4 for the different vibration regimes

For both the setups the STD of the torsional response is very low ($\tilde{\alpha} = 0.005$ rad and $\tilde{\alpha} = 0.004$ rad, respectively), while the STD of the vertical response is rather larger for setup #1 ($\tilde{h} = 0.029$ m) than for setup #4 ($\tilde{h} = 0.011$ m). This would make one expect larger correlation lengths for setup #1, the opposite of what it was found.

For the torsional lock-in regime the values of the STD response measured for setup #1 ($\tilde{h} = 0.014$ m, $\tilde{\alpha} = 0.070$ rad) and setup #4 ($\tilde{h} = 0.010$ m, $\tilde{\alpha} = 0.074$ rad) are similar. In spite of that the correlation coefficients are quite different. In setup #1 the correlated portion of torque is 54% (d=0.54) and that of lift is 14% (d=0.14), while in the setup #4 these values are 24% and 50%, respectively. For both setups the correlation portion of drag is lower (d=0.10 for setup #1 and d=0.15 for setup #4).

For the torsional lock-in regime, and especially in the case of setup #1, the presence of fully correlated and partially correlated components of the aerodynamic forces is clear, and the latter are characterised by small values of the correlation length (Tab.8.3). This result is in agreement with the approach used for the evaluation of the shedding induced response at lock-in, in which some aeroelastic stiffness and damping forces are introduced, to account for the fully correlated, motion dependent forces. To these an external excitation is added, with a correlation length of few times the dimension of the section. Moreover, from the results of setup #1 it can be observed that the largest correlation corresponds to the DoF of largest amplitude of oscillation, while for setup #4 the largest correlation is that of the force component associated with the DoF in which the amplitude of oscillation is smaller.

For setup #4 the wind speed of U=3.7 m/s has also been considered, which corresponds to a lock-in in the vertical DoF. This is an unusual condition, in which the shedding frequency correspond to the Strouhal frequency, and the vibration frequency in both DoFs gets locked to it. In this regime the forces are globally more correlated than in torsional lock-in. The correlated portion of torque increases from 24% to 76%, but the correlation length remains about the same. The correlated portion of lift, however, is the same, but the correlation length is almost doubled (from 2.2D to 4.2D). The correlated portion of drag goes to zero, and the correlation length strongly increases (from 2.1D to 11.4D). The same increase in the correlation length was observed for the base pressure (from 1.3D to 7.4D). Like for the torsional lock-in, also in this case the largest correlation is associated with the lowest dynamic response.

The wind speeds of U=12.7 m/s in setup #1 and U=12.1 m/s in setup #4 were chosen such to compare the correlation of the aerodynamic forces in the two regimes of torsional lock-in and flutter, with the same torsional amplitude of oscillation, and it was found that the characteristics of the correlations are rather different for the two regimes. In particular, for setup #1 the correlated portion of torque is 35%, as opposed to 54% of lock-in, while that of lift is 22% as opposed to 14%, in agreement with the increase of the amplitude of the vertical oscillation from $\tilde{h} = 0.014$ to $\tilde{h} = 0.049$. The correlated portion of drag is zero, as opposed to 10% of lock-in. The correlation length is larger at flutter for all the aerodynamic components, with a maximum difference for the lift force (L_{CL}=11.4D compared to L_{CL}=0.2D). As a result the interpolating curves in Fig. 4 are quite different for the two vibration regimes.

In the case of setup #4, the correlated portion of torque is 34%, as opposed to 24% of lock-in, while those of lift (0%) and drag (2%) are much lower than at lock-in (50% and 15%, respectively). The decrease of the correlated portion of lift is somehow unexpected, as at flutter there is an increase in the vertical vibration ($\tilde{h} = 0.022$ m) with respect to lock-in ($\tilde{h} = 0.010$ m). It can be concluded that the correlated portion of the aerodynamic forces decreases from lock-in to flutter, but the decay of the correlated forces is higher at lock-in.

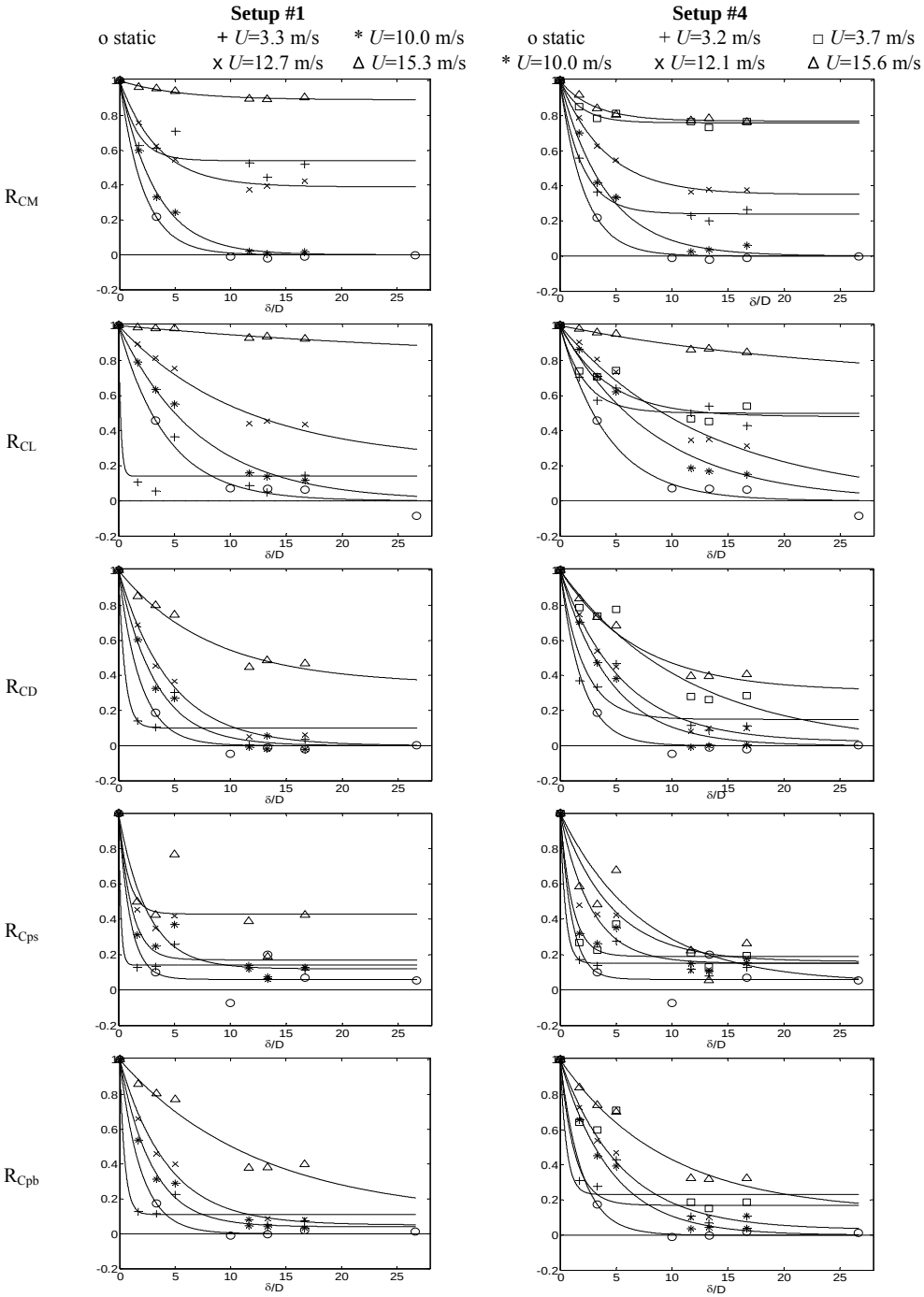

Figure 8.4 Correlation coefficient of aerodynamic forces and of stagnation and base pressure

The last vibration regime considered is that of a fully developed flutter (U=15.3 m/s in setup #1 and U=15.6 m/s in setup #4). Consistently with the large torsional vibration amplitude ($\tilde{\alpha} = 0.36$ rad and $\tilde{\alpha} = 0.20$ rad, respectively), the correlation is the highest, with the correlated portion of the forces ranging for a minimum of 31% for drag in setup #4 to a maximum of 89% for torque in setup #1. So large values indicate the large amount of self-excited flutter forces. Also the correlation length increases for all the aerodynamic components, except for torque in setup #4, where it decreases from 4.1D to 3.0D.

8.3 TRAPEZOIDAL SINGLE-BOX GIRDER DECK

In this section, some results obtained by tests on a trapezoidal single-box girder deck are reported. The same section model has been used for static and aeroelastic tests. The model is made of aluminum and its weight (without supporting system) is as high as 9.2 kg. The model is build around a circular tube with a diameter of 45 mm, to which 16 ribs supporting the external 0.5 mm sheet-aluminum, are connected. The model, whose main geometric features can be seen in Fig. 8.5, is 2380 mm long (the tube is 2800 mm long), 450 mm wide and 70 mm deep. Therefore the width-to-thickness ratio is B/D = 6.43 and the length-to-width ratio is L/B = 5.29. It is a bare-deck configuration, without non-structural details.

First, static tests are performed on the model, which is placed in the wind tunnel test section as shown in Fig. 8.6a. Six load cells (three on each side) are assembled to form a force measuring system according to the scheme of Fig. 8.6. Before starting the tests the whole system is calibrated applying known drag, lift and moment loads in order to build a calibration matrix.

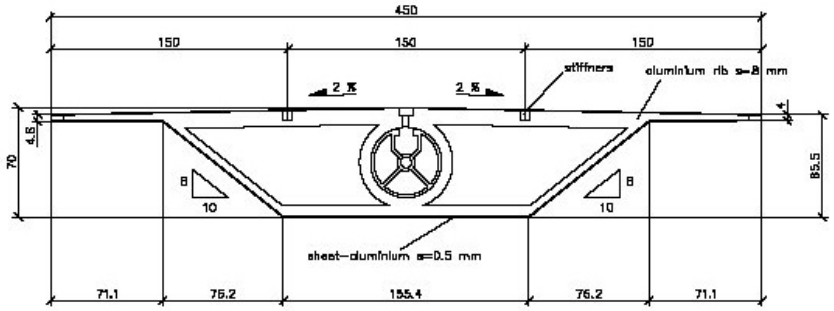

Figure 8.5 Geometric characteristics of the cross section of the section model (dimensions in mm)

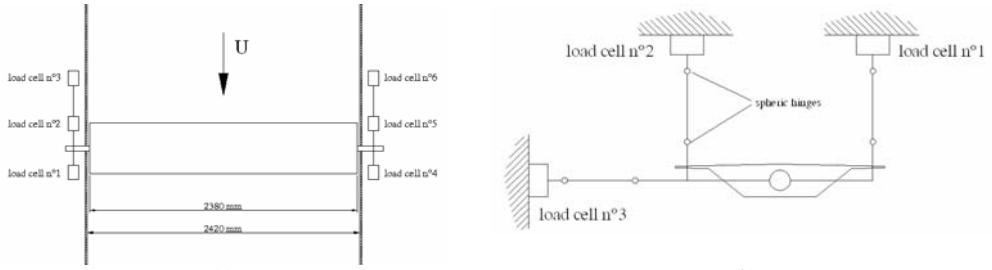

(a) (b)

Figure 8.6 Sketch of the setup for the static measurements: (a) top view; (b) lateral view

The influence of Reynolds number on the static behavior of the section model is investigated at three different angles of attack (-5°, 0°, +5°) increasing the wind speed approximately in the range 3 - 28 m/s ($9 \cdot 10^4 < Re < 8 \cdot 10^5$) and measuring the aerodynamic force coefficients (according to the reference system of Fig. 8.7). Fig. 8.8 shows that Reynolds number effects are definitely non-negligible for this type of section.

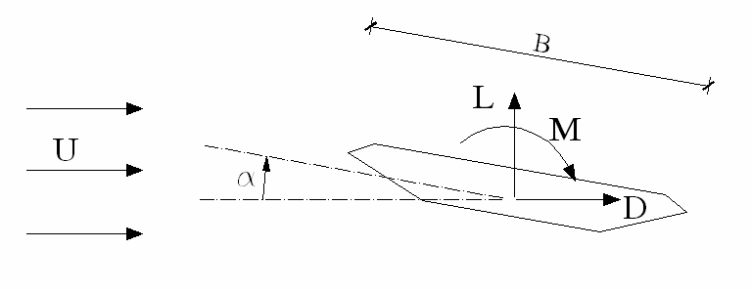

Figure 8.7 Reference system for the aerodynamic coefficients

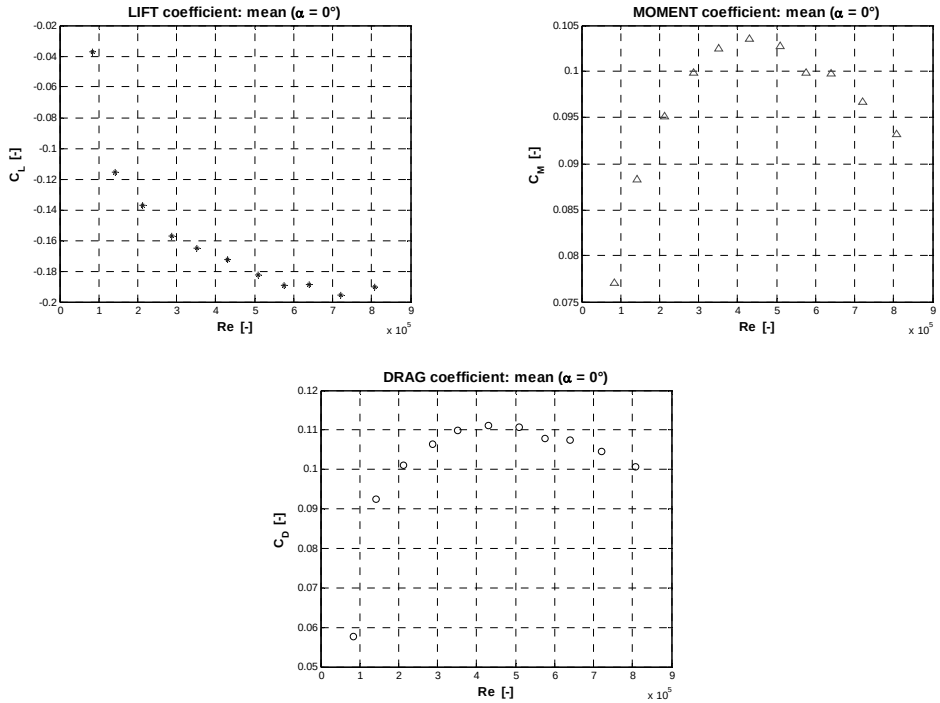

Figure 8.8 Mean values of the aerodynamic coefficients as functions of Reynolds number (α = 0°)

Next, the aerodynamic coefficients are measured at different angles of attack (static polars), choosing the highest Reynolds number, compatible with the wind-tunnel limits and the model safety exigencies ($Re = 5.8 \cdot 10^5$). Results are reported in Fig. 8.9.

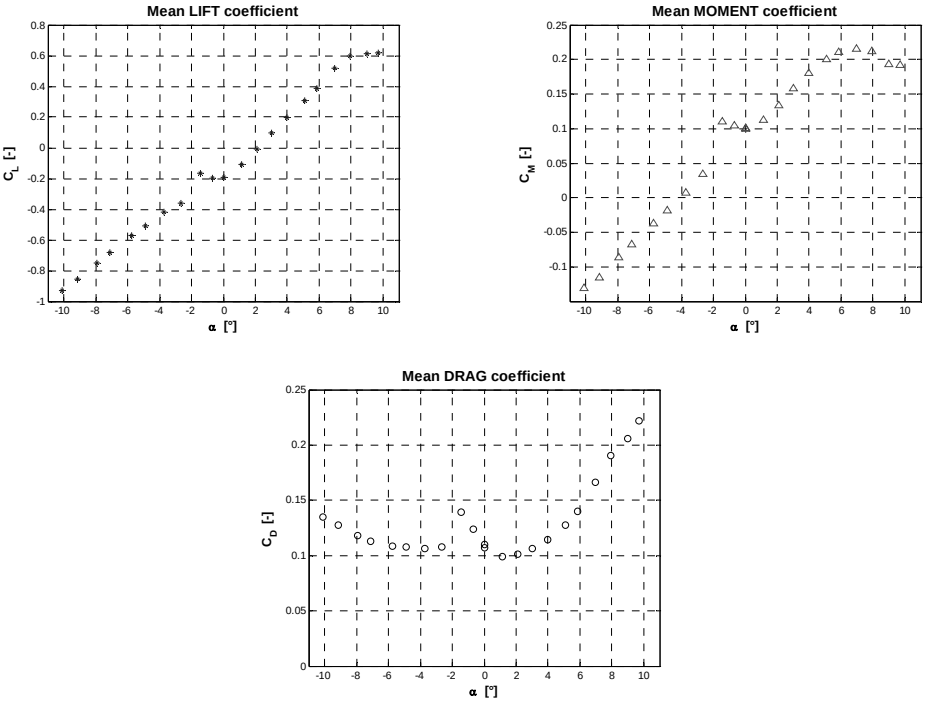

Figure 8.9 Mean aerodynamic force coefficients for different angles of attack

The strange behavior in the range $-2° < \alpha < 0°$, where also the mean force fluctuations increase a great deal, is qualitatively independent from the Reynolds number and consequently from the actual wind speed at which the aerodynamic coefficients are measured. In addition, it is confirmed by the behavior of the section model during the aeroelastic tests.

The Strouhal number, that is the non-dimensional frequency of vortex shedding, is measured for three different angles of attack, opportunely placing a hot-wire anemometer in the wake of the model. This measure is not easy at all, since this cross-section does not present a very strong shedding of eddies and the process is also disturbed by the unavoidable flow oncoming turbulence. Nevertheless, the Strouhal number seems to be independent on Reynolds number in the investigated range of wind speed, with values 0.24 for $\alpha = \pm 5°$ and about 0.21 for $\alpha = 0°$.

Experiments on a very similar section model (Sunshine Skyway Bridge, Florida; see Fig. 8.10) have already been performed at the Boundary Layer Wind Tunnel Laboratory, Canada ([f]). The main difference with the section model tested by CRIACIV concerns the box lower corners, which are purposely sharpened by small triangular appendices. Since the results are very different both for the mean aerodynamic coefficients and Strouhal number, some CFD simulations are performed, in the framework of a collaboration with the German Aerospace Center (DLR) of Göttingen, in order to try to understand the reason for these discrepancies. Two-dimensional Unsteady Reynolds-Averaged Navier-Stokes (URANS) simulations are performed on the DLR-Göttingen computer cluster, using the finite-volume unstructured flow solver DLR-Tau code ([2]), which solves the compressible URANS equations with the second-order accuracy in both space and time. Linearized Explicit Algebraic (LEA) two-equation turbulence model is chosen to simulate

the turbulent Reynolds stresses. Careful temporal and spatial grid convergence studies are performed. The adopted hybrid grid is shown in Fig. 8.11, while the results of the numerical simulations and experiments are compared in terms of mean aerodynamic coefficients in Fig. 8.12 and in terms of Strouhal number in Tab. 8.4. It can be noted that the agreement between experiments and numerical simulation is quite good in case of sharp edges and satisfactorily in case of rounded edges and interestingly the numerical simulations seem to be able to explain the difference between the two sets of experiments, especially concerning the opposite sign for lift and the very different Strouhal number. In Fig. 8.13 it is possible to appreciate the complete different flow field around the bridge section in the two cases.

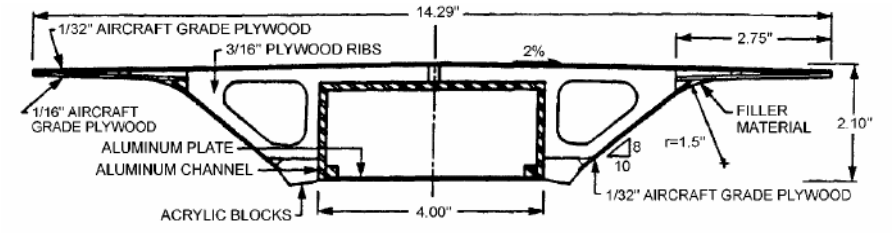

Figure 8.10 Sunshine Skyway Bridge (SSB) section model (dimensions in inches) [g]

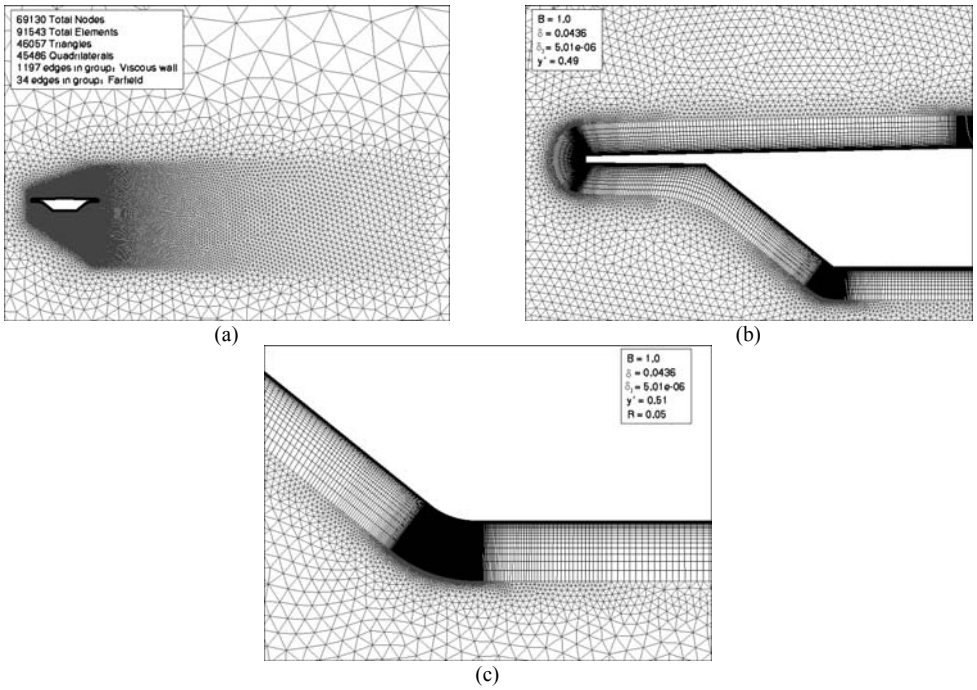

(a) (b)

(c)

Figure 8.11 Hybrid mesh used in the CFD simulations: (a) refinement around the body and in the wake; (b) near body grid; (c) detail of one of the lower edges in the configuration with rounded corners. δ is the total height of the structured grid, δ_1 is the first layer height, R is the corner radius of curvature, y^+ is a computational variable strongly correlated to δ_1

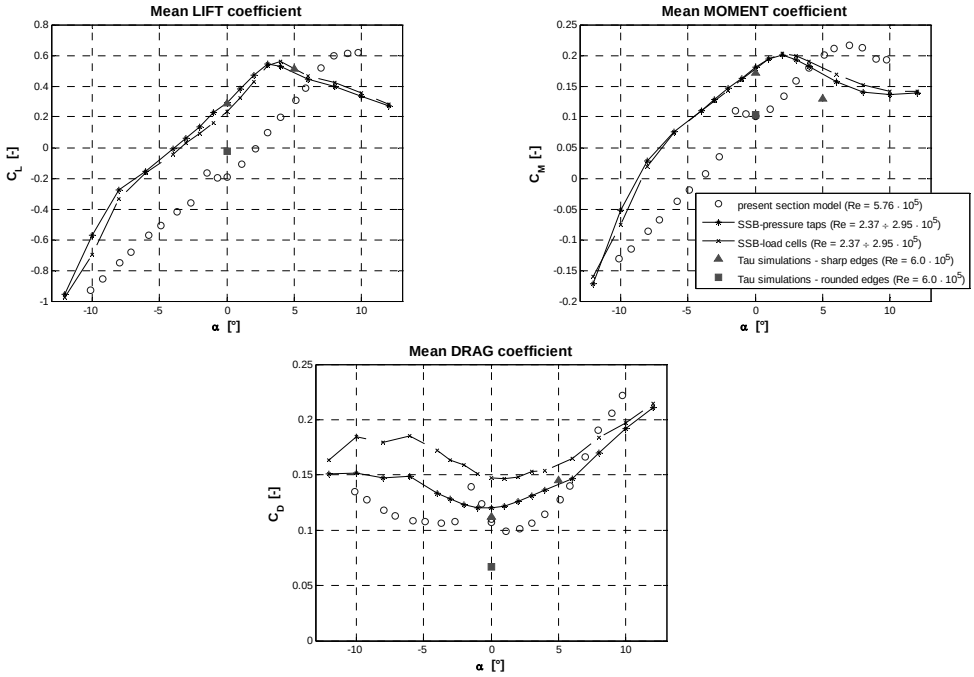

Figure 8.12 Experimental and numerical aerodynamic force coefficients for the Sunshine Skyway Bridge (SSB)

α [°]	Experiments (rounded edges)	Experiments (sharp edges)	Tau-simulation (sharp edges)	Tau-simulation (rounded edges)
0	0.21	0.146	0.154	0.255
+5	0.24	0.091	0.081	-

Table 8.5 Strouhal number for the bridge section

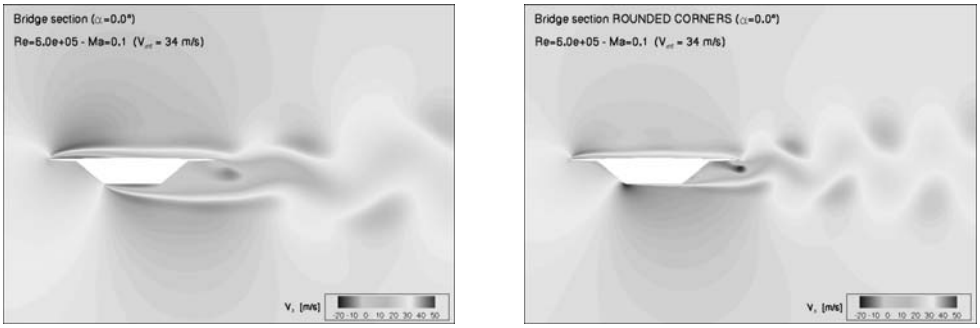

(a) (b)

Figure 8.13 Horizontal velocity field corresponding to the instant of maximum lift: (a) configuration with sharp edges; (b) configuration with rounded lower edges

This analysis is a very good example of the fruitful complementarities of CFD techniques and wind-tunnel tests, which conversely are often seen as being in strong competition. In addition, these results should warn about the extreme importance of model details sometimes erroneously considered as marginal, such as the bridge profile edges.

After the static tests the section model is elastically suspended and an extensive aeroelastic campaign is performed. The main target of this part of the experimental investigation was the identification of the aeroelastic functions, called flutter derivatives, via free-vibration tests at different mean angles of attack. The assumed linearity of the flutter derivatives with respect to the amplitude of vibration and the statistic characteristics of the measured functions are also deeply investigated.

For aeroelastic tests a setup is necessary in which the section model is elastically suspended and vertical heaving and pitching modes are allowed. This is obtained clamping the core-tube of the model to rigid suspension arms and then connecting eight springs to them. Each suspension arm consists of two aluminum plates connected together, in order to be very stiff with respect to bending in the vertical plane but as light as possible. The connection between the springs and the suspension arms is realized with steel ropes, in order to minimize the mechanical friction and let the springs work as regularly as possible. The springs are placed at a distance of 500 mm and opportunely prestressed. Those springs which are mounted above the section model (T42630) are stiffer than those mounted under it (T42150), since they have to support also the weight of the model and the suspension arms.

Since only two degrees of freedom should be allowed, it is necessary to restrain the oscillation of the model in the along wind direction, as well as the rotation with respect to a vertical axis. This is realized with long steel anti-drag cables which are connected to the model by means of two low-friction pillow blocks, in order not to disturb the pitching (Fig. 8.15a). A schema and some pictures of the setup are reported in Figs. 8.14 and 8.15. Finally, since the flutter derivatives are identified by measuring the in-wind heaving-pitching free-decay motion, a system to give a controlled and as regular as possible heaving-pitching initial condition is needed. This is obtained with two magnets and two iron devices that are able to release two steel cables which are connected to the model suspension arms (Fig. 8.15d). In order to limit as much as possible the rolling motion (rotation with respect to a horizontal axis perpendicular to the model axis), it is important that the two magnets release at same time the steel ropes and that the initial vertical displacements are the same on both sides of the model.

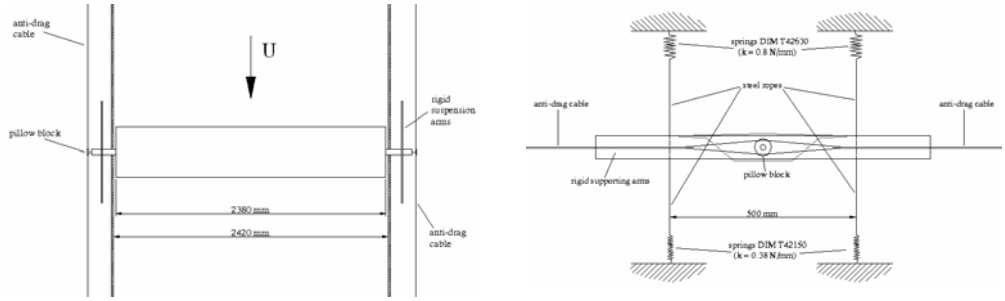

(a) (b)

Figure 8.14 Sketch of the setup for the aeroelastic measurements: (a) top view; (b) lateral view

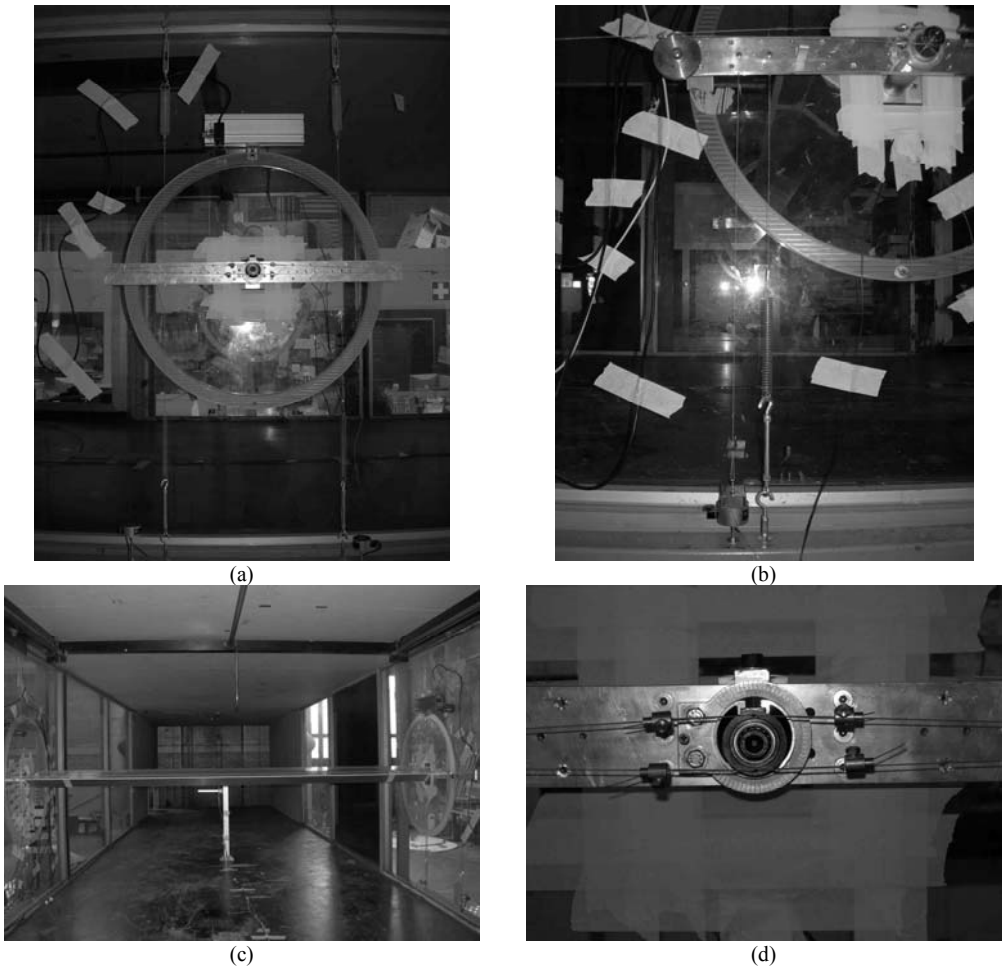

Figure 8.15 Setup for the aeroelastic measurements

Fig. 8.16 gives an example of heaving and pitching free-decaying motion in still-air: it is particularly worth noting the very small contribution of the rolling mode to the vibration signal after the proper adjustment of the initial condition release system.

Flutter derivatives are identified using the Unified Least Square (ULS) method ([h]) in the modified algorithm proposed by Righi [i]. This time-domain method is based on complex modal analysis and consequently on a linear mechanical model but it seems to be definitely adequate to interpret the measured heaving-pitching decaying signals, as demonstrated by the signal reconstruction reported in Fig. 8.18.

Particular attention is paid to the investigation about the dependence of the aeroelastic coefficients from the motion amplitude. For this purpose the flutter derivatives are identified for three different initial conditions, as reported in Tab. 8.6. Flutter derivatives are reported in Fig. 8.19 according to the Scanlan's convention (Fig. 8.17).

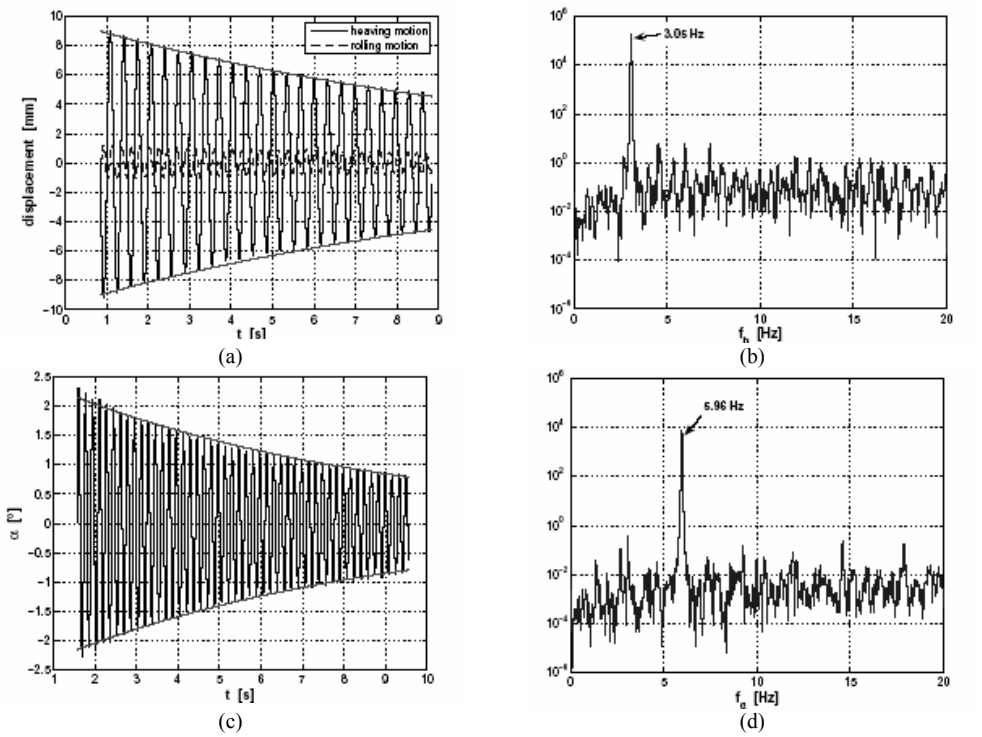

Figure 8.16 Still-air free-decay heaving and rolling modes (a) and heaving signal power spectral density (b); still-air free-decay pitching mode (c) and its power spectral density (d)

	$h_{i.c.}$ [mm]	$\alpha_{i.c.}$ [°]
"Large"	+9.6	-2.5
"Small"	+5.5	-1.4
"Very small"	+2.2	-0.6

Table 8.6 Still-air initial conditions for flutter derivatives identification

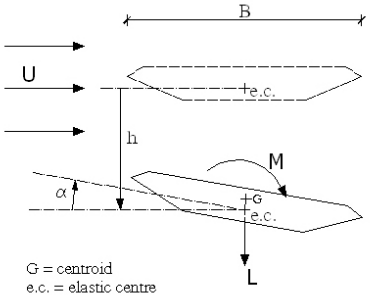

Figure 8.17 Scanlan's reference system for bridge self-excited forces

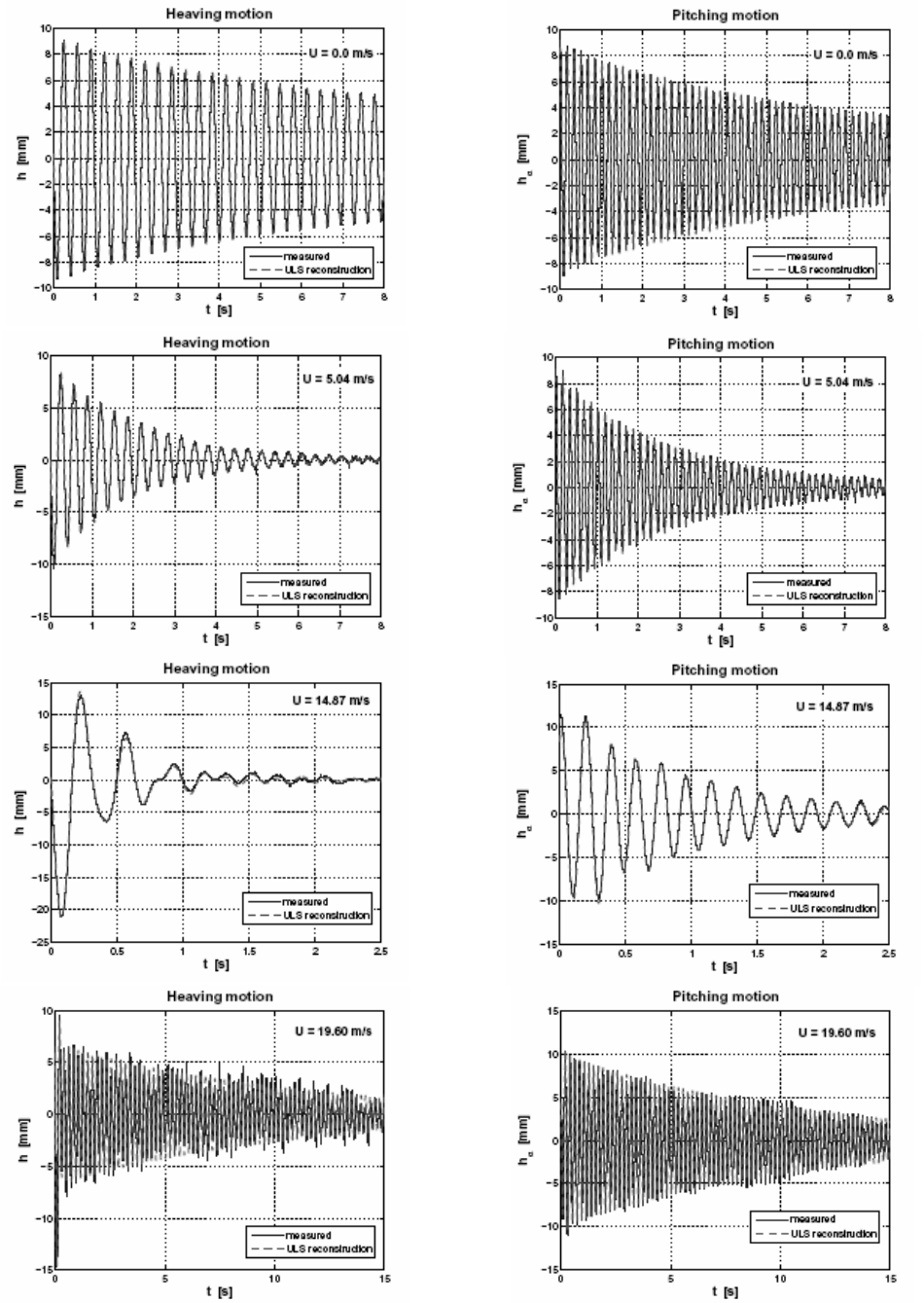

Figure 8.18 ULS reconstruction of measured heaving and pitching signals at different wind speeds. The pitching signal is expressed as $h_\alpha = B/2 \cdot \alpha$. The last case is taken immediately before flutter.

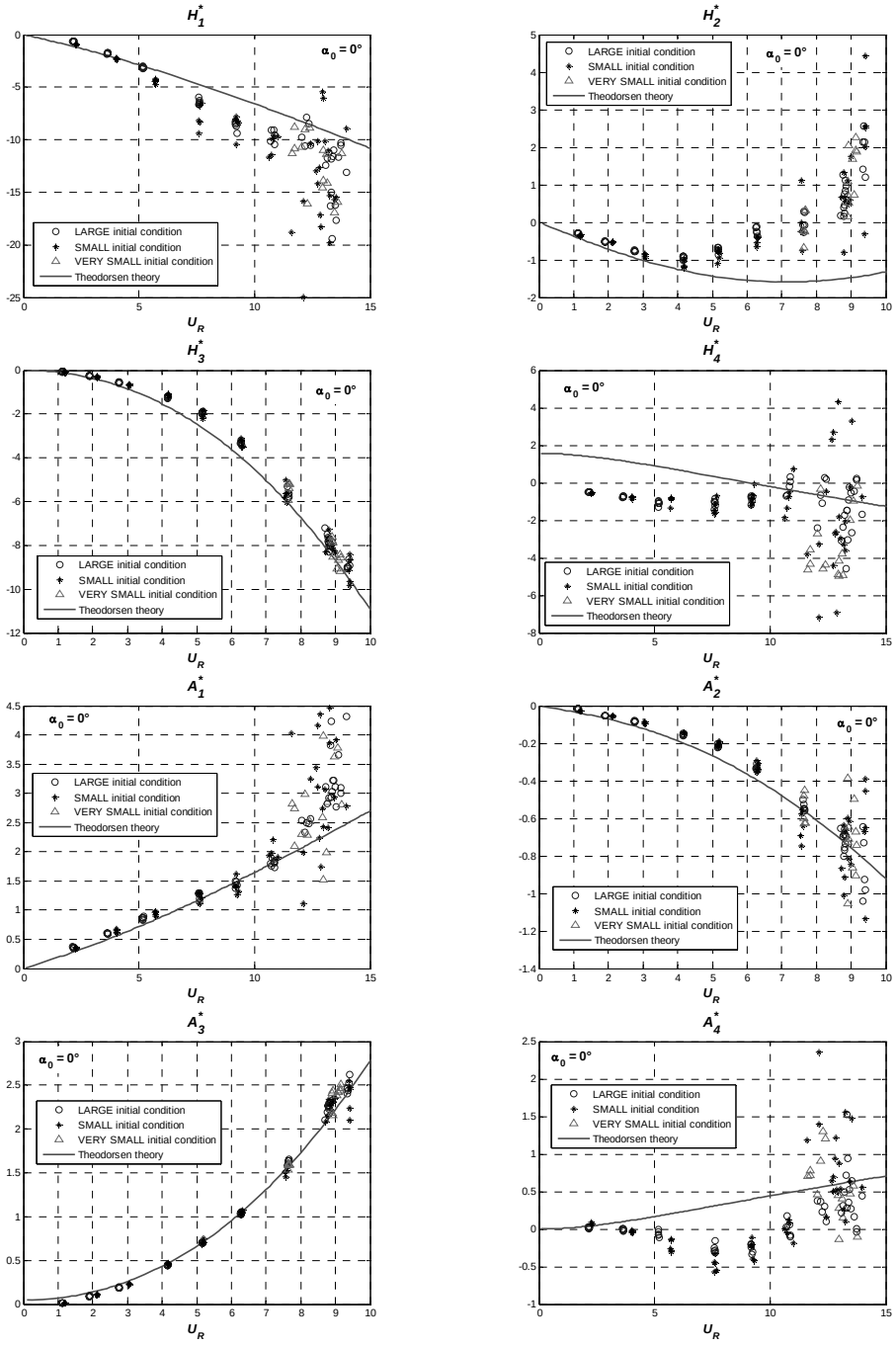

Figure 8.19 Flutter derivatives for three different initial conditions of the heaving-pitching free-decay motion. In still air the section model is horizontal ($\alpha_0 = 0°$).

The graphs of Fig. 8.19 suggest the first important conclusion: for this particular cross-sectional geometry the amplitude of the decaying motion does not seem to have a significant influence on the flutter derivative values. In other words the flutter derivatives are linear with respect to the amplitude of the motion. It is also evident that a certain degree of dispersion affects the measured values and this scattering increases with the reducing wind speed, becoming very large near the flutter instability limit. Consequently, it is very important to repeat several times the measures, especially when flutter derivatives are identified via free-vibration tests. Further, it can be remarked that surprisingly for many functions the measured values are not very far from the theoretical ones corresponding to a thin flat plate (Theodorsen's theory). Excluding the almost meaningless H_4^* and A_4^* functions, the largest discrepancy can be observed for H_2^*.

It is also worth noting that due to the non-zero mean aerodynamic moment, the cross-section presents a mean angle of attack which progressively increases with the wind speed. Since the non-linear dependence of flutter derivatives on the mean angle of attack is well known (e.g. [j]), it is necessary to express the aeroelastic coefficients as functions not only of the reduced velocity U_R but also of the mean angle of attack. In Fig. 8.20 this non-linear behavior is highlighted by reporting the flutter derivative curves corresponding to the still-air initial angle of attack α_0. For each reduced wind speed the mean value of the measured data is considered. It can be observed that the influence of the mean angle of attack is dramatic when small negative angles are concerned, corresponding to the range where an evident nonlinear behavior is observed in the static tests (Fig. 8.9).

Since the aeroelastic coefficients are mainly used to predict flutter, the validity of the measured functions is checked by calculating the critical flutter wind speed in three test cases for which the flutter boundaries are known (Tab. 8.7). In particular, "test case 0" is the one on which the flutter derivatives are actually measured, whereas the other two test cases are obtained by adding eccentric masses, so reducing the frequency ratio. In Tab. 8.8 the measured critical flutter wind speed and frequency are compared to the values calculated through eigenvalue analysis using the mean values of the experimental flutter derivatives and the Theodorsen's theory. In two out of the three test cases the results are very close to the measured values, while the Theodorsen's theory significantly overestimates the flutter critical wind speed. In the third case, characterized by the smallest frequency separation, the flutter derivatives do not correctly predict the flutter instability limit. The reasons for this discrepancy is still not clear.

Flutter derivatives are often considered as deterministic functions but it is to understand from the data scattering of Fig. 8.19 that they are not. Consequently, it is very interesting to understand how the uncertainty affecting the input (flutter derivatives) is transferred to the output (flutter critical wind speed and frequency). A probabilistic flutter approach was already proposed in [3] and [4] and interestingly applied to two rectangular cylinders, tested some years ago under smooth and turbulent flow in the CRIACIV wind tunnel [i]. The model is based on the assumption that the flutter derivative values at each reduced wind speed are extractions of independent normally-distributed random variables. While the independency assumption is quite obvious, the Gaussian distribution is positively checked via Lilliefors and Jarque-Bera tests with level of significance of 5 % (Fig. 8.21). The probability distribution function of the critical wind speed and frequency is calculated through the Monte-Carlo simulation of the flutter derivatives and then performing the classical eigenvalue analysis. The resulting critical wind speed distribution for "test case 0" (Tabs. 8.7 and 8.8) is reported in Fig. 8.22. It is worth noting that, due to the high non-linearity of the flutter equations, the resulting distribution is no longer Gaussian but in this particular instance well concentrated around the mean value, which is very close to the deterministic result. The coefficients of variation of the critical wind speed and frequency are in this case very small (between 1 and 3%), confirming the high reliability of the results.

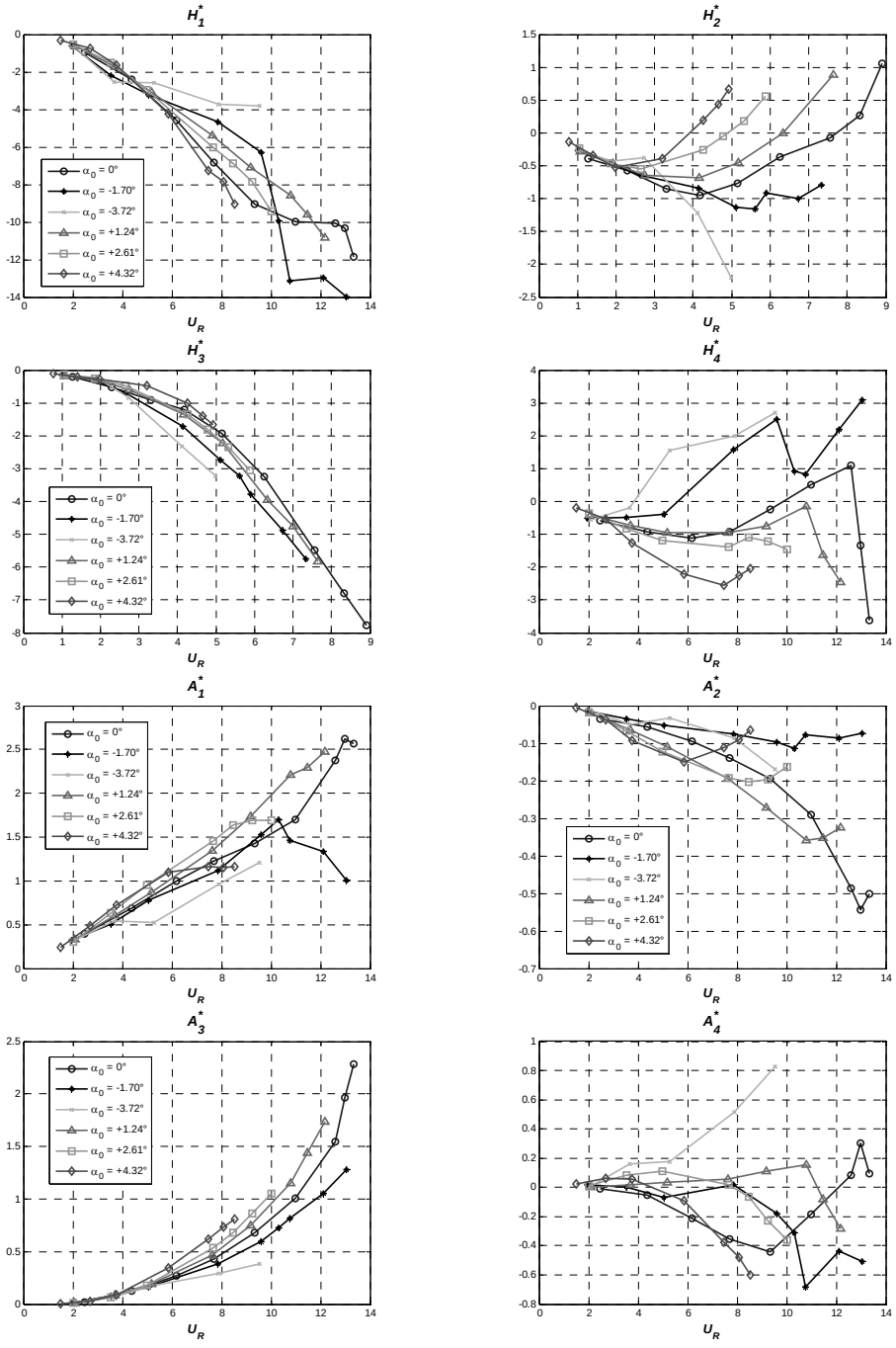

Figure 8.20 Flutter derivative comparison for four different still-air angles of attack α_0

Test case	ρ [kg/m^3]	m [kg/m]	I [kgm^2/m]	f_h [Hz]	f_α [Hz]	γ_ω [-]
0	1.195	5.449	0.0955	3.055	5.953	1.948
1	1.212	6.047	0.1917	2.906	4.165	1.433
2	1.212	6.289	0.2311	2.847	3.788	1.331

Table 8.7 Dynamic parameters of the three test cases for flutter calculation

Test case			Measured			Eig. Analysis			Theodorsen's theory		
	ζ_h [%]	ζ_α [%]	U_{Rc} [-]	f_c [Hz]	U_c [m/s]	U_{Rc} [-]	f_c [Hz]	U_c [m/s]	U_{Rc} [-]	f_c [Hz]	U_c [m/s]
0	0.24	0.18	9.30	4.74	19.86	9.43	4.69	19.91	11.24	4.35	22.00
	0.00	0.00				9.38	4.70	19.85	11.13	4.37	21.87
1	0.35	0.17	9.13	3.70	15.20	9.19	3.69	15.27	9.83	3.63	16.04
	0.00	0.00				9.08	3.70	15.13	9.64	3.64	15.79
2	0.34	0.17	7.24	3.56	11.60	9.10	3.44	14.08	9.28	3.42	14.27
	0.00	0.00				8.96	3.45	13.90	9.04	3.43	13.95

Table 8.8 Measured and calculated flutter critical reduced wind speed (U_{Rc}), frequency (f_c) and dimensional wind speed (U_c)

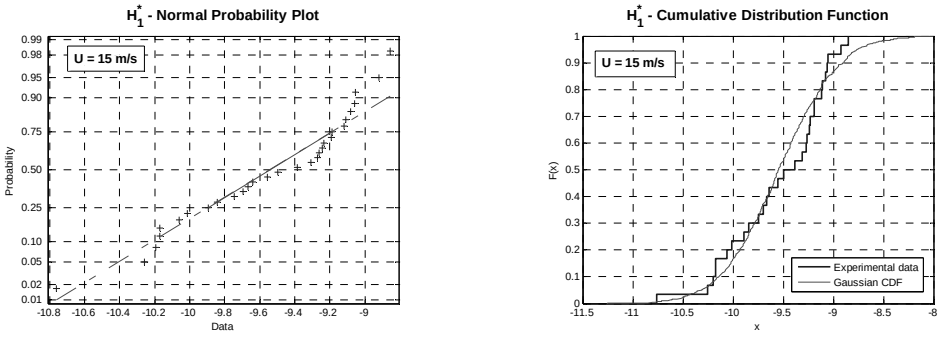

(a) (b)

Figure 8.21 Probability plot (a) and cumulative distribution function (b) for the flutter derivatives H_1*, measured at a wind speed of 15 m/s (sample size N = 30)

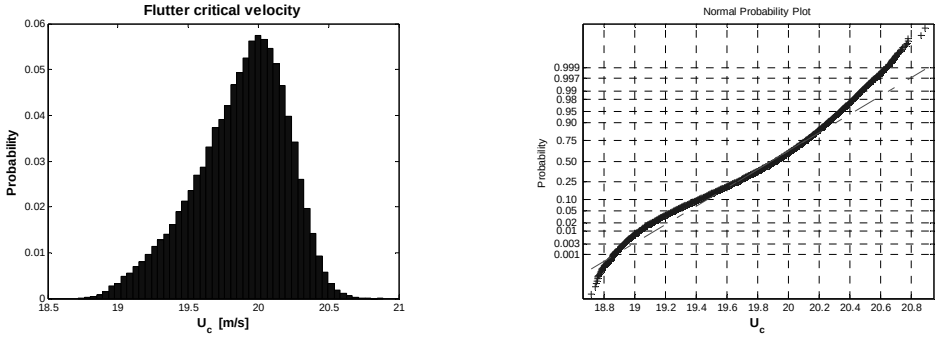

(a) (b)

Figure 8.22 Probability distribution and Normal probability plot (N = 100000) of the flutter critical wind speed (U_c) for “test case 0"

The small variance of the results is quite astonishing, given the high dispersion of some flutter derivatives at high reduced wind speed. This is due to the characteristics of the flutter equations but also to the fact that several flutter derivatives, and in particular the most dispersed ones, are known not to contribute significantly to flutter [5]. Finally, this probabilistic approach to flutter is able to highlight some "irregular" behaviors in the flutter calculation [3] and, also in the most clear cases, such as that one considered here, it allows to derive important information about the reliability of the results.

8.4 MULTI-BOX GIRDER DECK

The last wind-tunnel test campaign about bridge aerodynamics and aeroelasticity concerns multi-box girder decks. This structural solution is quite innovative and mainly adopted in very large bridges in order to obtain small aerodynamic forces (in particular low drag) and large stability with respect to flutter. For these reasons a three-box girder was chosen for the proposed design of Messina Strait Bridge, whose basic cross-sectional geometry is taken as reference case study in the CRIACIV wind-tunnel campaign. The main objectives of this research work is to study the sensitivity of the aerodynamic and aeroelastic properties of the deck with respect to the distance between the boxes and the non-structural elements which complete the cross-section.

Four wooden section-models were built, only changing the total width of the deck, ranging from 561.6 mm to 432.0 mm (Fig. 8.23), always keeping the same geometry of the boxes. With respect to Messina Bridge design the scale of the widest model (Deck 1) is 1:107.5. Static and aeroelastic tests are performed using the same setups previously described.

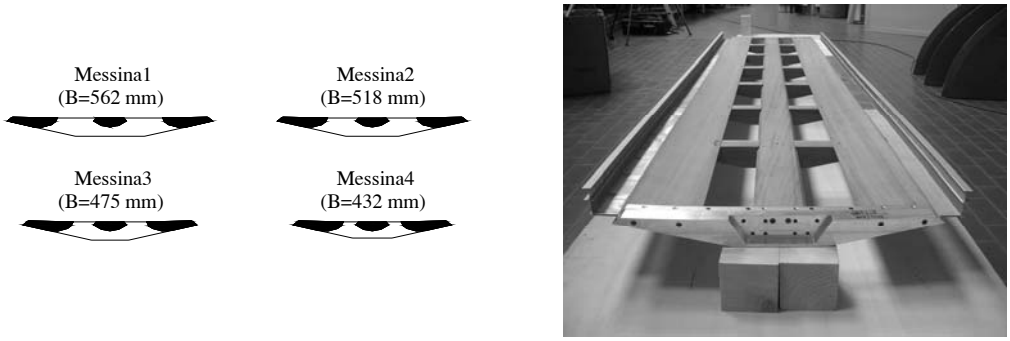

(a) (b)

Figure 8.23 (a) Schematic drawing of the four section models and (b) picture of "Deck 1" (with spoiler)

As a first step the mean aerodynamic forces of the four section models in the bare deck configuration are compared both normalizing them with respect to the chord length of the concerned deck or to that of Deck 1, which is taken as reference (Figs. 8.24 and 8.25). It is very interesting to remark that in the second case the curves are almost parallel: consequently, assuming at least qualitatively valid the quasi-steady approach which relates the flutter derivatives to the slope of the static polars, these results suggest that the aeroelastic behavior of the four section models differs for a scale factor proportional to the actual width of the deck. It is worth noting in Fig. 8.26 the strong sensitivity of the aerodynamic coefficients of Deck 1 in the bare configuration with respect to Reynolds number effects.

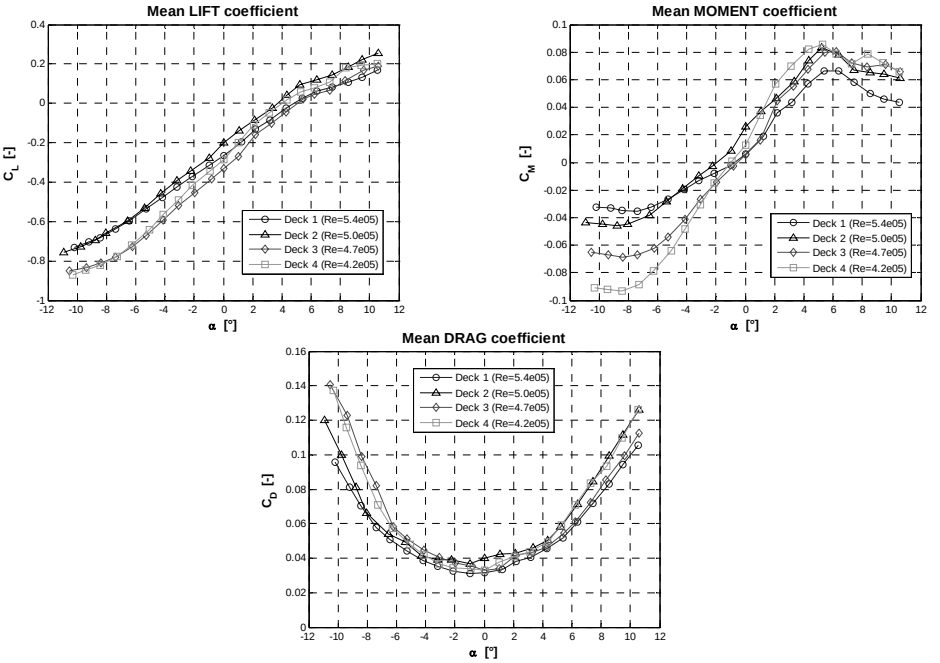

Figure 8.24 Static aerodynamic coefficients of the studied section models in the bare deck configuration (normalization with respect to actual width of the models)

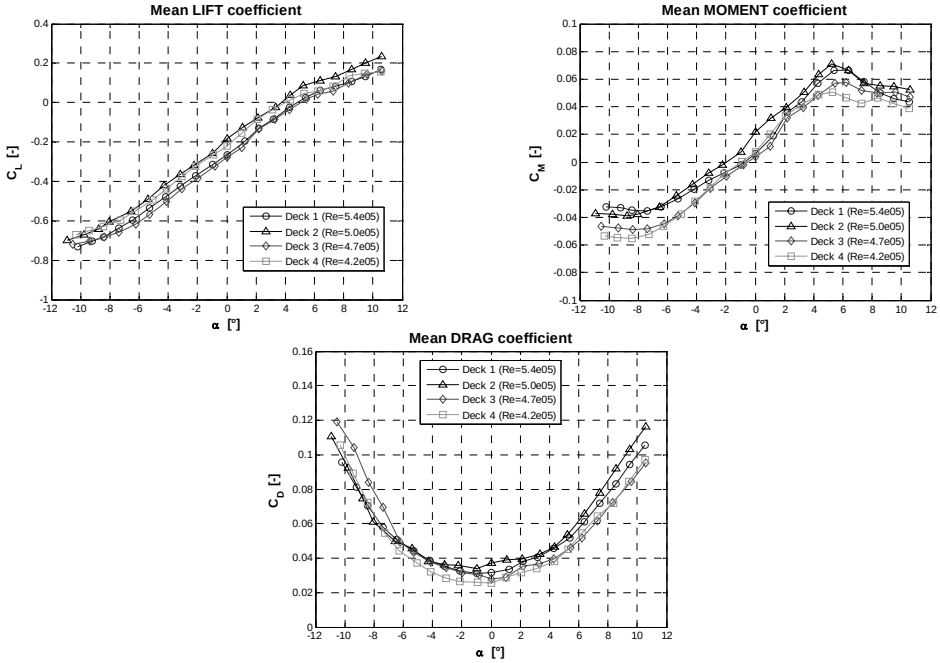

Figure 8.25 Static aerodynamic coefficients of the studied section models in the bare deck configuration (normalization with respect to width B_1 = 561.6 mm of Deck 1)

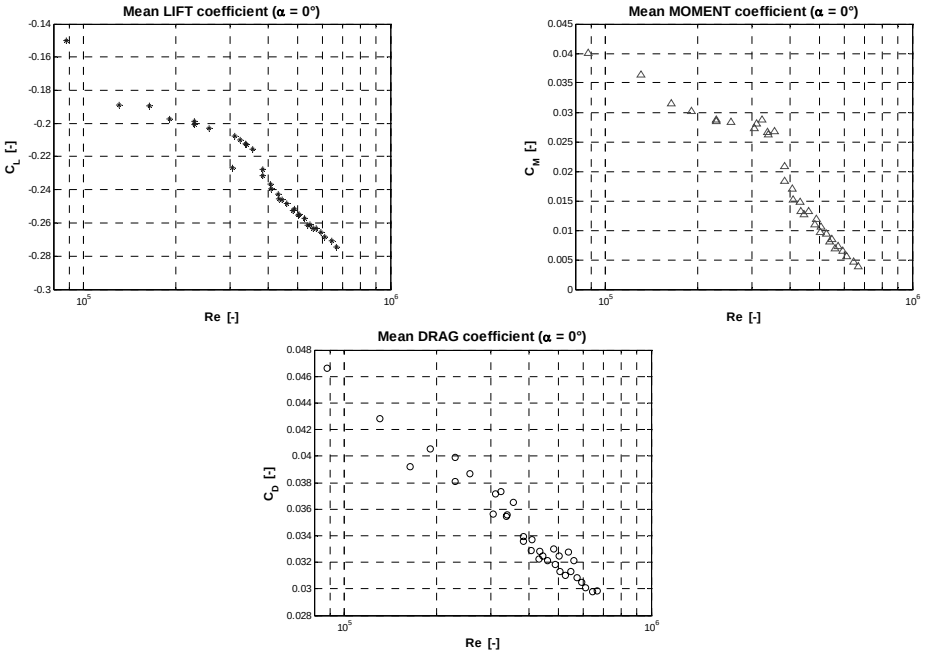

Figure 8.26 Reynolds number effects for the model Deck 1 in the bare deck configuration

The second part of the research is devoted to understand the sensitivity of the aerodynamic behavior with respect to non structural details such as lateral spoiler (see Fig. 8.23b) and grids of different porosity placed in correspondence of the spoilers and between the boxes. For this purpose only the model called Deck 1 was tested. The nomenclature adopted to describe the results is explained in Fig. 8.27, while the characteristics of the grids is detailed in Tab. 8.9. The measured aerodynamic coefficients (Fig. 8.28) show a strong variability with respect to these non structural details. In particular, it is worth noting that the drag coefficient is minimum for the bare deck configuration and it is obviously very sensitive to the grid porosity in correspondence of the spoiler and much less to that of the grid between the boxes. Conversely, the lift coefficient, particularly its slope, is very sensitive to all type of grids and only the configuration with non-porous screens between the boxes shows higher lift slope with respect to the bare deck. Finally, the moment coefficient seems to be dramatically affected by the presence of spoiler and grids. In particular, all kind of grid in the spoiler position makes the sign of the slope change from positive to negative and this slope gets larger when the degree of porosity decreases. That means that the flow field around the body completely changes when these grids are added.

The final step of this study is the comparison between the aerodynamic and aeroelastic behavior of two models with different chord lengths in the same deck configuration (spoiler without any grid, called “abcdP0” in Fig. 8.28). The static coefficients of Deck 2 (B_2 = 518.4 mm) for different Reynolds numbers are reported in Fig. 8.29, showing significant scale effects for Re < 560000 but not in the range 560000 < Re < 750000. In Fig. 8.30 the static polars for Deck 1 and Deck 2, both normalized with respect to B_1 = 561.6 mm are compared, confirming the aforementioned tendency to show the same lift and moment slopes.

Afterwards, flutter derivatives are measured for the two section models using the same free-vibration method previously described. In Fig. 8.31 the aeroelastic coefficients for Deck 2 are re-

ported showing once again the large scattering of the data especially near the flutter critical wind speed. It can also be observed that the amplitude of the motion does not seem to affect significantly the pattern of the functions. Finally, in Fig. 8.32 the mean values of the aeroelastic coefficients for the two decks are compared, showing very similar curves. The most visible differences concern A_1^* and A_3^*, although they seem to be limited to a multiplicative coefficient.

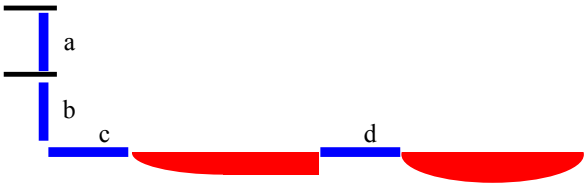

Figure 8.27 Nomenclature adopted for the position of the grids

Position		Porosity	
a	upper part of the spoiler	**PP**	no porosity
b	lower part of the spoiler	**P1**	very little porous grid
c	base of the spoiler	**P2**	grid with 2 mm holes
d	space between the boxes	**P3**	grid with 6 mm holes
		P0	no grid

Table 8.9 Nomenclature adopted for position and porosity of the grids

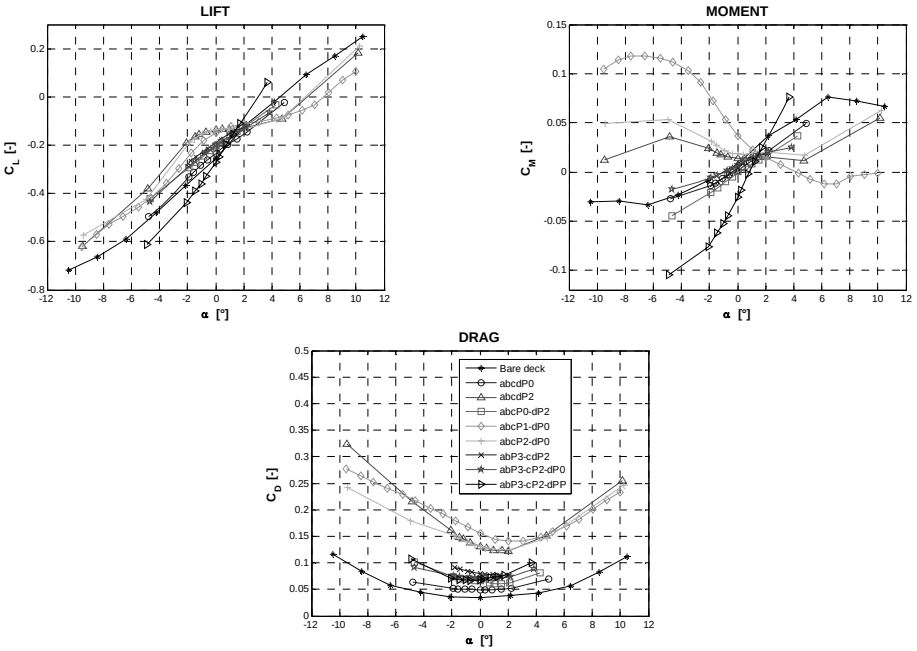

Figure 8.28 Sensitivity study on the aerodynamic coefficients with respect to the considered non structural details (Deck 1; Re ≈ 600000)

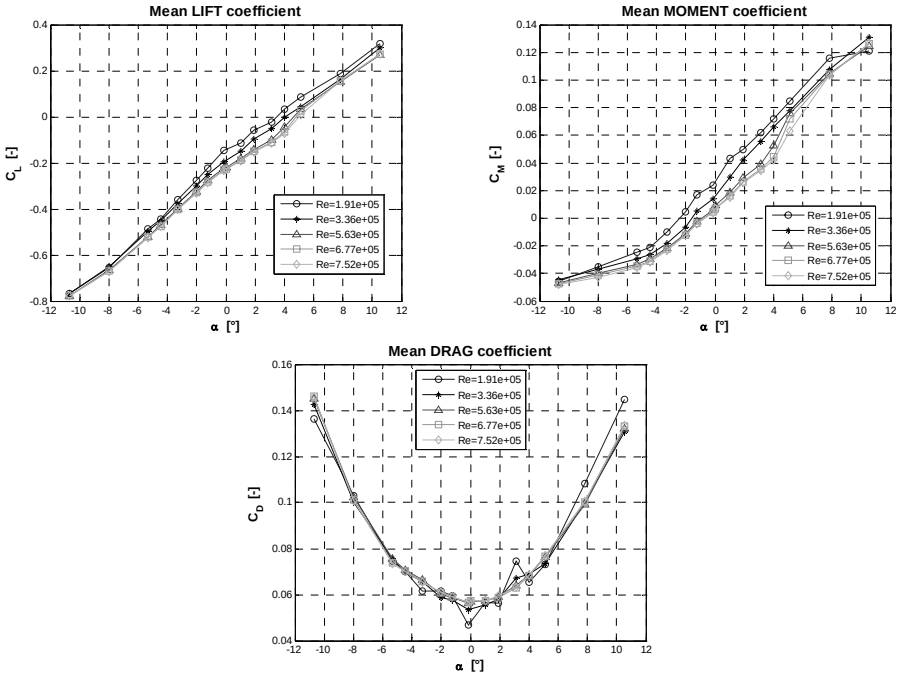

Figure 8.29 Deck 2 static polars for different Reynolds number (normalization with respect to B_2)

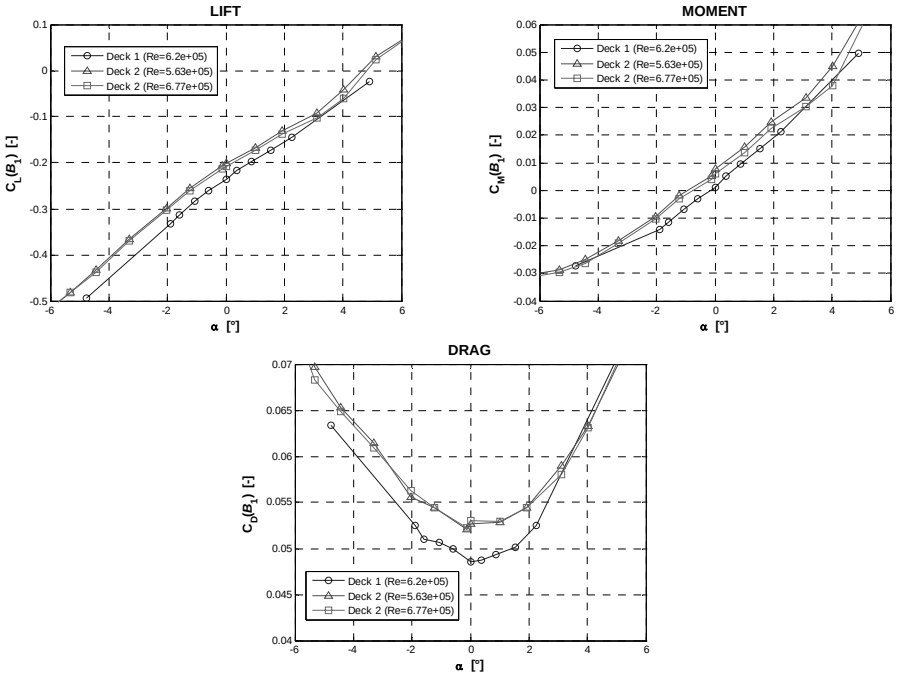

Figure 8.30 Comparison between Deck 2 and Deck 1 static polars (normalization with respect to B_1)

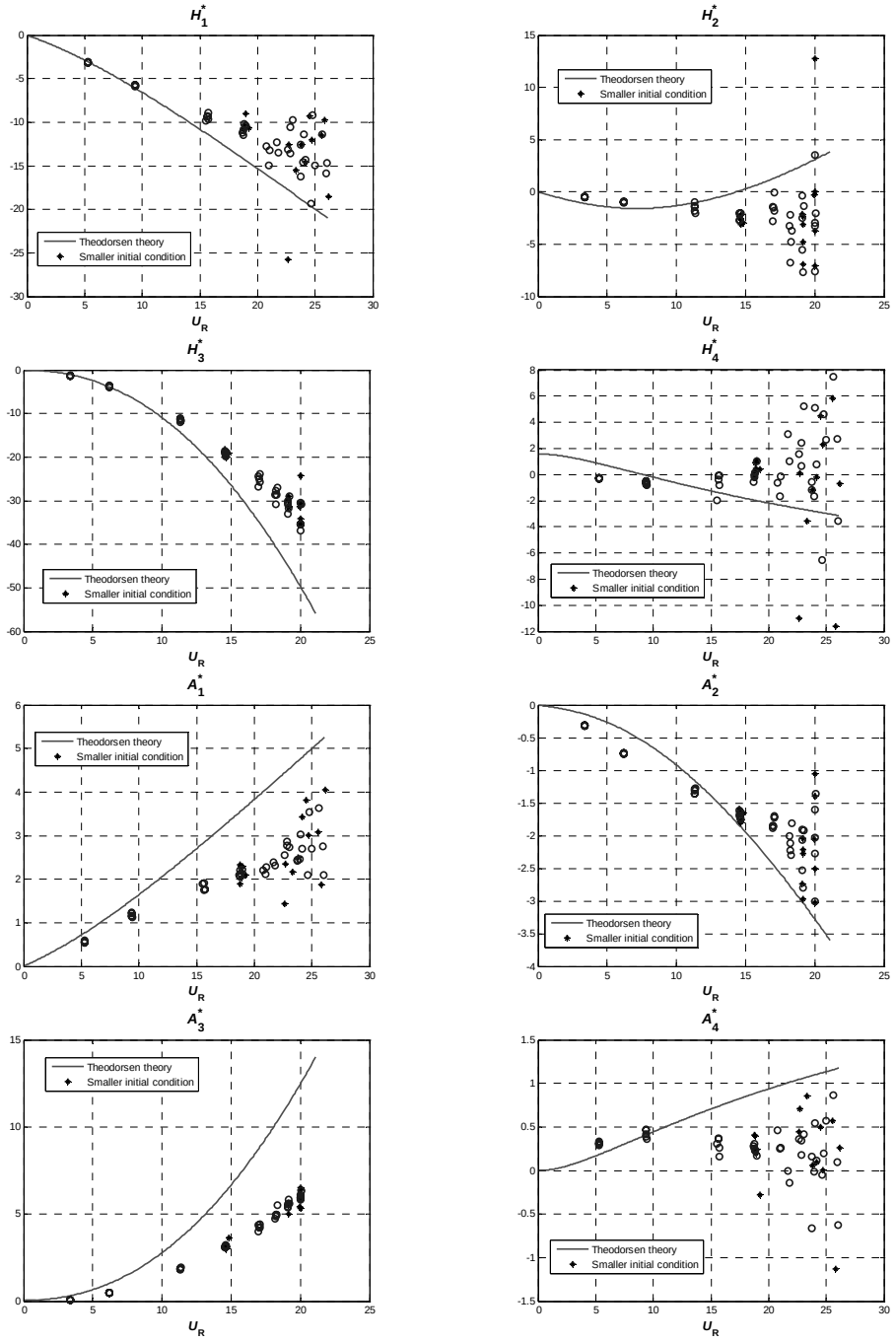

Figure 8.31 Flutter derivatives for Deck 2

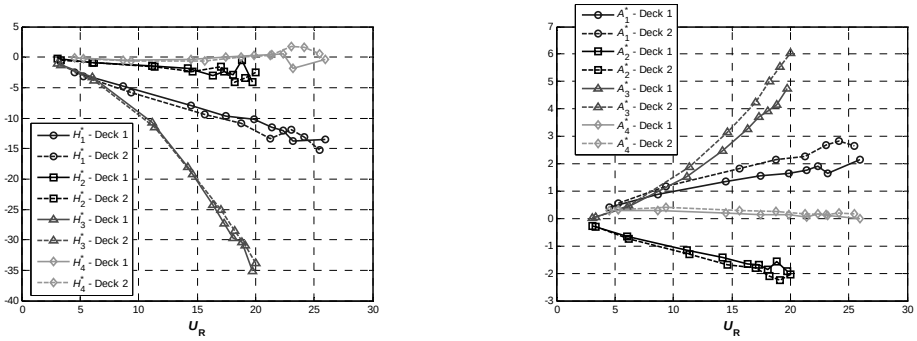

Figure 8.32 Flutter derivatives comparison for Deck 1 and Deck 2

8.5 BASIC REFERENCE

[a] Dyrbye C., Hansen S.O. 1997. *Wind loads on structures*. John Wiley & Sons, New York.

[b] Simiu E., Scanlan R.H. 1996. *Wind Effects on Structures. Fundamentals and Applications to Design*. 3rd Edition, Wiley, New York.

[c] Haan F.L. jr, Kareem A., Szewczyk A.A. 2000. Experimental measurements of spanwise correlation of self-excited forces on a rectangular cross section. *Fourth Int. Coll. on Bluff Body Aero. and Appl.*, Bochum, 439-442.

[d] Ricciardelli F., de Grenet E.T., Hangan H. 2002. Pressure distribution, aerodynamic forces and dynamic responce of box bridge sections. *J. Wind Eng. Ind. Aerodyn.,* **90** (10): 1135-1150.

[e] Ricciardelli F., de Grenet E.T., Solari G. 2002. Analysis of the wind loading of a bridge deck box section using Proper Orthogonal Decomposition. *J. Fluid Mech. Res.*, **29** (3-4): 312-322.

[f] Ricciardelli F., Hangan H. 2001. Pressure distribution and aerodynamic forces on stationary box bridge section. *Wind and Structures,* **4** (5): 399-412.

[g] Davenport A., King, J. 1982. *A study of the wind effect for the Sunshine Skyway Bridge, Tampa, Florida*. BLWT-SS24-1982, The BLWT Laboratory, UWO, London, Canada.

[h] Gu M., Zhang R., Xiang H. 2000. Identification of flutter derivatives of bridge decks. *J. Wind Eng. Ind. Aerodyn.,* **84**: 151-162.

[i] Righi M. 2003. *Aeroelastic stability of long span suspended bridges: flutter mechanism on rectangular cylinders in smooth and turbulent flow*. Ph.D. Thesis, Università di Firenze (Italy).

[j] Diana G., Bruni S., Rocchi D. 2005. A numerical and experimental investigation on aerodynamic nonlinearities in bridge response to turbulent wind. *Proc. 6th European & African Conference on Wind Engineering* (J. Náprstek & C. Fischer eds.), Prague.

8.6 LIST OF PUBLICATIONS

[1] de Grenet E.T., Ricciardelli F. 2005. The span-wise correlation of aerodynamic forces on a rectangular cylinder for different vibration regime. *6th European Conference on Structural Dynamics EURODYN'05*, Paris, France, 4-7 September 2005

[2] Mannini C., Soda A., Voß R. 2006. Computational Investigation of Flow around bridge sections. *Proc. SECON Conference "Bridges"*. Dubrovnik, Croatia

[3] Bartoli G., Mannini C. 2005. Reliability of bridge deck flutter derivative measurements in wind tunnel tests. *Proc. 9th International Conference On Structural Safety And Reliability* (Millpress, Rotterdam), Roma: 1193-1200.

[4] Mannini C. 2006. *Flutter vulnerability assessment of flexible bridge decks*. Ph.D. Thesis, Università degli Studi di Firenze (Italy) - TU Braunschweig (Germany).

[5] Bartoli G., Mannini C. 2005. A simplified method to evaluate the critical flutter speed for flexible bridge decks, *Proc. 6th European & African Conference on Wind Engineering* (J. Náprstek & C. Fischer eds.), Prague.

WITH CONTRIBUTION FROM:

Piero D'Asdia, University "G. D'Annunzio" of Chieti-Pescara
Enrico T. de Grenet, University "Mediterranea" of Reggio Calabria
Sofia Febo, University "G. D'Annunzio" of Chieti-Pescara
Claudio Mannini, University of Florence
Stefano Pastò, University of Florence
Lorenzo Procino, CRIACIV BLWT
Francesco Ricciardelli, University "Mediterranea" of Reggio Calabria
Vincenzo Sepe, University "G. D'Annunzio" of Chieti-Pescara

9 Numerical analyses

Luca Facchini
University of Florence

9.1 INTRODUCTION

This chapter is divided into two main sections, the former regarding the statistical characterization and the consequent numerical simulation of Gaussian and non-Gaussian wind induced pressure fields; the latter is devoted to the optimization problem of structures which undergo wind induced loads.

The chapter is a summary of the research work carried out by two research units of the Project, namely Florence (DIC) and Perugia, which has also been published as in the list of publications reported at the end of the chapter.

9.2 CHARACTERIZATION AND SIMULATION OF NON GAUSSIAN PRESSURE FIELDS BY MEANS OF MEMORYLESS TRANSFORMATIONS

In this section, a statistical characterization is given of the non-Gaussian pressure field induced by wind on the surface of a reduced scale model of an isolated cooling tower. Subsequently, the non Gaussian pressure field is simulated by means of a memory less transformation applied to a proper underlying Gaussian field.

The model was tested in the CRIACIV boundary layer wind tunnel in Prato, and pressure coefficients were estimated from measured pressures by means of the usual relation

$$c_{p,h}(t) = \frac{p_h(t) - p_{0,h}}{\rho v^2(z_h)/2} \tag{9.1}$$

where $p_h(t)$ is the recorded pressure in the h-th tap, $p_{0,h}$ is the constant "static" pressure of the undisturbed flow in the position of the tap, and the denominator represents the dynamic increment on the pressure of the undisturbed flow; z_h is the height of the h-th tap. At the end of the experiment, for each tap it was possible to obtain a global population of 516348 samples which showed a more or less marked non-Gaussianity, and was therefore characterized by means of a memory less transformation applied to an underlying Gaussian process which had to be defined.

From this point of view, in order to completely characterize the non-Gaussian pressure field acting on the tower surface, two objects are necessary:

- a Gaussian field with proper characteristics;
- a non linear function to apply to the Gaussian field in order to obtain the desired non-Gaussian field.

The actual pressure coefficient is a function of time and position on the tower surface, and can be expressed by

$$c_p(\mathbf{x},t) = f\left(\mathbf{x}, c_g(\mathbf{x},t)\right) \tag{9.2}$$

where $c_p(\mathbf{x},t)$ is the pressure coefficient evaluated in position $\mathbf{x}$ at time t, and $c_g(\mathbf{x},t)$ is the Gaussian pressure coefficient evaluated in the same position and at the same time. Function f is a nonlinear function which must be identified and depends on position as well.

The pressure coefficients are known in correspondence of the pressure taps, so it is necessary to proceed following these steps:

- Estimate function f and the Gaussian coefficients in correspondence of the position of the pressure taps for the performed experiment;
- Extend the function f outside of the pressure taps;
- Estimate the mean and spectral density of the underlying Gaussian field;
- Simulate the underlying Gaussian field and apply function f to it in order to obtain the desired non-Gaussian field of the actual pressure coefficients.

9.2.1 Estimation of transfer function in correspondence of pressure taps

The population of 516348 samples obtained in each pressure tap was rearranged in 20 classes in order to build the histogram of each c_p. Subsequently, an approximation of each pdf was computed by means of Gram-Charlier type III (see f.i. Muscolino [a]) expression:

$$p_{c_{p,h}}\left(c_{p,h}\right) = N_h \exp\left(\sum_{k=1}^{N_{gc}} \frac{\gamma_k H_k\left(\left(c_{p,h} - \mu_{c_{p,h}}\right)/\sigma_{c_{p,h}}\right)}{k}\right) \tag{9.3}$$

where N_h is a normalizing constant, N_{gc} is the order of the expansion, μ_{cp} and σ_{cp} are the mean and standard deviation of each pressure coefficient, respectively, and H_k is the k-th order Hermite polynomial.

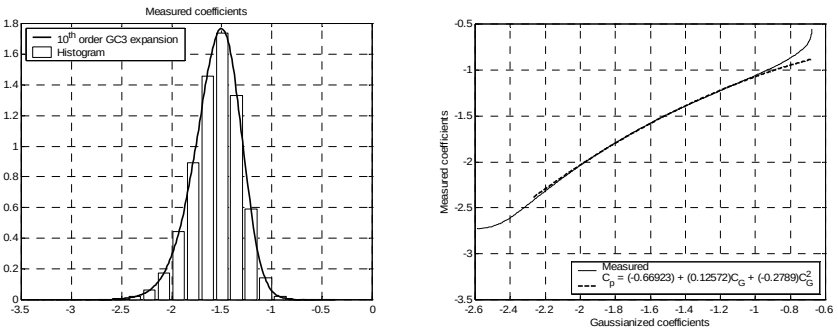

Figure 9.1 On the left, histogram and 10th order Gram-Charlier type III approximation of the pdf of the c_p measured in tap # 10 ; on the right, the estimated transfer function andits best polynomial fit.

It was found that a 10^{th} order expansion gave extremely satisfactory results for each tap (see f.i. Figure 9.1). The relation between the computed c_p and the corresponding underlying Gaussian c_g can be evaluated by means of different procedures (see f.i. Choi and Kanda [b]). Here, the

cumulative density function (CDF) was computed for both variables and subsequently plotted against each other. In other words, the CDF for each pressure coefficient was computed as

$$P_{c_{p,h}}(c) = \int_{-\infty}^{c} p(u)du \;;\; P_{c_{g,h}}(c) = \int_{-\infty}^{c} N\left(u, \mu_{c_{p,h}}, \sigma_{c_{p,h}}\right)du \tag{9.4}$$

where N stands for the normal distribution function; since the variables defined by

$$c_{pu_{,h}} = P_{c_{p,h}}\left(c_{p,h}\right) \;;\; c_{gu_h} = P_{c_{g,h}}\left(c_{g,h}\right) \tag{9.5}$$

are both uniformly distributed and therefore may be set to equal (see Bartoli et al. [c]), the underlying normal variable can be defined by the relation

$$c_{g_h} = P^{-1}_{c_{g,h}}\left(P_{c_{p,h}}\left(c_{p,h}\right)\right) \tag{9.6}$$

The obtained relation, together with a quadratic least squares fit, is shown in Figure 9.1 on the right side.

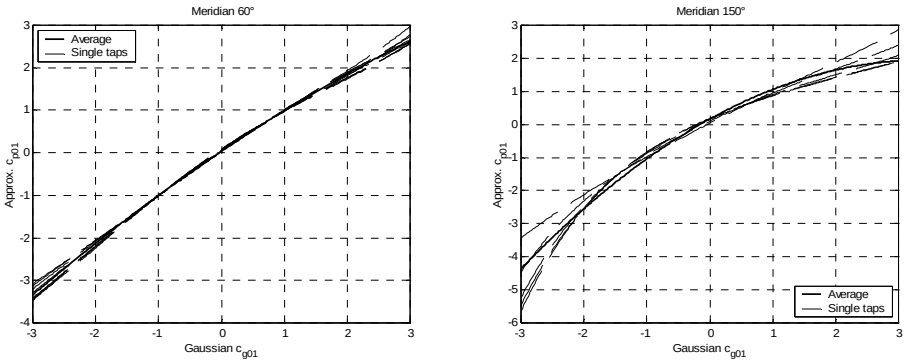

Figure 9.2 The best (left) and worst (right) assessment of the dependence of the transfer function on the anomaly θ only.

A very interesting observation can be made if the relation between the standardized pressure coefficients and their underlying Gaussian counterparts are grouped together for each meridian of the tower; the relation between $c_{p0,1} = (c_p - \mu_{cp})/\sigma_{cp}$ and $c_{g0,1} = (c_g - \mu_{cg})/\sigma_{cg}$ for each pressure tap lying on a given meridian is almost constant with height and consequently it depends only on the anomaly θ measured from the reference meridian (the one which is directly invested by the turbulent flow).

A polynomial approximation is estimated for such relation, and the coefficients of the 2nd and 3rd order polynomials are shown in Figure 9.3. A quadratic form is chosen from the observation that higher order approximations show very small leading coefficients, thus resulting in quadratic forms themselves; therefore, terms of order higher than 2 have been neglected.

If a quadratic expression is used for the relation between $c_{p0,1}$ and $c_{g0,1}$, then it must be of the form (taking also in account the fact that the first order term is always very close to unity, see Figure 9.3)

$$c_{p,01} = ac^2_{g,01} + c_{g,01} + b \tag{9.7}$$

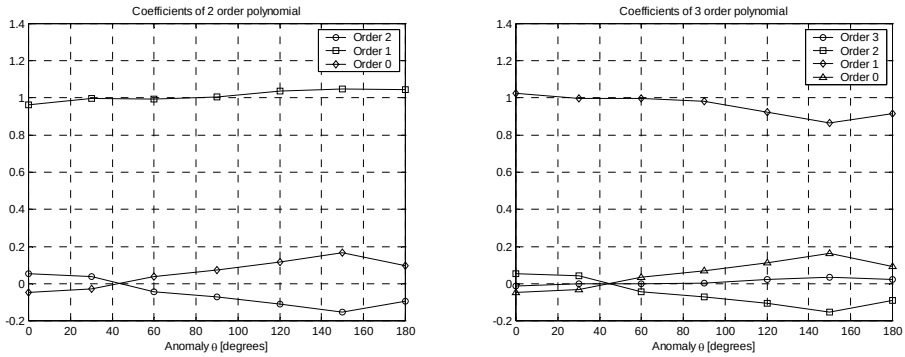

Figure 9.3 The coefficients of II order (left) and III order (right) approximating polynomials for transformations of standard Gaussian pressure coefficients.

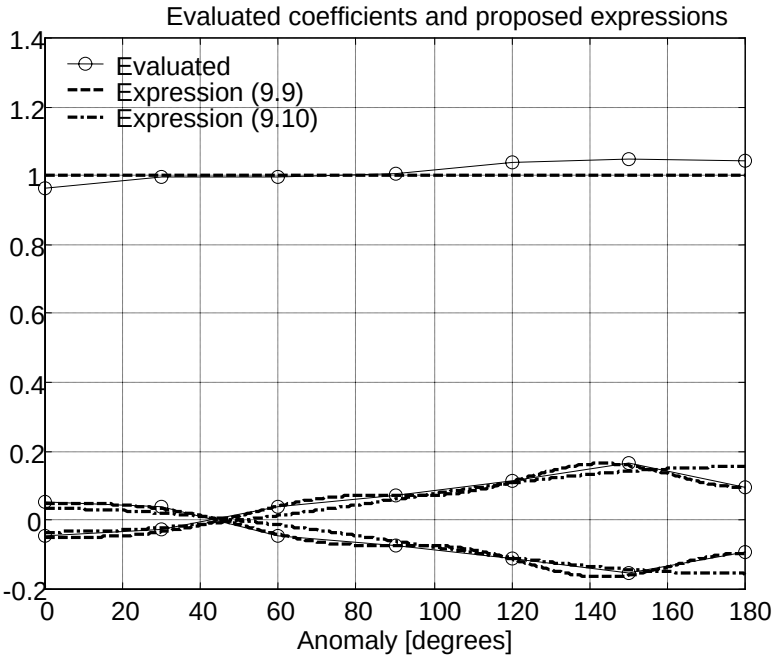

Figure 9.4 The two proposed expressions (9.9) and (9.10) for the polynomial approximation (9.8)

Imposing that $E[c_{p0,1}] = 0$ and $E[c^2_{p0,1}] = 1$, it is obtained that $b = -a$, and thus the proposed relation may be put in the form

$$c_{p,01} = a\left(c^2_{g,01} - 1\right) + c_{g,01} \tag{9.8}$$

where two possible expressions for the coefficient a are

$$a(\theta) = -0.0599 + 0.0914\cos(2\theta) + 0.0213\cos(4\theta) + \ldots + 0.0154\cos(8\theta) - 0.0201\cos(10\theta) + 0.0039\cos(12\theta) \tag{9.9}$$

$$a(\theta) = -0.06 + 0.10\cos(2\theta) \tag{9.10}$$

where θ is expressed in radians starting from the windward meridian (see Figure 9.4).

9.2.2 Characterization of underlying Gaussian field

The Gaussian field $c_{g,01}$ is completely characterized by its covariance structure, or equivalently by its spectral density function, its mean being zero all over the shell surface. Since the standard deviation is unitary all over the shell surface, a normalized expression has been used to describe the spectral densities.

Two different kind of power spectral density must be taken into account: the taps which are directly subject to the incoming flow show a rather smooth spectral density, while the ones subject to vortex shedding exhibit a spectral density with a marked peak: such characteristic must be properly described.

As for the transfer functions, the spectral density of the windward taps shows no marked variation with height along the 0° meridian. An approximating expression was searched in the form

$$\begin{aligned} \frac{fS_0(f)}{\sigma^2} &= \frac{Af}{\left[1 + Bf^{\beta}\right]^{\alpha}} \\ A &= \left[\int_0^{\infty} \frac{df}{\left[1 + Bf^{\beta}\right]^{\alpha}}\right]^{-1} = \frac{B^{1/\beta}\Gamma(\alpha)}{\Gamma\left(\alpha - \beta^{-1}\right)\Gamma\left(1 + \beta^{-1}\right)} \end{aligned} \tag{9.11}$$

where Γ(•) is the Gamma function; the coefficients were found B = 0.0216, β = 1.7034, α = 1.3608 and eventually A = 0.0879 for the taps with anomaly θ = 0.

The product αβ deviates significantly from its expected value 5/3, being approximately 2.32; in fact, as the wind velocity is also Gaussian, a linear relation between the two fields should hold, thus leading to a product αβ = 5/3 also for the Gaussian pressure coefficients.

Such deviation is currently under examination.

The spectral densities of the Gaussian coefficients obtained for the other taps shows a more or less defined peak, which corresponds to the phenomenon of vortex shedding. The spectral density of the taps is obtained by superposition of the spectral density obtained for the 0 degrees meridian and a function of the type

$$\begin{aligned} \hat{S}(\theta, f) &= \hat{A}(\theta) f^{\hat{\beta}_\theta} \exp(-\hat{\gamma}_\theta f) \\ \hat{A}(\theta) &= \left[\int_0^{\infty} f^{\hat{\beta}_\theta} \exp(-\hat{\gamma}_\theta f) df\right]^{-1} \end{aligned} \tag{9.12}$$

The final expression of the spectral density can be put in the form

$$\frac{fS(\theta, f)}{\sigma^2} = C(\theta)\frac{Af}{\left(1 + Bf^{\beta}\right)^{\alpha}} + (1 - C(\theta))\hat{A}(\theta) f^{1+\hat{\beta}_\theta} \exp(-\hat{\gamma}_\theta f) \tag{9.13}$$

For the coherence and phase angle it was found that standard relations (see f.i. Simiu and Scanlan [d]) gave results in good agreement with experiments.

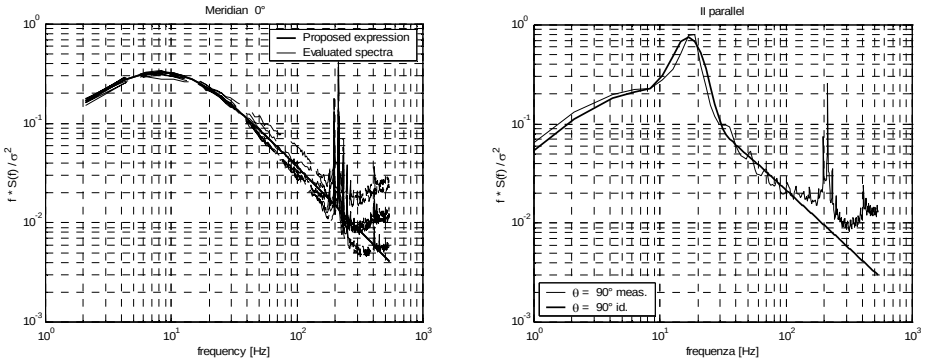

Figure 9.5 The evaluated and approximated spectral densities for the standardized Gaussian coefficients over the windward meridian (θ = 0°) and the 90° meridian, II level tap.

9.2.3 The simulation of the underlying Gaussian field

In order to obtain the simulation of the actual pressure coefficients c_p, the underlying $c_{g0,1}$ must be simulated and subsequently transformed.

The field of Gaussian coefficients $c_{p0,1}$ was simulated by means of RBF (radial basis functions) approach: in fact, it was modeled with an expression such

$$c_{g,01}(\mathbf{x},t) = a(t) + \mathbf{b}(t)\cdot\mathbf{x} + \mathbf{w}(t)\cdot\boldsymbol{\varphi}(\mathbf{x}) \tag{9.14}$$

Expression (9.14) is composed of three different terms:

- the first one, denoted by the symbol a, is constant with position, and is a function of time;
- the second one is linear with position, and can be represented by means of a scalar product between a vector **b** (which is function of time)and the position vector **x**;
- the last one is a completely nonlinear function of position **x**, and is modeled by means of a combination of a number N of functions $\varphi_i(\mathbf{x})$ times N time-dependent coefficients $w_i(t)$.

The expression of the nonlinear functions $\varphi_i(\mathbf{x})$ can be chosen among a wide variety (see f.i. Broomhead and Lowe [e], Gotovac and Kozulic [f], Haykin [g], Poggio and Girosi [h]). The main requirements are the following two:

- The generic function $\varphi_i(\mathbf{x})$ must be a function of the distance between the position **x** and another point $\mathbf{c}^{(i)}$, characteristic for each function, which is called the *center of the function*;
- Each function must tend to zero for increasing values of such distance.

An expression which is often employed for functions $\varphi_i(\mathbf{x})$ is the Gaussian bell:

$$\varphi_i(\mathbf{x}) = \exp\left(-\left\|\mathbf{x}-\mathbf{c}^{(i)}\right\|^2 \Big/ \sigma_i\right) \tag{9.15}$$

where σ_i denotes a decaying parameter.

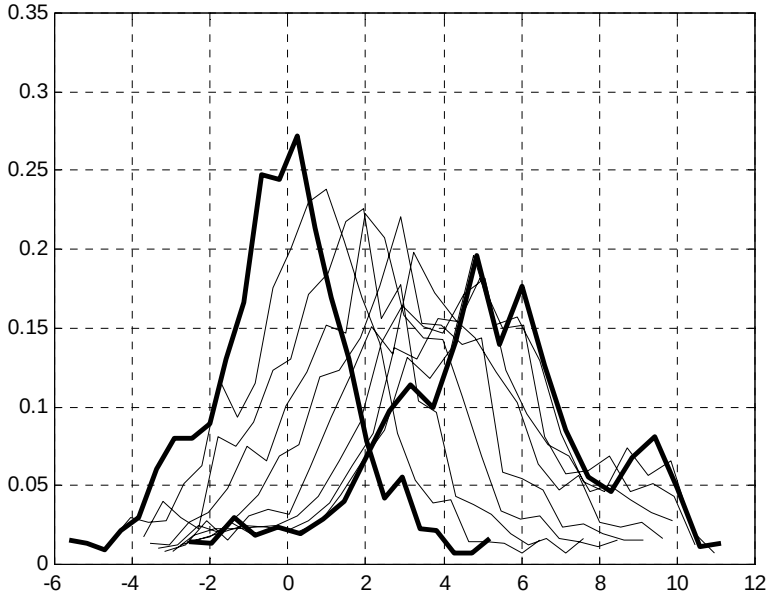

Figure 9.6 The distortion of the PDF of the pressure field from one tap to the adjacent one: the thick lines represent the pdf of the pressure in two adjacent taps, while the thin ones represent the pdf of the pressure field in intermediate positions.

Expression (9.14) can be rearranged in the form

$$\begin{aligned} c_{g,01}(\mathbf{x},t) &= \sum_h u_h(t)\cdot g_h(\mathbf{x}) = \mathbf{g}^t(\mathbf{x})\mathbf{u}(t) \\ \mathbf{g}^t(\mathbf{x}) &= \left[1 \quad \mathbf{x}^t \quad \boldsymbol{\varphi}^t(\mathbf{x})\right] \\ \mathbf{u}^t(t) &= \left[a(t) \quad \mathbf{b}^t(t) \quad \mathbf{w}^t(t)\right] \end{aligned} \tag{9.16}$$

With such positions, the random vector $\mathbf{u}(t)$ can be found by minimizing the error between the left and right term of the first of eqs. (9.16), obtaining that

$$\varepsilon(t) = \int_D \left[\sum_h u_h(t)\cdot g_h(\mathbf{x}) - c_{g,01}(\mathbf{x},t)\right]^2 d\mathbf{x} = \min \tag{9.17}$$

where D is the space domain of the simulation (i.e., the tower surface); thus

$$\frac{\partial \varepsilon}{\partial u_k} = \int_D \left[\sum_h u_h(t)\cdot g_h(\mathbf{x}) - c_{g,01}(\mathbf{x},t)\right] g_k(\mathbf{x}) d\mathbf{x} = 0 \tag{9.18}$$

Eq. (9.18) is a linear system, which can be put in matrix form by means of the following positions:

$$\int_D g_h(\mathbf{x}) g_h(\mathbf{x}) d\mathbf{x} = G_{hk}$$
$$\int_D g_h(\mathbf{x}) c_{g,01}(\mathbf{x},t) d\mathbf{x} = c_h(t) \tag{9.19}$$

thus obtaining that

$$G_{hk} u_k(t) = c_h(t) \Rightarrow \mathbf{u}(t) = \mathbf{G}^{-1}\mathbf{c}(t) \tag{9.20}$$

Correspondingly, for the spectral densities it can be found that

$$\mathbf{S}_{uu}(f) = \mathbf{G}^{-1}\mathbf{S}_{cc}(f)\mathbf{G}^{-t}$$
$$\mathbf{S}_{cc}(f) = \int_{D\times D} S_{c_{g,01}c_{g,01}}(\mathbf{x}_1, \mathbf{x}_2, f)\mathbf{g}(\mathbf{x}_1) \otimes \mathbf{g}(\mathbf{x}_2) d\mathbf{x}_1 d\mathbf{x}_2 \tag{9.21}$$

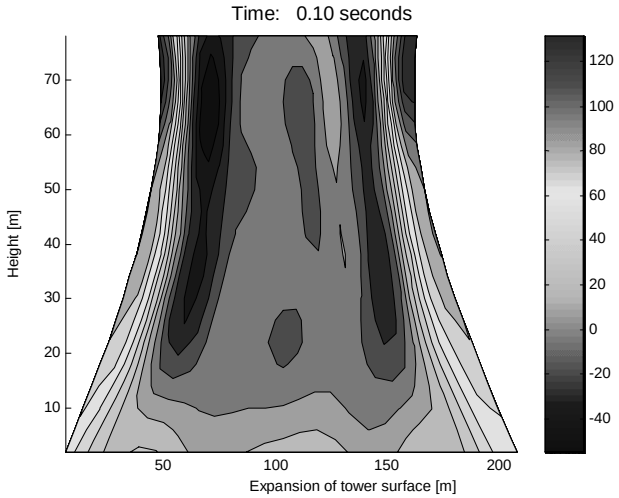

Figure 9.7 An example of the pressure field on the surface of the cooling tower at time t = 10 seconds. The view was taken from the leeward side.

9.3 Optimization of Structures Subjected to Wind Load

The optimal design of structures aimed at fulfilling safety and serviceability requirements may be a complex task, especially when the dominant loading excites the dynamic response, whose effects cannot be neglected in the optimization process. A typical case is that of flexible structures exposed to turbulent wind.

Instead, in structural dynamics problems, the analytical relationship between the target functions involving the unsteady response and the design variables can be found only in a few cases, unless resorting to approximations. This is the case of the wind excited response of structures, which can be expressed in closed form through the assumption of Gaussian wind pressure, linear structural behavior and statistical independence of the modal responses.

Moreover, even if the objective function can be evaluated analytically, it may present several local minima and therefore a global optimization technique, capable of escaping from the local minima and finding the global minimum of the problem, is needed.

To overcome these difficulties, a simulation procedure combined with a global optimization technique can be used. In this way, it is possible to take advantage of the global algorithms' capability to avoid local minima and of the simulation procedures' capability to correctly represent the stochastic nature of the physical phenomenon involved. This can be achieved through the evaluation of the objective function in correspondence of a large number of realizations of the response process.

For this purpose the Simulated Annealing algorithm can be chosen, among the global optimization techniques, for its effectiveness and easiness of implementation. The strength of the procedure mainly lies in its adaptability to different design situations. Therefore, it is also suitable to solve multiple objective optimization problem, which occur in most practical cases.

9.3.1 The Optimization Technique

9.3.1.1 The Simulated Annealing Algorithm

The Simulated Annealing algorithm owes its name to the similitude with the process of melting and subsequent slow crystallization of a metal. During the annealing, the particles slow down from the rapid movement typical of the liquid phase and set in pure crystals, reaching the minimum energy state.

The Simulated Annealing algorithm is composed by a sequence of Metropolis algorithms, that simulate a series of system's states towards the thermal equilibrium, calculated in correspondence of decreasing values of a suitable control parameter representing the temperature [i].

It can be demonstrated that under proper hypotheses on the convergence parameters, corresponding to a sufficiently slow cooling, the succession of the system's states converges to the global minimum [j].

The implementation of the Simulated Annealing algorithm requires the definition of the following data: 1) a large set of possible configurations, which represents the possible states of the physical system; 2) an objective function to minimize, corresponding to the internal energy of the system; 3) a control parameter and a cooling schedule, which represents the temperature and its rate of decrease, respectively; 4) a generator of random changes of the system configuration that simulates the path of the system towards the lower energy state.

The algorithm consists essentially of two main loops. The external one controls the temperature decrease and the internal one is the implementation of the Metropolis algorithm, which provides the system perturbation and checks for the acceptability of the new configuration (Figure 9.8).

To make the optimization procedure usable for problems with continuous variables a modified generator of random changes is needed. The procedure proposed in the present paper uses the Downhill Simplex Method to create the random sequence. In the neighborhood of the trial point a simplex is generated and the values of the objective function at its edges are calculated. Then, the simplex is subjected to proper reflections, expansions and contractions. In each vertex of the modified simplexes the acceptance criterion is checked.

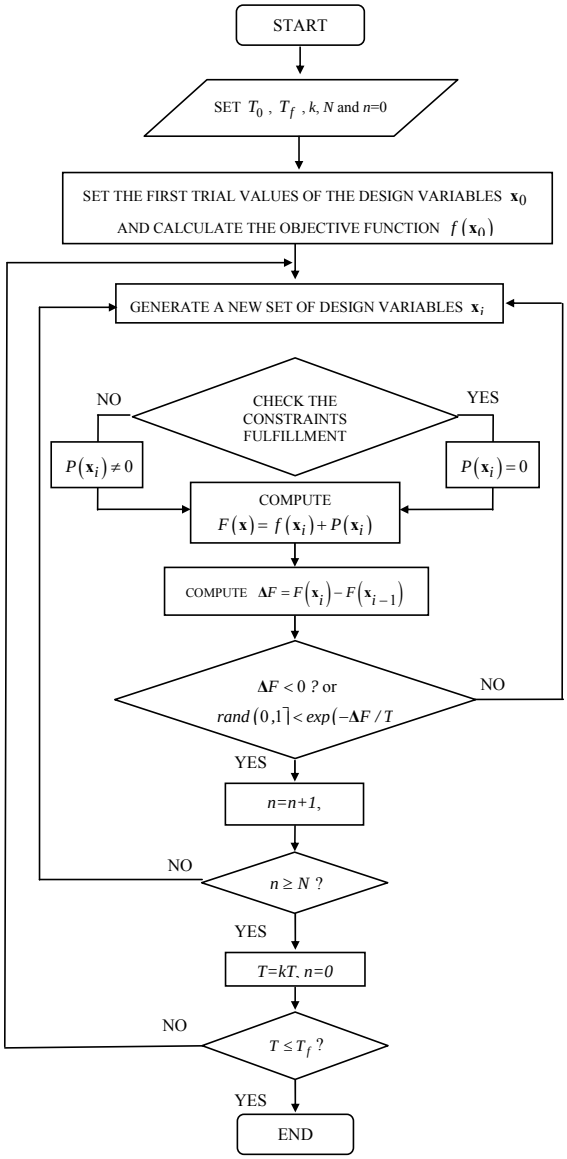

Figure 9.8 Block diagram of the simulated annealing algorithm.

In this continuous design variables case, a non-classical Metropolis acceptance criterion is used. A positive, logarithmically distributed, random variable is added to the value of the objective function in correspondence of each vertex and an analogous random variable is subtracted to the trial value of the objective function. In this way, the configurations in the downward direction are always accepted but sometimes a set of random variables in the upward direction may be accepted too. This allows the algorithm to escape from local minima.

9.3.1.2 The multiple objective problem

The multi-objective optimization method used herein is based on the simple weighting technique that generates effective solutions every time the objective space $f(\Omega)$, projection of the feasible decision space Ω into the objective space, is convex and some compensation between the objectives is allowed.

Considering an optimization problem with two competing targets $f_1(\mathbf{x})$ and $f_2(\mathbf{x})$, the method consists in solving, for each weighting coefficients set (α_1, α_2), the following single objective optimization problem:

$$\min f(\mathbf{x}) = \alpha_1 f_1(\mathbf{x}) + \alpha_2 f_2(\mathbf{x}) = f_1(\mathbf{x}) + \alpha f_2(\mathbf{x}) \qquad s.t.: \mathbf{x} \in \mathbf{\Omega} \tag{9.22}$$

where $\alpha=\alpha_2/\alpha_1$ ($\alpha_1>0$). Given different values for α, many optimal solution can be generated. Than, the best compromise solution may be chosen on the basis of trade off considerations.

9.3.1.3 Implementation of the procedure

In the proposed procedure several structural analysis methods can be implemented, depending on the problem under investigation. If the analyzed structure is subjected to a static loading, the target function will be determined by static analysis of the response. If the structure is subjected to dynamic loading, the objective function is evaluated using linear or non-linear step-by-step analysis or random dynamic analysis, as required by the dynamic system.

As the wind velocity is modeled as a stochastic process, in order to obtain a reliable solution of the optimization problem, the procedure may be repeated many times following a Monte Carlo scheme, modifying, in each run, the initial seed used by the random number generating routine. The statistical analysis of the results leads to the evaluation of the probabilistic structure of the response.

The multi-objective function is evaluated at each step, in correspondence of different trial values of the design variables.

The problem's constraints are considered through suitable penalty functions by adding a penalty term to the objective function if the restraints are not satisfied. In this case the configuration is automatically discarded. The penalty function approach, using a feasible design only strategy, is suitable for problems with a jointed feasible design space. The case of disjointed feasible domains is not considered in this study as it seldom occurs in structural engineering problems which this study is devoted to.

In the frequency domain the structural response is obtained by modal superposition.

In the time domain approach, a realization of the uni-dimensional multi-variate wind velocity process is artificially generated and the corresponding wind load time histories are applied to the joints of the discretized structure, in each trial configuration. The simulation of the wind velocity process is performed using well established techniques.

As each optimization analysis requires over one thousand structural analyses to be solved and considering that every time history is generated changing at random the starting phase angle, the probabilistic structure of the wind process is taken into account accurately.

The time domain analysis of the structural response allows to take into account properly the geometric non-linearity, that can be significant for flexible structures.

The Newmark's constant-average-acceleration integration method is used to perform the direct integration of the equations of motion following a step-by step procedure. The geometric nonlinearity is considered in the procedure by updating the stiffness matrix obtained, for each member, as the sum of the linear stiffness matrix and the geometric stiffness matrix. The geometric stiffness matrix is updated, at each iteration, using the value of the member's axial load

T at the previous step. The convergence tolerance of the nonlinear iterations can be assigned as a suitable percentage of the maximum axial loads.

9.3.2 Numerical Application

The previously described procedure has been applied to optimize the configuration of a guyed broadcasting antenna for telecommunications or mobile-phone networks, subjected to turbulent wind loading.

The structure is a 33 m high cable-stayed mast whose main pole is built with a steel hollow circular cross-section, having outer diameter D =16.83 cm and area A = 58.8 cm2, constant along the height, and supported by two orders of stays having diameter D = 2.7 cm (Figure 9.9).

The same structure was object of previous experimental studies in the wind tunnel aimed at investigating the aerodynamic loads acting upon it and the directionality effects of the wind loading [k].

Without any restriction to the applicability of the procedure, a schematic representation of the structure in two dimensions is considered in the analyses.

The finite-element model of the structure along with the joints numbering is shown in Figure 9.9. The pole and the cables are represented using frame and truss elements, respectively. The stays pretension is taken into account by means of proper thermal loads applied to the relevant members.

9.3.2.1 Formulation of the optimization problem

As the main constraints to the design of broadcasting antennas are the need of satisfying severe deformability limits and the requirement of restrain the overall dimensions in plan, two proper indicators of the above restrictions have been chosen as components of the multiple objective function: the first one, $f_1(\mathbf{x})$, is the sum of the squares of the displacements δ_i and the second one, $f_2(\mathbf{x})$, is the width in plan of the structure.

The design variables are the positions of the cables anchorages along the pole, h_1 and h_2, and the distance d between the cable anchorages to the ground (Figure 9.9).

Therefore, the optimization problem is expressed as follows:

$$minimize_{\mathbf{x}\in\Omega}\, f(\mathbf{x}) \tag{9.23}$$

where: $\mathbf{x} = (h_1, h_2, d)$

$$f(\mathbf{x}) = f_1(\mathbf{x}) + \alpha\, f_2(\mathbf{x}) = \sum \delta_i^2(\mathbf{x}) + \alpha \cdot d(\mathbf{x})$$

$$\Omega = \left\{ \mathbf{x} : \left| \boldsymbol{\sigma}_{members}(\mathbf{x}) \right| \le \bar{\boldsymbol{\sigma}} \cap \boldsymbol{\sigma}_{stays}(\mathbf{x}) \ge 0 \right\}$$

The problem constraints are represented by the fulfillment of the safety and serviceability requirements. In particular, the cables prestress must be greater than zero and the internal element stresses can not exceed the allowable value $\bar{\sigma}$.

The cooling schedule providing the best compromise between algorithm efficiency and computational effort was preliminarily calibrated: the control parameter T is reduced by 1% in each external loop, starting from an initial value T = 100, until the final value $T = 10^{-3}$ is reached. The maximum number of the accepted configurations N was set to 150.

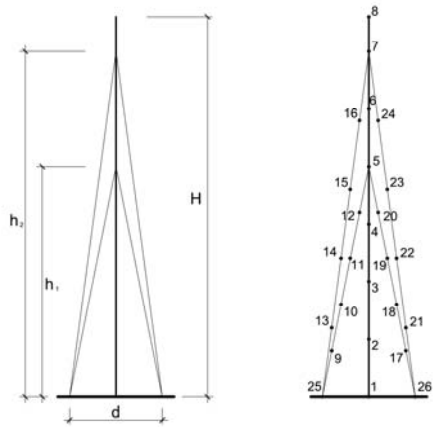

Figure 9.9 Schematic of the analyzed structure and joint numbering of the finite elements model.

The ratio α between the weighting coefficients α_1 and α_2 in Eq. 1.2 have been chosen to accommodate the differences in the physical dimensions of the components $f_1(\mathbf{x})$ and $f_2(\mathbf{x})$ and to make $f_1(\mathbf{x})$ and $\alpha f(\mathbf{x})$ comparable in magnitude. In particular the ratio $\alpha = 0.5$ was chosen to enhance the role of the displacements in the optimization process. As α_1 was set to unity, α_2 was taken as 2.

9.3.2.2 Results

The optimization problem is solved considering several structural analysis techniques: the static analysis under equivalent loads, the dynamic analysis in the frequency domain (FD) and the non-linear dynamic analysis in the time domain (TD).

In the case of the dynamic analysis in the frequency domain, the structural response is evaluated through the superposition of the first four natural modes, that proved to give a non negligible contribution in a preliminary spectral analysis.

The stability of the solution with respect to the choice of the first guess set of design variables has been investigated considering both the equivalent static analysis and the dynamic analysis of the response in the frequency domain. The results of Table 9.1 show that the algorithm is reasonably independent from the first guess configuration. However, the accuracy could be improved increasing the number of loops, i.e. refining the cooling schedule.

The small discrepancy between the values of the objective function may be ascribed to numerical tolerances and rounding. To study in detail this problem a parametric analysis was performed oriented to the systematic investigation of the feasible designs. Figure 9.10 shows that the objective function has a unique minimum in a low gradient that can lead to solutions slightly different from each other.

	Static analysis				*Dynamic analysis in the FD*			
First guess design variables (m)	Optimal design variables (m)			Objective function	Optimal design variables (m)			Objective function
21.00; 31.00; 6.00	18.462	31.595	3.369	1.977	15.869	27.003	3.226	1.816
19.00; 30.00; 5.00	19.262	31.742	3.302	1.975	15.053	27.193	3.085	1.799
22.00; 29.00; 4.00	18.772	31.568	3.354	1.972	14.921	27.419	3.518	1.838
20.00; 30.50; 3.00	19.059	31.469	3.328	1.973	16.349	27.887	3.288	1.856

Table 9.1 Optimal configurations (h1, h2, d) and values of the objective function obtained using static analysis and dynamic analysis in the frequency domain

The results in Table 9.1 highlight the discrepancy between the optimal design solutions obtained with the static analysis and those computed with the dynamic analysis. One of the reasons for this behavior is that the static analysis is based on the definition of equivalent static loads, which are calibrated on the first modal response of a free-standing cantilever beam. This type of load fails to simulate accurately the dynamic response of cable stayed masts, whose first modal shape displays inversion points. Moreover, for this class of structures, the contribution of the higher modes may hardly be neglected, as pointed out, among others, by Davenport and Sparling [l].

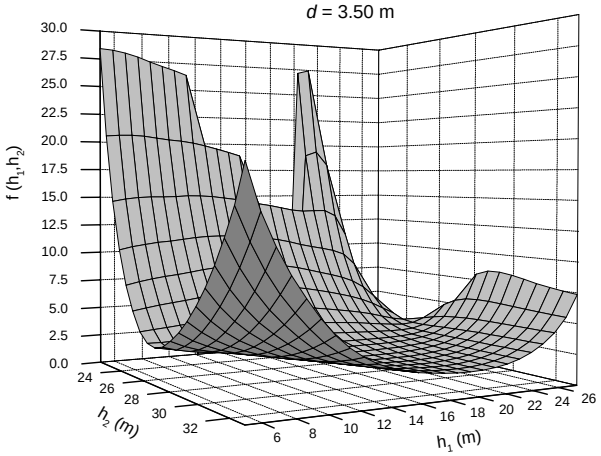

Figure 9.10 3D view of the objective function.

To demonstrate the applicability of the non-linear structural analysis in the optimization procedure, both TD and the FD optimizations were carried out.

Since the computation time required to perform a step-by-step analysis is about 100 times higher than the time needed for a frequency domain analysis, the comparison between the two procedures was carried out considering a short duration of the loading, corresponding to 60 seconds, though sufficient to excite the structure's dynamic response.

As the main purpose of the numerical applications is to illustrate the proposed procedure from a methodological point of view, a single run of the TD optimization was carried out instead of the

large number required by the Monte Carlo simulation which should be performed to take into account properly the stochastic nature of the applied load.

Table 9.2 summarizes the optimal configurations and the values of the objective function obtained using both the frequency and time domain analyses. The optimization in the time domain yields to a further reduction of the objective function with respect to the frequency domain analysis.

	Dynamic analysis in FD		*Dynamic analysis in the TD*	
First guess design variables (m)	Optimal design variables (m)	Objective function	Optimal design variables (m)	Objective function
21.00; 31.00; 6.00	20.04; 30.63; 5.82	1.94	21.79; 29.04; 5.06	1.89

Table 9.2 Optimal configurations (h_1, h_2, d) and values of the objective function obtained using dynamic analyses in frequency and time domain.

The time domain procedure has a wider field of applicability, but requires a significant computational effort. On the contrary the use of the frequency domain procedure is faster and represents a preliminary design tool whenever non-linear effects are negligible or attention must be paid to serviceability requirements.

9.4 BASIC REFERENCE

[a] Muscolino G., Ricciardi G., Cacciola P. 2003. Monte Carlo simulation in the stochastic analysis of non-linear systems under external stationary Poisson white noise input. *International Journal of Non-linear Mechanics*, **38**: 1269-1283.

[b] Choi H., Kanda J. 2003. Translation method: a historical review and its application to simulation of non-Gaussian stationary processes. *Wind & Structures*, **6** (5): 357-386.

[c] Bartoli G., Borri C., Facchini L. 2002. Simulation of non-Gaussian Wind Pressures on a 3D Bluff Body and Estimation of Design Loads, *Computer and Structures.* **80:** 1061-1070

[d] Simiu E., Scanlan R. H. 1996. *Wind effects on structures. Fundamentals and Applications to Design*. 3rd edition, John Wiley & sons, New York.

[e] Broomhead D.S., Lowe D. 1988. Multi-variable functional interpolation and adaptive networks. *Complex Syst.*, **2**: 269-303.

[f] Gotovac B., Kozulic V. 1999. On a selection of basis functions in numerical analyses of engineering problems. *International Journal for Engineering Modelling*, **12** (1-4): 25-41.

[g] Haykin S. 1996. *Adaptive Filter Theory*. Prentice Hall, Upper Saddle River.

[h] Poggio T., Girosi F. 1990. Networks for approximation and learning. *Proc. IEEE*, **78**: 1481-1497.

[i] Kirkpatrick S, Gelatt Jr. CD, Vecchi M.P. 1983. Optimization by simulated annealing. *Science;* **220**: 671-680.

[j] Van Laarhoven P.J.M., Aarts E.H.L. 1983. *Simulated Annealing: Theory and Applications*. D. Reidel Publishing Co., Dordrecht, Holland.

[k] Gioffrè M., Gusella V, Materazzi AL, Venanzi I. 2004. Removable guyed mast for mobile phone networks: wind load modeling and structural response, *J Wind Eng Ind Aerodyn,* **92**: 463-475.

[l] Davenport A.G., Sparling B.F. 1992. Dynamic gust response factors for guyed towers. *J Wind Eng Ind Aerodyn*; **41-44**: 2237-2248.

9.5 LIST OF PUBLICATIONS

[1] Facchini L. 2004. On the statistical characterization and simulation of wind induced pressure fields. In Impact of Wind and Storm on City Life and Built Environment, proceedings of *International Conference on Urban Wind Engineering and Building Aerodynamics*, von Karman Institute, Rhode-Saint-Genèse, Belgium, 5-7 maggio 2004.

[2] Biagini P., Borri C., Facchini L. 2004. Wind induced effects on an isolated cooling tower. In Impact of Wind and Storm on City Life and Built Environment, proceedings of *International Conference on Urban Wind Engineering and Building Aerodynamics*, von Karman Institute, Rhode-Saint-Genèse, Belgium, 5-7 maggio 2004.

[3] Biagini P., Facchini L. 2004. Analisi dell'affidabilità di strutture non lineari mediante il metodo della riduzione modale – il caso di una torre di raffreddamento sotto carico da vento. *Proceedings of IN-Vento-2004, VIII National Congress of Wind Engineering*, Reggio Calabria, 21-23 giugno 2004 (in Italian).

[4] Betti M., Borri C., Facchini L., Volpi S. 2004. Caratterizzazione e simulazione del campo di pressioni su una copertura aperta di grande luce (nuovo stadio di Manfredonia). *Proceedings of IN-Vento-2004, VIII National Congress of Wind Engineering*, Reggio Calabria, 21-23 giugno 2004 (in Italian).

[5] Biagini P., Facchini L. 2005. Analysis of complex systems under non-gaussian excitations by means of modal reduction. *Proceedings of Safety and Reliability of Engineering Systems and Structures*, ICOSSAR 2005, Rome 19-23 giugno 2005

[6] Materazzi A.L., Venanzi I. 2005. Structural Optimization under wind load via simulated annealing. *Proceedings of the Eurodyn 2005*, Paris, France.

[7] Materazzi A.L., Venanzi I. 2005. Optimal design of a cable-stayed mast exposed to turbulent wind. *Proceedings of Safety and Reliability of Engineering Systems and Structures*, ICOSSAR 2005, Rome 19-23 giugno 2005.

[8] Materazzi A.L., Venanzi I. Ottimizzazione in campo dinamico di antenne strallate. *Proceedings of 2nd National Congress on Vibration Problems in Civil Structures and Mechanical Constructions*, Perugia (in Italian).

[9] Materazzi A.L., Venanzi I. Progettazione ottimale di strutture flessibili esposte all'azione del vento. *Proceedings of IN-Vento-2004, VIII National Congress of Wind Engineering*, Reggio Calabria, 21-23 giugno 2004 (in Italian).

WITH CONTRIBUTIONS FROM:

Gianni Bartoli, University of Florence
Michele Betti, University of Florence
Paolo Biagini, University of Florence
Maurizio Orlando, University of Florence
Annibale Luigi Materazzi, University of Perugia
Ilaria Venanzi, University of Perugia